THE UNIVERSITY *of* EDINBURGH

Investigating the role of E3 ubiquitin ligase, UBR2, in chromosome stability

Veronica Duffy

Presented for the degree of

Doctor of Philosophy

Genetics and Molecular Medicine

The University of Edinburgh

February 2023

Declaration

I hereby declare that the work presented within this PhD thesis is my own, unless explicitly stated. This thesis has not been submitted for any other degree, diploma or professional qualification.

Veronica Duffy

28th February 2023

This thesis is dedicated to my mum Rosemary Duffy.

I owe everything in life to you.

Acknowledgements

First of all, I would like to thank my supervisor Ian Adams who provided knowledge, support and valuable insight throughout my PhD. Thank you for having me in your research group.

To all the members of the Adams lab, past and present, who created a warm and supportive environment to work in. Special thanks to Karen Dobie, who was my technical support through it all and was on hand to offer advice and most importantly the great chat. Also, thank you to Jen Lawson for always helping with mouse work and listening to me grumble as it does get like that sometimes. To my fellow PhD peer, Matilda Bui, you were the greatest ally I could have over the last few years. I am sure you will not miss me hovering around your desk for a debrief but I hope you realise how important you were to me over the last 3 years. I don't think I can ever repay you mate. James Crichton, the man who taught me all about testes, thank you for helping me and never judging the random stuff that would come out my mouth. I promise you there was some thought behind it all. Simon Brown, Issy MacGregor, Apiwat Moolnangdeaw, Cova Vara and Alex Pegg provided support, chat and snacks that were very much needed. I am especially grateful to Eleanor Raymond who gave me the grounding in my project at the beginning and Fiona Kilanowski for all your support with the ES cells.

To my PhD cohort: Alex, Jenny, Katy, Kirsty, Stuart and Zahra you were vital in maintaining a sense of fun that we all needed as we went through this

experience together. Thanks for all the amazing lunch banter, nights out and your belief in me. Thank you to my Twix girlies who were championing me from home and for the trips up to see me in my Edinburgh castle. Special thank you to Chelsea for being my best friend and supporting every decision I make regardless of whether it's good or bad.

Thank you to my family whose belief in me never wavered even when I did not have any in myself. My mum Rosemary you are the reason that I have achieved so much with your love, care and dedication. To my dad Thomas and my brother David thank you for instilling your hard work ethic into me. My big sister Rebecca and Darren for keeping the family together through all the ups and downs. My other big sister Mary for always checking in and sending photos of the family to give me a much needed boost. I am grateful for my nieces Sophie, Suzanne, Clara, Eilidh and Hannah and my nephew Albert for being the biggest inspiration and for showing me that life carries on. Thanks to Stella Henderson without you I would not have clean clothes.

Finally, I thank Susan. You came into my life at the same time as this PhD and I would never have completed it without you. Thank you for your patience, sympathy and encouragement even in the most testing of times. Here's to our future together.

Abstract

Ubiquitination is an essential cellular mechanism where ubiquitin attaches to proteins to regulate their function or target them for degradation via the proteasome. The transfer of ubiquitin from E2 ubiquitin conjugating enzymes to target proteins is regulated by the highly diverse group of E3 ubiquitin ligases. One prominent family of the E3 ubiquitin ligases are the seven UBR proteins, four of which have overlapping roles in the N-end rule pathway where they, canonically, bind either basic (Type I) or bulky hydrophobic (Type II) amino acids at the N-terminus of the substrate. However, at least some of these UBR proteins also have non-canonical roles outwith the N-end rule pathway, and even non-catalytic roles in stabilising some proteins. Null genetic mutations in *Ubr2* cause increased amounts of cohesin associating with chromosomes, defects in chromosome synapsis during meiosis, male infertility and female-specific embryonic lethality. However, it is not clear whether these phenotypes relate to UBR2's role in the N-end rule pathway or its non-canonical roles.

As UBR2 has a role in chromatin-bound cohesin maintenance in mitotic cells, I investigated whether UBR2 might localise to chromosomes to regulate chromatin-associated cohesin directly. I overexpressed FLAG-tagged UBR2 in HEK293T cells and imaged the cells throughout the cell cycle. Although I could not detect localisation of wild-type UBR2 to chromatin at any stage of the cell cycle, a version of UBR2 with mutations in its ELL domain did localise to chromosomes during mitosis in 30% of HEK293T cells suggesting that this

mutation increases the affinity of UBR2 to bind to chromosomes and regulate chromosome-associated substrates.

Next, I wanted to investigate how UBR2 regulates chromosome-associated substrates. In order to dissect which domains of UBR2 are involved in this function, I used CRISPR-Cas9 technology to introduce separation-of-function point mutations into the endogenous *Ubr2* locus, and characterised the effects of these mutations on known UBR2 substrates. Using these cells along with *Ubr2*$^{-/-}$ cells, I was able to use mass spectrometry to identify potential N-end rule substrates and non-canonical substrates of UBR2.

Finally, I used CRISPR-Cas9 technology to introduce these separation-of-function mutations into mice in order to determine how the distinct biochemical roles of UBR2 relate to the *Ubr2*$^{-/-}$ null mouse phenotypes. Surprisingly, I found that the major phenotypes in *Ubr2*$^{-/-}$ mice are not recapitulated by mutations that specifically affect N-end rule substrate ubiquitination, that non-canonical protein ubiquitination is likely involved in *Ubr2*-dependent regulation of cohesin, and that the well-established role for UBR2 during spermatogenesis does not appear to act through either N-end rule or non-canonical UBR2-dependent ubiquitination. I propose that the key physiological role of UBR2 in meiosis and spermatogenesis relies on non-catalytic roles of UBR2 in binding to, and stabilising, its binding partner TEX19.1.

Lay Summary

Proteins are the products of genes in a cell which need to be maintained throughout the cells life span to ensure normal function. To make sure protein levels are tightly maintained in a cell, an efficient recycling process has evolved to label proteins that need to be turned over- this is called ubiquitination. A small molecule, called ubiquitin, is transferred by a specialised protein to label proteins and direct it towards a recycling centre called the proteasome. One of these proteins is called UBR2 which has a role in the N-end Rule pathway, where UBR2 can bind to proteins that have certain degradation signals at one end and tag them to ensure they enter the recycling centre for turnover. UBR2 also has a role outwith the recycling process where it can stabilise other proteins in the cell such as the defence gene, TEX19.1. When UBR2 is removed in mice, the problems arise during sperm development that cause male infertility, and there are defects in the turnover of protein molecule called cohesin that helps hold chromosomes together. Previous work determined that the N-end rule pathway role of UBR2 may not be responsible for male infertility and cohesin turnover. I hypothesised that the effects on tissues that occur when UBR2 is removed is due to its role in labelling proteins with degradation signals in internal regions of proteins known as the non-N-end rule pathway.

To investigate UBR2 and its functions in cells, I placed mutations into different parts of the UBR2 protein using CRISPR-Cas9 genome editing in embryonic stem cells and mice. The embryonic stem cells allowed me to identify potential substrates recognized by the different domains of UBR2.

The mice models showed me that interrupting the transfer of the ubiquitin tag to UBR2 affects the recycling of cohesin on chromosomes but not the issues with male fertility. This suggests that alternative non-N-end rule pathway is important for cohesin turnover. The male infertility that is found when UBR2 is removed may be due to roles of UBR2 outwith the recycling process such as stabilising binding partners like TEX19.1.

Contents

List of figures

List of tables

Abbreviations

Ac ————— Acetyl protein modification

ACA ————— Anti-centromeric antibody (CREST patients)

AcSMC3 ————— Acetylated SMC3

APC/C ————— Anaphase-promoting complex, or cyclosome

Arg —————Arginine

Arg/N-end ——— N-terminal degron sequence for substrate ubiquitination

ATF3 ————— Activating transcription factor 3

AID ————— Autoinhibitory domain

AE ————— Axial element

BSCR ————— Barrier to sister chromatid repair

BioID ————— Biotinylated protein identification

CHD —————Cap helical domain

CTCF————— CCCTC-binding factor

CE ————— Central element

Ct ————— C-terminal

C-lobe ————— C-terminal lobe

CRLs ————— Cullin-RING ligases

DSB ————— Double-strand break

ESCs ————— Embryonic stem cells

FACS ————— Fluorescence-associated cell sorting

FC —————Fold change

GFP ————— Green fluorescent protein

GID ————— Glucose-induced degradation

HDR ————— Homology directed repair, a type of CRISPR-Cas9

HECT ————— Homologous to E6-associated Protein C-terminus

H3K9me3 ————— Histone 3 Lys-9 trimethylation

γH2AX ————— Histone H2AX at serine 139

IF ————— Immunofluorescence

IMM ————— Inner mitochondrial membrane

JNK ————— C-Jun N-terminal kinase

kDa ————— Kilodaltons

LFQ ————— Label-free quantitation

LE ————— Lateral elements

LIF ————— Leukaemia inhibitory factor

LINE-1 ————— Long interspersed nuclear element protein 1

MAPKKK ————— MAPK kinase kinase family

MS ————— Mass spectrometry

MEFs ————— Mouse embryonic fibroblasts

Met-Φ ————— Non-acetylated substrates of the Ac/N-end Rule pathway

MSCI ————— Meiotic sex chromosome inactivation

MSUC ————— Meiotic silencing of unsynapsed chromatin

Nt ————— N-terminal

N-lobe ————— N-terminal lobe

ORF ————— Open reading frame

PAGE ————— Polyacrylamide gel electrophoresis

PFA ————— Paraformaldehyde

PBS ————— Phosphate buffered saline

PI ————— Propidium iodide

PP2A ————— Protein phosphatase 2A

PINK1————— PTEN-induced kinase 1

RBR ————— RING-between-RING

RN ———— Recombination nodules

RING ———— Really Interesting New Gene

RBS ———— Roberts syndrome

Sgo ———— Shugoshin

SMC ———— Structural maintenance of chromosomes

SAC ———— Spindle assembly checkpoint

SA ———— Stromal antigens

SC ———— Synaptonemal complex

TAD ———— Topologically associated domains

TAR ———— Trans-activation response

TEX19.1 ———— Testis-expressed protein 19.1

TFAP2C ———— Transcription Factor AP-2 Gamma

TAK1 ———— Transforming growth factor-β-activated kinase 1

TF ———— Transverse filaments

TI ———— Type I (N-end Rule, Arginine)

TII ———— Type II (N-end Rule, Phenylalanine)

U2BR ———— Ubc2-binding region

Ub ———— Ubiquitin

UPS———— Ubiquitin-proteasome system

UAIN ———— UBR autoinhibitory domain

UBLC ———— UBR/Leu/Cys

UBR2 ———— UBR-domain protein 2

Ubr2$^{-/-}$ ———— *Ubr2* null mouse line

Ubr2$^{T1/T1}$ ———— *Ubr2* with the D118A point mutation

Ubr2$^{T2/T2}$ ———— *Ubr2* with the D233A point mutation

Ubr2$^{ELL/ELL}$ ———— *Ubr2* with the K834A point mutation

Ubr2$^{RD/RD}$ ———— *Ubr2* with the W1177A point mutation

WABS ———— Warsaw Breakage syndrome

WHD ———— Winged helical domain

WR ———— Working reagent

Chapter 1:
Introduction

1.1 Meiosis and Genomic Stability during Reproduction

There are two ways in which cells can divide and transmit chromosomes to their progeny. Mitosis is the more common of the two types of cell division that occurs during cell proliferation involving one round of DNA replication followed by one round of chromosome segregation. This leads to the generation of two daughter cells with the same number of chromosomes as the parental cell. Meiosis is the second type of cell division that is important for the production of haploid gametes.

1.1.1 The Two Meiotic Divisions

The meiotic cell cycle is characterised as one round of DNA replication followed by two rounds of chromosomes segregation (Meiosis I and Meiosis II) leading to the production of haploid gametes (Figure 1.1). Haploid gametes combine during fertilisation to produce a diploid zygote, which will continue through development. Chromosome structure and behaviour during meiosis differ from mitosis and are largely similar between oogenesis and spermatogenesis. However, there are key differences between the female and male reproductive systems that lead to certain adaptations in chromosome behaviour between spermatogenesis and oogenesis.

The timing of meiosis differs between females and males. In females, meiotic prophase is initiated in germ cells during foetal development and progresses until the oocytes enter a phase of dictyate arrest. In response to reproductive hormones, groups of arrested oocytes are then stimulated to grow, mature and eventually progress through meiotic divisions from puberty until menopause occurs later in adult life. Whereas in males, meiotic prophase is

initiated continuously in adult life, with no meiotic arrest, resulting in continuous gamete production from puberty and throughout adult life (Handel and Eppig, 1997; Morelli and Cohen, 2005).

In mammalian males, the completion of meiosis is monitored under several layers of regulation such as the pachytene checkpoint, kinase activation, meiotic sex chromosome inactivation and translational control (Sun and Handel, 2008; Burgoyne, Mahadevaiah and Turner, 2009; Sun, Palmer and Handel, 2010; Ichijima *et al.*, 2011; Jordan, Karppinen and Handel, 2012). Male prophase is accompanied by robust alterations of gene expression programmes (Schultz, Hamra and Garbers, 2003; Shima *et al.*, 2004; Green *et al.*, 2018; Grive *et al.*, 2019) and epigenetic status (Maezawa *et al.*, 2020) but how these are controlled during meiotic prophase is unknown. Whereas in mammalian females, there are two arrest stages throughout oogenesis, the longest being dictyate arrest which can last decades in humans, where age-related degradation of chromosomal components, such as chiasmata, impairs accurate division that leads to aneuploidy (Hunt and Hassold, 2008; Jessberger, 2010; Burkhardt *et al.*, 2016). Most meiotic errors are detected during oogenesis i.e. chromosome missegregation during female meiosis, as opposed to chromosome missegregation in the male meiotic cells (Hassold and Hunt, 2001). This may contribute to errors in spermatogenesis that leads to spermatocyte death in males so is not detected in humans and transmitted to offspring. However, there are still multiple issues that can arise during male meiosis that are detected which causes aneuploidy leading to infertility.

Figure 1.1: Schematic of chromosome dynamics during Meiosis I and II. In meiosis I, homologous chromosomes are segregated in opposite directions. At anaphase I, homologous chromosomes are segregated toward opposite poles of the spindle by dissolution of chiasmata. In meiosis II, sister chromatids are segregated. Adapted from Ishiguro, 2019.

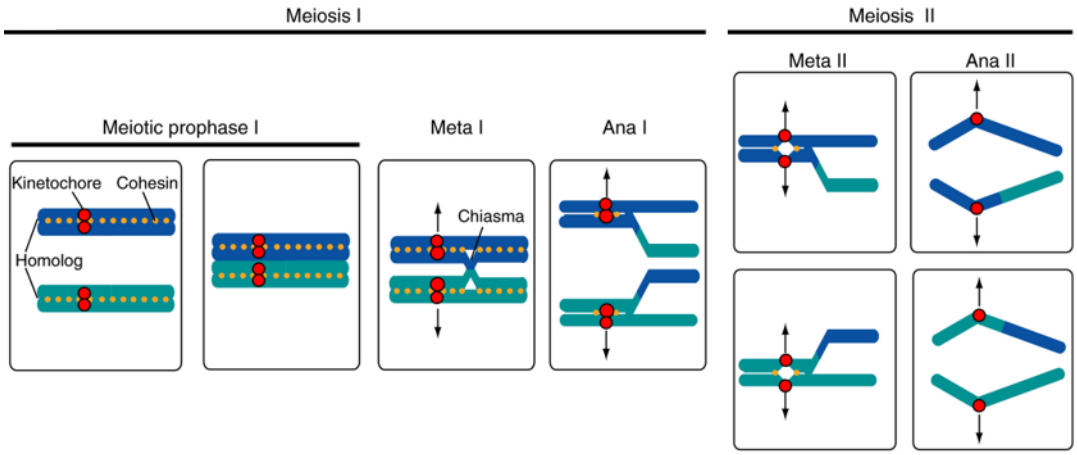
Meiosis I
Meiosis II
Meiotic prophase I
Meta I
Ana I
Meta II
Ana II
Kinetochore
Cohesin
Homolog
Chiasma

1.1.2 Meiosis I

1.1.2.1 Prophase I: Synapsis and Recombination

During meiotic prophase I, sister chromatids are organised into the axial element (AE) or chromosome axis where the synaptonemal complex (SC) is assembled and homolog recombination is completed (Zickler and Kleckner, 1999). The meiotic chromosomes undergo dynamic movements to facilitate homologue pairing and synapsis, driven by recombination and require telomere attachment to the nuclear membrane (Shibuya and Watanabe, 2014). In this way, the chromosome architecture and dynamics during meiotic prophase are markedly different from those in mammalian mitosis.

In most, but not all, mammals, meiotic recombination is initiated by selection and activation of DNA recombination sites that are marked by trimethylation of histone H3 on lysine4 (H3K4me3); in mammals, the DNA-binding zinc-finger protein, PRDM9 is expressed in prophase stages, leptotene and zygotene. (Parvanov, Petkov and Paigen, 2010; Sun *et al.*, 2015; Powers *et al.*, 2016; Zelazowski and Cole, 2016). PRDM9's zinc finger domain determines binding specificity, the SET domain possesses histone tri-methyl transferase activity whereas the KRAB domain is required for protein-protein interactions (Imai *et al.*, 2017). After this selection and activation with histone methyl marks, recombination sites become associated with the chromosome axis and undergo widespread double-strand break (DSB) formation an endonuclease that comprises SPO11 and TOPOVIBL subunits (Baudat, Imai and De Massy, 2013; Borde and de Massy, 2013; Robert *et al.*, 2016) which is followed by 5' DNA resection to yield 3' single-stranded tails (Neale, Pan

and Keeney, 2005; Neale and Keeney, 2006). This initiates a homology search and 3' tails undergo strand invasion of their intact homolog, leading to recombination products that resolves into either crossover or non-crossovers (Allers and Lichten, 2001; Baudat and de Massy, 2007).

During prophase, chromosome synapsis occurs – synapsis is achieved by the formation of the SC which is the 'zipper' that binds the homologous chromosomes together (Page and Hawley, 2004). The SC is made up of two parallel axial element/lateral elements (LE) and the central element (CE) connected by overlapping transverse filaments (TFs) (Page and Hawley, 2004). The lateral element is made up of proteins such as SYCP2 and SYCP3 that localise to chromosomes in leptotene (Figure 1.2). The LE forms individual axes by polymerisation along each homolog (Baier, Alsheimer and Benavente, 2007) and as they align during DSB repair during zygotene.

The LE forms alongside the cohesin cores, establishing the axis required to support meiotic recombination (Figure 1.2, Llano *et al.*, 2012; Biswas *et al.*, 2016; Ward *et al.*, 2016). Throughout prophase I, sister chromatids are held together by the cohesin complex (Figure 1.2), which is a tripartite protein ring complex where mutations in each subunit leads to meiotic arrest. It is proposed that the cohesin complex forms a ring structure that encircles sister chromatids during DNA replication prior to the beginning of Meiosis I but is also being loaded onto chromatin during leptotene (Ishiguro, 2019). The structure of cohesin in meiosis is discussed in detail in section 1.2.2. Sororin, a cohesin stabilizer, is important for meiotic G2-M transition and loss of

sororin results in either meiotic prophase I arrest or spindle defects due to APC/C-mediated degradation of Cyclin B2 and compromised Cdk1 activity (Zhou *et al.*, 2021). Therefore, it seems that different cohesin complexes and cofactors are vital for progression throughout meiosis, each being tightly regulated and carrying out specific functions.

Following LE assembly, the CE of the SC is formed and compromised of at least five proteins (SYCE1–3, TEX12 and SIX6OS1) and although the full picture remains unclear, the SC is composed of two distinct layers formed by TFs, made from SYCP1, that forms a ladder-like structure that holds two homologs together in a long axis (Costa *et al.*, 2005; Hernández-Hernández *et al.*, 2016; Dunne and Davies, 2019). Based on partial SC structures investigated in mice mutants of individual CE components, SYCE1, 3 and SIX6OS1 recruitment destabilises the SYCP1 tetrameric lattice and remodels it whereas SYCE2 and TEX12 are required for SC extension along the LE (Bolcun-Filas *et al.*, 2007, 2009; Hamer *et al.*, 2008; Schramm *et al.*, 2011; Gómez-H *et al.*, 2016; Crichton *et al.*, 2023).

Pachytene is the stage of prophase I when chromosomes in the nucleus are fully synapsed, except for the XY chromosomes in males, and the LE and CE are fully formed along the length of the SC. CE establishment coincides with the disappearance of axis-associated HORMAD1/2 that also have a role in DSB formation and repair (Figure 1.2, Daniel *et al.*, 2011; Wojtasz *et al.*, 2012). The mismatch repair heterodimer MLH1/MLH3 localises and carries out crossover repair during pachytene (Falque *et al.*, 2007; Rogacheva *et al.*,

2014). In mitosis, recombinant repair events act between sister chromatids which are held together by cohesin rings following replication. However, this is different in meiosis, as meiocytes have to guarantee recombination between homologs. This is described as a barrier to sister chromatid repair (BSCR) or interhomolog bias leading to further complexity of crossover regulation (Lao and Hunter, 2010). How BSCR occurs in mammals is still not fully understood but similar to other model organisms, the SC and associated proteins (SYCP3, HORMAD1/2) appear to have a critical role (Li, Bolcun-Filas and Schimenti, 2011; Shin, McGuire and Rajkovic, 2013; Kobayashi *et al.*, 2017; Rinaldi *et al.*, 2017). Homologous chromosomes synapsis and DSB repair is also ensured by recombination-proteins such as DMC1, RAD51, RPA and MSH4/5 (Figure 1.2).

Diplotene is the final stage of prophase I when chromosomes desynapse in preparation for the first meiotic division where the homologous chromosomes are held together by their recombination points. The SC dissociates and crossovers mature into chiasmata, to mark the onset of prometaphase I. At this time, HORMAD proteins once again mark the desynapsed axes (Daniel *et al.*, 2011; Wojtasz *et al.*, 2012). Chiasmata are physical connections between DNA at crossover points that maintain bivalent structure without protein scaffolds such as the SC or cohesin complexes (Nasmyth, 2001). Chiasmata have an essential role in positioning homologous chromosomes so that they are captured by microtubules from opposite poles during metaphase I (Sakuno *et al.*, 2011).

The DNA recombination process is required as a quality control of meiosis I where the primary goal is to ensure crossover formation and prevention of deleterious and disease-causing chromosomal loss. In men, 10% of patients with non-obstructive azoospermia show a higher rate of recombination failure (Gonsalves *et al.*, 2004), while up to 45% of men whose partner suffer from recurrent pregnancy loss, and who have normal sperm density, motility, and morphology have increased sperm aneuploidy (Ramasamy *et al.*, 2015). These findings could explain many cases of “idiopathic infertility”.

SC is essential for meiotic recombination and crossover formation. Significant disruption to the formation of the SC leads to meiotic failure, infertility and embryonic death through aneuploidy (de Vries *et al.*, 2005; Kouznetsova, Benavente and Pastink, 2011; Yuan *et al.*, 2002). Defective SC formation in humans has been associated with 15% of infertile couples, 5% having recurrent miscarriages as well as non-lethal aneuploidies such as Down syndrome (Matzuk and Lamb, 2002; Bolor *et al.*, 2009).

Figure 1.2: The four stages of Prophase I and the chromosome axis in meiosis. A schematic to illustrate both meiotic prophase I chromosome dynamics and the spatiotemporal coordination of the chromosomal axis and synaptonemal complex assembly with the recombination machinery. Male and female meiosis are illustrated by a schematic spermatocyte and oocyte with three pairs of homologous chromosomes, including the sex chromosome pair. Pairs of sister chromatids are aligned and held together by cohesin cores, and DSBs form in leptotene. Each pair of homologous chromosomes begins to line up as a result of the homology search in zygotene, and once the full lengths of the homologs are aligned and synapsed, the cell progresses into pachytene where DNA recombination and crossing over occur. Then the synaptonemal complex begins to break down for desynapsis except for the crossover points in diplotene. Proteins that assemble into cytologically visible complexes termed recombination nodules (RNs). Spermatocytes progress to metaphase I and complete meiotic divisions without interruption, whereas oocytes arrest at the dictyate stage until meiotic resumption months or years later, with another arrest at metaphase I just before ovulation. Taken from Bolcun-Filas and Handel, 2018.

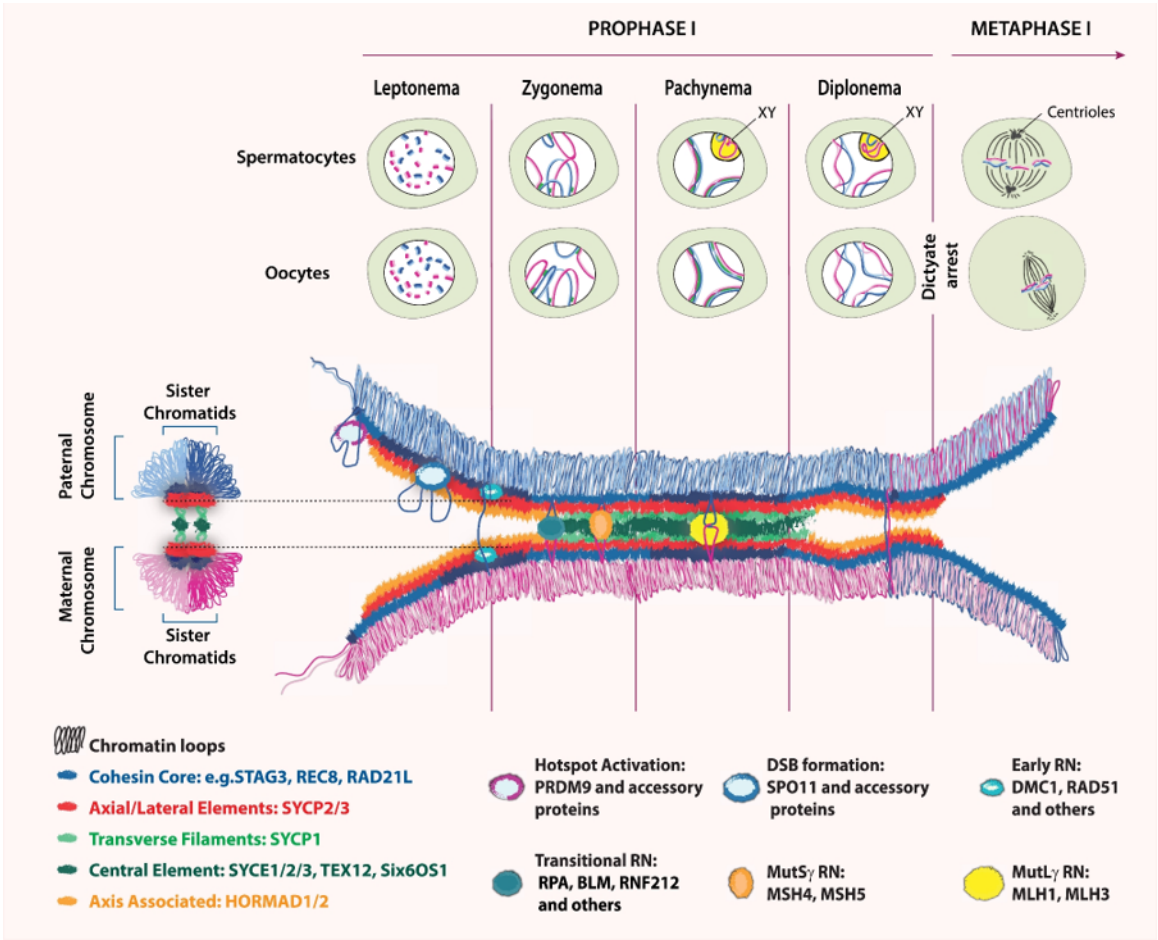
PROPHASE I
METAPHASE I
Leptonema
Zygonema
Pachynema
Diplonema
XY
XY
Centrioles
Spermatocytes
Oocytes
Dictyate arrest
Sister Chromatids
Paternal Chromosome
Maternal Chromosome
Sister Chromatids
Chromatin loops
Cohesin Core: e.g.STAG3, REC8, RAD21L
Axial/Lateral Elements: SYCP2/3
Transverse Filaments: SYCP1
Central Element: SYCE1/2/3, TEX12, Six6OS1
Axis Associated: HORMAD1/2
Hotspot Activation: PRDM9 and accessory proteins
DSB formation: SPO11 and accessory proteins
Early RN: DMC1, RAD51 and others
Transitional RN: RPA, BLM, RNF212 and others
MutSγ RN: MSH4, MSH5
MutLγ RN: MLH1, MLH3

1.1.2.2 Sex Chromosomes in Prophase I

Heterogametic sex chromosomes pose specific challenges in meiosis. In mammalian oocytes, the two X chromosomes experience no impediment to their pairing or recombination and behave like autosomal chromosomes. Whereas, in male mammalian germ cells X and Y chromosomes are quite different in length and sequence which affects their behaviour.

Sex chromosomes form a unique chromatin domain in spermatocytes called the “sex” or “XY” body in a large variety of mammals (Solari, 1974; Handel, 2004). The XY body is a domain of repressed chromatin associated with unique and incompletely understood array of proteins involved in DNA damage repair, chromatin modifications and protein translation (Hu, Sun and Handel, 2018). The XY body is a domain of unpaired chromatin that is different from the synapsed autosomal chromosomes within the spermatocyte nucleus. It is transcriptionally inactivated by a process known as meiotic sex chromosome inactivation (MSCI) which is a special case of a more general phenomenon: meiotic silencing of unsynapsed chromatin (MSUC) (Schimenti, 2005).

MSUC is a surveillance mechanism for chromosome asynapsis after homologous autosomes have completed synapsis in pachytene. In normal male meiosis, MSUC of unsynapsed X and Y chromosomes where only a small region of homologous sequence pairs and synapses called the pseudoautosomal region (Ellis and Goodfellow, 1989). At the onset of mid-pachytene, the initiation of MSCI leads to sex chromosomes separating away

from recombining and transcriptionally active autosomes and are transformed into the XY body (Turner, 2015).

MSUC and MSCI are directed by DNA damage response pathways that mediate the phosphorylation of histone H2AX at serine 139 (γH2AX) (Ichijima *et al.*, 2011; Ichijima, Sin and Namekawa, 2012). Unsynapsed chromosome axes (XY chromosomes in MSCI) are recognised by ATR, a serine/threonine-protein kinase, and TOPBP1, an ATR activator (Perera *et al.*, 2004; Royo *et al.*, 2013; ElInati *et al.*, 2017). ATR phosphorylates H2AX which draws MDC1, a γH2AX binding partner, leading to the spread of γH2AX into a chromosome-wide domain (XY chromatin in MSCI) which then continues the loop until there is chromosome-wide silencing including the XY chromosomes (Ichijima *et al.*, 2011). When present as autosomal transgenes, Y-linked transcription factor *Zfy* genes evade MSCI and are expressed ectopically during pachytene triggering germ cell apoptosis during stage IV of the spermatogenic cycle (Royo *et al.*, 2010). Extensive germ cell apoptosis at this tubule stage is seen in other models where MSCI, and in particular Y chromosome silencing is impaired (e.g. XYY males, *H2afx*$^{-/-}$, *Hormad2*$^{-/-}$) (Fernandez-Capetillo *et al.*, 2003; Royo *et al.*, 2010; Wojtasz *et al.*, 2012). Defective MSCI leads to meiotic failures which triggers efficient elimination of developing gametes carrying univalent chromosomes in male meiosis to prevent transmission to the next generation.

1.1.2.3 Completion of Meiosis I

Following completion of prophase I, the first meiotic division begins where the homologous chromosomes are segregated. The end result of prophase I is the physical connection between homologous chromosomes by chiasmata which aid in subsequent chromosomal capture by microtubules from opposing cellular poles during metaphase I (Sakuno *et al.*, 2011). The homologous chromosomes then separate from one another during anaphase I, segregating to opposite poles of the spindle following chiasma dissolution (Buonomo *et al.*, 2000; Kudo *et al.*, 2006). All of this leads to the reduction of the number of chromosomes by half in the daughter cells at the end of meiosis I (Watanabe, 2012).

To achieve this, major processes are specifically modified in meiosis in comparison with mitosis. The first difference of meiosis from mitosis is the behaviour of kinetochores to achieve bipolar attachment. Kinetochores are large proteinaceous structures that form at the centromere of each sister chromatid and act, alongside other regulatory functions, as attachment points for the spindle microtubules (Joglekar and Kukreja, 2017; Thomas, Renjith and Manna, 2017). In mitosis, sister kinetochores attach in a bipolar orientation to the opposite poles. Whereas in meiosis I, sister kinetochores attach to the same pole (monopolar kinetochore orientation) and homologous kinetochores attach to opposite poles. This allows for segregation of the sisters within each homolog pair towards the same direction and are co-

segregated into the same daughter cell (Sakuno, Tada and Watanabe, 2009; MacLennan *et al.*, 2015).

Chromosomes align on the spindle fibres in metaphase I. Chromosome segregation in spermatogenesis similar to mitosis where centrosomes located at the opposite ends (spindle pole) organise microtubules into spindles which interact with the chromosomes via their kinetochores. The movement of chromosomes is due to the polymerisation and depolymerisation of microtubules as well as microtubule motors such as CENP-E and dynein, which allow for the movement of chromosomes on microtubules (Klaasen and Kops, 2022) and centromeric cohesion holds each pair of sisters together.

Chiasmata act to provide tension against the spindle forces until chromosomes fully align, reducing the incidence of premature separation that could lead to aneuploidy (Sacristan and Kops, 2015). The spindle assembly checkpoint (SAC) is a crucial mechanism that ensures correct segregation of the chromosomes by monitoring any lack of microtubule attachment to kinetochores and a lack of tension to block or delay anaphase through inhibition of the anaphase-promoting complex/cyclosome (APC/C) (Lara-Gonzalez, Westhorpe and Taylor, 2012). Once chromosomes are aligned on the metaphase plate correctly, anaphase I commences: arm cohesin is removed and homologous chromosomes are pulled to opposite sides.

Ooocytes are one of the few cell types where the poles are not organized by centrosome, instead multiple acentriolar microtubule-organizing centres are

required for normal cell division and production of euploid cells (Szollosi, Calarco and Donahue, 1972; Baumann *et al.*, 2017). The meiotic spindle is asymmetrically positioned by activity of actin filaments to carry out the unequal divisions and polar body extrusion that maintain maternal resources in the cytoplasm (Mogessie, Scheffler and Schuh, 2018).

Proteolytic removal of cohesin along chromosome arms trigger separation of homologous chromosomes towards opposite poles during metaphase I-anaphase I transition. Removal of cohesin during meiosis is further discussed in section 1.2.3 but for now, the cysteine protease, Separase, cleaves the kleisin (REC8) subunit in meiosis (Buonomo *et al.*, 2000; Kitajima *et al.*, 2003; Kudo *et al.*, 2006). At the onset of anapahase I, REC8-cohesin is cleaved by separase along chromosome arms but is maintained at the centromere until meiosis II, allowing chiasmata resolution and release of homologous chromosomes (Figure 1.1). REC8 in the centromere is protected from cleavage to ensure sister chromatid separation in meiosis II, a period when bipolar attachment is established by the preserved centromeric cohesion. Shugoshin (Sgo)/Mei-S332 family protect centromeric cohesion during meiosis I each of which forms a complex with protein phosphatase 2A (PP2A) that contains the B56 subunit (Kitajima *et al.*, 2006). Shugoshin, SGO2, forms a complex with PP2A and SGO2-PP2A localizes to the centromeres to protect centromeric REC8 cohesin by counteracting phosphorylation and separase-mediated cleavage during anaphase I (Lee *et al.*, 2008; Llano *et al.*, 2008).

Cohesin and subsequent chromosome cohesion are extremely important in meiosis, especially in oogenesis which is not a continuous process and begins during embryonic development of the ovary, undergoing dictate arrest at the end of prophase I (MacLennan *et al.*, 2015). Loss of cohesin has been linked to reduced cohesion of chromatids leading to aneuploidy (Liu and Keefe, 2008).

1.1.2.4 Meiosis II: Segregation of Sister Chromatids

After the first meiotic division is complete, oocytes and spermatocytes progress into MII. Sister chromatids are held together by centromeric cohesin complexes and the kinetochores are bi-orientated on spindle fibres, much like in mitosis. Spermatocytes progress through cell division, but oocytes arrest again at Metaphase II until fertilisation with mature sperm, upon which centromeric cohesion is cleaved by separase which results in segregation of sister chromatids into each gamete (MacLennan *et al.*, 2015). Oocytes require asymmetric positioning of the spindle which is achieved by actin anchoring against the egg's surface (Mogessie, Scheffler and Schuh, 2018). As cell division occurs, the second polar body is extruded and one sister chromatid from each pair remains in the oocyte which then fuses with the haploid sperm nucleus to produce a diploid single-cell zygote.

1.2 Cohesin regulation during cell division.

Cohesin is the protein complex that is required for sister chromatid cohesion to be established which is essential for genomic stability during DNA synthesis and ensures accurate chromosome segregation in both mitosis and meiosis (Nasmyth and Haering, 2009).

Cohesins are a group of protein complexes that associate with chromosome axes during S phase and the mitotic/meiotic cycles as well as having regulatory roles during interphase. They generate intramolecular loops of chromatin and hold sister chromatid together until chromosome division in mitotic anaphase or meiotic anaphase II. The complex is made up of three subunits that make up a tripartite ring (Figure 1.3): two members of the SMCs (structural maintenance of chromosomes) protein family, SMC1α and SMC3 and the kleisin protein RAD21/SCC1.

SMC proteins form the core of the cohesin complex. There are 6 mammalian SMC proteins that form the basis of three major known complexes: cohesin (SMC1/SMC3), condensin (SMC2/4) and the SMC5/6 complex (Skibbens, 2019). These are highly conserved 110-170kDa proteins which consist of a globular ATPase that encompasses both N- and C-terminal domains, anti-parallel coiled-coil domain and a globular hinge domain that interacts with the hinge domain of other SMC proteins (Haering *et al.*, 2002). The ATPase domain mediates the interaction between cohesin and its host DNA molecule to entrap two strands of DNA between the kleisin and SMC ATPase heads (Hirano, 2002; Çamdere, Carlborg and Koshland, 2018; Chapard *et al.*,

2019). There are no implications for roles of the ATPase in sister chromatid cohesion but it is implicated in the cohesin complexes interaction with chromatin motor proteins, for cohesin translocation in the loop extrusion model of chromatin organisation (Nuebler *et al.*, 2018). The canonical mitotic cohesin complex is made up of SMC3 and SMC1α. SMC3 is present in all cohesin complexes, but SMC1β is mainly expressed and can form complexes during meiosis (Anderson *et al.*, 1999).

Kleisin proteins are highly evolutionary conserved family, and the major mammalian cohesin kleisin is RAD21, which is homologous to the S. cerevisiae kleisin Scc1 (McKay *et al.*, 1996). There are meiosis-specific cohesin kleisins REC8 and RAD21L which form a variety of different cohesin complexes in a meiotic context (Anderson *et al.*, 1999). The N- and C-terminal domains that interact with either SMC protein are the only conserved domains between all kleisins. The major function of the kleisins is to close the cohesin ring and hold the complex together which leads to the cohesion of DNA molecules together and leads to the recruitment of the Stromal antigens (SA) protein of the complex (Gligoris *et al.*, 2014).

Accessory proteins such as SA1/STAG1 or SA2/STAG2 (Stromal antigens 1 and 2) and other interactors bind and regulate the complex's behaviour (Nasmyth and Haering, 2009). SA1 or SA2 bind to the kleisin subunit (Zhang *et al.*, 2013). SA1/2 are the most implicated of all cohesin complex components in oncogenic mutations associated with chromosome cohesion (Smith *et al.*, 2016). SA1 is required for telomeric stability and depletion of

the protein results in aneuploidy during mitotic cell cycle (Canudas *et al.*, 2007). SA2 is required for maintenance of centromeric sister chromatid cohesion as well as chromatin structure and replication fork integrity during S-phase (Canudas and Smith, 2009; Mondal *et al.*, 2019). SA2 is also important in S/G2 phase for cohesin-mediated DNA damage repair, but both SA1 and SA2 are necessary for the S phase DNA damage checkpoint (Kong *et al.*, 2014). Meiotic SA3, or STAG3 (stromal antigen 3), is expressed in meiotic cells and localised along the chromosome axes during meiosis (Prieto *et al.*, 2001) and is required for the formation of the axis and synapsis of meiotic homologs during prophase I (Winters, McNicoll and Jessberger, 2014). Alongside SA3, both SA1 and SA2-cohesin complexes are found along the chromosome axis during meiosis (Prieto *et al.*, 2002) indicating the highly varied roles for different cohesin setups.

The interaction between chromatin and cohesin is thought to be topological. However, the cohesin ring structure appears to interact with DNA through non-specific sequences in the chromatin (Haering *et al.*, 2002). The ring model and the handcuff model are two major models for how this interaction takes place. The ring model utilises one cohesin ring to hold two DNA strands in close conformation such as cis-acting DNA strands in chromatin structural regulation or pairs of sister chromatids during cell division. The handcuff model suggests that each DNA strand is held by a single cohesin ring that interact together in a dimeric complex to bring the strands together. This dimer may be mediated through anti-parallel interaction of two RAD21 kleisin subunits which requires direct interaction with SA1 or SA2 (Zhang *et*

al., 2008, 2013). This handcuff model would be advantageous in adaptability of cohesin-regulated interactions of regions such as loop formation without unloading and reassembly of the cohesin complex.

Other accessory proteins, PDS5A/PDS5B (Losada, Yokochi and Hirano, 2005; Shintomi and Hirano, 2009) , WAPL (Gandhi, Gillespie and Hirano, 2006; Kueng *et al.*, 2006) and cohesin maintenance factor, Sororin (Schmitz *et al.*, 2007; Nishiyama *et al.*, 2010, 2013) are weakly associated with the cohesin complex and regulate interactions between cohesin and chromatin. Sororin is recruited by the AcSMC3 subunit and binds to PDS5B which stabilises sister chromatid cohesion by counteracting the WAPL-PDS5B interaction (Nishiyama *et al.*, 2010).

The cohesin complex has a major role in chromatin organisation during interphase alongside CCCTC-binding factor (CTCF) in the formation and maintenance of loops and TADs (topologically associated domains) (Hansen *et al.*, 2017). Cohesin is associated with interphase chromosomes (Wendt *et al.*, 2008), implying CTCF acts to organise cohesin's ability to restructure chromatin, but the loading and regulation of cohesin itself involves other mechanisms. This is regulated by the binding of WAPL that has been associated with chromatin loop size and regulation of cohesin's ability in loop extrusion (Wutz *et al.*, 2017). This is important for chromatin compartmentalisation and long-range transcriptional regulation (Schwarzer *et al.*, 2017; Wutz *et al.*, 2017). Acetylation of the cohesin subunit SMC3 has a role in maintaining the length of loops and TADs during the mitotic cell cycle

which requires the ATPase inhibitor PDS5 (Bastié *et al.*, 2022; van Ruiten *et al.*, 2022).

Figure 1.3: The cohesin complex. Cohesin has four core subunits, SMC1α and SMC3 which each have an ATPase head and interact through their globular hinge domain alongside the kleisin family protein RAD21 and SA1 or SA2. In meiosis there are two meiotic kleisin subunits, REC8 and RAD21L, and SMC1β and SA3 substitutes SMC1α and SA1/2. Cohesin is loaded on onto chromosomes during G1 phase with the help of the NIPBL-MAU2 complex. PDS5A/PDS5B, WAPL and Sororin are associated with the cohesin complex and regulate the dynamic interaction between cohesin and chromatin.

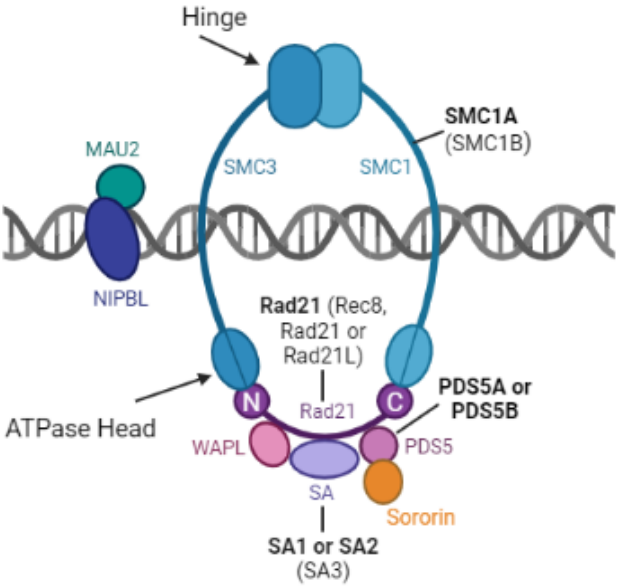
Hinge
SMC1A
(SMC1B)
MAU2
SMC3
SMC1
NIPBL
Rad21 (Rec8,
Rad21 or
Rad21L)
ATPase Head
N
Rad21
C
PDS5A or
PDS5B
WAPL
PDS5
SA
Sororin
SA1 or SA2
(SA3)

1.2.1 Cohesin in mitosis

The mammalian mitotic cell cycle is made up of four stages: G1, S, G2 and M phase. G1 is the first growth phase and followed by the S phase where DNA replication occurs. The cell enters a second growth phase (G2) and then enter mitosis (M phase) leading to the cell division into two daughter cells. Following DNA replication in S-phase, pairs of sister chromatids need to be held together throughout G2 and early mitosis through a mechanism called sister chromatid cohesion. This enables accurate chromosome segregation in anaphase and the physical connection must be maintained until the mitotic division. The binding and holding of sister chromatids together is partly mediated by the cohesin complex. The cell cycle and dynamics of the cohesin complex through the stages are summarised in Figure 1.4.

The heterodimeric chaperone complex NIPBL-MAU2 interact with each other through their conserved N-terminal domains to form a complex which then aids in cohesin loading onto chromosomes during G1 phase (Ciosk *et al.*, 2000; Seitan *et al.*, 2006; Watrin *et al.*, 2006; Bermudez *et al.*, 2012). The complex assembles fully before chromatin association (Losada, 2014) and is loaded onto DNA through an entry gate between the two SMC subunits (Collier and Nasmyth, 2022). Throughout G1, the cohesin complex is dynamically loaded and unloaded, as WAPL associates with the kleisin subunit and catalyses dissociation of the kleisin with SMC3, opening an ‘exit’ gate (Tedeschi *et al.*, 2013).

Eco1 homologues, ESCO1 and ESCO2, can acetylate the SMC3 subunit of cohesin at the two lysine residues towards the proteins N-terminus (K105 and K106 in human SMC3), which acts for the establishment of cohesion and regulation of cohesin dynamics on the chromatin (Zhang *et al.*, 2008; Minamino *et al.*, 2015; Alomer *et al.*, 2017). ESCO1 and ESCO2 have distinct patterns of expression throughout the cell cycle. ESCO1 is present at constant levels throughout the cell cycle, ESCO2 is a substrate of the APC/C, an E3 ubiquitin ligase that is activated at the metaphase-anaphase transition (Hou and Zou, 2005; Lafont, Song and Rankin, 2010; Song *et al.*, 2012). So ESCO2 levels are low in G1 and only increase as APC/C activity drops during S phase. The majority of SMC3 acetylation is due to the activity of ESCO1, while cohesin establishment during S phase requires ESCO2 (Alomer *et al.*, 2017).

The acetylation of SMC3 recruits sororin, which is antagonistic of WAPL activity, to maintain the cohesin complex by inhibiting the opening of the ‘exit’ gate (Nishiyama *et al.*, 2010). PDS5A or PDS5B have been associated both with cohesin removal (Nishiyama *et al.*, 2010; Wutz *et al.*, 2017) and cohesin establishment by the promotion of SMC3 acetylation by acetyltransferase ESCO1 or ESCO2 (Carretero *et al.*, 2013; Hons *et al.*, 2016). This indicates an essential cohesin regulatory function of PDS5 proteins as well as acting as WAPL cofactors.

Cohesin dissociation in mitosis occurs during prophase and anaphase and begins on chromosomes arms as sororin is phosphorylated by Aurora B and

CDK1 kinases (Nishiyama *et al.*, 2013; Borton *et al.*, 2016). WAPL can then open the ‘exit’ gate between SMC3 and the kleisin subunit. Centromeric cohesin is protected from dissociation by the centromeric localisation of Shugoshin 1 (SGO1) and Protein Phosphatase 2A (PP2A) that dephosphorylates sororin and maintains WAPL antagonism established earlier in the cell cycle (Figure 1.4). SGO1 and WAPL directly compete for binding sites on the SA1 or SA2 subunit that enhances cohesin protection at the centromere (Hara *et al.*, 2014).

Centromeric cohesion must be maintained until the spindle fibres attach to the kinetochores at the centromeres, ensuring accurate chromosomes segregation and cell division. This cohesion is important for pairwise alignment of the chromosomes on the mitotic spindle to ensure bipolar attachment of the chromosomes leading to the generation of tension across the centromeres. The SAC is a quality control mechanism that maintains genome stability by preventing anaphase until all the chromosomes are stably attached to the spindle (Nezi and Musacchio, 2009). Once the SAC has been satisfied, anaphase begins where SGO1 and PP2A dissociate from the centromere (Figure 1.4) and physical forces are put onto bioriented sister chromatid kinetochores as they pull away during spindle depolymerisation (Nerusheva *et al.*, 2014). SGO1 and PP2A inhibit the enzyme separase (Holland *et al.*, 2007; Clift, Bizzari and Marston, 2009; Sun *et al.*, 2009; Lianga *et al.*, 2018) and once SGO1-PP2A dissociation, separase cleaves the kleisin, RAD21 (Uhlmann, Lottspeich and Nasmyth, 1999).

APC/C also regulates separase-mediated kleisin cleavage. Separase is bound to the chaperone protein called securin, to inhibit its enzymatic activity until the SAC is satisfied (Holland *et al.*, 2007; Luo and Tong, 2018). APC/C can then phosphorylate securin (Toda *et al.*, 2012) to allow separase activity and cohesin dissociates from the DNA and chromosomes can divide. Cohesin is recycled and SMC3 is deacetylated by histone deacetylase, HDAC8 (Deardorff, Bando, *et al.*, 2012). The cohesin subunits can then form new cohesin complexes in the G1 phase in the next cell cycle (Dasgupta *et al.*, 2016).

Figure 1.4: Cohesin Dynamics in the Mitotic Cell Cycle. Cohesin is loaded onto chromatin in early G1 phase which is assisted by the NIPBL-MAU2 heterodimer. Cohesin subunits, SMC1A and SMC3, form a hinge region between them where DNA is thought to gain entry and exits cohesin between SMC3 and the kleisin subunit by WAPL activity. In S-phase, SMC3 is acetylated by cohesin acetyltransferases, ESCO1 and ESCO2, leading to sororin recruitment which inhibits WAPL activity to maintain chromosome cohesion. Upon entry to mitosis, cohesin dissociates during prophase and anaphase due to sororin phosphorylation, WAPL activity and seperase activity. Cohesin is recycled into G1 of the daughter cells and the cycle begins again. Taken from Losada, 2014.

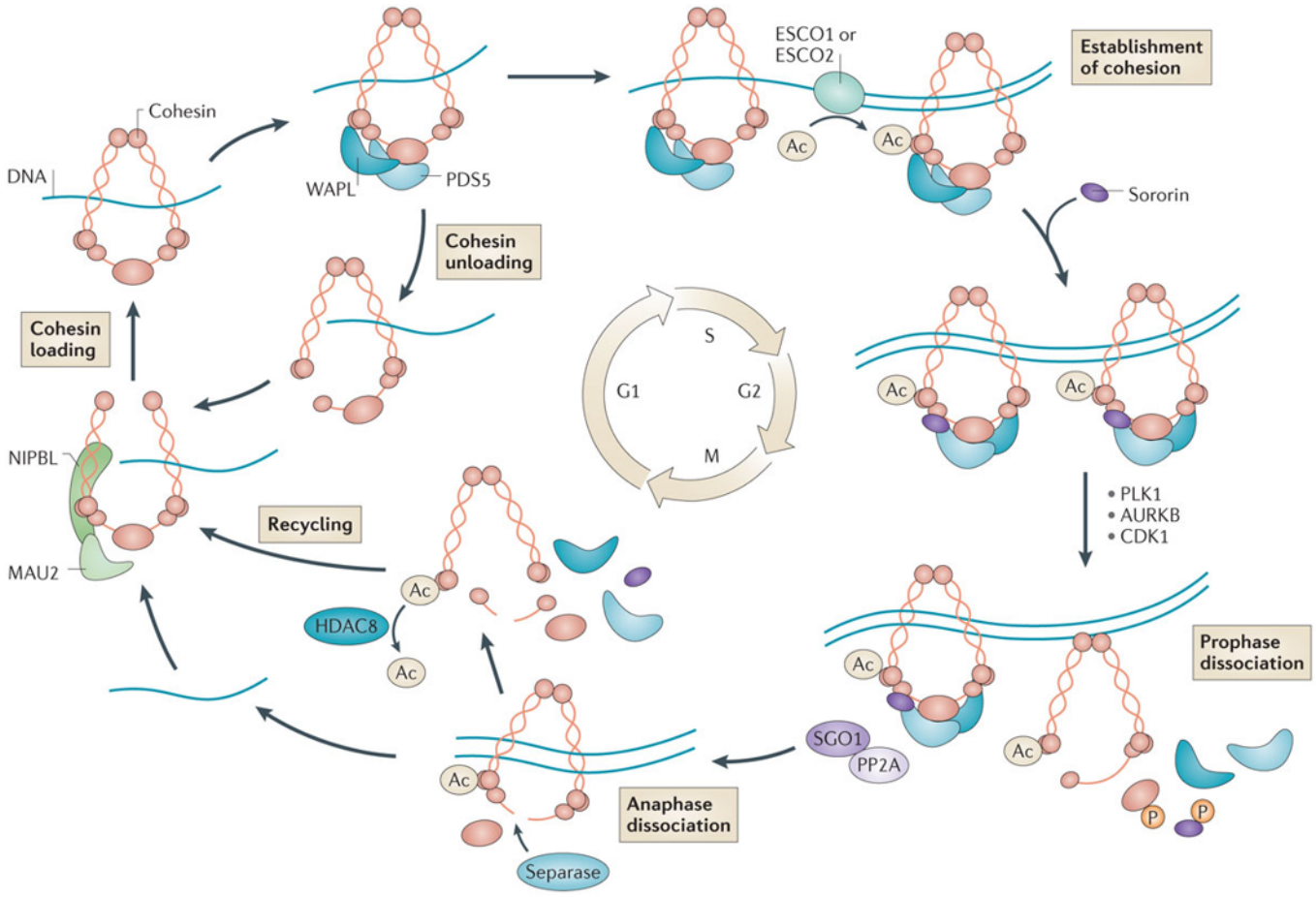
Cohesin
DNA
WAPL
PDS5
ESCO1 or
ESCO2
Establishment
of cohesion
Ac
Sororin
Cohesin
unloading
Cohesin
loading
S
G1
G2
M
NIPBL
MAU2
Recycling
HDAC8
• PLK1
• AURKB
• CDK1
Prophase
dissociation
SGO1
PP2A
P
Anaphase
dissociation
Separase

1.2.2 Cohesin in meiosis.

As previously explained in section 1.1, the cohesin complex is crucial in meiosis for sister chromatid cohesion and the formation of the AEs of the chromosomes and for the SC assembly during prophase I. Interestingly, the cohesin complex in meiosis is structurally different to that in mitosis. In mammalian germ cells, there are two meiosis-specific kleisin subunits, REC8 (Parisi *et al.*, 1999) and RAD21L (Gutiérrez-Caballero *et al.*, 2011; Ishiguro *et al.*, 2011) in addition to the mitotic kleisin subunit, RAD21 (Parra *et al.*, 2004). REC8 and RAD21L containing cohesin complexes are spatially distinct along the chromosome axis of spermatocytes and oocytes (Rong *et al.*, 2016) and are required for distinct roles in SC formation and chromosome synapsis (Herrán *et al.*, 2011; Ishiguro *et al.*, 2011; Fukuda *et al.*, 2014; Ward *et al.*, 2016). REC8-cohesin is the main complex required for sister chromatid cohesion in metaphase I and centromeric cohesion, whereas RAD21L-cohesin is required for normal clustering of pericentromeric heterochromatin (Ward *et al.*, 2016). Both REC8- and RAD21L-cohesin complexes, are required for chromosome axis formation (Llano *et al.*, 2012; Ishiguro *et al.*, 2014).

REC8-cohesin localise along chromosomes before meiotic DNA replication and persist throughout meiosis, at least at the centromeres, until metaphase II whereas RAD21L-cohesin appears on the chromosomes after DNA replication and dissociates after late pachytene in meiotic prophase I (Lee and Hirano, 2011; Ishiguro *et al.*, 2014). Cohesin removal triggers separation

of homologous chromosomes toward opposite poles during metaphase I–anaphase I transition and is mediated by WAPL similar to the mechanism in mitosis (Brieño-Enríquez *et al.*, 2016) and REC8-cohesin is cleaved by separase (Kudo *et al.*, 2006, 2009). REC8 phosphorylation increases susceptibility to cleavage and in mice, phosphorylation by Polo-like kinase 1 makes REC8 susceptible to separase cleavage *in vitro* (Kudo *et al.*, 2009). REC8-cohesin is cleaved along the chromosome arms by separase but is maintained at the centromere throughout anaphase I until meiosis II to allow chiasmata resolution and the release of homologous chromosomes (Buonomo *et al.*, 2000; Kitajima *et al.*, 2003; Kudo *et al.*, 2006).

Centromeric cohesion has to be preserved until meiosis II where centromeric REC8-cohesin is cleaved by separase leading to the segregation of sister chromatids into each gamete (Wassmann, 2013, 2022). Shugoshin-like protein, SGO2, forms a complex with PP2A phosphatase and SGO2-PP2A localises to the centromere to protect REC8-cohesin from separase cleavage during anaphase I (Lee *et al.*, 2008; Llano *et al.*, 2008). Notably, it remains unclear whether RAD21L is also cleaved by separase.

RAD21 is found in mitotic cells in testis before disappearing in early leptotene and is detectable again in late pachytene parallel with RAD21L dissociation (Parra *et al.*, 2004; Ishiguro *et al.*, 2011; Lee and Hirano, 2011). From diplotene onwards, RAD21 dissociates from AEs and is localised around centromeres at metaphase I in spermatocytes (Parra *et al.*, 2004; Xu *et al.*, 2004; Ishiguro *et al.*, 2011). It still remains to be clarified what is the role of

mitotic RAD21 kleisin during meiosis as well as the mechanism of loading RAD21-cohesin onto chromosomes at pachytene.

Also during meiosis, the SMC1α subunit is largely replaced by SMC1β (Revenkova *et al.*, 2001) and SA1/SA2 is replaced by SA3/STAG3 (Prieto *et al.*, 2001). Although it has been shown that a small proportion of meiotic cohesin contains SA2 and/or SMC1α in spermatocytes (Prieto *et al.*, 2002; Revenkova *et al.*, 2004), it remains unclear what is their precise role during meiosis. Transfection studies in somatic cells suggest that SA3 interacts with REC8 to import it into the nuclei (Wolf *et al.*, 2018) suggesting a specific role of the SA3 subunit in the assembly of meiotic cohesin. In SA3 KOs, AE formation is impaired resulting in short axes indicating that SA3, not SA1/2, is essential for AE formation and DSB repair (Fukuda *et al.*, 2014; Hopkins *et al.*, 2014; Winters, McNicoll and Jessberger, 2014; Ward *et al.*, 2016).

SMC1α can substitute SMC1β-containing cohesins in SC axial length regulation and homologue synapsis but SMC1β is specifically required for telomere integrity in the AE (Revenkova *et al.*, 2004; Hodges *et al.*, 2005; Biswas, Stevense and Jessberger, 2018). These proteins may have redundant roles in cohesion at chromosome arms, at the centromeric region SMC1β plays an essential role during meiosis (Biswas *et al.*, 2013; Biswas, Stevense and Jessberger, 2018). So in addition to mitotic cohesin complexes, different combinations of meiotic cohesin subunits lead to distinct cohesin complexes with different spatiotemporal localisation patterns in mammalian chromosomes during meiosis.

1.2.3 Cohesinopathies

1.2.3.1 Mitotic effects of mutations in cohesin

Mutations in cohesin subunits or its regulatory pathways result in a group of pathologies known as cohesinopathies. One of the most characterised Human cohesinopathies is Cornelia de Lange syndrome which is a rare genetically heterogeneous disorder that affects multiple organs and system. It is characterised by intellectual disability and distinctive craniofacial and limb developmental morphologies (Kline *et al.*, 2018). To date five genes are associated with the development of CdL syndrome: cohesin chaperone NIPBL, SMC1α, SMC3, RAD21 and HDAC8 (Krantz *et al.*, 2004; Tonkin *et al.*, 2004; Deardorff *et al.*, 2007; Deardorff, Bando, *et al.*, 2012; Deardorff, Wilde, *et al.*, 2012). Mutations in NIPBL, SMC3 and RAD21 lead to the autosomal dominant form of cdLS whilst SMC1α and HDAC8 are the X-linked CdLS with the most common cause of CdLS being mutations in NIPBL (Kaiser *et al.*, 2014).

Other cohesinopathies include Roberts syndrome (RBS) and Warsaw Breakage syndrome (WABS). RBS patients have growth and mental disabilities, limb deformities and craniofacial defects due to autosomal recessive loss-of-function mutation in essential acetyltransferase ESCO2. Mutations in ESCO2 leads to a loss of cohesin acetylation, which is localised to pericentromeres and acetylates the SMC3 subunit (Dupont *et al.*, 2014; Kawasumi *et al.*, 2017) so promotes the sister chromatid dissociation leading to potential segregation errors in the cell cycle. This results in widespread

translational errors, stemming from defects in chromatin architecture and pericentromeric heterochromatin morphology (Whelan *et al.*, 2012) as well as widespread mitotic aneuploidies and cell apoptosis (Mfarej and Skibbens, 2020). *Esco2* and *Esco1* null mice are embryonic lethal and there are no documented human ESCO1 mutations suggesting that this could be embryonic lethal (Gordillo *et al.*, 2008; Banerji, Skibbens and Iovine, 2017).

There are widely varied roles for cohesin in the mitotic cell, both in interphase and during mitosis, so molecular consequences of mutations vary from transcriptional changes due to chromatin remodelling in CdLS to mitotic cell failure as a result of aneuploidy and apoptosis that is associated with RBS (Banerji, Skibbens and Iovine, 2017).

1.2.3.2 Meiotic effect of mutations in cohesin

In addition to the developmental disorders and association with cohesin defects discussed above, there is also an association between cohesin defects during mammalian meiosis and infertility/aneuploidy. In mammalian spermatocytes, cohesin deficiency leads to infertility and meioitic arrest at various stages in prophase I. Partial loss of cohesion, telomere deficiencies, partial asynapsis, and shortened AEs/SCs is present in *Smc1β*$^{-/-}$ spermatocytes (Revenkova *et al.*, 2004; Adelfalk *et al.*, 2009). Absence of REC8 leads to spermatocytes arresting at zygotene-like stage where SYCP1 is deposited between sister chromatids and not between homologs (Bannister *et al.*, 2004; Xu *et al.*, 2004). RAD21L deficient spermatocytes do not form AEs properly and arrest at a zygotene-like stage (Herrán *et al.*,

2011) whereas deficiency in both REC8 and RAD21L leads to no AEs and SCs development contributing to the arrest at a leptotene-type chromosomal stage (Llano *et al.*, 2012).

Even when SA3 is deficient, there is very short AEs, synapsis failure and loss of centromeric and telomeric sister chromatid cohesion leading to meiotic arrest and sterility (Fukuda *et al.*, 2014; Hopkins *et al.*, 2014; Winters, McNicoll and Jessberger, 2014). Removal of two meioisis specific subunits such as in *Smc1β*$^{-/-}$ *Rec8*$^{-/-}$ and *Smc1β*$^{-/-}$ *Rad21L*$^{-/-}$ spermatocytes leads to different reductions in AE length, synapsis deficiency and telomere disruptions (Biswas *et al.*, 2016) indicating that cohesion depends on meiosis-specific cohesins. The different kind and or severity of phenotypes of mutants in distinct cohesin proteins indicate that specific cohesin complexes contribute to distinct processes, with partial overlap, during spermatogenesis. The functional complexity of cohesin in spermatocytes is still not completely understood.

In mammalian oocytes, meiosis begins in the foetal ovary and then oocytes enter dictyate, where they undergo long-term cell cycle arrest until puberty for meiosis to resume (Charalambous, Webster and Schuh, 2023). The time interval from the establishment to the final resolution of sister chromatid cohesion is prolonged in female meiosis, which lasts months in mice and decades in humans. Aneuploidy arises predominantly due to chromosome missegregation in female meiosis that leads to miscarriage or birth defects such as Down syndrome (Hassold T and Hunt P, 2001). Clinically recognised

trisomy's are largely correlated to advancing maternal age (Nagaoka, Hassold and Hunt, 2012; Herbert *et al.*, 2015) indicating that premature loss of sister chromatid cohesion is one of the primary causes of chromosome missegregation in oocytes due to cohesin loss.

There is an expanding evidence suggesting that cohesin levels are decreasing in aged human and mouse oocytes (Liu and Keefe, 2008; Chiang *et al.*, 2010; Lister *et al.*, 2010; Tsutsumi *et al.*, 2014; Sakakibara *et al.*, 2015; Zielinska *et al.*, 2015). Despite there being no difference in total REC8 protein levels in old and young mouse oocytes, the amount of chromosome-bound REC8 is reduced at the centromere and on the arms (Liu and Keefe, 2008; Chiang *et al.*, 2010; Lister *et al.*, 2010) suggesting that REC8-cohesin has dissociated from chromosomes in aged cells. This leads to aged oocytes having a high incidence of homologous chromosomes with no chiasma compared to younger oocytes (Lister *et al.*, 2010). *Rad21L*$^{-/-}$ mice also have maternal age-related infertility (Herrán *et al.*, 2011). This is accompanied by a significant reduction in the proportion of bivalents with a single chiasma, observed in *Smc1β*$^{-/-}$ oocytes, where terminally associated homologues without skewed crossover sites are prevalent (Hodges *et al.*, 2005). Live imaging analysis has also shown that chromosomes segregation errors are preceded by separation of bivalents into univalent during metaphase I in aged oocytes (Sakakibara *et al.*, 2015). Dissociation and degradation of chromosome-bound cohesin over time may account for increased aneuploidy in aged oocytes. It appears that sister chromatid cohesion in oocytes is

maintained on the chromosomes without turnover as there is no de novo loading of cohesin during prolonged arrest (Burkhardt *et al.*, 2016).

There is still a requirement to investigate cohesin and identify its regulators in meiosis due to impaired regulation of cohesin complexes, particularly in oocytes, being associated with chromosome missegregation, aneuploidy and subfertility (Jessberger, 2012; Herbert *et al.*, 2015). The E3 ubiquitin ligase, UBR2, is needed for successful meiosis progression as *Ubr2*$^{-/-}$ mice are infertile with chromosomal asynapsis and defects in early meiotic recombination (Kwon *et al.*, 2003; Crichton *et al.*, 2017). Also,UBR2 is important for embryonic development as there is female embryonic lethality present in *Ubr2*$^{-/-}$ mice (Kwon *et al.*, 2003) and has a role in cohesin regulation due to a significant increase in the level of the AcSMC3 subunit in *Ubr2*$^{-/-}$ spleen (Reichmann *et al.*, 2020), a phenotype that has been also identified in embryonic stem cells (Karen Dobie, Unpublished). It remains unclear how loss of *Ubr2* leads to these phenotypes.

1.3 The roles of UBR2

Among many other molecular functions, the E3 ubiquitin ligase, UBR2, has been shown to have a role in genomic stability (Ouyang *et al.*, 2006), regulation of cohesin complexes in the mice mitotic spleen (Reichmann *et al.*, 2020), male meiotic progression and embryonic development (Kwon *et al.*, 2003; Crichton *et al.*, 2017). The E3 RING ubiquitin ligase UBR2 is encoded by the *Ubr2* gene which is conserved between mouse and human genomes. *Ubr2* is a 46 exon gene that encodes a 200kDa protein, which is one of the four UBR E3 ubiquitin ligase proteins that have been shown to be active in the N-end Rule (Tasaki *et al.*, 2005). UBR2 has a prominent Type II N-end rule substrate binding but there is some Type I ability detected in *in vivo* genetics studies (Tasaki *et al.*, 2009, 2012; Rageul *et al.*, 2019).

More recently, UBR2 has been shown to have a role in degradation of N-end rule targets such as inflammasome NLRP1 in response to O_3 exposure, myosin heavy chain in muscle wasting and stress regulator, SDE2 (Xu *et al.*, 2019; Ferrara *et al.*, 2022; Gao *et al.*, 2022).These have not been identified as prominent phenotypes in an *Ubr2*$^{-/-}$ context and SDE2 can also be regulated by another UBR family member, UBR1. As there is lots of potential for redundancy between UBR proteins it is surprising that there appears to be a very specific subset of phenotypes in *Ubr2*$^{-/-}$ mice indicating essential functions of UBR2 in the testis and embryonic development (Kwon *et al.*, 2003). *Ubr2*$^{-/-}$ embryonic stem cell lines also have a phenotype which matches the cohesin phenotype found in *Ubr2*$^{-/-}$ mouse spleen, indicating a role for UBR2 in cohesin regulation in these cells, as well as in retrotransposon repression (Maclennan *et al.*, 2017; Reichmann *et al.*, 2020; Karen Dobie,

Unpublished). This similarity between the phenotypes of ESCs and splenocytes may be due to the spleen having rapid cell division and being a potential source of naturally occurring multipotent stem cells with possible pluripotent potential (Faustman and Davis, 2010). This indicates that ESCs in culture at G2/M may potentially mimic cohesin levels of splenocytes.

UBR2 is a member of the UBR protein family that are generally implicated in protein turnover, whether through the N-end Rule or non-N-end Rule substrate binding pathways (Tasaki *et al.*, 2009; Vu and Varshavsky, 2020). Alongside the role in protein turnover, UBR2 also has an unconventional role in protein stabilisation, as seen with the germline genome defence protein, TEX19.1, in germ cells (Yang *et al.*, 2010; Reichmann *et al.*, 2020), discussed in section 1.3.2. It remains unclear whether protein turnover, N-end rule or non-N-end rule, or protein stabilisation is important for UBR2's specific phenotypes in *Ubr2*$^{-/-}$ tissues.

1.3.1 Protein turnover

1.3.1.1 Ubiquitination and Protein Turnover

Cellular pathways such as DNA replication, cell cycle and responses to various stimuli, such as stress, require turnover of certain proteins (Hicke, 2001; Bedford *et al.*, 2010; Sadowski and Sarcevic, 2010). The major signalling pathway involved in protein turnover is the ubiquitin-proteasome system (UPS). Ubiquitination is a post-translational process involving the attachment of ubiquitin (Ub) molecules to lysine residues on a substrate protein. Ub is a 9kDa covalently-bound signalling protein with multiple

functions in the cells, predominantly in protein level regulation and turnover (Pickart and Eddins, 2004). Ub covalently conjugates to lysine residues of targeted proteins or onto itself through its own lysines or via its N-terminal methionine residue (Sadowski *et al.*, 2012). Polyubiquitin chains are built up by lysine ubiquitination. There are seven lysine residues within the molecule but the most common ubiquitin chains are built along K48, K33, K29, K11 or K63 residues (Li and Ye, 2008). Generally, K48 or K63 polyubiquitin chains are the residues utilised for protein turnover (Tsuchiya *et al.*, 2017; Ohtake *et al.*, 2018). However, the variety of different polyubiquitin chains carry out other diverse ubiquitination functions including those in signalling and endocytosis (Sadowski *et al.*, 2012) whereas monoubiquitination can regulate processes such as DNA repair, viral budding, and gene expression (Sarcevic *et al.*, 2002; Haglund, Fiore and Dikic, 2003; Bergink and Jentsch, 2009). Different combinations of ubiquitin-lysine linkages results in branched chains that perform certain proteostatic functions such as modulation of the RING E3 Ring1B ligase activity to induce histone H2A monoubiqutination (Ben-Saadon *et al.*, 2006). UPS also has a vital function during the quality control in protein synthesis, and there are functions for ubiquitination outside of protein degradation, such as protein regulation by interacting with proteins containing ubiquitin binding domains (Tsuchiya *et al.*, 2017).

Ubiquitin is the first identified member of a structurally similar family of small ubiquitin-like proteins, such as NEDD8 and SUMO amongst others, which can be conjugated to target proteins for signalling purposes similar to ubiquitin itself. These undergo similar but distinct conjugating enzyme cascades to

perform multiple signalling functions in eukaryotes through promoting targets to interact with SIM (SUMO-interacting motifs) or other UBL-binding proteins (Hochstrasser, 2010).

1.3.1.2 The E1-E2-E3 Ubiquitination Cascade

The ubiquitin pathway involves three consecutive enzymatic steps that act in a cascade which permits the conjugation of Ub and Ub-like molecules to specific protein substrates. This is called the E1-E2-E3 cascade (Figure 1.5). The first step requires the ATP-dependent activation of the Ub C-terminus and the assembly of multi-Ub chains that bind via a thioester bond with an active site cysteine residue in the E1 component also known as the Ub-activating enzyme (Schulman and Wade Harper, 2009). The activated Ub can then be transferred to the ubiquitin-conjugating enzyme (E2) via a transthiolation reaction to generate the Ub-E2 complex (Olsen and Lima, 2013).

Substrate specificity in this pathway is granted through the interaction of the target protein with the largest group of ubiquitination enzymes, the E3 ubiquitin ligase. An Ub ligase (E3) can bind both substrate and Ub-E2 complex to mediate Ub transfer from the E2 to the protein substrate. E3 Ub ligases are separated into three major classes each defined by their interaction with the E2 enzyme: HECT (Homologous to E6-associated Protein C-terminus), RING (Really Interesting New Gene) or RBR (RING-between-RING) (Berndsen and Wolberger, 2014).

Interactions between E2-E3 are transient due to the requirement of fast transfer of newly ubiquitin-charged E2 enzymes for the extension of the substrate ubiquitin chain. E3 ubiquitin ligase interact with multiple E2s which makes it difficult to predict E2-E3 pairs. It is thought that E2s only bind to the RING domain after thioesterification and ubiquitin-charging and uncharged E2s bind to E1s or E3 RING domains (Metzger *et al.*, 2014). E2 ligases physically bind to the RING domain, the Ub molecule is transferred to the target protein. This is different to ubiquitin transfer in HECT domains as ubiquitin does not bind to the RING domain rather straight onto the substrate. A HECT domain consists of two different lobes, the N-terminal lobe (N-lobe) and C-terminal lobe (C-lobe), connected by a flexible linker. The N-lobe is required for E2 binding and the C-lobe contains the catalytic cysteine that accepts ubiquitin from the E2 to make an E3-ubiquitin complex (Qian *et al.*, 2020; Shah and Kumar, 2021). So HECT E3s must be physically conjugated with ubiquitin before transferring to the substrate.

The transfer of Ub is most commonly onto the ε-amino group of a lysine in the target protein resulting in an isopeptide bond. Cell protein regulation requires both monoubiquitination or multiubiquitination (Sadowski and Sarcevic, 2010) but a large proportion of ubiquitinated target proteins are polyubiquitinated. This requires multiple interactions between charged E2 and E3 enzymes to build the ubiquitin chain on the substrate. So E2/E3 interactions must be transient but last long enough to allow ubiquitin-transfer to occur. E2 enzymes that no longer have Ub bound have lower binding affinity to HECT or RING domains of an E3 which allows the dissociation of

the E2/E3 complex after ubiquitin transfer (Metzger *et al.*, 2014; Sluimer and Distel, 2018).

A polyubiquitinated substrate is recognised by components of the 26S proteasomal lid complex such as Rpn10, Rpn13 or Sem1 (Paraskevopoulos *et al.*, 2014; Hamazaki, Hirayama and Murata, 2015; Kragelund *et al.*, 2016). The target protein is deubiquitylated by the proteasome-asssociated DUB enzyme so the protein can be degraded within the complex (Bedford *et al.*, 2010). Ubiquitin molecules and amino acids are then recycled back into the proteasome.

Figure 1.5 Ubiquitin-proteasome-mediated protein degradation. The UPS pathway is shown. E1 is Ub-activating enzyme, E2 is Ub-conjugating enzyme, and E3 is Ub-ligase protein. HECT and RBR-type E3 ligases perform a two-step ubiquitination, whereas RING E3s perform direct Ub transfer. Ubiquitin molecules are added to target proteins, resulting in the protein being targeted for degradation by the 26S proteasome. DUBs can rescue substrate expression or alter cell signalling by removing Ub moieties. Black arrows represent the intracellular destiny of ubiquitinated proteins. DUBs=deubiquitinating enzymes. Ub=ubiquitin. Taken from (LaPlante and Zhang, 2021)

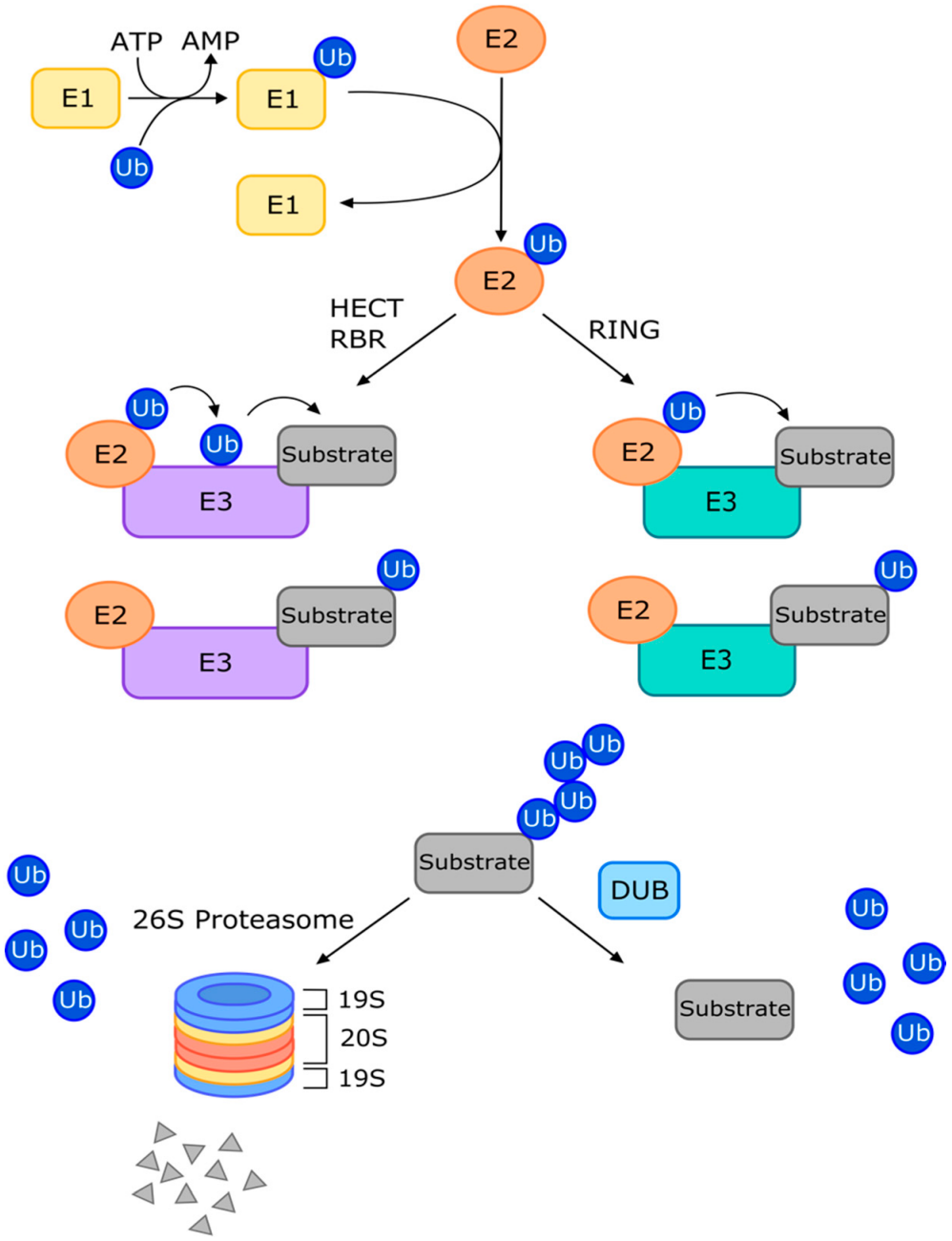
ATP AMP
E1
Ub
E1
E2
E1
Ub
E2
HECT
RBR
RING
Ub
Ub
E2
Substrate
E3
Ub
E2
Substrate
E3
Ub
E2
Substrate
E3
Ub
E2
Substrate
E3
Ub
Ub
Ub
Ub
Substrate
DUB
Ub
Ub
Ub
26S Proteasome
19S
20S
19S
Substrate
Ub
Ub
Ub
Peptides

1.3.1.3 The N-end Rule Pathway for Protein Degradation

E3 ubiquitin ligases are by far the largest and most diverse group of enzymes within the E1- E2-E3 cascade, with more than 500 distinct E3s in any given mammal (Li et al., 2008), and it is these that provide substrate specificity for the UPS. In contrast, there are only 2 known mammalian E1 ubiquitin activators enzymes, UBA1 and UBA6 (Jin et al., 2007; Schulman and Wade Harper, 2009), which are promiscuous for binding to the mammalian E2 enzymes, of which there are around 40 known (Stewart et al., 2016).

One of the earliest discovered E3 substrate binding pathways, the N-end rule, depends on the N-terminal sequence of the substrate, which acts as a degron binding site for the E3 ubiquitin ligase to carry out ubiquitination (Bachmair, Finley and Varshavsky, 1986). This was first discovered in *S. cerevisiae*, with identification of the E3 substrate recognition protein *UBR1* encoded by the *ubr1* gene (Bartel, Wünning and Varshavsky, 1990). u*br1* is a homolog of mammalian genes *Ubr1* and *Ubr2*, which are 47% sequence conserved, with 68% sequence similarity to each other (Tasaki *et al.*, 2005). Mammals encode a family of seven UBR proteins, of which UBR1 is the best characterised to carry out N-end recognition (Tasaki et al., 2005). The N-end rule pathway, as for most E3s, also requires at least one internal lysine residue in the target protein to act as the site for initial ubiquitin attachment by the associated E2 enzyme.

Overall structure of the *Ubr1*'s initiation complex has a base that is a helical scaffold with four regions separated by the Ubr-Box1, which is the highly conserved UBR box found in mammalian UBR proteins, Ubr-Box2 (also known as the N-domain) and a winged helical domain (WHD) (Figure 1.6, (Pan *et al.*, 2021)). Similar helical bundle repeats have been observed for other E3 ligases (Baek *et al.*, 2020; Rusnac and Zheng, 2020; Horn-Ghetko *et al.*, 2021). The E2, Ubc2, is primarily bound by a single helix of Ubr1, termed the Ubc2-binding region (U2BR) which is followed by a RING finger domain that interacts with Ubc2 and the loaded ubiquitin. A previously unidentified domain with a new fold termed the cap helical domain (CHD) follows the RING finger domain. Finally, the UBR/Leu/Cys (UBLC) (Du *et al.*, 2002) domain (also known as the UBR autoinhibitory domain UAIN) interacts with Ubr-Box and WHD through a putative zinc-binding site (Pan *et al.*, 2021). The structure of Ubr1 is important for its role in N-degron recognition and ubiquitin transfer within the N-end rule pathway.

Figure 1.6 Domain diagram and Cryo-EM maps of Ubr1 of *S. cerevisiae*

(**A**) Domain diagram of Ubr1 of S. cerevisiae. The residue boundaries are indicated. The dotted lines represent unresolved linkers and regions. The grey box indicates the substrate-recruiting domains, and the pink box indicates the E2 Ubc2-recruiting domains. Winged helical domain (WHD). Cap helical domain (CHD). (**B**) Cryo-EM maps of the initiation complex. The colour code of Ubr1 is the same as in (**A**). Taken from Pan et al 2021

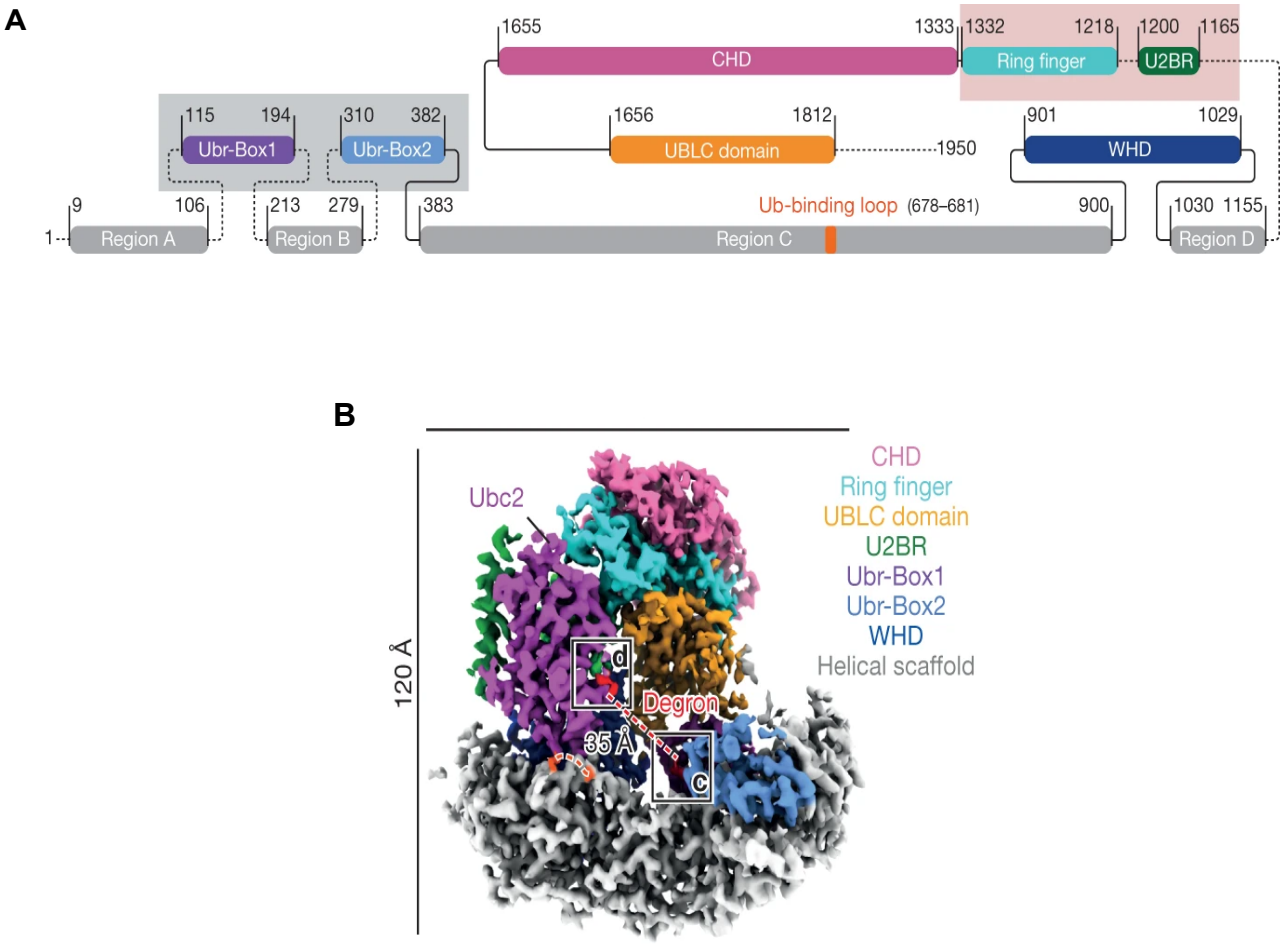
A
1655
1333
1332
1218
1200
1165
CHD
Ring finger
U2BR
115
194
310
382
1656
1812
1950
901
1029
Ubr-Box1
Ubr-Box2
UBLC domain
WHD
9
106
213
279
383
Ub-binding loop (678–681)
900
1030
1155
1
Region A
Region B
Region C
Region D
B
Ubc2
CHD
Ring finger
UBLC domain
U2BR
Ubr-Box1
Ubr-Box2
WHD
Helical scaffold
120 Å
a
Degron
35 Å
c

1.3.1.3.1 Classes of N-terminal degron pathways

N-terminal degron sequences are classified into three subcategories: the Arg/N-end rule, the Ac/N-end rule and the Pro/N-end rule pathway (Figure 1.7). Nascent proteins are expressed with an N-terminal methionine, encoded by the start codon ATG. However, N-terminal post-translational modifications are not uncommon, which results in the altered protein being targeted for degradation by the N-end rule pathway.

The Arg/N-end Rule pathway is the more studied of the three pathways (Kim and Hwang, 2014) and cleaved proteins that undergo this particular modification of the N-terminus are classified into having either Type I or Type II N-terminal recognition sequences. These are defined by the N-terminal residues of the target protein. Type I N-terminal residues are basic with the most common being arginine (Arg) and Type II are defined as bulky hydrophobic residues such as phenylalanine or tryptophan (Tasaki *et al.*, 2005).

The Ac/N-end rule pathway involves the cotranslational N-terminal acetylation of nascent proteins whose N-termini are either Met or the small uncharged residues: Ala, Val, Ser, Thr or Cys. This is a lesser understood category of the N-end Rule and was only discovered in 2010 (Hwang, Shemorry and Varshavsky, 2010) but this cotranslational modification occurs in 90% of mammalian proteins (Polevoda, Arnesen and Sherman, 2009; Nguyen *et al.*, 2019). As there are many Ac/N-end target proteins, the acetylated N-terminus is shielded by structural folding or interactions with a

protein complex (Shemorry, Hwang and Varshavsky, 2013). Human RGS2, a regulator of Specific G proteins, is a short lived substrate of the Ac/N-end rule pathway and can bind to E3 ubiquitin ligase TEB4 to induce degradation via the UPS and maintains proteomic integrity (Park *et al.*, 2015).

Acetylation at the N-terminus depends on the amino acid immediately after the N-terminal methionine. The small second residue, such as alanine or leucine, results in cleavage of methionine and acetylation of the second residue. But if the second residues is large or hydrophobic, the N-terminal methionine is preserved and acetylated directly. These proteins are classed as Met-ϕ and are degraded by the Ac/N-end rule or by the Arg/N-end rule when unacetylated to allow for quick degradation of misfolded proteins. There is evidence to suggest that, at least UBR1, is able to bind to non-acetylated Met-Φ proteins, aiding in their degradation as a redundant role for the degradation of acetylated Met-Φ proteins by the Ac-N-end Rule pathway (Kim and Hwang, 2014). This non-acetylated Met-ϕ turnover depends on components of the Type II Arg/N-end rule pathway where binding to the second, bulky residue with a similar conformation as to the bulky hydrophobic Type II N-degron (Kim and Hwang, 2014; Nguyen *et al.*, 2019).

The third N-end rule pathway and the most uncharacterised is the Pro/N-end rule pathway which is mediated by the GID (glucose-induced degradation) Ub ligase. Gid4, a subunit of GID that is the Pro/N-recognin, targets proteins that bear the N-terminal Pro residue or Pro at position 2, as well as the adjoining sequence motifs (Chen *et al.*, 2017). Physiological substrates of the

Pro/N-end rule pathway include gluconeogenic enzymes: Fbp1, Mdh2, Icl1, and Pck1, which are long-lived in cells deprived of glucose but are selectively destroyed when returning to glucose-replete conditions (Alibhoy and Chiang, 2011; Menssen *et al.*, 2012; Chen *et al.*, 2017).

There has been a discovery that the Nt-formylation of proteins, which is a long-known posttranslational protein modification previously thought to be confined to bacteria can occur at the start of translation by cytosolic ribosomes of eukaryotic *S. cerevisiae.* Nt-formylation of yeast cytosolic proteins is caused by the endogenous *Sc*Fmt1, whose translocation from the cytosol to the inner matrix of mitochondria. Nt-formylated cytosolic proteins are targeted by the Psh1 E3 Ub ligase (together with the Ubc3 E2 enzyme), which acts as the recognition component of the previously unknown eukaryotic fMet/N-end rule pathway that destroys Nt-formylated proteins by binding to the formyl group of the Nt-fMet residue (Kim *et al.*, 2018).

Figure 1.7: N-degron pathways. N-terminal residues at the top of the figure are indicated by single-letter abbreviations of twenty DNA-encoded amino acids arranged into 3 sets of N-degrons in *S. cerevisiae* corresponding to the three N-degron pathways. (A) The Arg/N-degron pathway. (B) The Ac/N-degron pathway. (C) The Pro/N-degron pathway. Taken from (Melnykov, Chen and Varshavsky, 2019).

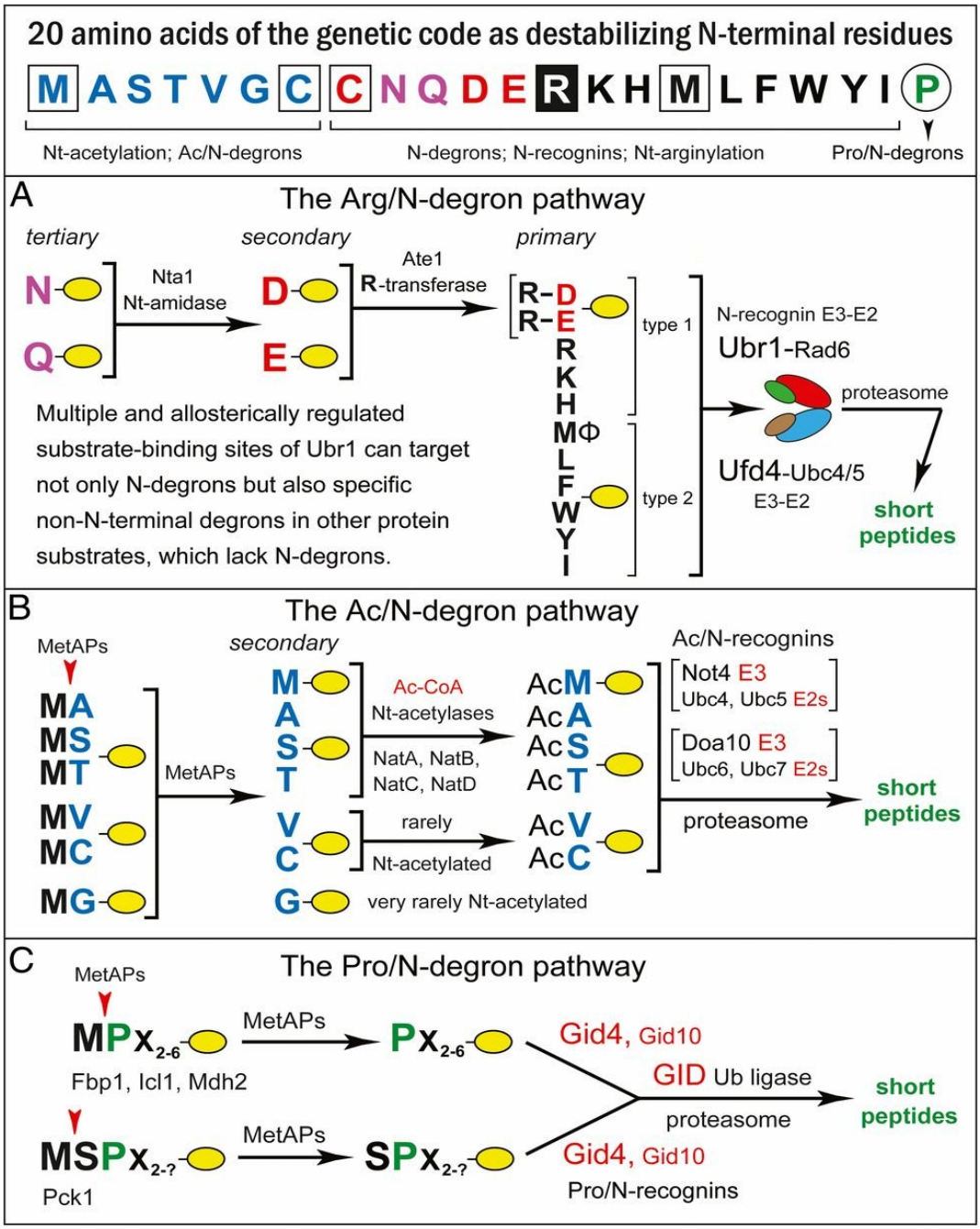
20 amino acids of the genetic code as destabilizing N-terminal residues
M A S T V G C C N Q D E R K H M L F W Y I P
Nt-acetylation; Ac/N-degrons
N-degrons; N-recognins; Nt-arginylation
Pro/N-degrons
A
The Arg/N-degron pathway
tertiary
secondary
primary
N
Q
Nta1
Nt-amidase
D
E
Ate1
R-transferase
R-D
R-E
R
K
H
MΦ
L
F
W
Y
I
type 1
type 2
N-recognin E3-E2
Ubr1-Rad6
proteasome
Ufd4-Ubc4/5
E3-E2
short peptides
Multiple and allosterically regulated substrate-binding sites of Ubr1 can target not only N-degrons but also specific non-N-terminal degrons in other protein substrates, which lack N-degrons.
B
The Ac/N-degron pathway
MetAPs
secondary
MA
MS
MT
MV
MC
MG
MetAPs
M
A
S
T
V
C
G
Ac-CoA
Nt-acetylases
NatA, NatB, NatC, NatD
rarely
Nt-acetylated
very rarely Nt-acetylated
AcM
AcA
AcS
AcT
AcV
AcC
Ac/N-recognins
Not4 E3
Ubc4, Ubc5 E2s
Doa10 E3
Ubc6, Ubc7 E2s
proteasome
short peptides
C
The Pro/N-degron pathway
MetAPs
MPx2-6
Fbp1, Icl1, Mdh2
MetAPs
Px2-6
MSPx2-?
Pck1
MetAPs
SPx2-?
Gid4, Gid10
GID Ub ligase
proteasome
short peptides
Gid4, Gid10
Pro/N-recognins

1.3.1.3.2 N-terminal Modifications

N-terminal (Nt) amino acid residues are categorised into primary destabilising (Arg, Lys, His, Leu, Phe, Tyr, Trp and Ile), secondary destabilising (Asp and Glu) and tertiary destabilising residues (Asn and Gln, as well as Cys, under specific conditions) (Varshavsky, 2008). Proteins with a primary destabilising Nt amino acid residue are recognised by N-recognins (including UBR proteins such as UBR1 and UBR2) (Tasaki *et al.*, 2012). One of the first discovered and direct ways which Nt modification acts to generate an N-degron signal for the N-end rule is through arginylation. This process begins when the Nt methionine is cleaved and second position residues, such as asparagine and glutamine, are exposed. Nt-arginylation also occurs on Nt-Asn and Nt-Gln following deamidation into Nt-Asp and Nt-Glu or Nt-Cys is oxidised to generate Cys-sulfinic acid ($CysO_2$) or Cys-sulfonic acid ($CysO_3$) (Yoo *et al.*, 2018; Varshavsky, 2019). Recently, the formation of Cys-sulfinic acid has been shown to be mediated by cysteamine (2-aminoethanethiol) dioxygenase (ADO) (Masson *et al.*, 2019). L-Arg is conjugated to Nt-Asp and Nt-Glu by ATE1-encoded Arg-tRNA transferases to generate a canonical N-degron, Arg (Kwon, Kashina and Varshavsky, 1999). Transferases conjugate an arginine residue on the N-terminal end to generate an arginine Type I N-terminal degron sequence so it can bind to N-recognins, like UBR2, for ubiquitination. Other Type I, or Type II, N-terminal sequences can arise through other N-terminal modifications.

There are specific roles for the N-end rule in specific targeting of substrates in certain cellular conditions which is achieved by the generation of a neo-N-terminus through proteolysis. In *S. cerevisiae,* separase cleaves the Scc1 (RAD21 in mammals) kleisin subunit of cohesin, during removal in chromosome segregation, to generate a C-terminal fragment that bears Nt-Arg which is rapidly destroyed by the Arg/N-end rule pathway (Rao *et al.*, 2001). Failure to eliminate this Scc1 fragment (e.g. in an *ubr1*Δ mutant with no Arg/N-end rule pathway) results in chromosome instability. As the c-terminal fragment of Scc1 retains a physical affinity for the rest of the cohesin complex (Rao *et al.*, 2001), the chromosome instability in *ubr1*Δ cells could be due to cohesin mechanics containing cohesin-bound C-terminal fragment of Scc1 but this remains unproven. As the yeast Scc1 fragment has Nt-Arg, the degradation by the N-end rule pathway does not require Nt-arginylation (Rao *et al.*, 2001).

In mammals, the C-terminal (Ct) fragments generated by separase of mitotic RAD21 and meiotic REC8 subunits bear Nt-Glu, a substrate of the ATE1 R-transferase (Hauf, Waizenegger and Peters, 2001; Kudo *et al.*, 2009; Peters and Nishiyama, 2012). *Ate1*$^{-/-}$ mice are embryonic lethal (Kwon *et al.*, 2002) and post-natal ablation of *Ate1* using Cre recombinase technology causes a variety of phenotypes, including fat loss and hyperkinetic behaviour (Brower and Varshavsky, 2009). However, in an *Ate1*$^{-/-}$ mouse strain where the ablation of *Ate1* was confined to germ cells, resulted in reduced male fertility due to arrest and apoptotic death of spermatocytes at the end of meiosis I (Liu *et al.*, 2016), a phenotype that is similar to that found in *Ubr2*$^{-/-}$

spermatocytes (Kwon *et al.*, 2003). This *Ate1*$^{-/-}$ mouse line confirmed that the main C-terminal fragment of REC8 cleavage by separase, Glu^{455}-REC8, is a short-lived substrate of the Arg/N-end rule pathway and that the degradation of this fragment requires its Nt-arginylation by the ATE1 R-transferase (Liu *et al.*, 2016).

As previously stated, the separase-generated C-terminal fragment of yeast Scc1 retains some affinity to the rest of the cohesin complex (Rao *et al.*, 2001). The mouse Glu^{455}-REC8 fragment could interact with cohesin complexes *in vivo.* However, the model for the Scc1 Ct fragments affinity for the cohesin complex would require incorporation into new cohesin complexes loaded onto the chromosomes during S phase in the next cell cycle so would not be applicable for meiotic cells.

The N-end rule has a role in conditional protein regulation in the innate immune response. Exposure to bacterial infection by *B. anthracis* and to anthrax lethal toxin leads to the cleavage of the inflammasome component, NLRP1B, generating a neo-N-terminal Type II degron sequence of the C-terminal fragment (Xu *et al.*, 2019). Caspase-1 is activated by the cleaved Nt fragment of NLRP1B and this response depends on the degradation of the C-terminal fragment by the N-end rule. siRNA knockdown of UBR2 or the E2 ubiquitin conjugating enzyme UBE2O in macrophages resulted in increased vulnerability to *B. anthracis* infection and a loss of the immune response, implying UBR2 specifically binds the C-terminal fragment for proteasomal degradation.

Other described roles of the N-end Rule is in the regulation of DNA replication stress regulators such as SDE2, which has a neo-Type I N-degron following stress-induced cleavage (Rageul *et al.*, 2019). Also, in the potential conditional protein regulation of neurodegeneration, as the cleavage of Trans-activation response element (TAR) DNA-binding protein 43 (TDP43) leads to the degradation by the Arg/N-degron pathway (Brower, Piatkov and Varshavsky, 2013) which can lead the accumulation of aggregates of the ALS marker, TDP43 (Eldeeb *et al.*, 2022).

1.3.1.3.3 Substrate Binding Specificity of UBR proteins in the Arg/N-end rule

UBR proteins that act as N-end rule E3 ubiquitin ligases have their substrate binding specificity regulated by two protein domains: the UBR box, a highly conserved 70-residue zinc finger-like motif which is shared across all UBR proteins (Figure 1.8; Matta-Camacho *et al.*, 2010) and the N-domain, which has high homology with the bacterial ClpS domain and is common to both mouse UBR2 as well as UBR1. The UBR box is able to bind Type I , or arginine-containing, target peptides alone but both the UBR box and the N-domain are needed for Type II, or phenylalanine-containing, peptide binding in UBR1 and UBR2 (Tasaki *et al.*, 2009).

UBR1 is able to bind to non-acetylated Met ϕ proteins, aiding in their degradation as a redundant role for the degradation of acetylated Met-ϕ proteins by the Ac-N-end rule pathway (Kim and Hwang, 2014). This requires

both the UBR box and the N-domain and appears to be related to canonical Type II N-end Rule degradation pathways used by UBR proteins as the second residue is often a bulky hydrophobic amino acid such as phenylalanine.

UBR2 has a UBR box and N-domain which are needed for Type I (basic) and Type II (bulky hydrophobic/aromatic) substrate binding but it has the highest detectable binding to Type II substrates (Tasaki *et al.*, 2005). The UBR box isolated from UBR2 can bind Type I peptide substrate sequences in vitro to the same level as the UBR box isolated from UBR1 (Matta-Camacho *et al.*, 2010). This affinity changes when the whole UBR2 protein is present (Tasaki *et al.*, 2005), which suggests a conformation that favours Type II substrate binding. Other UBR proteins, UBR1/4/5, are strongly detectable in Type I binding assays and as they are ubiquitously coexpressed are likely to be the primary Type I regulators of the N-end Rule pathway. But UBR2 can bind to Type I substrate stress regulator SDE2 *in vivo* (Rageul *et al.*, 2019, p. 2). This shows that there are *in vivo* roles for proteins such as UBR2 that cannot necessarily be predicted by *in vitro* pulldown or binding assays.

UBR1/2/4/5 are likely to exhibit some redundancy in their substrate binding ability which has been functionally demonstrated between UBR1 and UBR2 which are the most genetically similar. *Ubr2*$^{-/-}$ mice exhibit developmental defects including a varying female-specific embryonic lethality (Kwon *et al.*, 2003) whereas a *Ubr1*$^{-/-}$ mouse is viable but exhibit growth defects particularly in the skeleton and adipose tissue (Kwon *et al.*, 2001). In a

double *Ubr1*$^{-/-}$ *Ubr2*$^{-/-}$ mouse there is a more penetrant embryonic lethality, associated with defects in neurogenesis and cardiovascular development not found in either single mutants (An *et al.*, 2006). This suggests that one can compensate for the other in different developmental pathways.

An example of redundancy outside of UBR1/UBR2 is the knockdown of *Ubr4* by RNAi in *Ubr1*$^{-/-}$ *Ubr2*$^{-/-}$ cells. Alone, *Ubr1*$^{-/-}$ *Ubr2*$^{-/-}$ embryonic fibroblasts have an increase in both type I and type II N-end rule reporter proteins, but knockdown of *Ubr4* results in a loss of type II N-end Rule turnover, although another component of the type I N-end Rule persisted in these cells- potentially UBR5. This indicates that UBR1, UBR2 and UBR4 may partially compensate each other for turnover for the same substrates but as this is a reporter system there is no *in vivo* evidence that UBR1/UBR2 have overlapping biological substrates with UBR4 (Tasaki *et al.*, 2005).

An example of Arg/N-end rule regulatory function is in the proteasomal degradation is the conditional degradation of the genome surveillance protein SDE2 (Rageul *et al.*, 2019). SDE2 is cleaved in response to DNA replication stress to prevent progression at DNA replication forks so it can protect against cellular stress and promote progression of DNA replication and S-phase (Jo *et al.*, 2016). Cleavage of SDE2 exposes the N-terminus of the C-terminal fragment that contains a TI N-degron which is turned over by proteolysis. Knockdown of *Ubr1* or *Ubr2* results in stabilisation of this C-terminal fragment but both must be removed to fully stabilise the C-terminal SDE2 protein (Rageul *et al.*, 2019). This is an *in vivo* Type I function of UBR2

despite peptide pulldown assays do not show a strong affinity for Type I peptide sequences by UBR2 protein (Tasaki *et al.*, 2005). This demonstrates that there are *in vivo* roles for UBR2 and potentially other proteins that cannot be predicted by *in vitro* pulldown assays.

Terminal degron pathways, such as the N-end rule pathway, offer a potential for therapeutic targeting. Successful development of small molecules that can inhibit E3 ubiquitin ligases binding to the N-terminus of its partner protein provide proof-of-concept that pockets binding to N termini are ligandable (Scott *et al.*, 2017; Zhou *et al.*, 2017). This has led to great pharmaceutical interest in developing small molecules that occupy substrate-binding pockets in E3s as these molecules can be used to generate degrader drugs that connect E3s and disease-causing proteins. Terminal degron-binding sites in substrate receptors have pockets that are the size of small molecules and are candidates for degrader drugs (Verma, Mohl and Deshaies, 2020). Thus, there is a drive to investigate E3s and how they target proteins to lead to rewiring for degradation of disease-causing targets.

Figure 1.8 Domains of the mammalian UBR box protein family. All UBR proteins have a UBR box (yellow ellipse) to recognize N-degrons, and this UBR box is the signature of the UBR family. UBR1 and UBR2 also have an N-domain (green ellipse) that recognizes the type II N-degrons. In addition, these UBR proteins have a RING (navy blue square), HECT (blue square), F-box (orange box), or PHD domain (purple box) for E2 binding or ubiquitin conjugation. Other domains include the CUE domain, which recognizes ubiquitin, the MLLE domain, known to regulate the catalytic activity of HECT and the UAIN which is the UBR auto-inhibitory domain. Adapted from Kim *et al.*, 2021

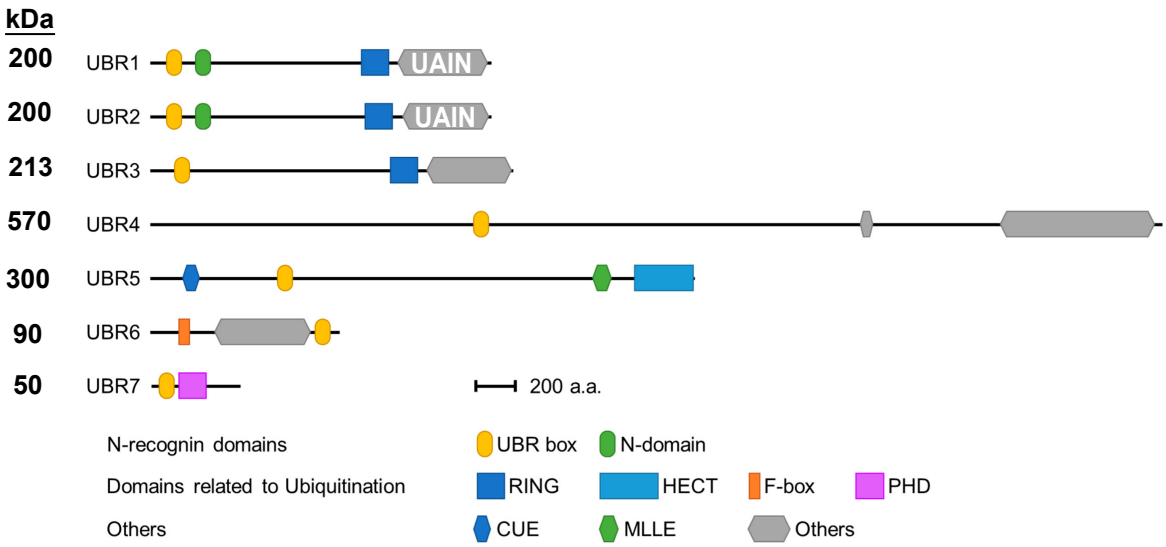
kDa
200
UBR1
UAIN
200
UBR2
UAIN
213
UBR3
570
UBR4
300
UBR5
90
UBR6
50
UBR7
200 a.a.
N-recognin domains
UBR box
N-domain
Domains related to Ubiquitination
RING
HECT
F-box
PHD
Others
CUE
MLLE
Others

1.3.1.3.4 E2/E3 Interaction Dynamics and the E3 RING Domain

There are three major classes for E3 ubiquitin ligases: those with a RING, HECT or RBR domains which determine how the E2 ubiquitin conjugating enzyme binds and ubiquitin is transferred to target proteins. The UBR family are variable in their E2 binding domains (Figure 1.8) so are expected to interact with a variety of E2 enzymes. UBR5 contains a HECT domain, that undergoes temporary ubiquitination as a proximal transfer point for build-up of ubiquitin chains before transfer to the substrate (Wang and Pickart, 2005; Sluimer and Distel, 2018). UBR5's HECT domain is present in its C-terminus and its catalytic cysteine is Cys2768 (Qian *et al.*, 2020). Within the N-end Rule, UBR5 has only been shown to be active in Type I N-degron binding (Tasaki *et al.*, 2009). There is no known UBR protein with a RBR domain, which is a highly specialised domain that catalyses ubiquitin transfer in an E2-independent manner (Spratt, Walden and Shaw, 2014).

UBR2 and UBR1 are E3 ubiquitin ligases that contain a RING domain, which interacts through sequence specific contacts on the RING domains surface (Deshaies and Joazeiro, 2009). E2-E3 interactions are highly variable but UBR2 has been shown to interact with UBE2A, USE1 (Lee *et al.*, 2011) and UBE20 (Xu *et al.*, 2019). UBE2A can bind to E1 ubiquitin activator UBA1 (Kwon *et al.*, 2003; Lee *et al.*, 2011). The ubiquitin conjugating enzyme USE1 is the only known E2 to accept and transfer ubiquitin solely from E1 ubiquitin activator, UBA6 (Aichem *et al.*, 2010). The UBA6-USE1 cascade is not as

well studied as other E1 proteins, like UBA1, due to being present in mammalian cells but not many eukaryotes such as *S.cerevisiae.*

UBE2O was more recently identified as a potential interactor of UBR2, both being required for the N-end Rule-mediated proteolysis of the NLRP1B inflammasome (Xu *et al.*, 2019). UBE2O is an E2/E3 hybrid ubiquitin-protein ligase and displays both E2 ubiquitin conjugating enzyme and E3 ubiquitin ligase activities and have been implicated in the turnover of orphan proteins that are misfolded due to protein complex loss (Yanagitani, Juszkiewicz and Hegde, 2017; Hormaechea-Agulla *et al.*, 2018). This appears to be independent of any canonical E3 ligase but is does seem that UBE2O has a role as an E2 alongside UBR2.

There are over 600 human genes encoding RING domain-containing proteins, most of which are expected to be partially active as E3 ubiquitin ligases (Li *et al.*, 2008). RING E3 ligases are divided into two big families: monomeric RING finger and multi-subunit E3 ligases. Monomeric RING E3 ligases not only have the domain for substrate binding and ubiquitination, but also have the function of autoubiquitination, such as COP1, MDM2, and TRAF6 and UBR2 (Joazeiro and Weissman, 2000). Multi-subunit E3 ligases like the cullin-RING ligases (CRLs) are a diverse class of ubiquitin ligases characterised by several common features. The cullin scaffold includes the N-terminus RING-box protein, adaptor protein and C-terminus substrate receptor. A crucial multi-subunit E3 ligases APC/C is assembled of 19 subunits including a RING subunit and cullin-like subunit (Apc2) which

connect with each other and perform functions like substrate recoginition and connections with other complex components (Primorac and Musacchio, 2013; Metzger *et al.*, 2014). RING E3s can be also regulated by different modifications, including autoubiquitination, neddylation, phosphorylation, and interaction with small molecules. The large number of proteins with RING domains suggests a level of redundancy and protection against mutations within eukaryotes indicating the importance of the UPS for proteome homeostasis.

The canonical RING domain is a cysteine-rich protein domain with conserved histidine residues that coordinate two zinc molecules in the structural core with some similarity to the zinc finger DNA-binding structure (Freemont, Hanson and Trowsdale, 1991; Freemont, 1993). Intervening amino acids in the RING domain can be variable but structural and mutational studies show that several residues are important for physical contacts to E2 ubiquitin ligases. For example, W408, a bulky hydrophobic Tryptophan, is located on the exposed surface of the RING domain in c-Cbl with its sidechain sitting in the binding cleft of the E2 enzyme (Deshaies and Joazeiro, 2009; Lee *et al.*, 2011). Some RING proteins need modifications to stabilise E2 interactions and promote Ub transfer across sometimes larger distances, like linkage proteins (Liu and Nussinov, 2010) or autoubiquitination of the E2 or E3 ligases (Patel, Sibbet and Huang, 2019). Given the large number of E2-E3 interactions, there is an even larger variability in the UPS in addition to the large number of ubiquitin ligase-encoding genes (Li *et al.*, 2008).

1.3.1.3.5 Non-N-end rule turnover

Outside of the N-end rule, a non-canonical role in protein quality control has been identified for *S.cerevisiae* Ubr1 (Eisele and Wolf, 2008; Heck, Cheung and Hampton, 2010; Nillegoda *et al.*, 2010) as well as *S.pombe* Ubr11 (Kriegenburg *et al.*, 2014). This is dependent on the interaction of the protein chaperone Hsp70 to misfolded proteins in the cytoplasm (Summers *et al.*, 2013; Kriegenburg *et al.*, 2014) and even though no pathway has thus far been identified for mammalian UBR proteins, they are still implicated in cytoplasmic protein quality control in mammals (Sultana, Theodoraki and Caplan, 2012). *S.cerevisiae* Ubr1 protein has substrate binding abilities to an internal degron site in the transcriptional repressor CUP9 (Turner, Du and Varshavsky, 2000; Du *et al.*, 2002). Ubr1 recognition of CUP9 depends on the c-terminus proximal UAIN, which has also been noted in some literature as region IV (Zenker *et al.*, 2005). The domain carries out auto-inhibition in Ubr1, whereby it acts to bind the N-terminal region of the Ubr1 protein, blocking binding of Ubr1 to CUP9 (Du *et al.*, 2002). CUP9 is a transcriptional repressor of peptide import proteins such as PTR2 (Byrd, Turner and Varshavsky, 1998; Kawai *et al.*, 2014) and so the addition of N-end rule peptides to Ubr1 relieves inhibition by the UAIN and exposes the CUP9 binding site on Ubr1 to promote CUP9 degradation, so positively regulating their own uptake (Turner, Du and Varshavsky, 2000). CUP9 has an internal degron sequence, which has been limited to the C terminal 33-residue region but the recognition domain for CUP9 within Ubr1 has not been identified. So it is not understood how the UAIN acts to physically block CUP9 interaction (Du *et*

al., 2002; Xia *et al.*, 2008). Although the protein sequence is conserved between species, there is very little published about the UAIN domain in mammalian UBR proteins.

Also, there are very limited studies on functions for mammalian UBR1 or UBR2 outside the N-end Rule pathway. The retrotransposon-expressed protein LINE-1 ORF1p can be turned over by UBR2 through an unknown mechanism – presumably by binding to an internal degron, similarly to the CUP9 substrate of *S. cerevisiae* Ubr1, as ORF1p does not contain a canonical N-degron sequence. The physical interaction domains between UBR2 and ORF1p have not been identified (Maclennan *et al.*, 2017), and it is unknown whether this depends on activity of the UAIN domain, or if binding to N-end Rule sequences are required for LINE-1 ORF1p binding.

More recently, chase-degradation assays showed that human UBR1 and UBR2 mediate the degradation of stress-inducible transcription factor ATF3 (Vu and Varshavsky, 2020). ATF3 does not have a distinguished N-degron site making it the first physiological substrate of the mammalian UBR1 and UBR2 that is targeted for degradation through an internal unmapped degron. It was unexpected that ATF3 interacted with a 123 kDa Nt-fragment of UBR1 but exhibited an ‘opposite’ binding pattern with UBR2, binding to a 81Kda Ct-fragment of UBR2 (Vu and Varshavsky, 2020). This suggests that UBR2 and UBR1 have a role as a regulator of gene expression and may have other substrates in non-N-end rule protein turnover.

1.3.2 UBR2 and histone modifications during meiosis

The E3 ubiquitin ligase, UBR2, has been implicated in a regulatory role for histone ubiquitination in meiotic spermatocytes, by monoubiquitination of histone H2A. In somatic cells, regulatory role for ubiquitination of histones is mediated by Polycomb complex and E3 ubiquitin ligase RING1B and is a repressive chromatin mark which is important for X-inactivation or transcriptional silencing (Cohen and Lee, 2002). In prophase I, IF staining in *Ubr2*$^{-/-}$ spermatocytes showed less monoubiquitinated H2A on XY chromosomes indicating a role for UBR2 in the silencing of sex chromosomes (An *et al.*, 2010). But the immunofluorescence (IF) staining from the *An et al* does not match IF staining using more specific anti-H2A mono-Ub antibodies (Hasegawa *et al.*, 2015; Luo *et al.*, 2015) indicating that the antibody staining is likely detecting other species of ubiquitinyated histones.

UBR2 was also suggested not to have a role in the initiation of meiotic recombination as it did not localise to recombination foci and was not required for normal recruitment of RAD51 or RPA to recombination foci during leptotene (An *et al.*, 2010). Also, further work completed in our group contradicts this as asynapsis in *Ubr2*$^{-/-}$ spermatocytes was associated with earlier defects in meiotic recombination as γH2AX abundance, DMC1 foci frequency and RAD51 foci frequency were reduced to 50%, 52% and 58% respectively of those seen during leptotene in *Ubr2*$^{-/-}$ mutants (Crichton *et al.*, 2017). Representative images and quantitative analysis of recombination foci in *Ubr2*$^{-/-}$ spermatocytes were not shown in *An et al*. This suggests that the

reduction in zygotene recombination foci in *Ubr2*$^{-/-}$ spermatocytes is a consequence of earlier defects in the meiotic recombination during leptotene, and that reduced meiotic recombination is contributing to the *Ubr2*$^{-/-}$ meiotic phenotype but it remains unclear how this is happening.

Furthermore, the idea that the meiotic arrest in *Ubr2*$^{-/-}$ spermatocytes is due to accumulation of ubiquitylated histone H2A at the sex body mediated by interactions with E2 ubiquitin conjugating enzyme, HR6B, does not align with the findings from *Crichton et al*. The functional data on HR6B's role in H2A ubiquitination was completed in IP experiments of GST-pulldown assay and Ubiquitination-coupled E3 binding assay with UBR2 (as a mixture with UBR1) immobilized on F-peptide-beads followed by immunoblotting (An *et al.*, 2010). Also, there is no IF staining showing HR6B localisation to the XY body alongside UBR2 and as previously shown that only small foci of HR6B in the nucleus and on the developing SCs are identified (Mulugeta Achame *et al.*, 2010). There is no convincing data showing UBR2 binding to HR6B is responsible for ubiquitination of H2A specific to the XY body in these assays.

1.3.3 UBR2 and TEX19.1

UBR2 interacts with the TEX19.1 protein (Yang *et al.*, 2010; Maclennan *et al.*, 2017) which is a germline genome defence protein expressed in hypomethylated tissues such as in testes, ovaries and the placenta (Öllinger *et al.*, 2008). TEX19.1 may inhibit the activity of UBR2 toward type II N-end rule substrates. Ectopic expression of *Tex19.1* in FlpIn-293 cell lines expressing different ubiquitin-GFP fusions showed there was a specific protection of GFP Type II N-end rule reporters (Reichmann *et al.*, 2020). TEX19.1 expression broadly overlaps the phenotypes found in *Ubr2*$^{-/-}$ mice (Kwon *et al.*, 2003; Öllinger *et al.*, 2008; Yang *et al.*, 2010) with the exception being the cohesin phenotype found in the spleen (Reichmann *et al.*, 2020) implying that UBR2 is able to negatively regulate the acetylated cohesin complex through direct turnover (via N-end rule or non-N-end rule) or through an indirect pathway not dependent on its interactions with TEX19.1.

The *Ubr2*$^{-/-}$ mouse model has three major phenotypes that are not compensated by other endogenous UBR proteins. The most well characterised of these is in male meiotic progression found in mice bred onto different genetic backgrounds (Yang *et al.*, 2010; Crichton *et al.*, 2017), female embryonic lethality that appears to vary depending on the genetic background (Kwon *et al.*, 2003) and the increase in AcSMC3-subunit of cohesin in mitotic spleen (Reichmann *et al.*, 2020).

1.3.3.1 Similarities between *Tex19.1*$^{-/-}$ and *Ubr2*$^{-/-}$ Phenotypes

In *Ubr2*$^{-/-}$ spermatogenesis, there is chromosome asynapsis in prophase I, which is associated with the loss of recombination foci and homology search defects (Crichton *et al.*, 2017). This leads to gross spermatocyte phenotypes and male infertility characterised by morphological changes in seminiferous testis tubules, low testis weight and no mature sperm (Kwon *et al.*, 2003). A very similar phenotype is characterised in *Tex19.1*$^{-/-}$ males which has asynaptic arrest and reduced frequency of recombination foci (Crichton *et al.*, 2017). TEX19.1 protein is destabilised in *Ubr2*$^{-/-}$ testis (Yang *et al.*, 2010), suggesting that their interaction is important for normal spermatogenesis and the similar phenotypes between *Tex19.1*$^{-/-}$ and *Ubr2*$^{-/-}$ testes are due to lack a functional TEX19.1-UBR2 complex (Yang *et al.*, 2010a; Crichton *et al.*, 2017). Aside from UBR2, UBR1 is the other UBR protein that has the highest N-end Rule affinity that is expressed in similar levels in the testis (Tasaki *et al.*, 2005) but *Ubr2*$^{-/-}$ testis have a lost a specific function in spermatocytes that cannot be compensated by redundancy with UBR1 resulting in the *Ubr2*$^{-/-}$ specific phenotypes.

The female embryonic lethality present in *Ubr2*$^{-/-}$ mice is also similar to that observed in *Tex19.1*$^{-/-}$ mice. TEX19.1 is expressed in the trophoblast-derived tissues of the placenta, and in a *Tex19.1*$^{-/-}$ environment there are embryonic growth restrictions and a placental defect that arises around E12.5 days of development (Reichmann *et al.*, 2013, p. 201; Tarabay *et al.*, 2013). This is associated with an intrauterine growth restriction and changes in trophoblast-derived tissue development in the placenta linked to derepression of

retrotransposons, particularly LINE-1 (Reichmann *et al.*, 2013). There are placental defects in an *Ubr2*$^{-/-}$ mouse that affect additional layers of the placenta than those found in *Tex19.1*$^{-/-}$ (Eleanor Raymond, unpublished), indicating TEX19.1-independent functions of UBR2 in the placenta.

Ubr2$^{-/-}$ females that do survive are reported to be subfertile but due to female-biased embryonic lethality the role of UBR2 in female meiotic processes has been difficult to study (Kwon *et al.*, 2003). *Tex19.1*$^{-/-}$ females have subfertility associated with chromosome missegregation and aneuploidy in the oocyte (Reichmann *et al.*, 2020) which was not observed in the *Ubr2*$^{-/-}$ oocytes (Eleanor Raymond, unpublished), indicating that UBR2 and TEX19.1 may also have independent roles during female meiosis. The chromosome missegregation in *Tex19.1*$^{-/-}$ mouse oocytes is linked to the misregulation and reduction of acetylated SMC3 subunit of the cohesin complex and chromosomes cohesion defects (Reichmann *et al.*, 2020). The dynamics of the cohesin complex are discussed in Section 1.2 but SMC3 acetylation is most well understood in mitosis, and it acts to recruit cohesin maintenance factor sororin (Ben-Shahar *et al.*, 2008) to “lock” cohesin onto the chromosome axis. AcSMC3 appears to be required for normal chromosome segregation and further study into how TEX19.1 regulates this cohesin subpopulation will give insights into the importance of SMC3 acetylation in this cell type.

As previously stated *Ubr2*$^{-/-}$ embryonic stem cells, also express *Tex19.1* mRNA but have no detectable TEX19.1 protein, have a significant increase of AcSMC3 protein levels at G2/M (Karen Dobie, unpublished) suggesting that UBR2 has a role in turnover of chromatin bound cohesin in these cells.

However, *Ubr2*$^{-/-}$ mouse mitotic spleen has a significant increase in AcSMC3 protein levels (Reichmann *et al.*, 2020) and TEX19.1 is not expressed in this tissue. This suggests that UBR2 alone is responsible for this cohesin-associated phenotype in mitotic tissue but it remains unclear if it is through UBR2's N-end rule/non-N-end rule protein turnover or protein stabilisation of an unknown substrate similar to its interactions with TEX19.1.

1.4 Thesis Objectives

As UBR2 has a role in chromatin-bound cohesin regulation I wanted to identify which of UBR2's function is important in this mechanism whether it be through N-end rule, Non-N-end rule protein ubiquitination or stabilisation of TEX19.1. Identifying which of these functions is responsible might help develop ways to influence meiotic chromosome missegregation and prevent oocyte aneuploidy. There is evidence that UBR2s Type II N-end Rule substrate binding ability is not responsible for phenotypes found in *Ubr2*$^{-/-}$ mice, so I hypothesised that these phenotypes were due to the non-N-end rule protein ubiquitination role of UBR2.

- Investigate whether UBR2 localises to chromatin and determine which domains of UBR2 might regulate its localisation
- Determine the in vivo consequences of mutating endogenous Ubr2 for the cellular proteome in cultured cells, and how the different domains of UBR2 contribute to this
- Dissect the contribution of N-end rule and non-N-end rule activities to the essential role of UBR2 in regulating cohesin abundance, meiotic progression and spermatogenesis in mice

Chapter 2:
Materials and Methods

2.1 Animal Work

Animals were maintained in a heterozygous colony with *Ubr2*$^{+/RD}$ x *Ubr2*$^{+/RD}$ and *Ubr2*$^{+/TT}$ x *Ubr2*$^{+/TT}$ crosses. Unless stated, animals used for experiments were 2-4 months old, with age-matched wild type (*Ubr2*$^{+/+}$) controls from the same colony. All animal work was carried out after ethical approval by the University of Edinburgh Animal Welfare and Ethical Review Body, under UK Home Office Project Licences PPL60/4424 or P3900/7F29. Husbandry and animal care followed local institutional guidelines (University of Edinburgh, Central Bioresearch Services). All animals were housed per ARRIVE guidelines in IVC blue line (1284) cage types with a dark/light cycle of 12 hours on, 12 hours off (7am-7pm) as well as a maintained ambient temperature of 20-24°C and humidity at 45-65%.

2.1.1 Dissection and tissue retrieval

All animals were culled by Schedule 1 termination, in accordance with UK Home Office regulations. Adults were culled by cervical dislocation, and the spleen and testis were dissected.

2.1.1.1 Testis and Spleen Weight

Whole spleen from each adult animal (6-12 weeks) were weighed. Both testes from each adult animal (6–12 weeks old) were weighed, and the mean testis weight was used for statistical comparison.

2.1.1.2 Sperm Count

For sperm count one epididymis from each animal was homogenised in 1 mL 1% sodium citrate and incubated for 5 minutes at room temperature to allow

the debris to settle. Sperm in the supernatant was then counted with a haemocytometer**.**

2.1.2 CRISPR-HDR microinjection into zygotes.

To generate the *Ubr2*$^{RD/RD}$ mouse lines, both wild type (with mutant PAM) and point mutant (W1177A) dsDNA repair templates (IDT, sequences in Table 2.1, 1.5 µg/µL), and an crRNA guide construct (IDT, sequences in Table 2.1) specific to the target site were designed. 5 µg of crRNA and 10 µg tracrRNA were annealed at 95°C for 5 minutes to form gRNA complex, then ramp down to 25°C at 5°C/min. Dilute gRNA complex in 80 µL of injection buffer and add Alt-R S.p. Cas9 Nuclease to a final concentration of 20 ng/µL. This was incubated at room temperature for 10-15 minutes. The repair templates were added to the injection mix at 20 ng/µL and the final volume was adjusted to 100 µL before centrifuging the injection mix at 13000 rpm for 10 minutes at room temperature. 80 µL of the supernatant was passed through a Millipore filter and the injection mix was injected into a single-celled mouse zygote on the F1 background. These were then transferred into the uterus of a host mother on a CD-1 background. Injections and embryo transfer were carried out by Bioresearch and Veterinary Services (BVS) at the University of Edinburgh. 2 founder animals were used for subsequent matings and generation of the *Ubr2*$^{RD/RD}$ mouse line used in experiments in Chapter 5. The *Ubr2*$^{TT/TT}$ mouse line was generated from a single founder mouse identified produced during CRISPR editing to generate the *Ubr2*$^{RD/RD}$ line. This founder was backcrossed to C57BL/6J mice and then these pups were used for generation of *Ubr2*$^{TT/TT}$ mouse line used in all experiments.

Mouse line	**cRNA sequence**	**Repair template**
Ubr2$^{RD/RD}$	CAAATTACCT TTGCCAACAA	*Ubr2*$^{RD/RD}$ TTGTTTTATAATGCAGAAAAATATGATCC ATTATTCATGCACCCCGATCTGTCTTGTG GGACACACACTGGCAGCTGTGGGCACG TTATGCATGC**G**CATTGT**GC**GCAAAGGTA ATTTGTATTCTTATATTACTCAGGGAACA CCATCTGAAGGCTCAGGATTGACTTTTAA AGCAAAGGAAAATTTGTGCTGGGGGTGG Wildtype: TTGTTTTATAATGCAGAAAAATATGATCC ATTATTCATGCACCCCGATCTGTCTTGTG GGACACACACTGGCAGCTGTGGGCACG TTATGCATGC**G**CATTGTTGGCAAAGGTA ATTTGTATTCTTATATTACTCAGGGAACA CCATCTGAAGGCTCAGGATTGACTTTTAA AGCAAAGGAAAATTTGTGCTGGGGGTGG

Table 2.1: cRNA and repair sequence used in Crispr microinjections.

Bases mutated are in **BOLD** and homology arms are underlined.

2.1.3 Genotyping assays

All mice used in this thesis were genotyped by earclipping at weaning (3 weeks post-partum). DNA was extracted using the DNAreleasy™ standard protocol (Anachem LS02), where each earclip was submerged in 20 µL DNAreleasy™ reagent and incubated on a thermocycler at 75°C for 5 minutes, 96°C for 2 minutes and 20°C for 10 minutes. After one freeze-thaw cycle (-20°C), the tissue was spun down using a microcentrifuge at maximum speed and the supernatant was used in following PCR experiments. In all genotyping assays, PCR products were observed using gel electrophoresis,

as per standard protocols. 2% agarose gel in TBE (0.13 M Tris/ 45 mM Borate/ 2.5 mM EDTA) buffer with 0.5 µg/mL ethidium bromide for visualisation (Electran®, VWR). Samples were combined with loading buffer (Gel Loading Dye, Purple (6X), no SDS (NEB #B7025)) and loaded alongside either 1 kb (NEB, N3232L) or 100 bp (NEB, N3231L) DNA ladder, as appropriate for expected sizes and run at 100 V/cm. DNA bands were visualised using a UV SynGene U:Genius 3 Geldoc system.

The *Ubr2*$^{RD/RD}$ mouse was genotyped using a two-step protocol: PCR amplification around the site of the mutation, with primers as in Table 2.2, and digestion using *FspI* restriction enzyme (NEB, R0135S). This was then assayed by gel electrophoresis, see Table 2.2 for expected band sizes. For each 25 µL PCR reaction: 2.5 µL 10x Platinum Taq buffer, 0.75 µL 50 mM $MgCl_2$, 0.5 µL 10 µM dNTP mix, 0.5 µL each primer at 100 µM, 0.1 µL Platinum Taq DNA polymerase (Invitrogen, 10966034) and 19.65 µL of dH_2O with 0.5 µL DNA. PCR protocol as in Table 2.3. The *Ubr2*$^{TT/TT}$ mice was genotyped by PCR amplification of the site, using the same primers used for *Ubr2*$^{RD/RD}$ (shown in Table 2.2) with PCR protocol in Table 2.3. In order to confirm all mutations and genotype *Ubr2*$^{TT/TT}$ mice, Sanger sequencing was implemented as in section 2.4.2.

Assay	Primers	Expected Results	Notes
Ubr2$^{RD/RD}$	Forward: 5'- ATGCACCCCGATCTGTCTTG Reverse: 5'- CCCCTTTTGGCTACAGCCTT	+/+: Single band at 499bp +/RD: 3 bands: 499bp, 431bp, 68bp RD/RD: 2 bands: 431bp, 68bp	FspI digest (NEB, R0135S)
Ubr2$^{TT/TT}$	Forward: 5'- ATGCACCCCGATCTGTCTTG Reverse: 5'- CCCCTTTTGGCTACAGCCTT	Single band at 499bp	

Table 2.2 Primers for mouse colony genotyping

Step	
1) Initial Denaturation	94°C, 2 minutes
2) Denaturation	94°C, 30 seconds
3) Annealing	62°C, 30 seconds
4) Extension	72°C, 1 minute
Cycles	40 cycles Return to (2) 39 times
5) Final Extension	72°C, 5 minutes

Table 2.3 PCR cycling conditions for mouse colony genotyping assays

2.2 Cell culture

2.2.1 Cell storage and general culture conditions

Cells were stored at -150°C in liquid nitrogen, in DMSO + foetal calf serum supplemented freezing media (culture media for each cell line, as in sections 2.2.2 and 2.2.3, was supplemented with 20% DMSO and 25% FCS). Cells were thawed in a 37°C waterbath and added to 9 mL of pre-warmed media, then pelleted by centrifugation (200 g, 5 minutes). The media was removed by aspiration and the cell pellet resuspended in fresh pre-warmed media. They were seeded into either T25 or T75 flasks (Corning, 25 cm^2 and 75 cm^2) at $2x10^4$ cells/cm^2, unless stated; HEK293T cells were seeded on uncoated flasks, and for mouse embryonic stem cells (ESCs), flasks were coated in 0.2% gelatin (Sigma) in phosphate buffered saline (PBS), which was removed by aspiration prior to addition of cell suspension in media.

All cells were cultured at 37°C and 5% CO_2. The standard passaging protocol for cell culture was: a 1x pre-warmed (37°C) PBS wash, then trypsinisation using pre-warmed trypsin-EDTA (1% trypsin/0.4% EDTA, Sigma Aldrich T4174) in PBS for 2 minutes at 37°C, 5% CO_2. Trypsin was inactivated using 10 volumes of pre-warmed media. Cells were transferred to 15 mL falcon tube to pellet by centrifugation (200 g, 5 minutes), media was removed by aspiration and cells were resuspended in fresh pre-warmed media. All cells were reseeded at $2x10^4$ cells/cm^2, unless stated.

2.2.2 HEK293T cell culture

Wild type HEK293T cells were obtained from ATCC (ATCC Cat# CRL-3216, RRID: CVCL_0063) and are used primarily as a vehicle for protein overexpression through transfection of CMV10-3xFLAG-UBR2 plasmids. HEK293T cells were cultured in serum-supplemented DMEM (Dulbecco's Modified Eagle's Medium, Gibco 41965-039) (10% foetal calf serum/FCS, 200 µg/mL penicillin-streptomycin, P/S, 8 mM L-Glutamine) and allowed to grow for 48-72 hours between passaging.

2.2.2.1 Transfection of CMV10-3xFLAG-UBR2 and pCAGGS-TEX19.1 plasmids in HEK293Ts

For overexpression experiments, HEK293T cells were seeded at $3.1x10^4$ cells/cm^2 onto gelatinised coverslips in 6-well plates (9.6cm^2) and allowed to grow for 24 hours. Then, the CMV10-3xFLAG-UBR2 and pCAGGS-TEX19.1-YFP plasmids outlined in Table 2.6 were transfected using the Lipofectamine 2000 (LF2000, Invitrogen 11668-019) standard protocol. 1 µg of plasmid was added to 50 µL Opti-MEM Reduced Serum Media (Invitrogen 31985-092) and a master mix of 3 µL LF2000 per 50 µL Opti-MEM was made up. Both were incubated at room temperature for 5 minutes, then combined (total volume 100 µL), gently mixed and incubated again at room temperature for 15 minutes. This mixture was then added dropwise to each well of the 6-well plate and the cells incubated for 24 hours. Cells were harvested at 24 hours post-transfection, by in-well cell lysis, or coverslips were fixed with 4% paraformaldehyde.

2.2.2.2 HEK293T synchronisation via single thymidine block

To synchronise HEK293T cells into G2/M, cells were seeded at $1x10^4$ cells/cm^2 in a 6 well plate, and after 24 hours of growth, media was changed with media that was supplemented with 1.25 mM thymidine (Sigma Aldrich T9250). Cells were cultured for 16 hours under thymidine treatment, then released for up to 10 hours (2 hour intervals). At 16 hours treatment and 2 hour intervals after release, HEK293T cells were harvested by trypsinisation and the cell pellet was washed in PBS. The suspension was spun down in a tabletop centrifuge and resuspended in 50% FCS in PBS. Cells were fixed with addition of 450 µL ice cold 70% EtOH dropwise over a vortex and incubated at 4°C. To stain for FACS, cells were centrifuged at 1000 RCF at 4°C for 5 minutes, washed twice in ice cold PBS, then resuspended in 50 µg/ml propidium iodide (Sigma, P4864-10ML), 100 µg/mL RNase A (Invitrogen, 12091021) in PBS and incubated at room temperature for 1 hour. Cells were stored on ice, protected from light, until analysis on a BD Biosciences LSR Fortessa™ (MRC HGU Core FACS Facility).

2.2.3 E14 embryonic stem cell culture

E14Tg2a mouse ESCs (RRID:CVCL_9108) were obtained from Fiona Kilanowski (MRC Human Genetics Unit, UK) and cultured on 0.2% gelatin-coated flasks in serum/LIF-supplemented GMEM (Glasgow Minimal Essential Medium, Gibco 21710-025) (10% FCS, 100 µg/mL P/S, 2 mM Gibco L-Glutamine, 1 mM Sigma Aldrich sodium pyruvate, 1x Sigma MEM non-essential amino acids, 50 µM Gibco β-mercaptoethanol and 1,000 U/mL Leukaemia inhibitory factor (LIF) and passaged at maximum every 48 hours.

2.2.3.1 CRISPR-Cas9 HDR for *Ubr2*$^{T2/T2}$, *Ubr2*$^{RD/RD}$ and *Ubr2*$^{ELL/ELL}$ ESC generation

I generated stable *Ubr2*$^{T2/T2}$, *Ubr2*$^{RD/RD}$ and *Ubr2*$^{ELL/ELL}$ lines on the E14 background with the D233A, W1177A and K834A point mutations by CRISPR-Cas9 HDR. E14 ESCs were transfected with the dsDNA repair oligo with 100 bp homology arms (IDT) encoding the mutant repair template containing both the point mutation and the mutant PAM sequence, alongside a Cas9 expressing plasmid and PX458 plasmids with the specific guide sequence cloned into it, see section 2.4.1.3 and Figure 4.1, 4.2 and 4.3. Transfection and picking of clonal colonies was carried out by Fiona Kilanowski (MRC HGU).

To genotype successful clones of the *Ubr2*$^{T2/T2}$, *Ubr2*$^{RD/RD}$ and *Ubr2*$^{ELL/ELL}$ lines, I designed a two-step protocol: PCR amplification followed by restriction digest (primers and restriction enzyme in Table 2.4, PCR protocol in Table 2.5). This was then assayed by gel electrophoresis, see Table 2.4 for expected band sizes. The mutations were confirmed by Sanger sequencing of the PCR product. Wild type untransfected E14 ESCs were used as a control comparison to the each *Ubr2* ESC line.

Assay	Primers	Expected Results	Notes
Ubr2$^{T2/T2}$	Forward: 5'- CGTCCGTTACCGTCTAGCTA Reverse: 5'- CTGTAGTTGCAAAGCCAATGG	+/+: Single band at 303bp *+/T2*: 3 bands: 303bp, 221bp, 82bp *T2/T2*: 2 bands: 221bp, 82bp	*ApaLI* (NEB, R0507S)
Ubr2$^{RD/RD}$	Forward: 5'- ATGCACCCCGATCTGTCTTG Reverse: 5'- CCCCTTTTGGCTACAGCCTT	+/+: Single band at 499bp *+/RD*: 3 bands: 499bp, 431bp, 68bp *RD/RD*: 2 bands: 431bp, 68bp	*FspI* digest (NEB, R0135S)
Ubr2$^{ELL/ELL}$	Forward: 5'- TAGTTCACAGTGGAGGTGCTG Reverse: 5'- GCTAGACAGGGTTGCTGTGT	+/+: Single band at 386bp *+/ELL*: 3 bands: 386bp, 231bp, 155bp ELL/ELL: 2 bands: 231bp, 155bp	*SfoI* (NEB, R0606S)

Table 2.4 Primers for mouse *Ubr2* genotyping

Step	*Ubr2*$^{T2/T2}$ (UBR2-D223A-T2) *Ubr2*$^{RD/RD}$ (UBR2-W1177A-RD) *Ubr2*$^{ELL/ELL}$ (UBR2-K834A-ELL)
1) Initial Denaturation	94°C, 2 minutes
2) Denaturation	94°C, 30 seconds
3) Annealing	62°C, seconds
4) Extension	72°C, 1 minute
Cycles	35 cycles Return to (2) 34 times
5) Final Extension	72°C, 5 minutes

Table 2.5 PCR cycling conditions for *Ubr2* genotyping assays

2.3 DNA analysis

2.3.1 Plasmids

Various plasmids were used for overexpression of proteins in cell culture (see section 2.2.2.1) and conduction of CRISPR-Cas9 in ESCs (section 2.2.3); all are noted in Table 2.6.

Name	Features	Antibiotic Resistance	Source
CMV10-3xFLAG (CMV10-FLAG)	N-terminal 3xFLAG epitope tag	Ampicillin	Sigma-Aldrich, E7658
CMV10-3xFLAG-KAP1 (FLAG-KAP1)	N-terminal 3xFLAG epitope tag Mouse Kap1 CDS	Ampicillin	Adams Lab (MRC HGU)
CMV10-3xFLAG-UBR2 (FLAG-UBR2)	N-terminal 3xFLAG epitope tag Mouse *Ubr2* CDS	Ampicillin	Adams Lab (MRC HGU)
FLAG-T1-UBR2	N-terminal 3xFLAG epitope tag Mouse Ubr2 CDS with D118A mutation in UBR box	Ampicillin	Adams Lab (MRC HGU)
FLAG-T2-UBR2	N-terminal 3xFLAG epitope tag Mouse Ubr2 CDS with D223A mutation in N-domain	Ampicillin	Adams Lab (MRC HGU)
FLAG-RD-UBR2	N-terminal 3xFLAG epitope tag Mouse Ubr2 CDS with W1177A mutation in RING domain	Ampicillin	Adams Lab (MRC HGU)
pCAGGS-TEX19.1-GFP	GFP epitope tag Mouse Tex19.1 CDS CAG promoter	Kanamycin	From Maclennan *et al.*, 2017
pCAGGS-GFP	GFP epitope tag CAG promoter	Kanamycin	From Maclennan *et al.*, 2017
pSpCas9(BB)-2A-GFP (PX458)	WT CRISPR-Cas9 machinery with GFP U6 promoter	Ampicillin	Gift from Feng Zhang (Ran *et al.*, 2013; Addgene plasmid # 48138)

Table 2.6: Plasmids used in various molecular biology assays

2.3.1.1 Bacterial culture and DNA extraction

Plasmids were amplified by transforming into subcloning efficiency DH5α competent E. coli cells (Invitrogen, 18265017) as per the manufacturer's instructions. Cells were thawed on ice prior to use. These were mixed and aliquoted into 50 µL, then incubated with 5-10 ng of DNA for 30 minutes on ice. The cells were heatshocked at 42°C for 20 seconds and then chilled on ice for 2 minutes. Then 950 µL prewarmed SOC medium was added and cells were incubated with shaking at 1 g at 37°C for 1 hour. 200 µL of cells in SOC medium were plated onto pre-poured LB agar plates (10 g/L NaCL, 10 g/L Bacto-tryptone, 5 g/L Yeast extract, 15 g/L Difco Agar) with either Kanamycin or Ampicillin antibiotic treatment for selection of successful transformants. Plates were inverted and incubated overnight at 37°C. Colonies were picked and outgrown overnight in 5 mL LB medium with 50 µg/L of antibiotic (Ampicillin or Kanamycin) at 1 g. DNA was isolated using the MiniPrep column spin kit (Qiagen) and yield was quantified using Nanodrop spectrophotometry (ThermoFisher Scientific).

2.3.1.2 Site directed mutagenesis

In order to introduce the K834A point mutation into the pCMV10-3xFLAG-UBR2 plasmid, I used Phusion Site-Directed Mutagenesis (Thermo Scientific F-541) as per manufacturer's instructions. A forward and reverse primer pair were designed to meet at their 5' end (Table 2.7), with the intended point mutation in the centre of primer F. They were ordered from IDT with 5'

phosphorylation in order to aid direct circularisation of the linear PCR product, and PAGE (polyacrylamide gel electrophoresis) purified.

Mutagenesis Target	**Forward**	**Reverse**
UBR2-K834A	5'–[Phos] ATGTATGAGCTGGCGCCA GAGTGTGC	5'–[Phos] GCCTCGCCCTGTGAGC CCAGGTTTCT

Table 2.7: Site-directed mutagenesis primers. The introduced point mutation is marked in red.

The 11 kb plasmid was added to the following PCR reaction; 31.8 µL dH_2O, 10 µL 5x Phusion buffer, 2.5 µL of each primer at 10 µM, 0.2µL CMV10-3xFLAG-UBR2 (10 ng total plasmid DNA), 1µL 10 mM dNTPs, 1.5 µL DMSO (final concentration at 3%) and 0.5 µL Phusion HotStart DNA polymerase. As CMV10-3xFLAG-UBR2 is a large (11 kb) plasmid, DMSO was added outwith the standard Phusion protocol. The extension time was calculated at 30 seconds/kb of plasmid. The PCR protocol was followed as outlined in Table 2.8**.** A negative control with no Phusion polymerase was also used to ensure no contamination was present in the sample and all plasmid was incorporated into the PCR reaction.

Step	FLAG-ELL-UBR2 (K834A)
1) Initial denaturation	98°C, 30 seconds
2) Denaturation	98°C, 10 seconds
3) Annealing	64°C, 30 seconds
4) Extension	72°C, 6 minutes
Cycles	25 cycles Return to (2) 24 times
5) Final Extension	72°C, 10 minutes

Table 2.8: PCR protocol for site-directed mutagenesis.

After PCR amplification, the linear product was treated with 1µl FastDigest DpnI per reaction and incubated at 37°C for 15 minutes to digest the methylated parental plasmid DNA. The product was circularised using T4 DNA ligase (NEB, M02025); 2 µL DpnI treated PCR product was combined with 2 µL 5x T4 buffer, 5.5 µL dH_2O and 0.5 µL T4 ligase, then incubated at room temperature for 5 minutes.

The mutated plasmids were then amplified using DH5α competent E. coli cells, as outlined in section 2.4.1.1, and screened for successful clones by Sanger sequencing of the whole ORF (open reading frame) to verify that no unintended mutation of the *Ubr2* CDS ORF had arisen.

2.3.1.3 RNA guide cloning for CRISPR-Cas9 editing in ESCs

In order to generate the CRISPR gRNA guide for generation of ESCs as in section 2.2.3.1, I introduced the guide sequence in Figures 4.1, 4.2 or 4.3 into the plasmid PX458 (Table 2.6). This plasmid encodes the wild type CRISPR-Cas9 guide machinery required for binding of the guide to wtCas9 protein and successful CRISPR mutational activity. Both sense and antisense guide sequences were ordered as 5'-phosphorylated single stranded DNA oligos (Table 2.9).

Mutation	**Sense**	**Antisense**
Ubr2$^{T2/T2}$ (D223A)	5'-[Phos] CACCGCTGCATGCTGTTTAATGATG	5'- AAACCATCATTAAACAGCATGCAGC
Ubr2$^{RD/RD}$ (W1177A)	5'-[Phos] CACCGCAAATTACCTTTGCCAACAA	5'- AAACTTGTTGGCAAAGGTAATTTGC
Ubr2$^{ELL/ELL}$ (K834A)	5'-[Phos] CACCGTTGAACTCTTTGGCACACTC	5'- AAACGAGTGTGCCAAAGAGTTCAAC

Table 2.9 CRISPR gRNA generation constructs. Additional bases indicated in red for generation of sticky ends required for cloning into PX458. [Phos] indicates a phosphate group on the 5' end of the next base in the sequence.

The PX458 plasmid was digested with the *BbsI* restriction enzyme (consensus 5'- GAAGAC$(N)_2$^ –3') in a 40 µL reaction, as follows: 2 µg PX458 plasmid, 2 µL *BbsI* (6 U/ml, NEB, R0539S), 2 µL Fast AP(NEB, 3U/ml), 4 µL 10x NEB RE CutSmart buffer and dH_2O up to a total volume of 40 µL. This was incubated at 37°C for 1 hour and check on agarose gel to ensure complete cleavage and the linearized plasmid was cleaned up using PCR purification kit (Qiagen) before use in ligations. During this, the sense and antisense oligos were diluted in dH_2O to 100 µM, combined in a 10 µL reaction, denatured at 95°C for 5 minutes and allowed to slowly cool to room temperature to anneal into a dsDNA structure. This was diluted 1:250 to a final concentration of 0.4 µM. the ligation reaction was carried out overnight at 4°C using T4 ligase, as follows: 50 ng linearized PX458, 1 µL 0.4 µM gRNA, 3 µL of 10x Roche ligation buffer, 1 µL T4 DNA ligase (Roche), and dH_2O to a total volume of 30 µL.

The ligation reactions were then used to transform into DH5α competenet E. coli cells for amplification, as outlined in section 2.4.1.1, and selection by Ampicillin antibiotic resistance. Plasmid DNA was isolated with the MiniPrep column spin kit (Qiagen) and verified using Sanger sequencing with primers specific to the sequence of the U6 promoter. For the CRISPR editing of the ESCs, this plasmid is transfected directly into the cells, as detailed in 2.2.3.1.

2.3.2 DNA Sequencing

All DNA Sanger sequencing was carried out using a 3730 or 3130XL Genetic Analyser (Applied Biosystems, MRC HGU, Core DNA sequencing Facility).

This was used for genotyping point mutations in CRISPR-Cas9 generated cell or mice lines and the verification of site directed mutagenesis in plasmids.

2.4 Immunoflourescent staining

2.4.1 Immunostaining of HEK293T spreads

Coverslips with HEK293Ts were fixed in 4% paraformaldehyde (PFA) for 15 minutes at room temperature. PFA was removed and cells were washed twice in 3% BSA-PBS before incubating in 0.5% Triton X-100 detergent for 20 minutes at room temperature. Blocking solution (0.15% BSA, 0.1% Tween-20, 5% goat serum in PBS) was made up fresh and primary antibodies were then added at the concentration described in Table 2.10, in 500 µL blocking solution per coverslip and incubated at room temperature for 2-3 hours. After primary antibody, coverslips were washed three times in PBS for 5 minutes and then incubated with secondary fluorescent (Alexa Fluor®, Invitrogen) antibodies (in 500 µL of 3% BSA-PBS with 0.1% Tween 20 at the indicated concentration in Table 2.10) and 20 µg/mL DAPI (Biotium, 40043, stock at 10 mg/mL) for 1 hour at room temperature, protected from the light. Coverslips were then mounted in PD mountant solution (1 mg/mL p-phenylene diamine in 90% glycerol), gently compressed onto a glass slide for approximately 15 minutes, then sealed with clear nail varnish and stored at 4°C, protected from light, until imaging using epifluorescent microscopy, as detailed in section 2.5.3.

2.4.2 Immunostaining of Meiotic Chromosome Spreads

Immunostaining of chromosome spreads from meiotic spermatocytes was performed essentially as described previously (Costa *et al.*, 2005). Briefly, testes were homogenized in PBS and 0.1 mL of cells were incubated in 0.5 mL 5% sucrose on a microscope slide for 1 hour. Cells were lysed with 0.1 mL 0.05% Triton-X-100 for 10 minutes and fixed with 0.8 mL of fixing solution (2% paraformaldehyde, 0.02% SDS in PBS) for 1 hour. The slides were then washed, blocked with 5% serum, 0.1% Tween in PBS and incubated with primary antibodies for 2-3 hours, anti-SYCP3 and anti-SYCP1 antibodies were added at the concentration described in Table 2.10. Fluorescently labelled secondary antibodies were used at 1 mg/mL (Invitrogen), and DNA was stained with 2 mg/mL DAPI.

2.4.3 Epifluorescence microscopy

After immunofluorescent staining, epifluorescent images were acquired using a Photometrics Coolsnap HQ2 CCD camera and a Zeiss Axioplan II fluorescence microscope with Planneofluar objectives (Carl Zeiss, Cambridge, UK), a Mercury Halide fluorescent light source (Exfo Excite 120, Excelitas Technologies) and Chroma #83000 triple band pass filter set (Chroma Technology Corp., Rockingham, VT) with the excitation filters installed in a motorised filter wheel (Ludl Electronic Products, Hawthorne, NY). Image capture was performed using scripts written by the IGMM-AIR (Advanced Imaging Resource) facility for Micromanager (https://open-imaging.com/). Objectives and magnifications used were set on

Micromanager prior to image capture, so this was captured in the image metadata and scale could be directly applied to images during analysis.

Unless specified, all 2-dimensional image analysis and quantifications were carried out using FIJI (Image J) with 64bit Java8. In order to avoid scoring bias, image names were randomized using a FIJI macro script written by James Crichton (MRC HGU) and analysed blind.

2.4.3.1 Staging of HEK293T cells

Nuclei were staged by the localisation of immunostaining of DAPI and the centromere marker ACA. Nuclei with DAPI in a circle shape and when ACA was present, random localisation of ACA is interphase. Prophase is determined when DAPI stained chromosomes condense but there is still random localisation of ACA. Metaphase is when the ACA is lined up in the centre of the DAPI staining and anaphase is when there are two sets of DAPI staining in a nucleus where the ACA staining is on the opposite edge of each DAPI-stained chromosomes.

2.4.3.2 Staging of spermatocyte nuclei

Nuclei were staged by immunostaining for the axial/lateral element markers SYCP3 and SYCP1 (Lammers *et al.*, 1994). Nuclei with short fragments of SYCP3 and no linear stretches of SYCP1 staining were classified as leptotene, nuclei containing some regions of axial element undergoing synapsis along with some regions of axial element not undergoing synapsis were classified as zygotene, and those with complete autosomal synapsis as pachytene. Immunostaining for the transverse filament component SYCP1

(Meuwissen *et al.*, 1992), were included in experiments to monitor synapsis. Asynapsed pachytene nuclei (Öllinger *et al.*, 2008) were identified due to the presence of at least one completely synapsed pair of autosomes or at least one incompletely synapsed pair of autosomes exhibiting asynapsis along at least half its length. Diplotene is defined as nuclei with accumulation of SYCP3 at telomeres and a loss of SYCP1 from desynapsed regions. Metaphase II is defined as accumulation of SYCP3 in very short fragments that correspond to accumulation of DAPI in the same regions with no SYCP1 staining detected.

2.5 Protein analysis

2.5.1 Preparation from cell culture

2.5.1.1 Whole cell lysate collection

HEK293T cells were transformed with combination of FLAG-UBR2, TEX19.1, FLAG or GFP expression plasmids, as described in section 2.2.2.1 and Table 2.6. Mouse embryonic stem cells were seeded at $1x10^5$ cell/mL in a T75 and cultured, as described in section 2.2.1. All cells were harvested by scraping them into ice cold PBS and pelleted by centrifugation at 200 g for 5 minutes at 4°C. 200 µL of lysis buffer (10 mM Tris, pH7.5, 0.15 M NaCl, 0.5 mM EDTA, 0.5% NP40 detergent, 1 mM PMSF and 1% Roche Complete Mini protease inhibitor in dH_2O) was added to the cell pellet and lysed on ice for 30 minutes. During this incubation, cells were occasionally gently mixed to avoid settling and ensure full cell lysis. Cell debris were pelleted by centrifugation at 16000 g for 10 minutes at 4°C and then the protein

supernatant was transferred to a fresh Eppendorf. A small aliquot of lysate is taken for BCA assays and the rest is added to Laemmli sample buffer (Sigma-Aldrich, S3401) and boiled at >95°C for 10 minutes. Protein samples were used immediately for Western blotting, or stored at - 20°C until later use.

2.5.1.2 Co-immunoprecipitation

HEK293T cells were transformed with combination of FLAG-UBR2, TEX19.1, FLAG or GFP expression plasmids, as described in section 2.2.2.1 and Table 2.6 and harvested by scraping cells into ice cold PBS. ChromoTek GFP-Trap® Magnetic Agarose (gtma20) were equilibrated in Dilution buffer (same as lysis buffer in section 2.6.1.1 but without 0.5% NP40 detergent) by washing 25 µL bead slurry per experiment three times in 500 µL dilution buffer, which was removed by the use of a magnetic tube rack, and stored on ice until use.

Transfected HEK293T cells were washed in ice-cold PBS, then resuspended in 200 µL Lysis buffer (Lysis buffer in section 2.6.1.1) and lysed on ice for 30 minutes. During this incubation, cells were occasionally gently mixed to avoid settling and ensure full cell lysis. Cell debris were pelleted by centrifugation at 16000 g for 10 minutes at 4°C and then the protein supernatant was transferred to a precooled tube and diluted in 800 µL dilution buffer to a total volume of 1 mL. A small aliquot of this was taken as an input sampled for each co-immunoprecipitation experiment and added to Laemmli sample buffer. The diluted lysate was added to the 25 µL equilibrated GFP-TRAP

beads and mixed by inversion overnight at 4°C. Beads, and bound proteins, were kept on ice throughout three washes in 500 µL ice-cold dilution buffer, then denatured and dissociated in Laemmli sample buffer at >95°C for 10 minutes. Protein samples were used immediately for Western blotting or stored at - 20°C until later use.

2.5.1.3 Peptide pulldown assays

Peptides specific to the N-terminal sequence of Type I (arginine) or Type II (phenylalanine) target proteins in the N-end Rule, or negative control (glycine) (see Chapter 3, Figure 3.5) were conjugated to resin via a C-terminal cysteine using the Sulfolink® Peptide Immobilisation Kit (Thermo Scientific, 44999) according to the manufacturer's instructions.

Briefly, each peptide Type I (R), Type II (F) and –ve (G, negative control) was diluted to 0.5 mg/mL in 2 mL of Sulflolink® coupling Buffer (50 mM Tris pH 8.5, 5 mM EDTA-Na) and oxidized with 100 µL TCEP (0.5 M Tris(2-carboxlethyl)phosphine, Sulfolink BondBreaker®). Followed by an incubation at room temperature for 30 minutes. Resin was equilibrated by three washes in Sulfolink® Coupling Buffer, then added the peptide solution and incubated end-over-end at room temperature for 15 minutes, and upright for a further 30 minutes to allow coupling of peptide to resin beads. Resin was washed four times in Sulfolink® Wash Solution (1 M NaCl, 0.05% NaN_3) and two times in Sulfolink® Coupling Buffer. Resin was then incubated in 7.9 mg/mL L-Cysteine-HCL in Sulfolink® Coupling Buffer end-over-end for 15 minutes at room temperature, and for an additional 30 minutes upright. Resin was

washed twice with storage buffer (0.05% sodium azide in 1x PBS) and stored upright in 2 mL of storage buffer at 4°C. The resin should be maintained at 50% resin, 50% storage buffer.

Peptide coupling efficiency was calculated by measuring the protein content of the flowthrough of the peptide solution before and after coupling by Nanodrop spectrophotometry. When comparing the protein content of before and after coupling, ≥80% coupling efficiency was deemed sufficient for peptide pulldown assays.

When pulldown assay is undertaken, resin was aliquoted- three 110 µL aliquots of preclear and one 220 µL aliquot of each Type I, Type II and –ve peptide per condition- and then prepared by removal of storage buffer and washed in 1 mL ice cold dilution buffer (10 mM Tris pH7.5, 150 mM NaCl, 0.5 mM EDTA, 1x Roche Protease Inhibitor in dH_2O). All centrifugation of resin performed at 8200 g and 4°C for 30 seconds. All resin was stored in 100 µL dilution buffer on ice until use.

HEK293T cells were seeded at $2x10^4$ cells/cm^2 in 3 wells of a 6-well plate and, after 24 hours were transfected with either FLAG-ELL-UBR2 or control plasmid FLAG-UBR2, as in section 2.2.2.1. 24 hours after transfection, cells were washed with ice cold 1x PBS and cells were lysed in-well with 200µl ice cold lysis buffer (10 mM Tris pH7.5, 150 mM NaCl, 0.5 mM EDTA, 0.5% NP-40, 1x Roche Protease Inhibitor in dH_2O) and incubated for 30 minutes at 4°C with continuous rocking. Lysates from three wells were combined and centrifuged at 16000 g for 10 minutes at 4°C to separate out cell debris.

Supernatant was transferred into a new tube and diluted to 3 mL with ice cold dilution buffer which reduces the concentration of NP-40 detergent. A 50 µL aliquot of each sample is taken to be the input control and added 50 µL Laemmli sample buffer before being boiled at >95°C for 5 minutes prior to Western blotting. Each sample was split evenly across 3 preclear resin tubes and incubated end-over-end at 4°C for 1 hour.

Preclear tubes were spun down with centrifugation at 200 g for 5 minutes at 4°C. Supernatants were combined and then split into Type I, Type II and –ve peptide-conjugated resin (1 mL per tube). These were incubated end-over-end at 4°C overnight. The supernatant was removed and the resin washed 3 times in 750 µL of ice-cold wash buffer (10 mM Tris pH7.5, 150 mM NaCl, 0.5 mM EDTA, 0.1% NP-40, 1x Roche Protease Inhibitor in dH_2O). Resin was resuspended in 50 µL Laemmli sample buffer and heated for 5 minutes at 95°C while pulse-vortexing every 1-2 minutes to ensure mixing. Resin would be centrifuged and supernatant isolated for Western blotting.

2.5.1.4 Cell pellets for whole proteome analysis by mass spectrometry

Mouse embryonic stem cells were seeded at $2X10^4$ cells/cm^2 in a T75 and cultured, as described in section 2.2.1. All cells were harvested by scraping them into ice cold PBS and pelleted by centrifugation at 200 g for 5 minutes at 4°C. Cell pellets were then frozen at -80°C until they were prepared for whole proteome analysis on the Q Exactive QE1 by the IGC Mass Spectrometry team.

Proteomics data was analysed using DIA-NN software to identify all the proteins (gene names) identified from the spectra and the calculated raw

intensities identified by the mass spectrometer. All comparisons between each mESC line were completed in the Spectronaut software and R.

2.5.2 Preparation from animal tissues

2.5.2.1 Chromatin preparation

Spleens were dissected from adult males and homogenised using razor blades and filtered through a 100 µm nylon cell strainer into 1.5 mL PBS. Cells were pelleted at 100 g for 4 minutes at 4°C, washed in ice-cold PBS and then resuspended in 500 µL Buffer A (10 mM HEPES, 10 mM KCl, 1.5 mM $MgCl_2$, 0.34 M sucrose, 1 mM DTT, 5mM sodium butyrate to prevent deacetylation of proteins, 1X Roche Complete Mini protease inhibitor and 10% glycerol in dH_2O) and added 0.1% Triton-X100 before lysing on ice for 5 minutes. Nuclei were separated by centrifugation at 1500 g for 4 minutes at 4°C, the washed in 700 µL Buffer A. Nuclei were separated by centrifugation as above, and resuspended in 500 µL Buffer B (3 mM EDTA, 0.2 mM EGTA, 1 mM DTT, 5 mM sodium butyrate to prevent deacetylation of proteins and 1X Roche Complete Mini protease inhibitor in dH_2O); this was incubated for 30 minutes on ice to lyse nuclei. Chromatin was separated by centrifugation at 1700 g for 4 minutes at 4°C, then washed with 700 µL Buffer B and pelleted as above. Chromatin was respuspended in 200 µL Laemmli 2x sample buffer, sonicated to shear chromatin for 20 cycles (30 seconds on, 30 seconds off – BioRuptor®, Diagenode) and then the protein sample was denatured at >95°C in a heat block for 10 minutes.

As spleen tissue has high cell number, protein isolated from spleen chromatin was diluted 1:10 in Laemmli after sonication and denaturation at >95°C in order to produce accurate Western blots. Protein samples were then stored at -20°C until analysis by Western blotting.

2.5.2.2 Testis Whole cell lysis

Testes dissected from adult mice (6-12 weeks) were homogenized in Laemmli buffer and denatured at 95°C for 10 minutes. As testis tissue has a much higher cell number compared to cell pellet isolated from cell culture, protein isolated from testis was diluted 1:10 in Laemmli after denaturation at >95°C in order to produce accurate Western blots. Protein samples were then stored at -20°C until analysis by Western blotting.

2.5.3 Western blotting and quantification

2.5.3.1 BCA protein assays

BCA assays were undertaken with the Pierce™ BCA Protein Assay Kit (Thermo Fisher Cat: 2322). The working reagent (WR) was made by mixing reagents A and B (50:1). 200 µL of WR was dispensed into Eppendorf tubes and 25 µL of the BSA standard or 20µL water + 5µL sample were added to WR. The tubes were vortexed and then incubate at 37°C for 30 minutes. Samples were spin at 12,000 RCF for 5 minutes. 100 µL of sample were placed into in each well of a 96 well plate and the OD was read at 562 nm on a Tecan plate reader.

2.5.3.2 Western blotting

For Western blotting, lysates were heated in Laemlli buffer for 5 minutes at 95°C, then 20 µg of protein (calculated by BCA analysis) into wells of 4-12% Bis-Tris gel (Invitrogen NuPAGE system) alongside a broad range Color Protein Standard (NEB, P7719S) marker. Gels were run in SDS MOPS buffer (NuPAGE™, Invitrogen NP00001) at 130 volts (V/cm) in order to separate proteins by molecular weight. Gels were transferred onto nitrocellulose blotting membranes using the iBlot2 dry transfer system (ThermoFisher, IB21001). The membranes were washed in PBS-T (0.1% Tween-20 in 1x PBS); membrane block and most antibody incubations were in 5% milk (Marvel milk powder) in PBS-T. Primary and HRP-conjugated (horseradish peroxidase) secondary antibodies are noted in Table 2.10. For high molecular weight proteins (i.e. UBR2), proteins were transferred onto PVDF (polyvinlyidene fluoride) membranes and blocked in 3% BSA (bovine serum albumin) in 1xPBS-T.

For visualisation of western blots, membranes were incubated in ECL (enhanced chemiluminescent reagent, Thermo Fisher SuperSignal system, 34577) and visualised on Image Quant 8000. If quantification was required, TIFF image files and protein band intensity quantified using the Gel analysis tool in FIJI (ImageJ).

Biological Target	Application	Dilution	Species	Reference/Source
FLAG-M2	Primary	Immunofluorescence, 1:1000 Western blotting, 1:10000	Mo	Millipore, F1804
ACA (anti-centromere)	Primary	Immunofluorescence, 1:1000	Hu	Antibodies, Inc. 15-235-0001
SYCP3	Primary	Immunofluorescence, 1:500	Mo	Abcam, ab97672
SYCP1	Primary	Immunofluorescence, 1:200	Rb	Abcam, ab15090
GFP	Primary	Western blotting, 1:5000	Rb	Abcam, ab290
AcSMC3	Primary	Western blotting, 1:500	Mo	Merk, MABE1925
SMC3	Primary	Western blotting, 1:500	Rb	Abcam, ab128919
SA2	Primary	Western blotting, 1:500	Rb	Abcam, ab155081
SMC1	Primary	Western blotting, 1:500	Rb	Abcam, ab9262
RAD21	Primary	Western blotting, 1:500	Rb	Abcam, ab992
Histone H3	Primary	Western blotting, 1:10000	Rb	Abcam, ab1791
UBR2	Primary	Western blotting, 1:500	Gt	Aviva, OAEB00482
TEX19.1	Primary	Western blotting, 1:1000	Rb	Gift from J. Wang (Yang et al., 2010)

DPPA3	Primary	Western blotting, 1:500	Rb	Sc-67249
β-actin	Primary	Western blotting, 1:5000	Mo	Abcam, ab8226
Lamin-B1	Primary	Western blotting, 1:5000	Mo	Sc-374015
TFPA2C	Primary	Western blotting, 1:500	Rb	PA5-49862
594 (red) anti-Mo	Secondary	Immunofluorescence, 1:500	Gt	Alexa Fluor® Invitrogen, A11020
594 (red) anti-Rb	Secondary	Immunoflourescence, 1:500	Gt	Alexa Fluor® Invitrogen, A11012
488 (green) anti-Hu	Secondary	Immunofluorescence, 1:500	Gt	Alexa Fluor® Invitrogen, A11013
488 (green) anti-Mo	Secondary	Immunofluorescence, 1:500	Gt	Alexa Fluor® Invitrogen, A11017
HRP anti-Mo	Secondary	Western Blotting, 1:5,000	Gt	BioRad, 170-6516
HRP anti-Rb	Secondary	Western Blotting, 1:5,000	Gt	Cell Signalling 7074S
HRP anti-Gt	Secondary	Western Blotting, 1:5,000	Rb	BioRad, 172-1034

Table 2.10: Antibodies used in various assays. Rb – rabbit. Mo – mouse. Hu – human. Gt – goat. 594, 488 – fluorescent wavelength. HRP – horseradish peroxidase

Chapter 3:

Localisation of UBR2 through the cell cycle

3.1 Introduction

As discussed in Chapter 1, the E3 ubiquitin ligase, UBR2, is one of seven UBR proteins that contain an UBR box. Four of these UBR proteins, including UBR2, have been shown to have activity in the N-end rule protein recognition system of the UPS (Tasaki et al., 2009) and are coexpressed in a wide variety of tissues with suspected redundancy between them (An et al., 2006). Even though UBR2 is ubiquitously expressed in all tissues, *Ubr2*$^{-/-}$ mice have a specific subset of phenotypes such as male infertility and female embryonic lethality (Kwon *et al.*, 2003). UBR2 has essential molecular functions in specific tissues, either through the N-end rule, or through other potential functions of the protein that cannot be compensated by UBR protein redundancy.

UBR2 has been found to have a 1:1 stoichiometric interaction with the germline genome defence protein TEX19.1 which is primarily expressed in hypomethylated tissues such as the testes, ovaries, placenta and embryonic stem cells (Öllinger *et al.*, 2008b; Yang *et al.*, 2010; Crichton *et al.*, 2017; Reichmann *et al.*, 2020). TEX19.1 can regulate, via UBR2, the turnover of Type II N-end rule reporters (Reichmann et al., 2020). The *Tex19.1*$^{-/-}$ males are also infertile with a zygotene-like asynaptic arrest and reduction in recombination rates (Crichton *et al.*, 2017). Also, TEX19.1 is destabilised in the *Ubr2*$^{-/-}$ testis (Yang *et al.*, 2010), indicating that their interaction is vital for normal spermatogenesis.

One role of UBR2 previously identified in our group is the turnover of chromatin associated cohesin, specifically the acetylated subpopulation of

cohesin as *Ubr2*$^{-/-}$ mitotic tissue such as spleen or embryonic stem cells have a significant increase in AcSMC3 in G2/M (Reichmann *et al.*, 2020; Karen Dobie, unpublished). However, it remains unclear where the UBR2 protein localises in cells during the cell cycle so it is unknown if UBR2 could be directly interacting with AcSMC3 or via an intermediate substrate. *An et al* (2012) showed by immunofluorescence (IF) that endogenous UBR2 is found predominantly in the nucleus of HeLa cells during interphase but the cell fractionation data contradicts this finding. Cell fractionation data did show that UBR2 localises to chromatin specifically during the G2/M phases of the cell cycle (An et al., 2012) which is the stage of the cell cycle in which UBR2 also influences chromatin-associated cohesin.

It is difficult to test UBR2 localisation in cells due to the available antibodies to endogenous UBR2 not working well in IF. To overcome this issue, a Cmv10-3xFLAG-UBR2 (FLAG-UBR2) plasmid was utilised to overexpress epitope-tagged UBR2 in HEK293T cells by transient transfection. To assess the importance of the N-end rule and non-N-end rule pathways in UBR2's localisation, point mutations in protein binding interfaces were introduced to *Ubr2* with a view to understand which domains of UBR2 might be involved in its localisation.

3.2 Results

3.2.1 Localisation of FLAG-UBR2 in HEK293T cells during the cell cycle

In order to confirm UBR2's localisation during interphase, FLAG-tagged UBR2 plasmid was transiently transfected into HEK293T cells. Our group had previously cloned the *Ubr2* CDS (coding sequence, exons only) into the plasmid p3XFLAG-Cmv-10, which encodes an N-terminal triple FLAG tag immediately upstream of a multiple cloning site where *Ubr2* CDS was cloned. The FLAG-UBR2 plasmid that is used in this experiment is functional in *in vitro* ubiquitylation assays (Lee *et al.*, 2011).

24 hours after transfection, the cells were fixed in 4% PFA and stained with α-FLAG and fluorescent antibodies before being imaged (Figure 3.1A). A control transfection using the empty plasmid containing only the promoter and the 3xFLAG tag (Cmv10-FLAG) and an untransfected control group was used to identify any background α-FLAG staining in the HEK293T cells. To aid identification of nuclear staining that can be distinguished from background, a Cmv10-3xFLAG-KAP1 (FLAG-KAP1) plasmid was transfected and stained in the same way. KAP1, a nuclear corepressor, is predominantly present in the nucleus (Wang *et al.*, 2007).

Examination of the control experiments showed that cells transfected with FLAG-KAP1 have strong readily detectable α-FLAG staining that is not present in the Cmv10-FLAG or untransfected controls (Figure 3.1A). Cells transfected with FLAG-UBR2 are similarly readily detectable by α-FLAG staining in this assay (Figure 3.1A). Based on the DAPI staining, which stains

DNA, the HEK293T cells scored in this experiment were in interphase. The α-FLAG staining of FLAG-UBR2 was classified into 3 groups: nuclear, cytoplasmic or nuclear-cytoplasmic based on the overlap with DAPI (Figure 3.1B). Overexpression of FLAG-UBR2 is predominantly nuclear in HEK293T cells; over 80% of the FLAG staining was nuclear and only a small percentage was found in the other two categories (Figure 3.1C). Western blots of the lysate following transfection confirmed that FLAG-KAP1 and FLAG-UBR2 protein successfully expressed from plasmids (Figure 3.1D). Immunoblotting with the α-FLAG antibody used in IF experiments revealed a ~100 kDa band in the FLAG-KAP1 lysate consistent with the predicted size of the FLAG-KAP1 fusion protein (89 kDa) and a band at the predicted size of FLAG-UBR2, 250 kDa, in the FLAG-UBR2 lysate.

Taken together, these data suggest that the FLAG-UBR2 plasmids can be successfully transfected into HEK293T cells and localise to the nucleus during interphase. The predominantly nuclear localisation of FLAG-UBR2 is consistent with IF of endogenous UBR2 protein (An *et al.*, 2012). The cytoplasmic and nuclear-cytoplasmic FLAG-UBR2 staining observed in the transfected HEK293T cells was not reported in previous IF studies on endogenous UBR2 protein in HeLa cells (An *et al.*, 2012).

Figure legend 3.1: FLAG-UBR2 localises to the nucleus in HEK293T cells. (**A**) Representative HEK293T cells, immunostained for FLAG in red, with DAPI shown in blue to mark DNA. HEK293T cells were fixed 24 hours after transfection of Cmv10-FLAG, FLAG-KAP1 or FLAG-UBR2 plasmids alongside an untransfected control. Scale bars are 10μm. (**B**) Examples of nuclear, cytoplasmic and nuclear-cytoplasmic staining categories for FLAG-UBR2 in HEK293T cells. (**C)** Interphase cells were identified by DAPI staining and the percentage of interphase cells with nuclear, cytoplasmic or nuclear-cytoplasmic anti-FLAG staining was determined for cells transfected with FLAG-UBR2. Data represents 3 independent transfections with 128, 241 and 253 interphase cells scored. (**D**) Western blot of HEK293T whole cell lysate following transfection. Blots were probed for FLAG, and for β-actin as a loading control. Arrow indicates FLAG-UBR2 protein.

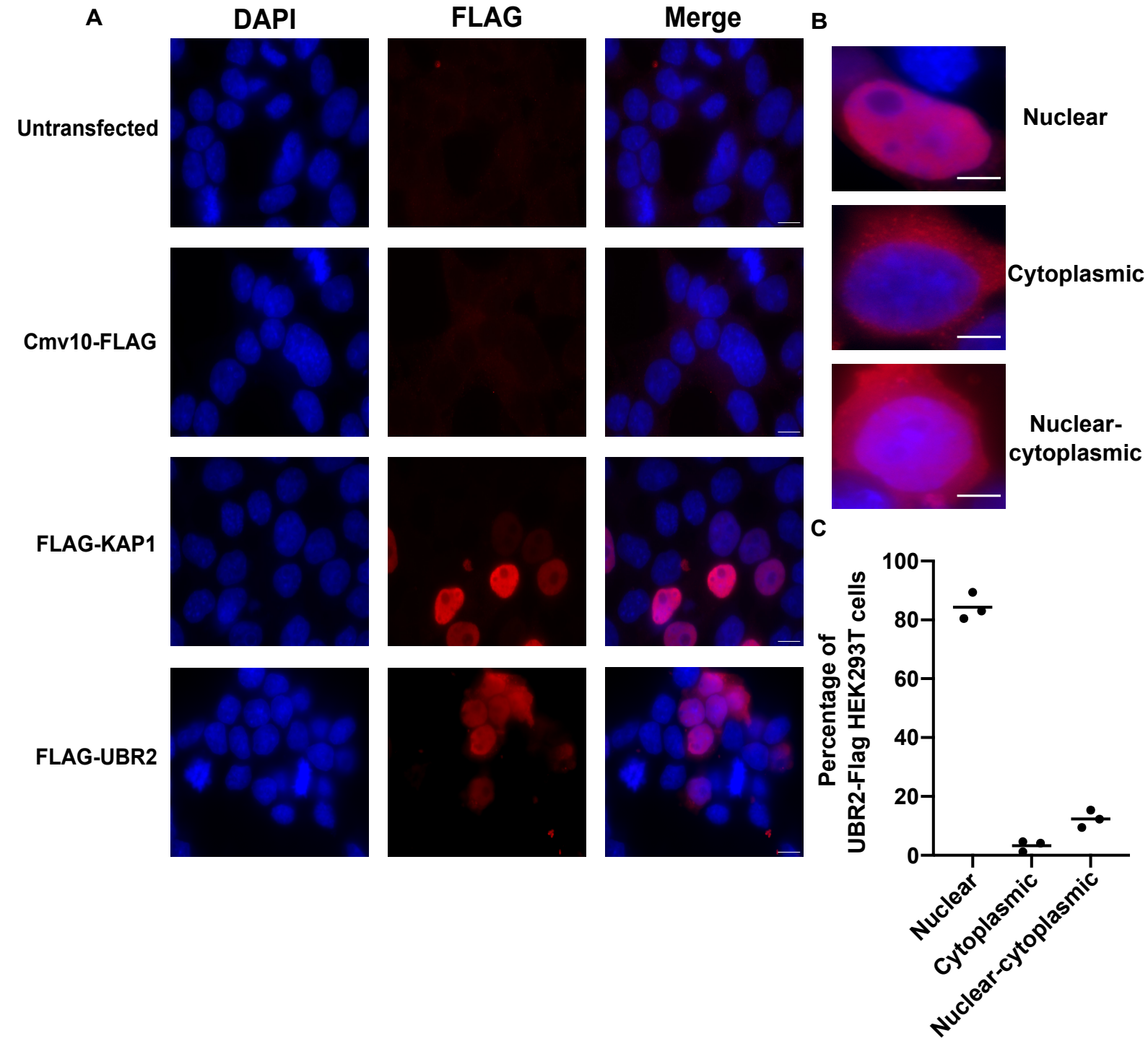
A
DAPI
FLAG
Merge
Untransfected
Cmv10-FLAG
FLAG-KAP1
FLAG-UBR2
B
Nuclear
Cytoplasmic
Nuclear-
cytoplasmic
C
Percentage of
UBR2-Flag HEK293T cells
100
80
60
40
20
0
Nuclear
Cytoplasmic
Nuclear-cytoplasmic

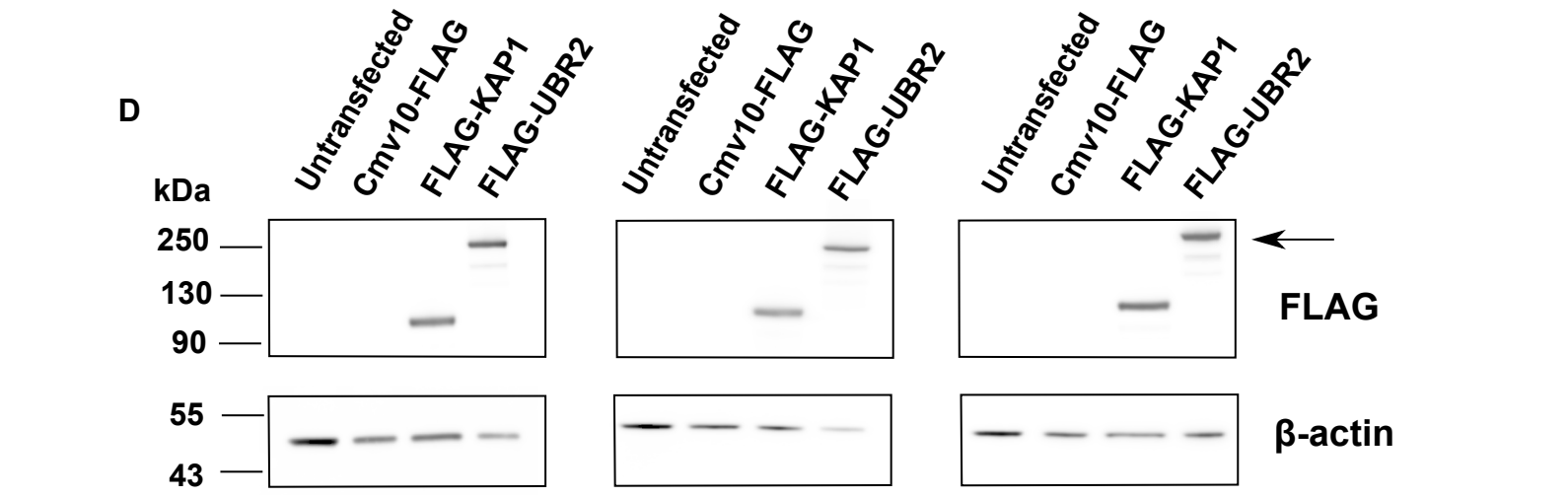
D
Untransfected
Cmv10-FLAG
FLAG-KAP1
FLAG-UBR2
kDa
250
130
90
55
43
FLAG
β-actin

UBR2 appears to have an impact on chromatin-associated cohesin during G2/M (Karen Dobie, unpublished). To see if there was any localisation of UBR2 to the chromatin during G2/M, HEK293T cells were synchronised with a single thymidine block which arrests cells mainly in S phase to ensure samples were collected within 48 hours after transfection. Following release, cells were taken at two hour intervals, up to 10 hours, to identify a time point where most of the cells were in G2/M (Figure 3.2A) which was determined to be around 6 hours post release. Subsequent transfections of the FLAG-UBR2 were undertaken and the cells were then synchronised with a single thymidine block and fixed after 6 hours release.

In this experiment, cells were immunostained with human auto-immune α-centromeric antigen (ACA) antibodies to visualise the centromeres. The α-FLAG localisation pattern appeared to be excluded from the DAPI-stained chromosomes at all mitotic stages (Figure 3.2B). The FLAG staining appears to surround the DAPI staining in the images which suggests there is no direct localisation of wild type FLAG-UBR2 to chromosomes in G2/M.

Figure legend 3.2: FLAG-UBR2 is excluded from the DAPI during G2/M. (**A**) FACS (fluorescence-associated cell sorting) plot of PI-stained (propidium iodide) cycling HEK293T cells has two peaks, one at G1 and one at G2/M, and a trough that was designated as S-phase. Profile for cycling HEK293T cells and at time points: 16hr thymidine, T+4, T+6, T+10. (**B**) Representative images of HEK293T cells following transient transfection of FLAG-UBR2 plasmid for 48 hours. HEK293T cells were enriched in G2/M by blocking the cells in thymidine then releasing for 6 hours, fixed and immunostained for FLAG in red, anti-centromeric antibody (ACA) in green with DAPI shown in blue to mark DNA. Stages of mitosis were identified by DAPI staining and the location of ACA. Scale bars are 10μm.

A

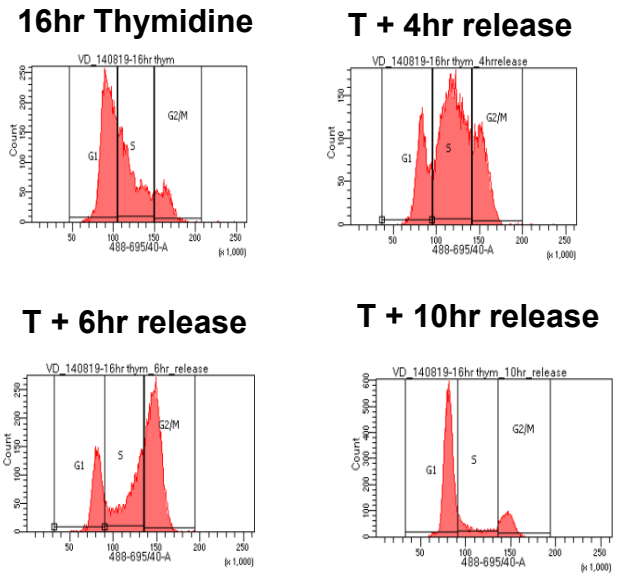
16hr Thymidine
T + 4hr release
T + 6hr release
T + 10hr release
G1
S
G2/M
Count
488-695/40-A

B

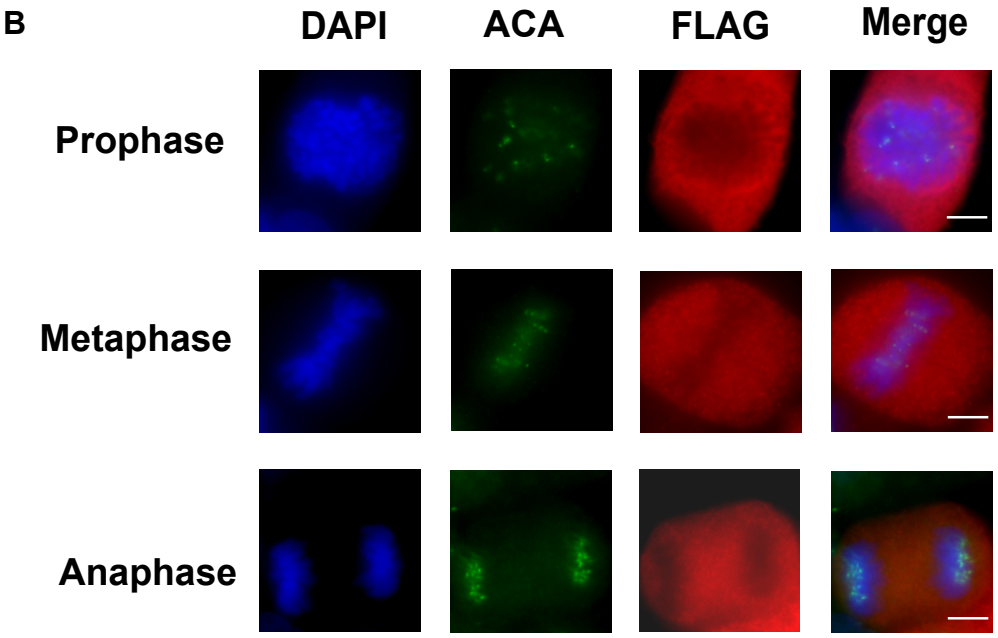
DAPI
ACA
FLAG
Merge
Prophase
Metaphase
Anaphase

3.2.2 Identification of mutations in protein-binding interfaces of UBR2

UBR2 has a role in the N-end rule protein recognition system of the UPS (Tasaki *et al.*, 2009). This is regulated by three protein domains (Figure 3.3A): the UBR box, a highly conserved zinc-finger-like structure that is found across all UBR proteins and binds to N-end rule substrates; the N-domain, which has high homology to bacterial ClpS domain and stabilises binding of type II N-end rule substrates to the UBR box; and the RING domain that mediates binding to E2 ubiquitin conjugating enzymes. Specific mutations in these domains can disrupt different aspects of UBR1/UBR2 function (Tasaki *et al.*, 2009).

Mutating D118A in the UBR box and D233A in the N-domain of UBR2 reduces binding of UBR2 to Type I and Type II N-end rule peptides respectively (Eleanor Raymond, unpublished). UBR2 appeared to have a much stronger affinity to Type II peptide recognition but there are known Type I substrates of UBR2 *in vivo*, such as the shared UBR1/UBR2 N-end rule Type I substrate SDE2 (Rageul et al., 2019). Mutating W1177A in the RING domain reduced the affinity of UBR2 for binding to the E2 ubiquitin conjugating enzymes USE1 and UBE2A/B (Lee *et al.*, 2011)

In further search of potential functional domains in UBR2, a lab member, Luis Sanchez-Pulido, analysed the predicted structure of UBR2 by aligning known structural variants in InterPro and identified a Winged Helix ELL-like domain (residues 779-858) between the N-domain and the RING domain (Figure

3.3A). This domain is highly conserved in eukaryotes and is found in both mammalian UBR1 and UBR3.

ELL-like domains are found in functionally diverse proteins where they mediate binding to diverse groups of ligands depending on the type of residues exposed by this domain. Cockayne syndrome group B protein (ERCC6) is a protein that has a winged helix ELL domain and its main function is ubiquitin binding (Takahashi *et al.*, 2019). Whilst forkhead box A3 (FOXA3) has a domain in a similar orientation to UBR2's winged helix ELL-like domain but has a role in DNA binding (Harami, Gyimesi and Kovács, 2013). However, the ELL-like domain in UBR2 does not have a similar conserved area or charge to the ligand-binding interface of the ELL domain in either of these proteins so it remains unclear if the domain in UBR2 is mediating binding to either ubiquitin or DNA.

A candidate residue in the UBR2 ELL domain that could potentially disrupt the structure of this domain when mutated, Lysine 834 (K834). K834 is highly conserved in mouse and humans as well as UBR1 and UBR3 (Figure 3.3B) and appears to coordinate a C-terminal capping of a key alpha helix within this domain (Figure 3.3C). The function of this conserved lysine residue and the whole ELL domain is unclear, but mutating this positively charged amino acid to a neutral amino acid could potentially disrupt the structure of this domain.

Figure 3.3: Structural prediction of the winged helix ELL-like domain in UBR2. (**A**) UBR2 domain structure with UBR box, N-domain, ELL domain, RING Domain and Autoinhibitory domain (AID) annotated (**B**) Protein sequence alignment of the ELL region in UBR proteins, showing homology. K834 (arrow) is conserved between human and mouse UBR1, UBR2 and UBR3 and UBR1 in yeast. (**C**) Predicted structure of the UBR2 ELL domain. K834 co-ordinates an α-helix in the centre of this domain. Adapted from image generated by Luis Sanchez-Pulido.

A

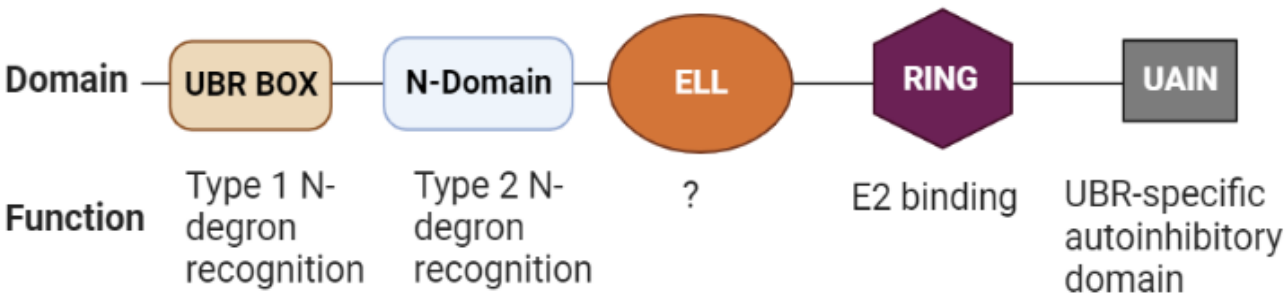

B

```
sp|P19812|UBR1_YEAST      ------FDEALEEVSVFV----EPKGLADNGVFKLKASLYAK-VDPLKLLNLENEFE---  996
sp|Q6ZT12|UBR3_HUMAN      IPGSYSFESVLSAVADFKAPVFEPGGSMQQGMYTPKAEVWDQEFDPVM-VILRTVYRRDV  878
sp|Q5U430|UBR3_MOUSE      IPGSYSFESVLSAVADFRAPIFEPGGSMQQGMYTPKAEVWDQEFDPVM-VILRTVYRRDV  878
sp|Q8IWV7|UBR1_HUMAN      -------ENVINKVATFKKPGV-----SGHGVYELKDESLK-DFNMYF-----YHYSKTQ  842
sp|O70481|UBR1_MOUSE      -------ENVINKVATFKKPGV-----SGHGVYELKDESLK-DFNMYF-----YHYSKTQ  842
sp|Q8IWV8|UBR2_HUMAN      -------ESVIEAVAHFKKPGL-----TGRGMYELKPECAK-EFNLYF-----YHFSRAE  852
sp|Q6WKZ8|UBR2_MOUSE      -------ESVIESVAHFKKPGL-----TGRGMYELKPECAK-EFNLYF-----YHFSRAE  852
                                 :..:. *: *            .*::  * .    .:          :
```

C

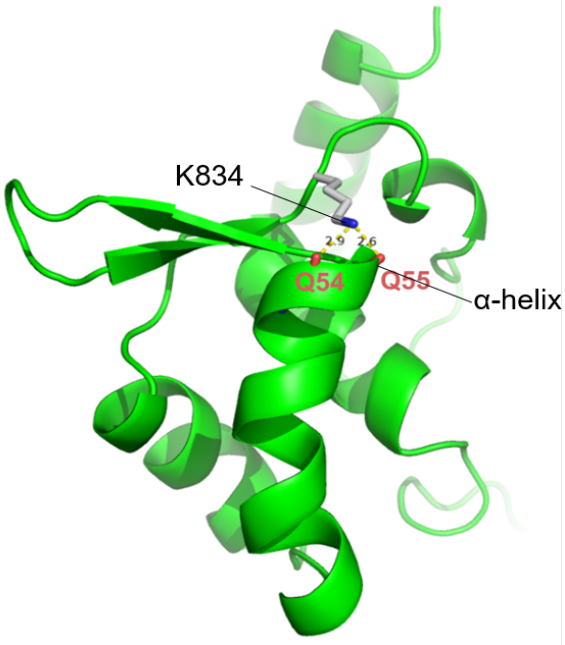

To determine if the ELL domain play a role in UBR2 function, the conserved K834 residue was mutated to alanine (K834A -GAC->GCC) by site-directed mutagenesis of the pCmv10-FLAG-UBR2 plasmid (Figure 3.4A). Oligonucleotide primers containing this point mutation were used generate a linear version of the pCmv10-UBR2-FLAG plasmid by PCR, which was then circularised. Sanger sequencing was used to verify the introductions of the K834A mutation (Figure 3.4B). This provided a tool to potentially identify a role of the ELL domain in UBR2's function.

Figure 3.4: Site-directed mutagenesis of the *Ubr2* CDS (**A**) Schematic representation of the pCmv10-FLAG-UBR2 plasmid, with the *Ubr2* CDS (coding sequence) inserted into the multiple cloning site of pCmv10-FLAG-UBR2 downstream of the N-terminal 3xFLAG tag sequence. Locations of the K834A residue are shown, which is mutated using site-directed mutagenesis in this screen. (**B**) Sanger sequencing data for the UBR2-K834A mutant CDS, the K834A mutation is underlined, GAC->GCC.

A

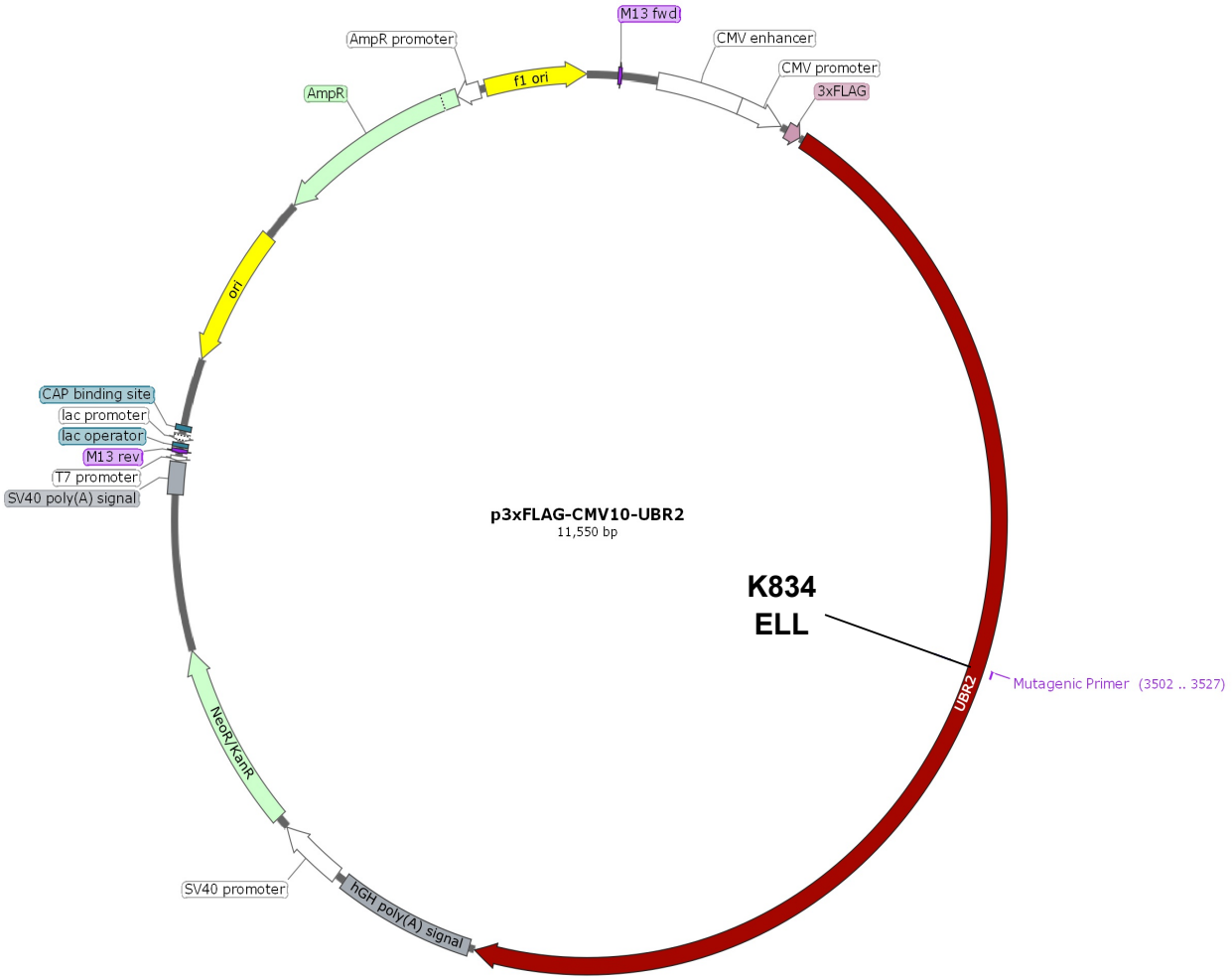

B

AAG > GCG
K834A

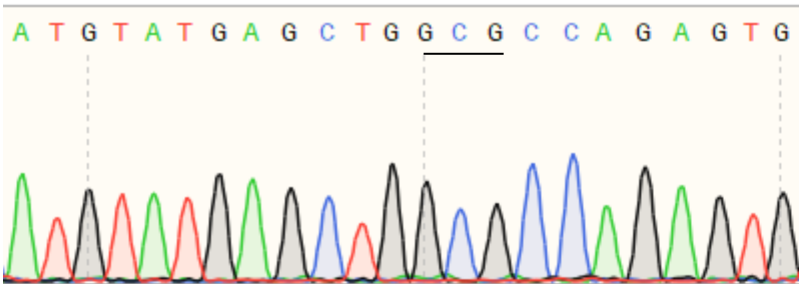

Firstly, to investigate if the ELL mutation affected UBR2's ability to bind to substrates in the N-end rule pathway, HEK293T cells were transfected with the FLAG-UBR2 or the FLAG-ELL-UBR2 plasmids to overexpress the protein. Cell lysates were collected and were used to perform a peptide pulldown assay.

Different peptides were chemically conjugated to resin beads via a C-terminal Cysteine residue, allowing immobilisation of the peptide via a thioether bond. Each peptide has a specific amino acid at their N-terminal end: Type I (arginine, TI), Type II (phenylalanine, TII) or a stabilising negative control (glycine, -ve) (Figure 3.5A). The beads were incubated in whole cell lysate from the transfected HEK293T cells to allow proteins that bind to these peptides to be isolated then assayed by Western blotting against the N-terminal FLAG-tag of the overexpressed UBR2 protein.

Previous studies have shown that wild-type UBR2 has low Type I (TI) binding and strong Type II (TII) binding ability (Tasaki *et al.*, 2005) which was observed in FLAG-UBR2 transfected HEK293T lysates but there did appear to have stronger TI binding than previously observed (Figure 3.5B). The –ve (stabilising, glycine) peptide is the negative control that pulls down a very low level of FLAG-tagged UBR2 protein in both FLAG-UBR2 and FLAG-ELL-UBR2 samples over all three repeats (Figure 3.5B). There was strong band in the input of the second FLAG-UBR2/FLAG-ELL-UBR2 repeat which was absent in the other two samples due to a technical error in loading. Similar amounts of FLAG-UBR2 and FLAG-ELL-UBR2 protein are present in the TI

and TII pull-downs over three independent repeats (Figure 3.5B) indicating that the K834A mutation does not impact the ability of UBR2 to bind to Type I or Type II N-end rule peptides in this assay.

Figure 3.5 ELL-UBR2 mutation does not prevent substrate binding (**A**) Sequences of peptides chemically conjugated to resin beads used in a peptide pulldown assay. N-terminal residues R, F or G are Type I, Type II or negative control peptide sequences, respectively. (**B**) Western blots showing 3 independent repeats of a peptide pulldown after overexpression of UBR2-FLAG and ELL-UBR2-FLAG (K834A) in HEK293T cells. I, 5% input protein. TI, Type I (arginine). TII, Type II (phenylalanine). –ve, negative (glycine, stabilising) control. Probed using anti-FLAG M2 antibody for the N-terminally FLAG tagged UBR2 protein. * indicates a possible isoform of the UBR2 protein. Arrow indicates the band of interest.

A

Type I (TI)	RIFSTDTGPGGC	Arginine (R)
Type II (TII)	FIFSTDTGPGGC	Phenylalanine (F)
-ve Control	GIFSTDTGPGGC	Glycine (G)

B

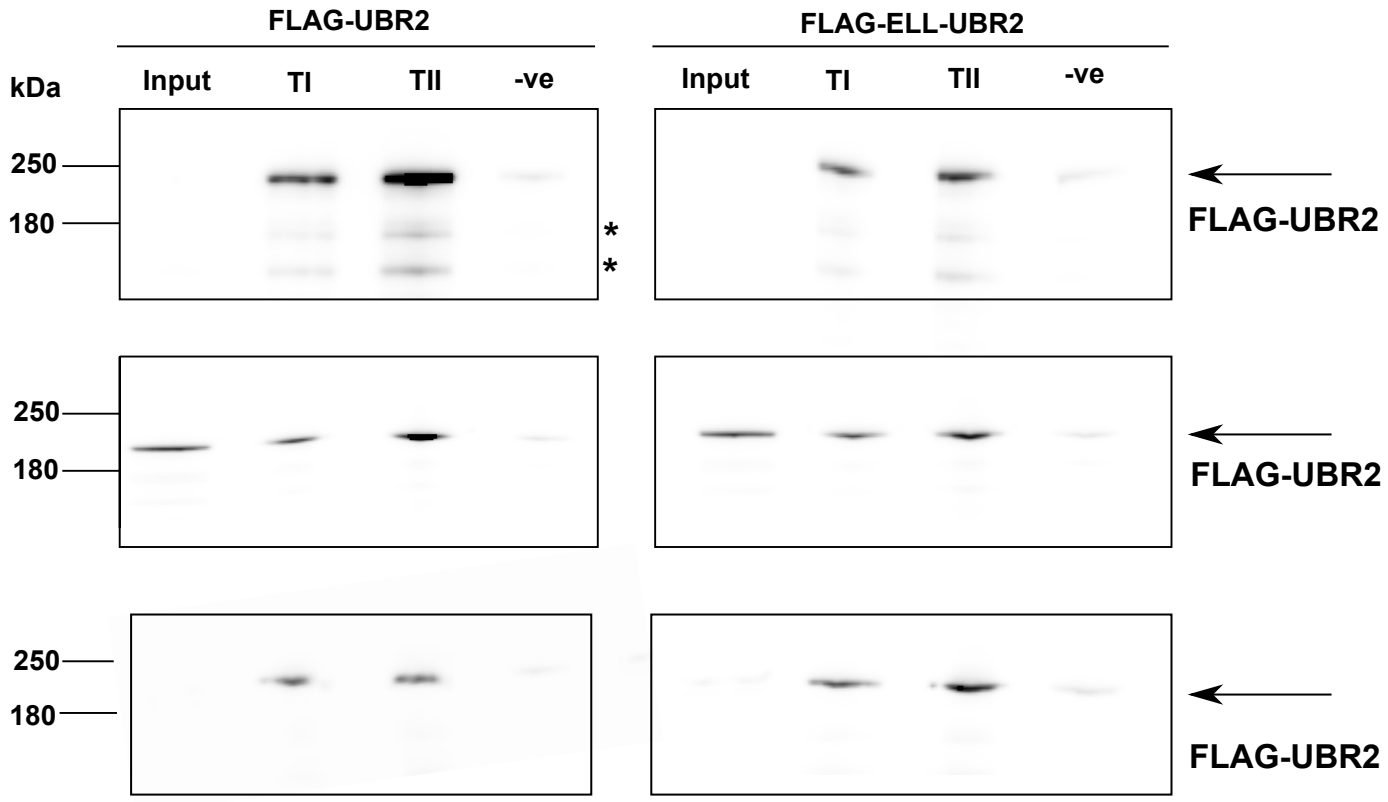

One other validated molecular function of UBR2 is the stoichiometric interaction with TEX19.1 (Reichmann *et al.*, 2020) so FLAG-UBR2 and FLAG-ELL-UBR2 plasmids and GFP-tagged TEX19.1 plasmid (pCAAGS-TEX19.1-GFP) were cotransfected into HEK293T cells. Co-immunoprecipitation was performed with GFP-Trap Agarose beads to pull down the TEX19.1 protein and any interacting proteins.

TEX19.1-GFP pulls down wild type FLAG-UBR2 (Figure 3.6, GFP-Trap, lane 2) but GFP alone cannot pull down FLAG-UBR2 (Figure 3.6, GFP-Trap, lane 4). FLAG-ELL-UBR2 can co-immunoprecipitate with TEX19.1-GFP (Figure 3.6, GFP-Trap, lane 3). As seen with FLAG-UBR2, pCAGGS-GFP does not pull down FLAG-ELL-UBR2 (Figure 3.6, GFP-Trap, lane 5). Two other controls were used in the Co-IP experiment, coexpression of the Cmv10-FLAG construct with TEX19.1-GFP and pCAGGS-GFP co expressed with Cmv10-FLAG construct did not pull down anything detectable with the FLAG antibody (Figure 3.6, GFP-Trap, Lane 1 and 6). The K834A mutation does not disrupt the ability of UBR2 to bind to TEX19.1.

In this section, using both peptide pulldown assays and coimmunoprecipation with known interactor TEX19.1, the ELL K834A point mutation within UBR2 was shown to have no impact on either Type I (Arg) or Type II (Phe) N-end rule or TEX19.1 binding. Therefore, the K834A mutation does not impact UBR2’s binding in peptide pulldown assays.

Figure 3.6 Mutating UBR2's ELL domain does not impair its interaction with TEX19.1 Representative Western blot from 3 co-immunoprecipitation assays with GFP-Trap beads, after co-transfection of either wild type FLAG-UBR2 or FLAG-ELL-UBR2 (pCmv10-FLAG-UBR2 or pCmv10-FLAG-ELL-UBR2) with TEX19.1-GFP (pCAAGS-Tex19.1-GFP). Controls: FLAG and GFP are the pCmv10-FLAG and pCAAGS-GFP transfected to ensure no crossreaction of the tags with proteins of interest. Probed using anti-FLAG M2 antibody for the N-terminally FLAG tagged UBR2 protein and anti-GFP antibody for the GFP-tagged TEX19.1 protein.

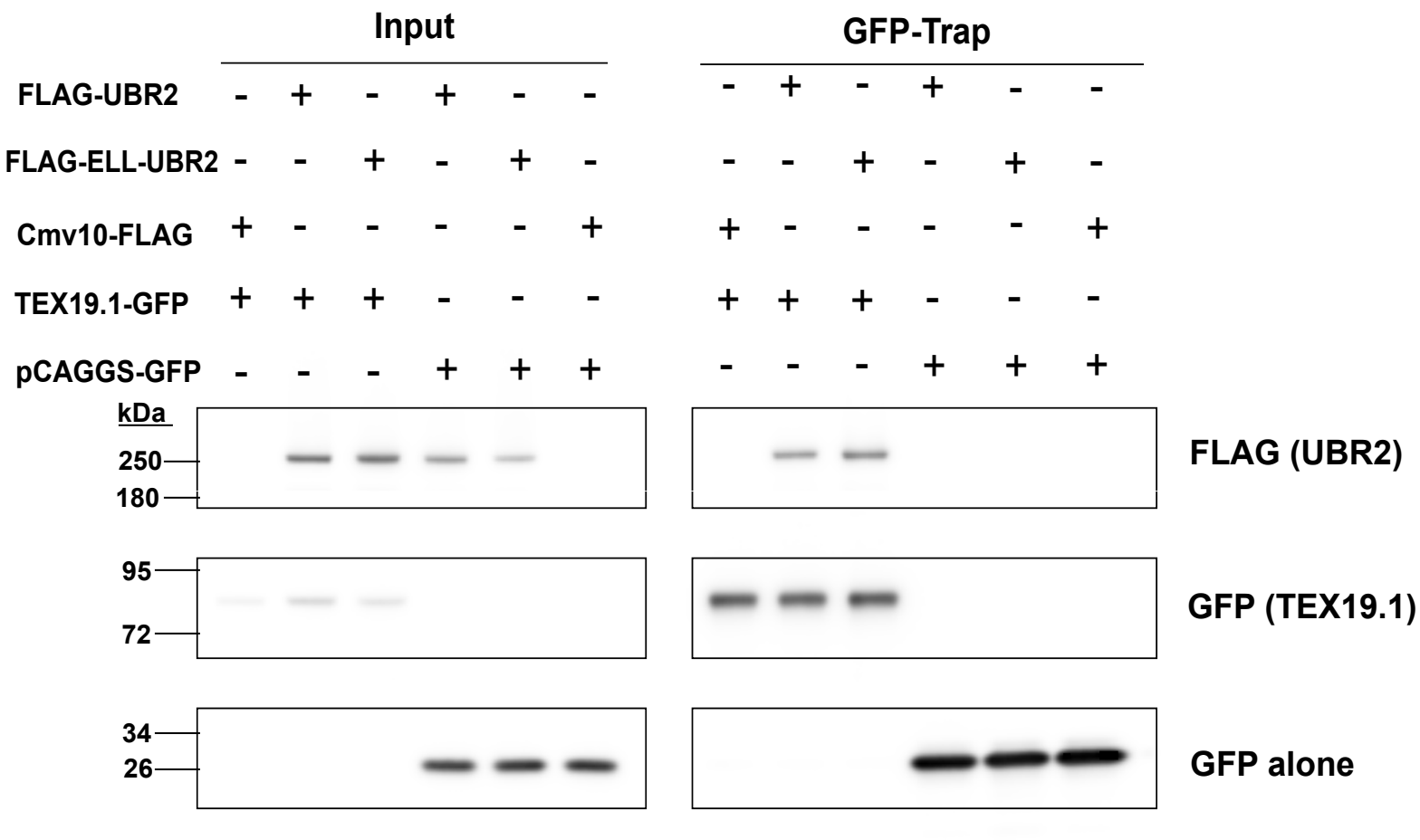
Input
GFP-Trap
FLAG-UBR2 - + - + - - - + - + - -
FLAG-ELL-UBR2 - - + - + - - - + - + -
Cmv10-FLAG + - - - - + + - - - - +
TEX19.1-GFP + + + - - - + + + - - -
pCAGGS-GFP - - - + + + - - - + + +
kDa
250
180
95
72
34
26
FLAG (UBR2)
GFP (TEX19.1)
GFP alone

3.2.3 Localisation of UBR2 plasmids with mutations in protein binding interfaces in HEK293Ts

The point mutations in protein binding interfaces impairing UBR2 N-end rule substrate binding (T1-UBR2 or T2-UBR2), E2 binding (RD-UBR2) or the ELL mutation (ELL-UBR2) can be used to test whether these interfaces are required to recruit UBR2 to the nucleus or to chromatin. As previously, FLAG-UBR2 was excluded from chromatin during mitosis by IF (Figure 3.2A) which did not match previous cell fractionation data showing an increase in UBR2 in chromatin during G2/M (An *et al.*, 2012).

To determine if mutations in these protein binding interfaces of FLAG-UBR2's could change its localisation during mitosis, these plasmids were transfected into HEK293T cells and synchronised into G2/M as above (Figure 3.7A). FLAG-ELL-UBR2 was used to determine if the ELL mutation had an impact on UBR2's localisation.

During metaphase, α-FLAG staining in the FLAG-T1-, T2- or RD-UBR2 transfected cells was excluded from DAPI-stained chromosomes and looked similar to FLAG-UBR2 staining (Figure 3.7A). However, the FLAG-ELL-UBR2 construct displayed a strikingly different localisation pattern showing strong enrichment on mitotic chromosomes, shown by DAPI staining, in a proportion of the transfected cells. Thus, the K834A mutation in the ELL domain of UBR2 appears to promote the localisation of UBR2 to mitotic chromosomes.

As only a proportion of mitotic FLAG-ELL-UBR2 transfected cells showed localisation of UBR2 to chromosomes. I quantified this proportion across

three replicate transfections and ~30% of FLAG-ELL-UBR2 transfected mitotic cells displayed chromosome-associated α-FLAG immunostaining, whereas this pattern was not seen in cells transfected with FLAG-UBR2 (Figure 3.7B). FLAG-ELL-UBR2 protein abundance in transfected HEK293T lysates was similar to the abundance of FLAG-UBR2 and other mutant FLAG-UBR2 proteins (Figure 3.7C). Thus, the FLAG-ELL-UBR2 protein appears to be stable and expressing at similar levels in the HEK293Ts as the other FLAG-UBR2 proteins.

However, it remains unclear as to why the K834A mutation leads to FLAG-UBR2 associating with chromatin in ~30% of transfected cells. One possible explanation is that the ELL mutation has made UBR2 have a higher affinity to chromatin-associated targets. Possible targets could be chromatin-associated cohesin or histones due to the link between UBR2 and AcSMC3 subpopulation of cohesin and histone ubiquitylation (An *et al.*, 2012; Reichmann *et al.*, 2020).

Figure 3.7 FLAG-ELL-UBR2 can colocalise with DAPI in HEK293Ts (**A**) HEK293T metaphase cells following overexpression of, FLAG-UBR2 or FLAG-T1-UBR2 (D118A), FLAG-T2-UBR2 (D233A) or FLAG-RD-UBR2 (W1177A) and FLAG-ELL-UBR2 (K834A) plasmids for 24 hours. HEK293T cells were synchronised following a thymidine block, fixed and immunostained for FLAG in red, anti-centromeric antibody (ACA) in green with DAPI shown in blue to mark DNA. Scale bars are 10μm. (**B**) Percentage of HEK293T mitotic cells with FLAG expression excluded from the DAPI or colocalised with the DAPI following FLAG-UBR2 transfection, data represents 3 independent transfections with 19, 21 and 24 metaphase cells scored, or FLAG-ELL-UBR2 transfection, data represents 3 independent transfections with 28, 27 and 22 metaphase cells scored. ** P-value <0.01, Students T-test. (**C**) Western blot images of the lysates from three independent repeats of the HEK293T cells following transfection of FLAG-UBR2, FLAG-T1-UBR2, FLAG-T2-UBR2, FLAG-RD-UBR2 and FLAG-ELL-UBR2, probed for FLAG and β-actin as a loading control. * indicates a possible isoform of the UBR2 protein.

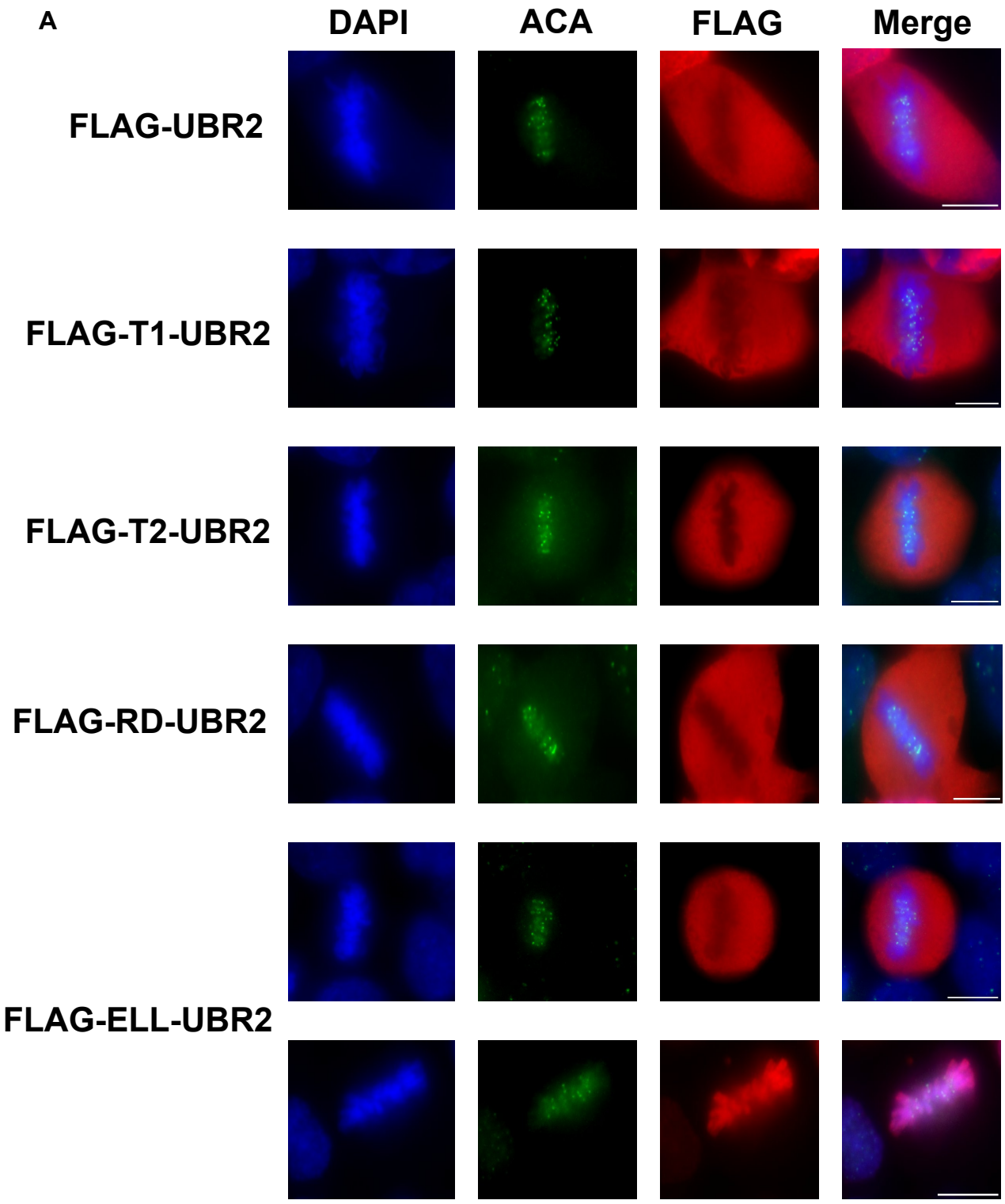
A
DAPI
ACA
FLAG
Merge
FLAG-UBR2
FLAG-T1-UBR2
FLAG-T2-UBR2
FLAG-RD-UBR2
FLAG-ELL-UBR2

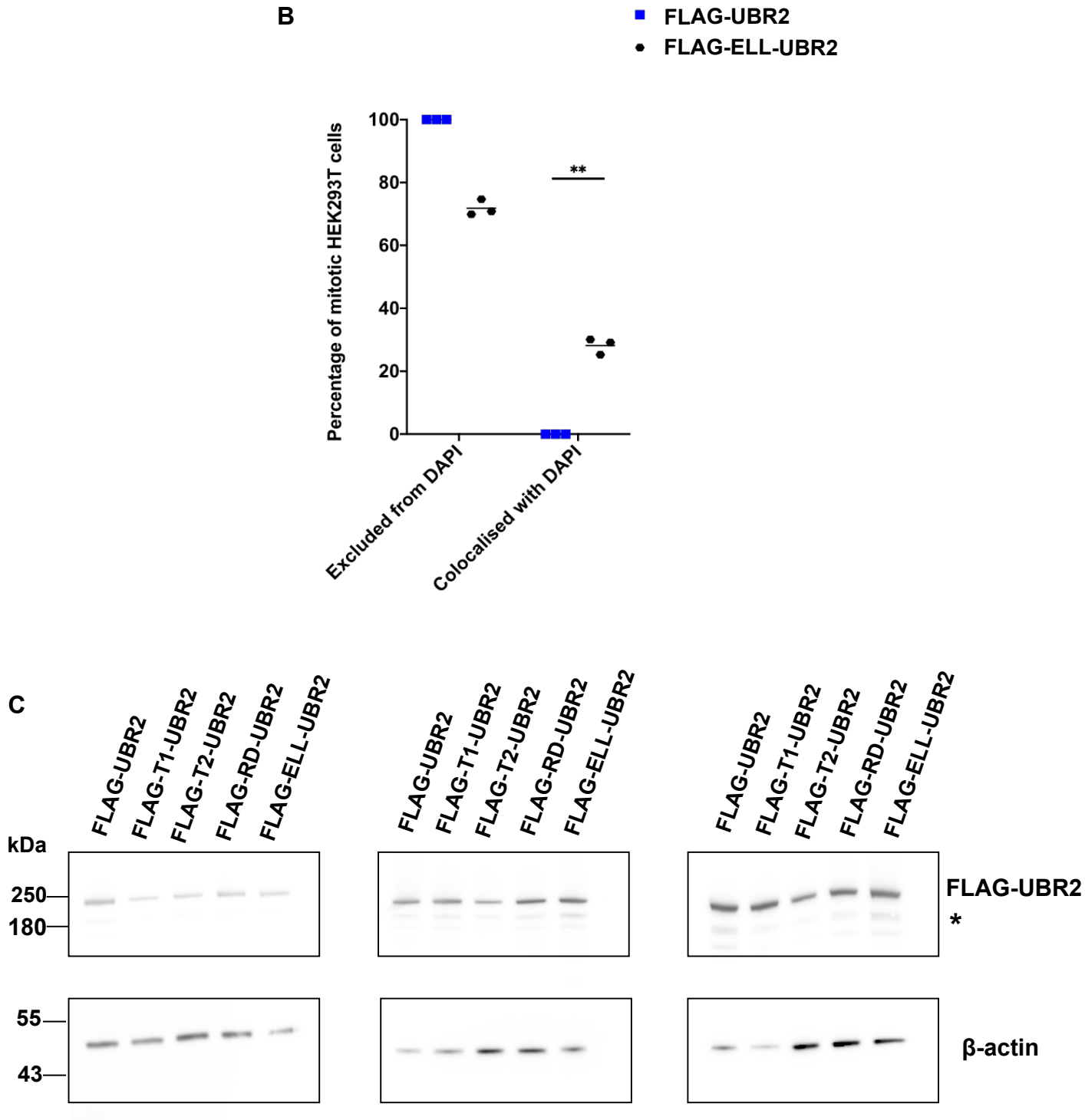
B
FLAG-UBR2
FLAG-ELL-UBR2
Percentage of mitotic HEK293T cells
100
80
60
40
20
0
**
Excluded from DAPI
Colocalised with DAPI
C
FLAG-UBR2
FLAG-T1-UBR2
FLAG-T2-UBR2
FLAG-RD-UBR2
FLAG-ELL-UBR2
kDa
250
180
55
43
FLAG-UBR2
*
β-actin

To determine whether cohesin could be a potential target for FLAG-ELL-UBR2, HEK293T cells transfected were analysed at anaphase. During mitosis, most of cohesin and cohesin associated proteins are removed from the chromosomes through the prophase pathway whereas others from centromeres at the onset of anaphase (Waizenegger *et al.*, 2000). Therefore if it is cohesin that FLAG-ELL-UBR2 is binding too, it would not be present along chromosome arms during anaphase. The colocalisation to the DAPI pattern can be seen in FLAG-ELL-UBR2 cells during anaphase (Figure 3.8A) which suggests that the change in FLAG-ELL-UBR2 localisation is not due to binding to chromatin-associated cohesin rather to some unknown substrate.

To identify any potential substrates that could be responsible for the change in localisation, anti-FLAG IP mass spectrometry (MS) was performed by Karen Dobie in our group. HEK293T cells were transfected with FLAG-UBR2 and FLAG-ELL-UBR2, synchronised in G2/M using a thymidine block and release and anti-FLAG immunoprecipitates analysed by label-free quantitative mass spectrometry. The Max Label-free quantification (LFQ) intensity of proteins identified in the mass spectrometry of FLAG-UBR2 and FLAG-ELL-UBR2 were compared (Figure 3.8B) and 34 proteins were pulled down with FLAG-ELL-UBR2 that were not detected with FLAG-UBR2, 10 of these proteins were of particular interest as they are primarily expressed in the nucleus (Figure 3.8C). These substrates should be investigated to determine if they could potentially be chromatin associated during mitosis and localises FLAG-ELL-UBR2 to chromatin.

Our group have previously shown that UBR2 has a role in splenocytes (Reichmann *et al.*, 2020) and embryonic stem cells (Karen Dobie, unpublished) in the regulation of the AcSMC3-containing subpopulation of cohesin complexes, which is thought to mediate sister chromatid cohesin. In *Ubr2*$^{-/-}$ splenocytes, chromatin-associated AcSMC3 increases, a phenotype that is also present in *Ubr2*$^{-/-}$ ES cells. Importantly, UBR2 specifically regulates AcSMC3-containing cohesin complexes, which is a relatively minor population of cohesin in cells, and specific effects on this population typically do not cause detectable changes in the abundance of other cohesin subunits, such as total SMC3. Interestingly, there were no cohesin subunits immunoprecipitates detected in the mass spectra following transfection with either FLAG-UBR2 or FLAG-ELL-UBR2 plasmids that may suggest that UBR2 is not binding directly to cohesin.

Regulatory monoubiquitination of histone H2A that leads to repressive chromatin structure and transcriptional silencing is important for processes such as X-inactivation (Cohen and Lee, 2002). In somatic cells, the canonical E3 ubiquitin ligase associated with this is RING1B (Cohen and Lee, 2002) but UBR2 has been implicated in the ubiquitylation of Histone H2A. This is reported to be important for transcriptional silencing in spermatocytes (An *et al.*, 2010) and chromosome stability in somatic cultured fibroblasts (An *et al.*, 2012). Multiple histone variants were identified, including a member of the H2A family, in the anti-FLAG immunoprecipitates in both FLAG-UBR2 and FLAG-ELL-UBR2 lysates (Figure 3.8D). Both FLAG-UBR2 and FLAG-ELL-

UBR2 bind all histone variants detected in the mass spectra indicating the UBR2 can bind directly to histones in HEK293T cells.

Figure 3.8 FLAG-ELL-UBR2 colocalises to DAPI during anaphase (**A**) Representative images of Anaphase stage HEK293T cells following overexpression of FLAG-ELL-UBR2. HEK293T cells were synchronised following a thymidine block, fixed and immunostained for FLAG in red, anti-centromeric antibody (ACA) in green with DAPI shown in blue to mark DNA. Scale bars are 10μm. (**B**) Comparison of max LFQ intensity of proteins identified by FLAG-IP mass spectrometry following transfection of FLAG-UBR2 and FLAG-ELL-UBR2 in HEK293T cells synchronised to G2/M. Points in blue are the hits identified to be pulled down in FLAG-ELL-UBR2 but not in FLAG-UBR2. (**C**) List of nuclear proteins identified that were pulled down in FLAG-ELL-UBR2 FLAG-IP only and the Max LFQ intensity. All IP hits were not pulled down in FLAG-UBR2 FLAG-IP. (**D**) Comparison of max LFQ intensity of proteins identified by FLAG-IP mass spectrometry following transfection of FLAG-UBR2 and FLAG-ELL-UBR2 in HEK293T cells synchronised to G2/M. Gene symbols of identified histone variants are in red.

A

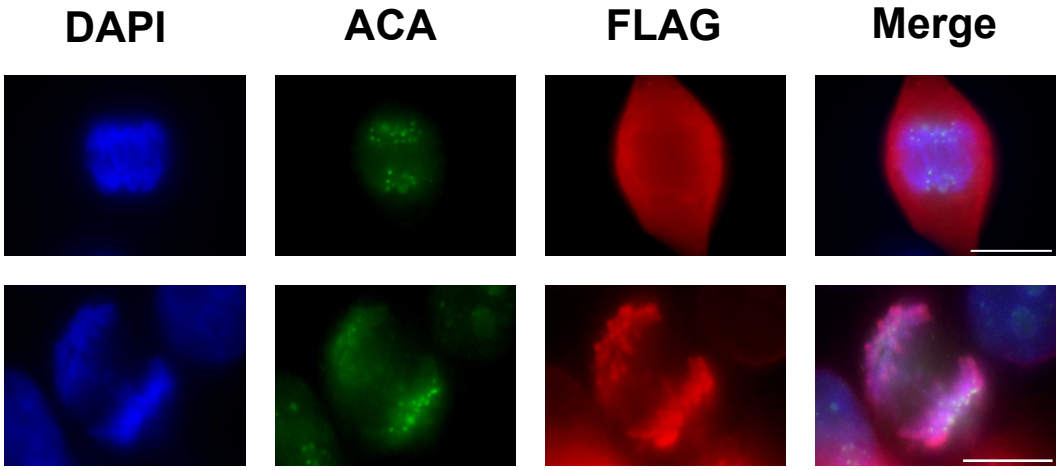

B

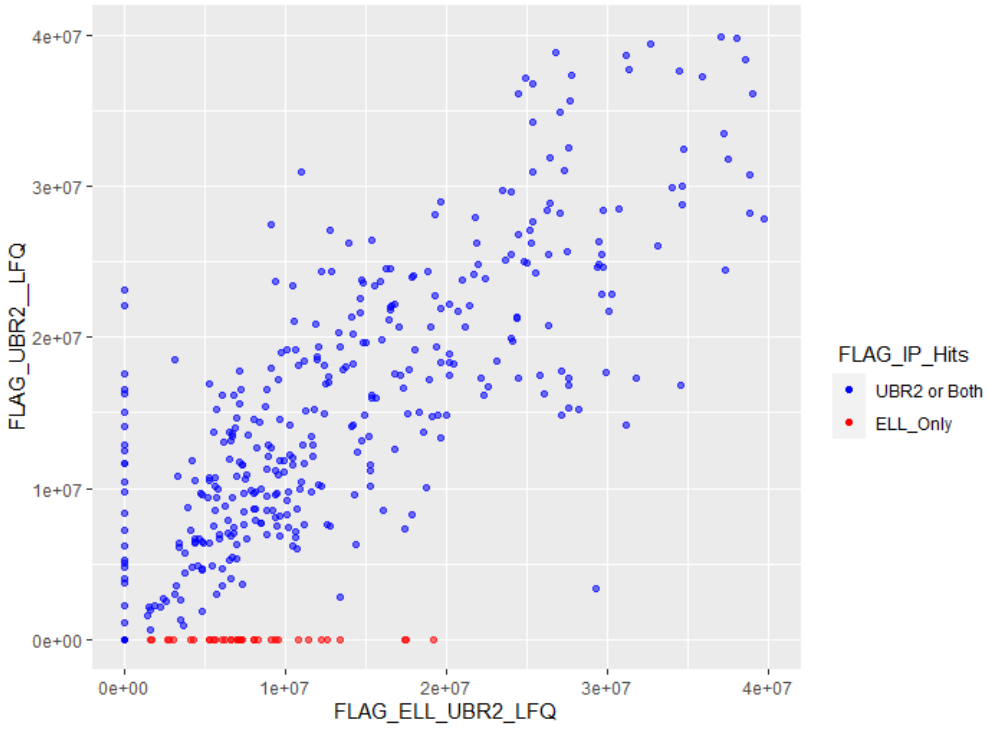

C

Gene	Protein Name	FLAG-ELL-UBR2 Max LFQ
XRCC6	Isoform 2 of X-ray repair cross-complementing protein 6	17385726
EDC4	Isoform 2 of Enhancer of mRNA-decapping protein 4	13323243
ZC3H11A	Zinc finger CCCH domain-containing protein 11A	8234615
TAB1	TGF-beta-activated kinase 1 and MAP3K7-binding protein 1	9535248
PES1	Isoform 2 of Pescadillo homolog	8010320
NOL4	Isoform 2 of Nucleolar protein 4	7216327
GATAD2A	Isoform 2 of Transcriptional repressor p66-alpha	7010249
PRKRIP1	PRKR-interacting protein 1	4244786
HNRNPA0	Heterogeneous nuclear ribonucleoprotein A0	3036983
SMARCAL1	SWI/SNF-related matrix-associated actin-dependent regulator of chromatin subfamily A-like protein 1	2644508

D

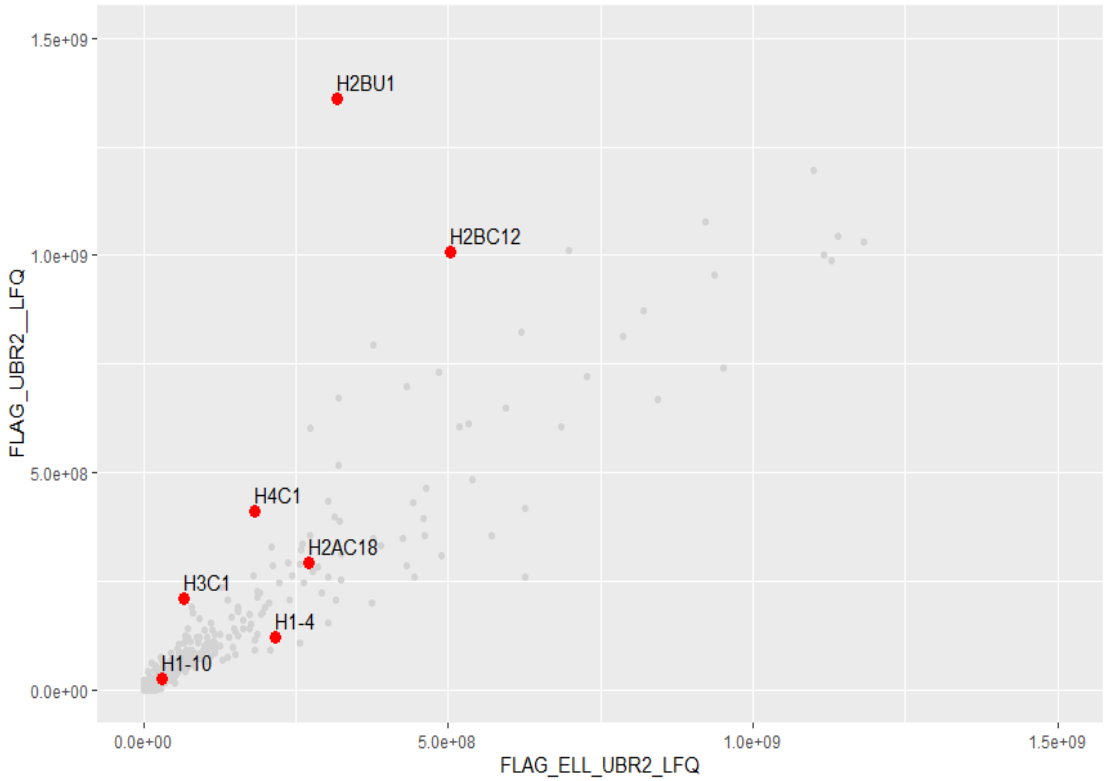
1.5e+09
1.0e+09
5.0e+08
0.0e+00
FLAG_UBR2__LFQ
H2BU1
H2BC12
H4C1
H2AC18
H3C1
H1-4
H1-10
0.0e+00
5.0e+08
1.0e+09
1.5e+09
FLAG_ELL_UBR2_LFQ

3.3 Discussion

In this chapter, I determined the localisation of FLAG-UBR2 in HEK293T cells and whether the localisation of FLAG-UBR2 depended on some of the known protein-binding interfaces of UBR2. Mutations in the UBR box, N-domain and RING domain did not change the localisation of FLAG-UBR2 at G2/M but there was a change in localisation to the chromatin in a subset of cells when the ELL K834A mutation was introduced to FLAG-UBR2.

3.3.1 FLAG-UBR2 does not localise to chromatin during G2/M

Anti-FLAG staining of FLAG-UBR2 was mainly found in the nucleus during interphase but surrounds the DAPI in G2/M which suggests there is no direct localisation of FLAG-UBR2 to chromosomes during G2/M. These observations do not align with the analysis of endogenous UBR2 localisation in fractionated cell compartments in HeLa cells where UBR2 is enriched with chromatin when synchronised to G2/M (An *et al.*, 2012).

This could be related to differences in cell types and behaviour between overexpressed FLAG-tagged UBR2 and endogenous UBR2 during G2/M. Expression levels of proteins in eukaryotes can vary by more than 10,000-fold (Kulak *et al.*, 2014), the degree of the overexpression of FLAG-UBR2 in these experiments may differ by some orders of magnitude. The data from the HEK293T cells in this section show the consequences of comparably strong production of FLAG-UBR2 and overexpression of proteins can cause deleterious effects on cells, promiscuous interactions or even impede cellular

growth (Moriya, 2015). However, overexpression of FLAG-UBR2 did not impair cell growth and anti-FLAG IF predominantly localised to the nucleus during interphase in HEK293T cells (Figure 3.1A) which mimics that seen by IF for endogenous UBR2 in mouse embryonic fibroblasts, U2OS and HeLa cells (An *et al.*, 2012) indicating that FLAG-UBR2 has the same localisation pattern to endogenous protein.

As previously stated, *An et al* reports UBR2 as nuclear associated in interphase stages of the cell cycle detected by IF staining in HeLa cells. Yet cell fractionation data (chromatin-bound, nuclear soluble and cytoplasmic) collected throughout the cell cycle shows very low UBR2 protein levels in the nuclear and chromatin-bound fractions in G1 and S-phase with a strong increase in chromatin-bound UBR2 protein levels at G2/M (An *et al.*, 2012). There is no IF staining of endogenous UBR2 at G2/M in this paper making it difficult to confirm whether UBR2 is localising to chromatin at this stage. This suggests that there may be issues with the endogenous antibody used in these experiments and that it may not be suitable for either IF or the Western blotting of the fractionation lysates. Repeats of experiments completed by *An et al* with a different endogenous UBR2 antibodies may help clarify this contradicting data.

UBR2 has a role in turnover of chromatin-associated AcSMC3 cohesin in somatic spleenocytes and ES cells during G2/M (Reichmann *et al.*, 2020, Karen Dobie, Unpublished) but it remains unclear whether UBR2 directly interacts with cohesin in cells or via intermediates. As the anti-FLAG IF signal

is specific for the FLAG-UBR2 construct, UBR2 is not chromatin bound during G2/M (Figure 3.2). One key thing that should be undertaken is to analyse fractionation data of the cells at G2/M following overexpression of FLAG-UBR2 and if an increase in FLAG-UBR2 leads to a change of AcSMC3 levels observed in splenocytes and ESCs. Also, overexpressing the FLAG-UBR2 construct in ESCs to identify localisation of UBR2 in the cell type that has the cohesin phenotype.

Three mutations in protein binding interfaces were introduced to the FLAG-UBR2 CDS. FLAG-T1-UBR2- and FLAG-T2-UBR2 mutations have been shown to perturb the type I and type II peptide binding ability of UBR2 (Eleanor Raymond, Unpublished). FLAG-RD-UBR2 has the W1177A mutation in UBR2's RING domain which has previously been shown to reduce the binding of E2s, USE1 and UBE2A (Lee *et al.*, 2011) were used to investigate whether perturbing UBR2's well characterised binding domains leads to a change in localisation. The mutations did not change the localisation of UBR2 during G2/M suggesting that the interfering with some of the known binding interfaces does not change is localisation. Further indicating the lack of any localisation between UBR2 and chromosomes in HEK293T cells at G2/M in this experiment setup.

3.3.2 FLAG-ELL-UBR2 localises to chromatin during G2/M

UBR2 appears to have an ELL-like structural domain located between the N-domain and the RING-domain. Recently, the molecular structure of yeast Ubr1 was elucidated and had a winged helical domain (WHD) after the Ubr-Box2 (known as the N-domain in UBR2) (Pan *et al.*, 2021). In the initiation complex, Ubr1 had a helical scaffold consisting of four regions interspaced by three domains: the Ubr1-Box1, Ubr-Box2 and the WHD. The WHD was shown to interact with other domains within Ubr1 like the autoinhibitory UBR/Leu/Cys (UBLC) domain and participate in the interaction with donor Ub alongside the RING finger domain during ubiquitination of target substrates (Pan *et al.*, 2021). The mutation K834A was introduced to FLAG-UBR2 plasmids due to the high conservation of K834 and exposure in this region of UBR2. Mutations to K834 is predicted to disrupt the structure of the ELL domain as the residue has a role in coordinating a central alpha-helix (Luis Sanchez-Pulido, Unpublished).

The introduction of the K834A mutation to FLAG-UBR2 did not produce different binding patterns to TEX19.1-GFP or TI or TII peptides to what was observed in wild type FLAG-UBR2. However, it is worthy to note that the variability of the TI and TII assay, which is difficult to standardise against loading controls, means that it’s difficult to detect if ELL mutation does perturb the type I or II binding ability of the UBR box and N-domain in a minor way.

The key difference between FLAG-ELL-UBR2 and the other FLAG-UBR2 plasmids is the change in localisation in FLAG IF staining in 30% of metaphase cells. It is unclear what would cause this change in localisation and why it only occurs in a subset of HEK293T cells rather than the majority. There may be specific post-translational modifications to the FLAG-ELL-UBR2 protein or misfolding in this subgroup of cells due to activation of processes such as signal-transduction pathways (Wang and Kaufman, 2016). A limitation of this study is that the cells are fixed before IF staining so there is only a snapshot of what is happening in the cell, live cell imaging that tracks FLAG-ELL-UBR2 throughout mitosis may give further insight into when the protein is localising to chromatin more transiently or are permanently localised in some cells.

One possible explanation for the change in localisation could be that FLAG-ELL-UBR2 is localising to chromatin at metaphase due to an increase in binding to a potential chromatin-associated substrate for protein turnover or stabilisation. To identify a substrate that may be of interest for further investigation, a FLAG-IP MS was undertaken and 10 proteins were pulled down with FLAG-ELL-UBR2 and not with FLAG-UBR2 that were predominantly nuclear (Figure 3.8C). FLAG-ELL-UBR2 was able to pull down 34 hits in the FLAG-IP not detected with wildtype FLAG-UBR2 indicating that the ELL mutation may have led to a change in conformation of the protein that alters binding affinity for protein turnover. Crystal structure of the UBR1/UBR2's UBR box has been characterised (Matta-Camacho *et al.*, 2010) due to its importance in type I N-end rule activity. Further structural

analysis into mammalian UBR2 may give insight into the importance of the ELL domain and whether it matches interactions with other domains identified in the similar region of yeast Ubr1 (Pan *et al.*, 2021).

The majority of the hits are involved in RNA processing from RNA binding activity (Takayanagi-Kiya *et al.*, 2014; Young *et al.*, 2014; Zhang *et al.*, 2017; Cheng *et al.*, 2019; Darweesh *et al.*, 2022) to degradation (Fenger-Grøn *et al.*, 2005). One hit of interest was TAB1, an adaptor protein required for Transforming growth factor-β-activated kinase 1 (TAK1) activation and associates with N-terminal kinase domain of TAK1. TAK1 is a member of the MAPK kinase kinase (MAPKKK) family that is activated by multiple stimuli and phosphorylates a series of target proteins which produce different signal transduction and cellular responses across cell types and activates nuclear factor NF-κB, c-Jun N-terminal kinase (JNK) and p38 (Fan *et al.*, 2010; Mukhopadhyay and Lee, 2020). TAB1 expresses as nuclear specs during interphase but it is unclear where it resides during G2/M.

SMARCAL1 which is an ATP-dependent DNA annealing helicase with homology to the ATP-dependent chromatin remodelling proteins (Yusufzai and Kadonaga, 2008). SMARCAL1 has been shown to localize at the double-strand break sites to maintain genome integrity at stalled replication forks during replication and following DNA damage (Bansbach *et al.*, 2009; Couch *et al.*, 2013). SMARCAL1 interacts with histones (Coleman *et al.*, 2003; Elizondo *et al.*, 2009) and has been shown to co-localizes with histone modification markers in the genome (Bansal *et al.*, 2020) making it important

for chromatin remodelling. Further IF experiments with FLAG-ELL-UBR2 and any one of these potential nuclear binding partner may show any colocalisation between these two proteins in the cells where FLAG-ELL-UBR2 is chromatin-bound to confirm if the K834A mutation is changing the affinity of UBR2 binding to substrates.

In this chapter, I have demonstrated that UBR2 does not localise to chromatin during mitosis and that the K834A mutation in the ELL region causes UBR2 to localise to chromatin in a subset of cells in G2/M. Further investigation of the change in localisation of FLAG-ELL-UBR2 during G2/M is required to determine why UBR2 appears to ‘stick’ to chromosomes and whether if it is due to an increase in binding to nuclear substrates, such as TAB1 or SMARCAL1, for protein turnover or non-canonical functions outside of ubiquitination.

Chapter 4:

Investigating the role of UBR2 in chromosome stability in ES cells

4.1 Introduction

As discussed in Chapter 1, UBR2 is one of seven UBR proteins that contain the UBR box; four of which, including UBR2, have been shown to have activity as E3 ubiquitin ligases in the N-end Rule protein recognition system of the UPS (Tasaki *et al.*, 2009). UBR proteins are coexpressed in a variety of cells and tissues with evidence that redundancy occurs between them (An *et al.*, 2006). However, removal of UBR2 leads to an array of tissue specific phenotypes indicating that UBR2 has important functions within these tissues. It remains unclear whether this could be through the N-end Rule or through other functions that cannot be compensated by UBR protein redundancy. UBR2 has been implicated in non N-end rule functions including ubiquitination of non-N-end rule substrates (An *et al.*, 2012; Maclennan *et al.*, 2017; Vu and Varshavsky, 2020), ubiquitination of misfolded proteins as part of protein quality control (Nillegoda *et al.*, 2010), and in stabilisation of some proteins that interact with UBR2 and form heteromeric complexes (Yang *et al.*, 2010; Reichmann *et al.*, 2020).

In this chapter, I generated a group of embryonic stem cell (ESC) lines with point mutations in protein-binding interfaces of UBR2 including the UBR box, N-domain, RING domain and the structural ELL domain in order to separate distinct biochemical roles of UBR2. By using these cells alongside *Ubr2*$^{-/-}$ ESCs, I was able to identify potential substrates of UBR2, and relate these potential substrates to biological processes that require UBR2 to function correctly.

4.2 Results

4.2.1 Generating stable *Ubr2* ESC lines with point mutations using CRISPR Cas9

4.2.1.1 Generation of *Ubr2*^{D233A} ESCs

It is apparent that the roles in chromosome stability of UBR2 could be modelled in ESCs in culture. For example, a specific upregulation of the AcSMC3 cohesin subunit in the *Ubr2*$^{-/-}$ genotype matches the phenotype found in the spleen of *Ubr2*$^{-/-}$ mouse (Reichmann *et al.*, 2020). It remains unclear if this phenotype, amongst others, could be due to UBR2's role in the N-end rule pathway or another ubiquitin pathway. Therefore, to further investigate which activities of UBR2 might be important for cellular functions, a CRISPR-Cas9 experiment was designed with homology-directed repair, with the aim to generate a stable *Ubr2*-T2D223A mutant ESC line, so perturbing the binding of UBR2 to type II N-end rule peptides. The D233A point mutation was first identified in an alanine-scanning mutagenesis screen of *Ubr1* (Tasaki *et al.*, 2009) which specifically perturbs detectable binding to Type II N-end rule peptides. The D233 amino acid sequence is conserved in the mouse *Ubr2* gene and is located in UBR2's N-domain (Figure 4.1A). Previous work has confirmed the D233A mutation lowers UBR2's affinity to TII N-end rule peptide in ectopic expression of a FLAG-UBR2 construct in HEK293T cells and following the introduction of the mutation into endogenous *Ubr2* in mice (Eleanor Raymond, unpublished). In order to carry out HDR, a dsDNA repair oligo with 100bp homology arms encoding the mutant repair template containing both the point mutation and the mutant

PAM sequence were cotransfected into E14 ESCs alongside a Cas9 expressing plasmid and PX458 plasmid with the specific guide sequence cloned into it (Figure 4.1B). These cells were transfected and clonal colonies picked by Fiona Kilanowski (MRC HGU), and genetic screening was carried out to identify successfully edited clones.

For screening of successfully edited stable *Ubr2*^{D223A} clones, the mutations introduced into the *Ubr2* gene contained a restriction site GTG^CAC that could be cut with the restriction enzyme, *ApaLI* (Figure 4.1C). The control band is 303bp with successful incorporation of the restriction site leads to two bands, 221bp and 82bp in size. The clone G3 was one of four successfully edited D233A homozygous clone from screening 192 clonal cell lines (2.1% success rate). All clones were confirmed by Sanger sequencing of the 303bp PCR fragment (Figure 4.1D), which shows the GCT alanine-encoding codon in position 223 and the PAM mutation of CCA > GCA (5' TGG>TGC). For further experiments G3 will be written as *Ubr2*$^{T2/T2}$.

Figure 4.1: *Ubr2*^{D233A} mutant ESC line design and screening. (**A**) Schematic of UBR2's domain structure. Arrow indicates domain where the D233A mutation is located. Genome browser to show T2_F and T2_R primers and D233's location in UBR2 sequence (**B**) CRISPR-HDR guide and repair sequences for the Ubr2-T2D233A CRISPR experiment. PAM sequence is shown in bold and cut site of wtCas9 enzyme marked by ^. Introduced point mutations are marked in repair templates in red. Homology arms are underlined. (**C**) Representative gel electrophoresis showing restriction digest with ApaLI for T2 clone genotyping. 100bp ladder shown on left. Successful clone G3 shown by *. (**D**) Sanger sequencing data for the successful *Ubr2*$^{T2/T2}$ (G3) ESC clone (GAT->GCT).

A

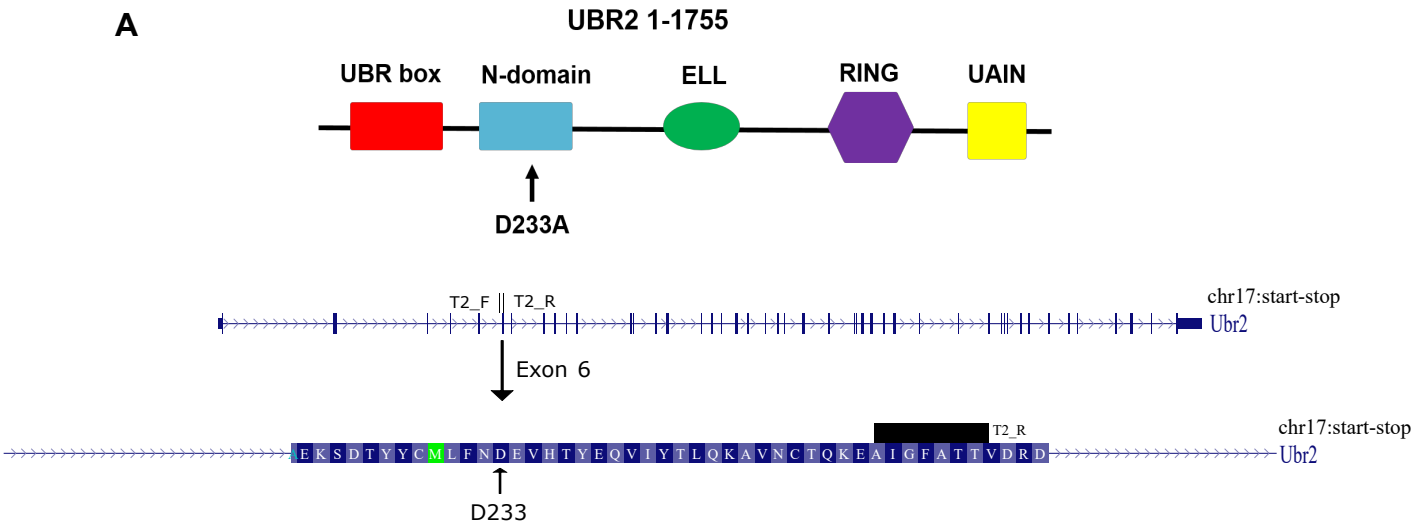

B

Experiment	Guide Sequence	Repair Template	Restriction site
T2 (D233A) GAT>GCT	CTGCATGCTGTTTA ATGATG Pam: AGG	CCCAGATGACACGCCCACTCTTTCCACAGCATT GATGGCATTGATGTTTTCTCC CCAGAGAGAAG AGTGACACCTACTACTGCATGCTGTTTAAT GCT GAAGTGCACACCTATGAGCAAGTCATTTATACC CTTCAGAAAGCTGTGAACTGTACACAGAAGGA AGCCATTGGCTTTGCAACTACAGTTGATCGAG ATGTA	GTG^CAC

C

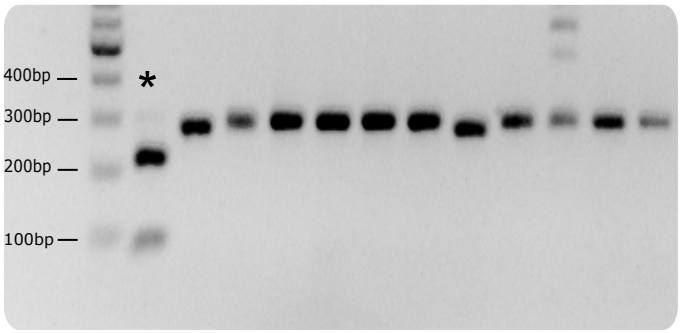

D

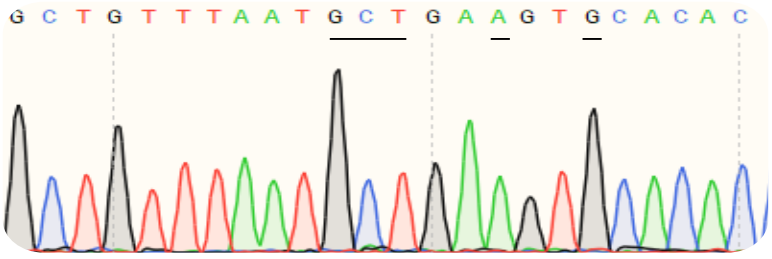

4.2.1.2 Generation of *Ubr2*^{W1177A} ESCs

To further investigate which activities of UBR2 might be important for functions, I designed a CRISPR-Cas9 experiment with homology-directed repair with the aim to generate a stable *Ubr2*^{W1177A} mutant ES cell line, by introducing a W1177A mutation into the UBR2 RING domain (Figure 4.2A). The W1177A point mutation was previously shown to disrupt the interaction between UBR2 and E2s, UBE2A and USE1, *in vitro* (Lee *et al.*, 2011) and in *in vivo* transient transfection and co-immunoprecipitation assays (Eleanor Raymond, unpublished). This mutation is expected to affect both N-end rule and non-N-end rule ubiquitination by UBR2.

A similar strategy to the one described previously to generate *Ubr2*$^{T2/T2}$ ESCs was used to generate *Ubr2*^{W1177A} ESCs (Figure 4.2B). For screening of successfully edited stable *Ubr2*^{W1177A} clones, the mutations introduced into the *Ubr2* gene contained a restriction site TGC^GCA that could be cut with the restriction enzyme, *FspI* and the digest products were identified by gel electrophoresis (Figure 4.2C). The control band is 499bp with successful incorporation of the restriction site leads to two bands, 431bp and 68bp in size. The clone A3 was the only one successfully edited W1177A homozygous clone from screening 192 clonal cell lines (0.5% success rate). This clone was confirmed by Sanger sequencing of the 499bp PCR fragment (Figure 4.2D), which shows the GCG alanine-encoding codon in position 1177 and the PAM mutation of CCA > GCA (5’ TGG>TGC). For further experiments this clone will be written as *Ubr2*$^{RD/RD}$.

Figure 4.2: *Ubr2*^{W1177A} mutant ESC line design and screening.

(**A**) Schematic of UBR2's domain structure. Arrow indicates domain where the W1177A mutation is located. Genome browser to show RD_F and RD_R primers and W1177s location in UBR2 sequence. (**B**) CRISPR-HDR guide and repair sequences for the *Ubr2*^{W1177A} CRISPR experiment. PAM sequence is shown in bold and cut site of wtCas9 enzyme marked by ^. Introduced point mutations are marked in repair templates in red. Homology arms are underlined. (**C**) Representative gel electrophoresis showing restriction digest with FSPI for RD clone genotyping. 100bp ladder shown on left. Successful clone A3 shown by *. (**D**) Sanger sequencing data for the successful *Ubr2*$^{RD/RD}$ (A3) ESC clone (TGG->GCG).

A

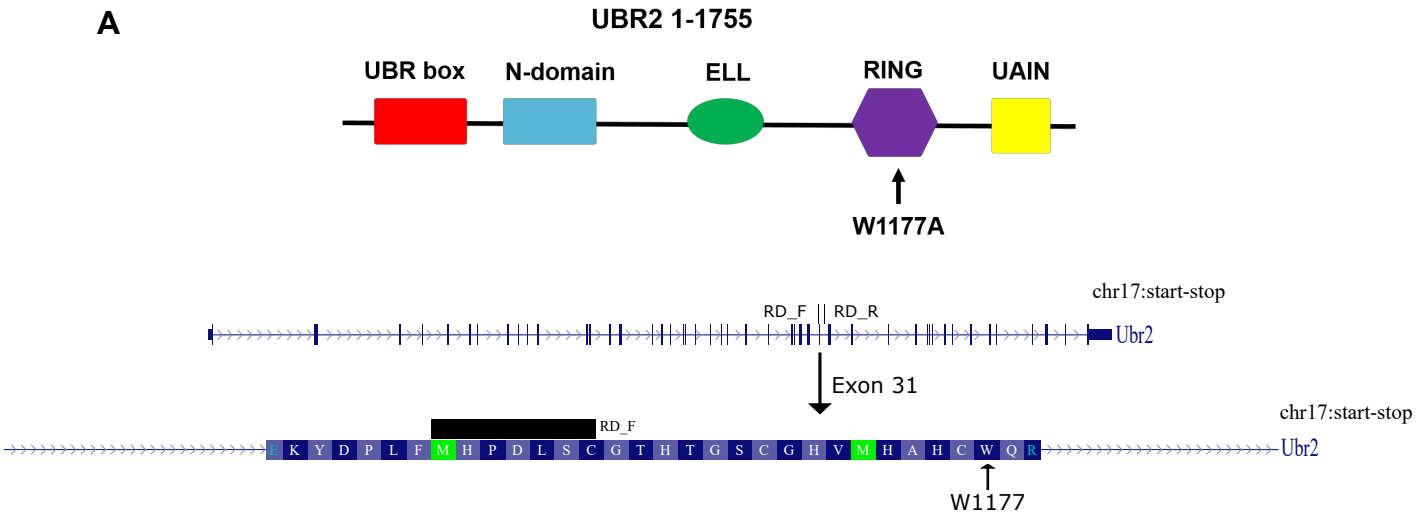

B

Experiment	Guide Sequence	Repair Template	Restriction site
*Ubr2*_RD (W1177A) TGG>GCG	CAAATTACCTTTGC CAA^CAA**TGG**	TTGTTTTATAATGCAGAAAAATATGATCCATTA TTCATGCACCCCGATCTGTCTTGTGGGACACAC ACTGGCAGCTGTGGGCACGTTATGCATGCGCA TTGTGCGCAAAGGTAATTTGTATTCTTATATTA CTCAGGGAACACCATCTGAAGGCTCAGGATTG ACTTTTAAAGCAAAGGAAAATTTGTGCTGGGG GTGG	TGC^GCA

C

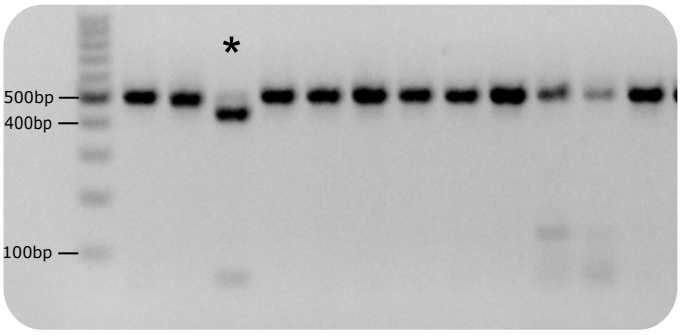

D

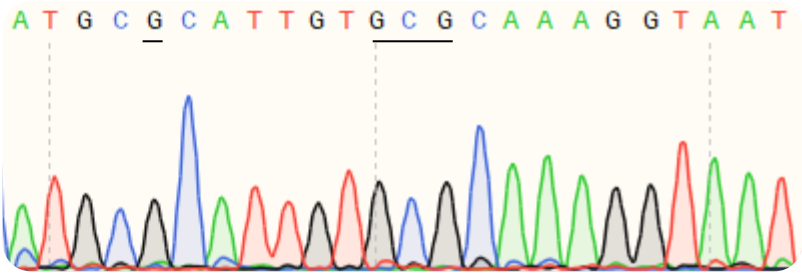

4.2.1.3 Generation of *Ubr2*^{K834A} ESCs

To further characterise the ELL domain and identify possible phenotypes, a CRISPR-Cas9 experiment with homology-directed repair was designed with the aim to generate a stable *Ubr2*^{K834A} mutant ESC line, to introduce the K834A mutation into endogenous *Ubr2* (Figure 4.3A). The ELL region was identified as a structural domain in UBR2 with a highly conserved residue of K834 that could be responsible for the stabilisation of a β-sheet in UBR2 structure. Mutating the K834 residue to alanine resulted in a change in localisation of the overexpressed FLAG-UBR2-ELL in HEK293T cells (Chapter 3, Figure 3.8). As the essential functions of UBR2 appears to not act through the N-end rule pathway, investigating non-canonical roles and uncharacterised domains of UBR2 is important to understand what regions of *UBR2* are important for roles in ESCs.

A similar strategy to the one described previously to generate *Ubr2*$^{T2/T2}$ ESCs was used to generate *Ubr2*^{K834A} ESCs (Figure 4.3B). For screening of successfully edited stable *Ubr2*^{K834A} clones, the mutations introduced into the *Ubr2* gene contained a restriction site GGC^GCC that could be cut with the restriction enzyme, *SfoI* (Figure 4.3C). The control band is 386bp with successful incorporation of the restriction site leads to two bands, 231bp and 155bp in size. The clone B10 was the one of 8 successfully edited K834A homozygous clone from screening 384 clonal cell lines (2.1% success rate); the other seven successful clones were E1, C8, D11, F9, G2, A10 and H2. I then validated these clones by Sanger sequencing of the 386bp PCR

fragment (Figure 4.3D), which shows the GCG alanine-encoding codon in position 834 and the base changes that were introduced in place of a PAM site mutation. The PAM site of the gRNA is CCA (5' TGG) in the repair template which is in frame and codes for proline leading to no appropriate silent mutations that would stop cutting in the sequence. For further experiments the B10 clone will be written as *Ubr2*$^{ELL/ELL}$.

Figure 4.3: *Ubr2*^{K834A} mutant ESC line design and screening. (**A**) Schematic of UBR2 domain structure. Arrow indicates domain where the K834 amino acid is located. Genome browser to show ELL_F and ELL_R primers and K834's location in UBR2 sequence. (**B**) CRISPR-HDR guide and repair sequences for the *Ubr2*^{K834A} CRISPR experiment. PAM sequence is shown in bold and cut site of wtCas9 enzyme marked by ^. Introduced point mutations are marked in repair templates in red. Homology arms are underlined. (**C**) Representative gel electrophoresis showing restriction digest with SfoI for ELL clone genotyping. 100bp ladder shown on left. Successful clone B10 shown by *. (**D**) Sanger sequencing data for the successful B10 ESC clone (AAG->GCG).

A

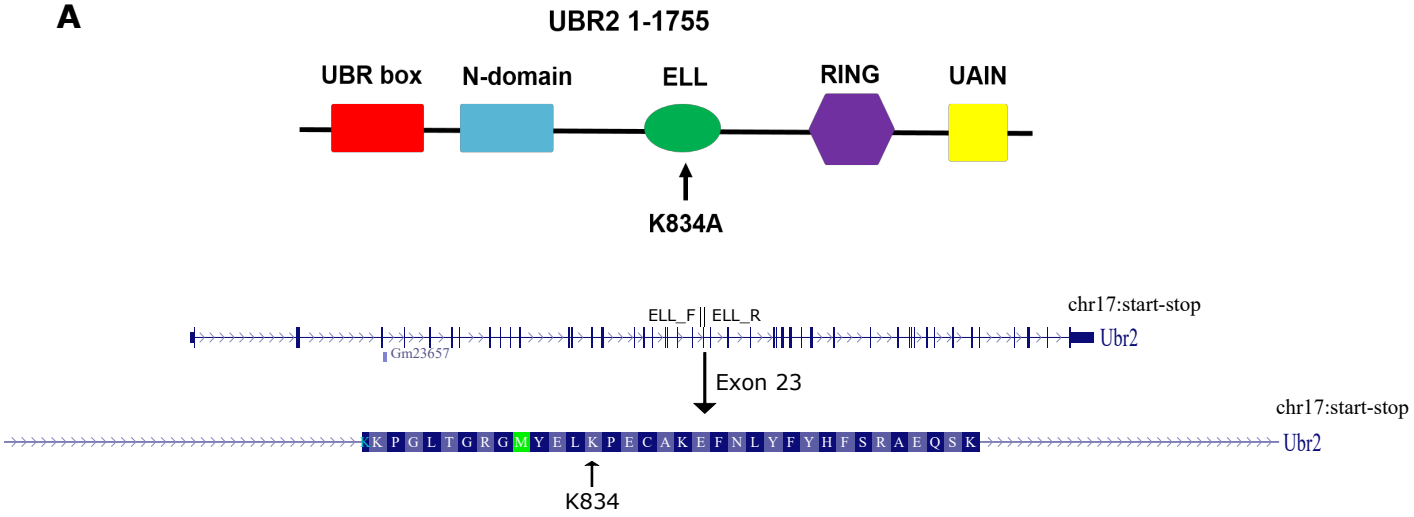

B

Experiment	Guide Sequence	Repair Template	Restriction site
ELL (K834A) AAG>GCG	TTGAACTCTTTGGC ACA^CTC**TGG**	GACCATCTAAGACTCTCGGCATGCGTGACTTTG CTAATGATACTCTTCCCACCAGGAAACCTGGGC TCACAGGGCGAGGCATGTATGAGCTG GCGCCA GAATGCGCTAAAGAGTTCAACCTGTATTTTTAT CATTTCTCCAGGGCAGAGCAGTCCAAGGTAAG GGGGAGCTCAGAGCAGTGGGAGGTGCTAAGT GTGT	GGC^GCC

C

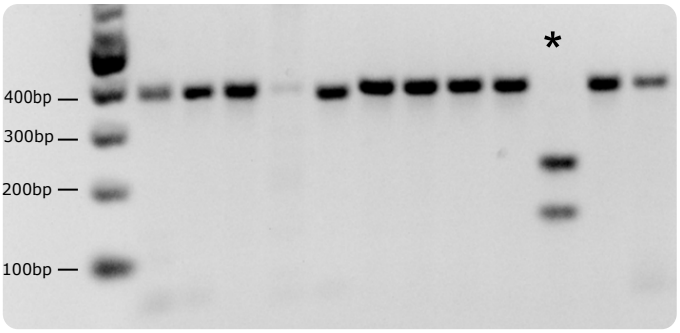

D

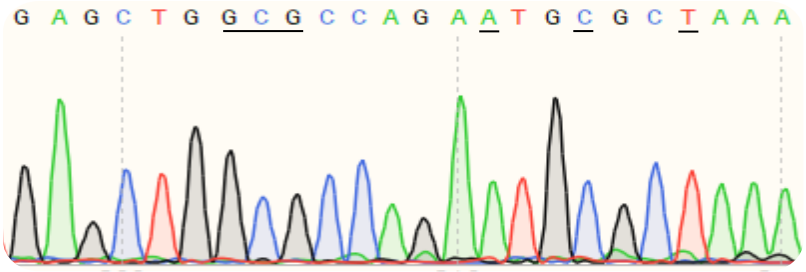

In order to confirm that UBR2 protein from *Ubr2*$^{T2/T2}$, *Ubr2*$^{RD/RD}$, *Ubr2*$^{ELL/ELL}$ and the previous generated *Ubr2*^{D118A} (*Ubr2*$^{T1/T1}$) ESCs is detectable at levels similar to wild type and the protein is stable, Western blotting was carried out to detect endogenously expressed UBR2 (Figure 4.4). One ESC clone from each mutant group were probed for UBR2 protein and lamin B1 as a loading control, alongside E14 wild type ESCs (*Ubr2*$^{+/+}$). UBR2 protein is detectable in wild type E14 (*Ubr2*$^{+/+}$) cells, and in all UBR2 mutant clones.

UBR2 stabilises TEX19.1, resulting in TEX19.1 protein being undetectable in *Ubr2*$^{-/-}$ testes (Yang *et al.*, 2010) and in *Ubr2*$^{-/-}$ ESCs (Karen Dobie, unpublished). When ectopically expressed, TEX19.1 is able to regulate the Type II N-end rule substrate binding activity of UBR2 so may regulate UBR2's ability to target Type II substrates for N-end rule ubiquitination (Reichmann *et al.*, 2020). Therefore, in order to determine if endogenous TEX19.1 is detectable in the mutant ESCs, Western blotting was used to detect TEX19.1 protein levels (Figure 4.4). The TEX19.1 protein is expected to be around 40kDa (Uniprot Q99MV2) and is observed in *Ubr2*$^{T1/T1}$, *Ubr2*$^{T2/T2}$, *Ubr2*$^{RD/RD}$, *Ubr2*$^{ELL/ELL}$ and *Ubr2*$^{+/+}$ ESC lysates, alongside lamin B1 as a loading control protein. Thus, endogenous TEX19.1 protein is stable in presence of all the mutated UBR2 protein, so none of these mutants affect UBR2-TEX19.1 stabilisation. This finding is consistent with previous experiments suggesting that each of these mutant UBR2 mutant is still able to co-immunoprecipitate with ectopically expressed TEX19.1 in a transiently transfected HEK293T cells (Eleanor Raymond, unpublished; Figure 3.6).

Figure 4.4: UBR2 and TEX19.1 are present in *Ubr2* mutant ESCs. Protein levels of UBR2 (~200kDa) and TEX19.1 (~40kDa) using Western blotting in wild type E14 *Ubr2*$^{+/+}$, *Ubr2*$^{T1/T1}$, *Ubr2*$^{T2/T2}$, *Ubr2*$^{RD/RD}$ and *Ubr2*$^{ELL/ELL}$ ESCs. Protein product of housekeeping gene lamin B1 (~80kDa) shown as a loading control. * are non-specific bands.

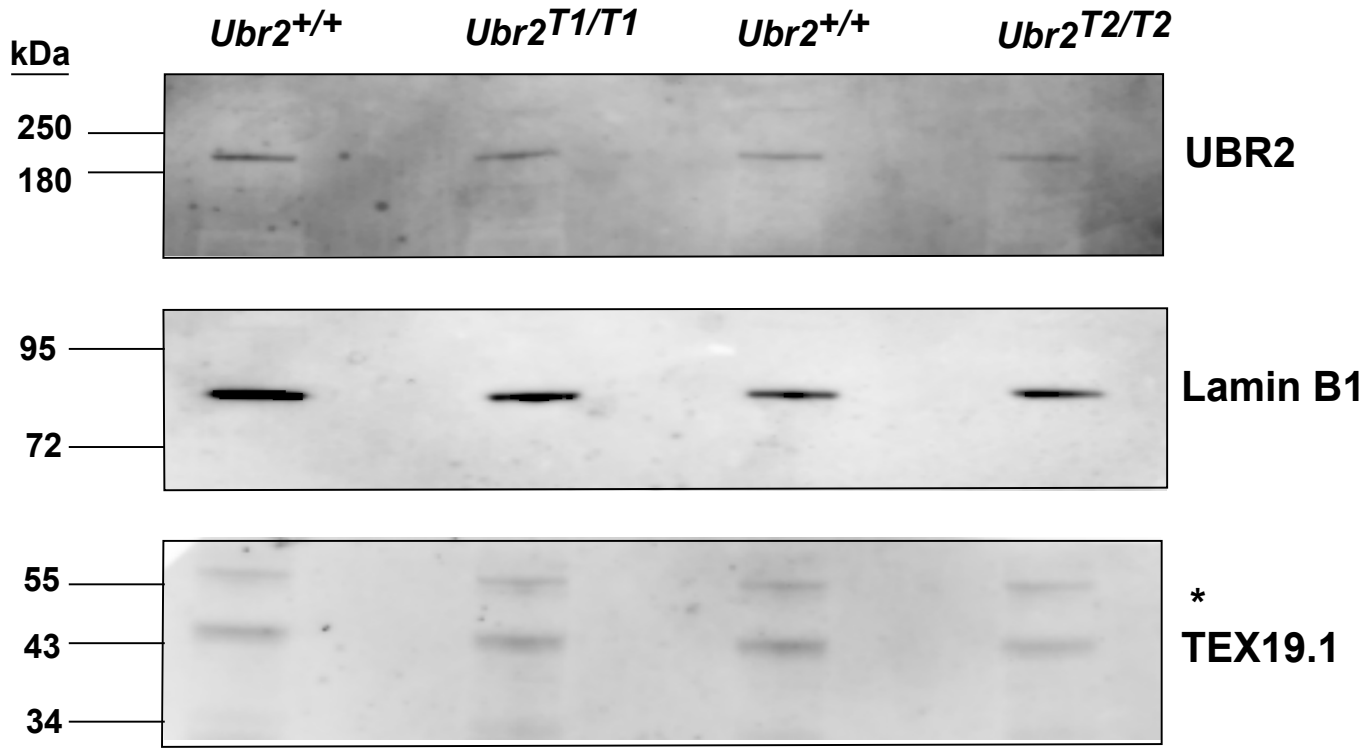
kDa
Ubr2+/+
Ubr2T1/T1
Ubr2+/+
Ubr2T2/T2
250
180
UBR2
95
72
Lamin B1
55
43
34
*
TEX19.1

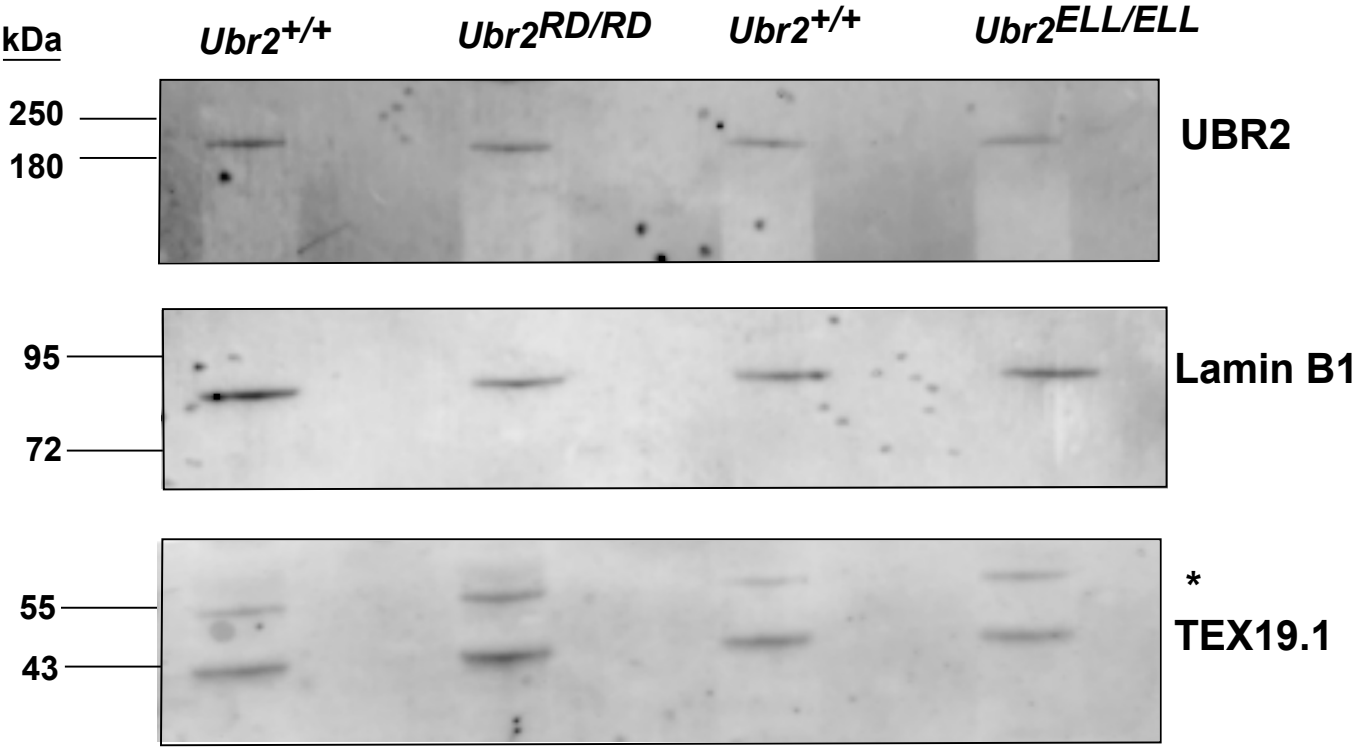
kDa
Ubr2+/+
Ubr2RD/RD
Ubr2+/+
Ubr2ELL/ELL
250
180
UBR2
95
72
Lamin B1
55
43
*
TEX19.1

To test whether the point mutations in *Ubr2* impairs cell growth and proliferation, cells were plated at $2x10^5$ cells/well in triplicate and counted after 24 and 48 hours. *Ubr2*$^{+/+}$ ESCs had $4.7x10^5$ $\pm 8.8x10^4$ (± standard deviation) cells/well after 24 hours and $9.83x10^5$ $\pm 1.2x10^5$ cells/well after 48 hours (Figure 4.5A). The *Ubr2*$^{T1/T1}$ mutant had $4.2x10^5$ $\pm 9.7x10^4$ and $1.1x10^6$ $\pm 1.5x10^5$ cells/well, *Ubr2*$^{T2/T2}$ had $5.2\ x10^5$ $\pm 6.8x10^4$ and $1.1x10^6$ $\pm 2.3x10^5$ cells/well, *Ubr2*$^{RD/RD}$ had $3.6x10^5$ $\pm 8.1x10^4$ and $8.6x10^5$ $\pm 1.4x10^5$ cells/well, *Ubr2*$^{ELL/ELL}$ $4.4x10^5$ $\pm 6.7x10^4$ and $1.1x10^6$ $\pm 1.6x10^5$ cells/well at 24 and 48 hours respectively. None of the *Ubr2* point mutations impair cell growth and proliferation in culture.

To check whether the mutations in *Ubr2* lead to aneuploidy in ESCs, chromosome numbers in the *Ubr2*$^{+/+}$, *Ubr2*$^{T2/T2}$, *Ubr2*$^{RD/RD}$ and *Ubr2*$^{ELL/ELL}$ ESCs at a higher passage number of at least 35 were counted by Fiona Kilanowski. 83% of wildtype control *Ubr2*$^{+/+}$ ESCs contained the expected 40 chromosomes (Figure 4.5B). *Ubr2*$^{T2/T2}$ ESCs had 78%, *Ubr2*$^{RD/RD}$ had 72% and *Ubr2*$^{ELL/ELL}$ had 75% with the expected 40 chromosomes so *Ubr* mutant ESCs at passages earlier than 35 were used for subsequent experiments.

Figure 4.5: ES cells with UBR2 point mutations grow normally (A) Cellular-growth curves determined by cell counts at 24 hours and 48hours of *Ubr2*$^{+/+}$, *Ubr2*$^{T1/T1}$, *Ubr2*$^{T2/T2}$, *Ubr2*$^{RD/RD}$, *Ubr2*$^{ELL/ELL}$ ES cells. All measures were performed in triplicate and error bars correspond to standard deviation. All mutants were compared to *Ubr2*$^{+/+}$ control with Student's t-test at each time point, p-value (24hr, 48hr). *Ubr2*$^{T1/T1}$ p=0.24, p=0.06. *Ubr2*$^{T2/T2}$ p=0.6, p=0.53. *Ubr2*$^{RD/RD}$ p=0.3, p=0.09. *Ubr2*$^{ELL/ELL}$ p=0.62, p=0.61. (**B**) Aneuploidy in *Ubr2*$^{+/+}$, *Ubr2*$^{T2/T2}$, *Ubr2*$^{RD/RD}$ and *Ubr2*$^{ELL/ELL}$ ES cells. Chromosome number was counted in N=30, 18, 18, 20 nuclei respectively from each cell line at passage 35. Each count were placed into two groups: the expected group of 40 chromosomes, or the aneuploidy groups of <40 chromosomes and >40 chromosomes.

A

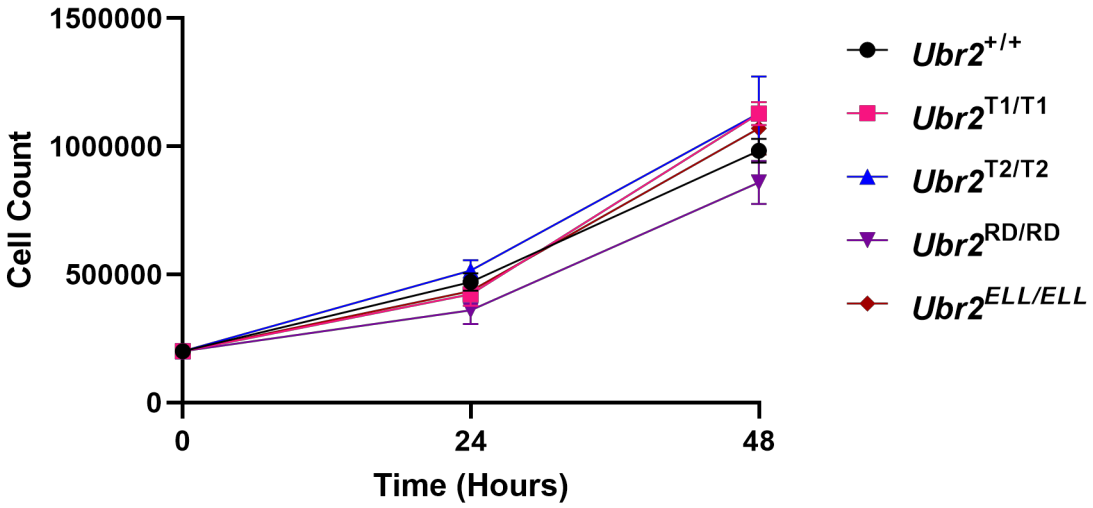
1500000
1000000
500000
0
Cell Count
0
24
48
Time (Hours)
Ubr2+/+
Ubr2T1/T1
Ubr2T2/T2
Ubr2RD/RD
Ubr2ELL/ELL

B

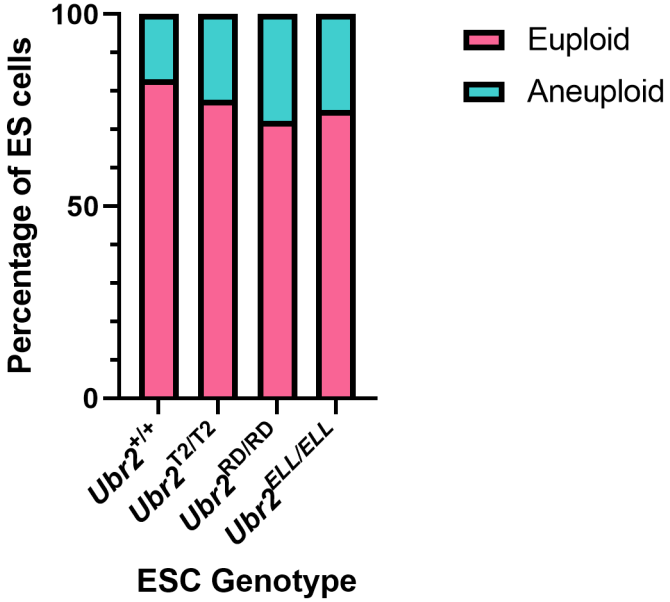
100
50
0
Percentage of ES cells
Euploid
Aneuploid
Ubr2+/+
Ubr2T2/T2
Ubr2RD/RD
Ubr2ELL/ELL
ESC Genotype

4.2.2 Mass spectrometry of *Ubr2* mutant proteomes.

4.2.2.1 *Ubr2*$^{-/-}$ ESCs have upregulated and downregulated proteins enriched in multiple biological processes.

To try identify proteins whose abundance is regulated by UBR2 in ESCs, cell pellets from *Ubr2*$^{+/+}$ and *Ubr2*$^{-/-}$ ESCs were analysed by mass spectrometry (MS). The raw data was analysed using Spectronaut software to produce a data matrix by calculating peak integration to allow for alignment, metabolite identification and then calculation of metabolite concentrations. Three ESC pellets from each cell line were ran through resulting in an observed abundance value for all for specimens within each experimental leading to over 5000 proteins identified. Protein abundances from *Ubr2*$^{-/-}$ ESCs was compared to wildtype *Ubr2*$^{+/+}$ controls and significant differences in abundance between the two cell types were calculated. All proteins that had a p-value <0.05 were used for further analysis and the definition of an upregulated protein is where the log Fold change (FC) calculated over the three repeats is above 1.5 and downregulated is when the calculated log FC is below -1.5 (Figure 4.6A). There were 485 upregulated proteins and 399 downregulated proteins identified in *Ubr2*$^{-/-}$ when compared to *Ubr2*$^{+/+}$ controls. UBR2 is an E3 ubiquitin ligase whose main role in cells is in N-end rule protein degradation (Tasaki *et al.*, 2009) so it was expected to identify a large amount of upregulated proteins in *Ubr2*$^{-/-}$ ESCs. However, there were more downregulated proteins identified suggesting that removal of UBR2 may lead to an increase in negative regulators of the downregulated proteins.

As UBR2 is an E3 ubiquitin ligase that is involved in the degradation of proteins, there was particular interest in the proteins that were upregulated in *Ubr2*$^{-/-}$ ESCs. The upregulated proteins were used to undertake GO enrichment analysis to determine which biological processes the proteins were enriched when compared to the total proteins (Figure 4.6B). The highest fold enrichment was in the process of mitochondrial ATP synthesis coupled proton transport which is important for the transport of protons across a mitochondrial membrane to generate an electrochemical gradient (proton-motive force) that powers ATP synthesis (Sgarbi *et al.*, 2006). This was one of many mitochondrial and ATP processes found to be enriched in *Ubr2*$^{-/-}$ ESCs indicating that UBR2 potentially has a role in mitochondria regulation in ESCs.

Interestingly, the downregulated proteins were enriched in multiple pathways with the largest fold enrichment being proteins involved in Histone H2B ubiquitination (Figure 4.6C). UBR2 has a previously described relationship with ubiquitination of Histone H2A (An *et al.*, 2012) which is disputed. But it is likely that UBR2 has an important role in ubiquitination pathways of other histones as several histones were identified in the MS. As well as apparently separate biological pathways, *Ubr2*$^{-/-}$ ESCs have decreased abundance of proteins involved in RNA associated and telomere localisation pathways (Figure 4.6C). Together, this indicates that the *Ubr2*$^{-/-}$ genotype leads to both positive and negative effects on proteins.

Figure 4.6 Whole proteomics *data of Ubr2*$^{-/-}$ ESCs shows that *Ubr2* has an enrichment of upregulated proteins in mitochondria processes. (**A**) Volcano plot of mass spectrometry results shows the proteins in *Ubr2*$^{-/-}$ compared to *Ubr2*$^{+/+}$ ESCs. Y-axis represents negative log10(p-value) where all protein changes that had p-values <0.05 were classed as significant. X-axis is the calculated Log2 fold change (Mean log2 Ratio) where proteins with a positive fold change >1.5 represent upregulated proteins (highlighted in red) and those with negative fold change <1.5 represent downregulated proteins (highlighted in blue) in the *Ubr2*$^{-/-}$ ESCs, respectively. Upregulated proteins= 485 and downregulated proteins = 399. Gene names were used to label proteins. (**B**) GO term analysis of the biological processes upregulated proteins from *Ubr2*$^{-/-}$ ESCs. Significant upregulated proteins were compared to the 5424 total background proteins identified in the MS. Enrichment FDR is the estimated probability that a gene set with a given enrichment score represents a false positive finding. nGenes is the number of genes found in the upregulated proteins, Pathway genes is the total number of genes in the BP pathway and Fold enrichment is the calculated increase in enrichment compared to the background. (**C**) GO term analysis of downregulated proteins from *Ubr2*$^{-/-}$ ESCs. Significant downregulated proteins were compared to the 5424 total proteins identified in the mass spectrometry. The headings are the same as in (**B**).

A

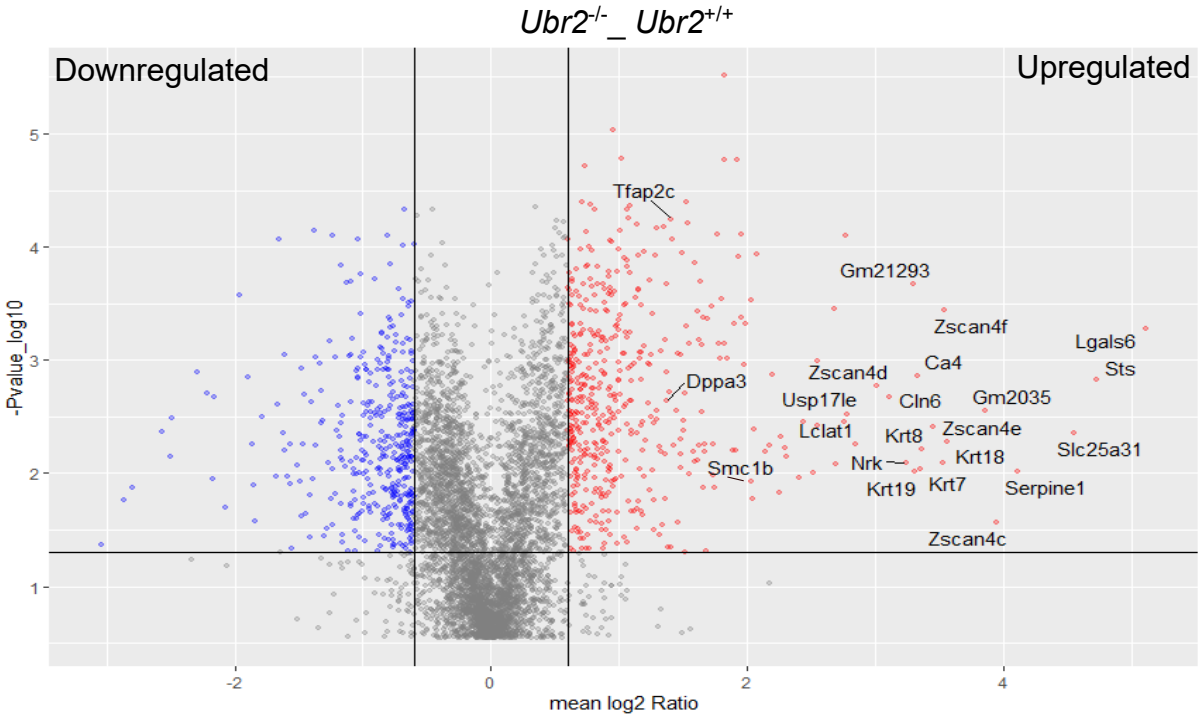

B Upregulated

Enrichment FDR	nGenes	Pathway Genes	Fold Enrichment	GO Biological Processes
1.10E-05	13	17	3.6	Mitochondrial ATP synthesis coupled proton transport
2.80E-02	6	26	3.6	Cellular response to angiotensin
2.80E-02	6	14	3.6	Sodium ion export across plasma membrane
9.90E-06	15	24	3.4	Energy coupled proton transport, down electrochemical gradient
9.90E-06	15	24	3.4	ATP synthesis coupled proton transport
2.10E-03	10	47	3.3	Metal ion export
1.80E-05	16	22	3.2	Mitochondrial cytochrome c oxidase assembly
2.40E-15	43	58	3.2	NADH dehydrogenase complex assembly
2.40E-15	43	58	3.2	Mitochondrial respiratory chain complex I assembly
4.00E-04	13	19	3.1	Protein import into mitochondrial matrix

C Downregulated

Enrichment FDR	nGenes	Pathway Genes	Fold Enrichment	GO Biological Processes
9.20E-03	8	12	3.1	Histone H2B ubiquitination
4.50E-02	6	12	3.1	UDP-N-acetylglucosamine metabolic processing
2.60E-04	14	16	2.9	Formation of cytoplasmic translation initiation complex
4.00E-03	11	13	2.8	Positive regulation of protein localisation to chromosome, telomeric region
2.70E-03	13	21	2.7	Proteasomal ubiquitin-independent protein catabolic proccessing
1.10E-02	11	16	2.6	Establishment of protein localization to telomere
4.50E-02	9	13	2.5	MRNA cleavage involved in mRNA processing
4.50E-02	9	12	2.5	Pre-mRNA cleavage required for polyadenylation
4.50E-02	9	12	2.5	Regulation of RNA binding
4.50E-02	9	16	2.5	DNA strand elongation

4.2.2.2 Point mutations in protein-interacting interfaces of UBR2 can identify potential substrates for ubiquitin-dependent degradation in ESCs

The MS of the *Ubr2* mutant ES cells (*Ubr2*$^{RD/RD}$, *Ubr2*$^{T1/T1}$, *Ubr2*$^{T2/T2}$ and *Ubr2*$^{ELL/ELL}$) was used to identify potential proteins that may be substrates for UBR2-mediated ubiquitin-dependent degradation, and to separate out N-end rule substrates and non N-end rule substrates. The W1177A mutation of *Ubr2*$^{RD/RD}$ has previously been shown to decrease the binding of E2s, UBE2A and USE1 (Lee *et al.*, 2011). To identify proteins that could be targeted for ubiquitin-dependent degradation by UBR2, *Ubr2*$^{RD/RD}$ and wildtype *Ubr2*$^{+/+}$ proteomes were compared to identify upregulated and downregulated proteins as described for *Ubr2*$^{-/-}$ ESCs.

To graphically represent this comparison data, a volcano plot $-\log_{10}$ (p-value) vs. $\log_2$ (fold change in *Ubr2*$^{RD/RD}$ vs *Ubr2*$^{+/+}$ ESCs) was constructed to graphically display the quantitative data (Figure 4.7A). The 514 differentially increased abundant proteins ($P < 0.05$ and fold change >1.5) was compared to the 485 proteins from Ubr2$^{-/-}$ ESCs (Figure 4.7B). ~49.1% of proteins upregulated in *Ubr2*$^{-/-}$ ESCs were also significantly upregulated in *Ubr2*$^{RD/RD}$ ESCs including the histone Hist1h2bp, H1-6 and the cohesin subunit Smc1β. These 238 proteins upregulated in both *Ubr2*$^{-/-}$ and *Ubr2*$^{RD/RD}$ ESC are potential substrates for UBR2-mediated ubiquitin-dependent degradation. As there were 276 proteins that were upregulated in the *Ubr2*$^{RD/RD}$ but not in the *Ubr2*$^{-/-}$ could indicate ubiquitin substrates of UBR2 that may also be targeted

by other E3 ligases such as UBR1. One hit of interest in this group was Haspin which has a role in modifying histones, a potential role of UBR2, by phosphorylating histone H3 at threonine-3 during mitosis, particularly at inner centromeres (Higgins, 2010). 247 proteins were only upregulated in *Ubr2*$^{-/-}$ ESCs and not *Ubr2*$^{RD/RD}$ ESCs indicating proteins that are UBR2 substrates for other non-canonical functions outside of ubiquitination.

Figure 4.7 *Ubr2*$^{RD/RD}$ ESCs have overlapping upregulated substrates to *Ubr2*$^{-/-}$ ESCs. (**A**) Volcano plot of mass spectrometry results shows the proteins in *Ubr2*$^{RD/RD}$ compared to *Ubr2*$^{+/+}$ ESC. Y-axis represents negative log10 p-value and proteins with a positive Log2 fold change (Mean Log2 Ratio) are upregulated and negative values represent downregulated proteins in the *Ubr2*$^{RD/RD}$ ESCs, respectively. Proteins changes that have Fold change >1.5 are highlighted in red, Fold change <-1.5 are highlighted in blue. Upregulated protein = 514 and downregulated protein = 258. Gene names of proteins with the highest Log(Fold change) are labelled alongside *Smc1b*, *Tfap2c* and *Dppa3*. (**B**) Venn diagram of comparisons of upregulated *Ubr2*$^{-/-}$ and *Ubr2*$^{RD/RD}$ proteins and identifying the number of sample-exclusive or common proteins. An example of proteins that were exclusive or common are included.

A

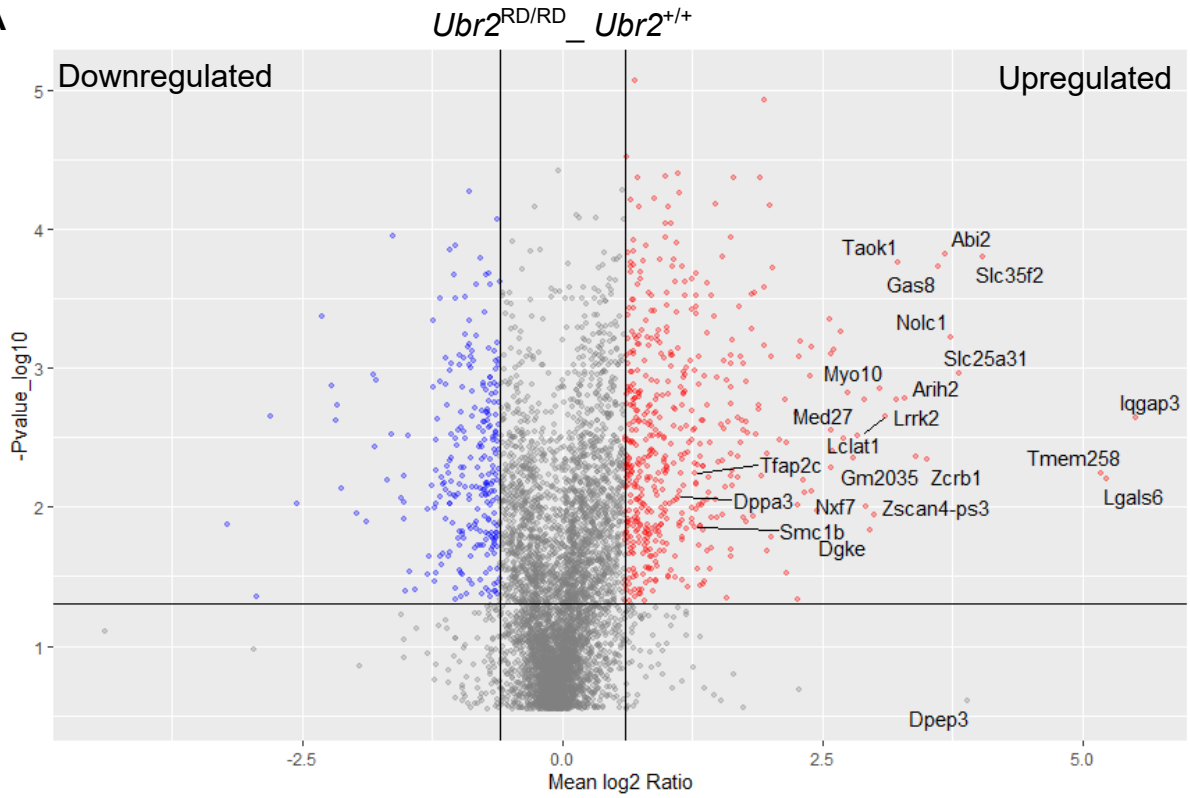

B Upregulated

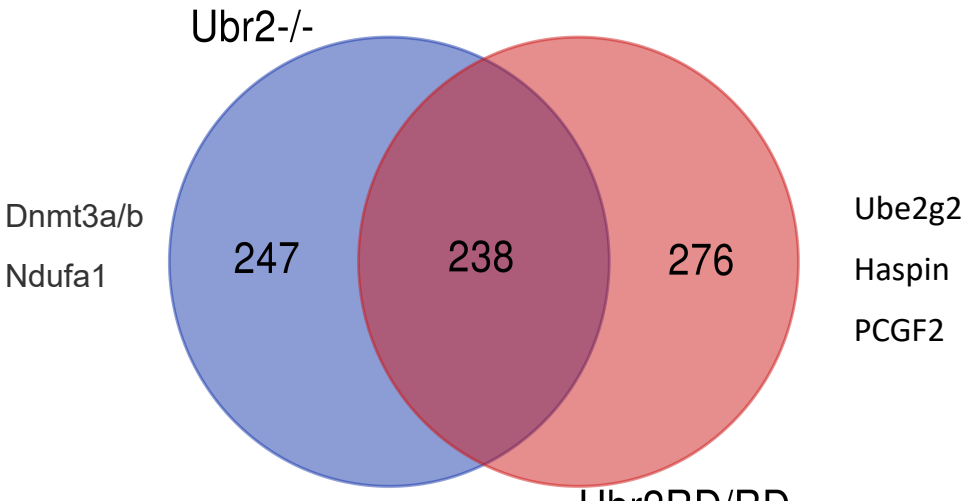

To identify proteins that might be regulated by the N-end rule activity of UBR2, I next performed mass spectrometry on *Ubr2*$^{T1/T1}$ and *Ubr2*$^{T2/T2}$ ESCs and compared these proteomes to wild type *Ubr2*$^{+/+}$ ESCs. 1246 proteins from *Ubr2*$^{T1/T1}$ and 1298 proteins from *Ubr2*$^{T2/T2}$ ESCs were upregulated > 1.5 fold ($p<0.05$) relative to wild type *Ubr2*$^{+/+}$ ESCs (Figure 4.8A). Only 7 proteins were upregulated in common between *Ubr2*$^{T1/T1}$, *Ubr2*$^{RD/RD}$ and *Ubr2*$^{-/-}$ ESCs but not *Ubr2*$^{T2/T2}$ ESCs (Figure 4.8A). These 7 proteins are potential type I N-end rule substrates regulated by UBR2. In contrast, 57 proteins were upregulated in common between *Ubr2*$^{T2/T2}$, *Ubr2*$^{RD/RD}$ and *Ubr2*$^{-/-}$ ESCs but not in *Ubr2*$^{T1/T1}$ ESCs (Figure 4.8A). These 57 proteins are potential type II N-end rule substrates regulated by UBR2. Furthermore, 21 proteins were upregulated in both *Ubr2*$^{RD/RD}$ and *Ubr2*$^{-/-}$ ESCs but not in either *Ubr2*$^{T1/T1}$ or *Ubr2*$^{T2/T2}$ ESCs (Figure 4.8A). These proteins are potential non-N-end rule substrates for UBR2-dependent ubiquitination.

Interestingly, there is overlap of 153 proteins that are upregulated in *Ubr2*$^{-/-}$, *Ubr2*$^{RD/RD}$, *Ubr2*$^{T1/T1}$ and *Ubr2*$^{T2/T2}$ ESC lines compared to *Ubr2*$^{+/+}$ ESCs suggesting that some N-end rule substrates are affected by both the type I and type II mutations. UBR2 was first thought to have a limited role in the type I N-end Rule pathway instead acting more in the turnover of type II substrates *in vitro* (Tasaki *et al.*, 2005) which may explain the low amount of type I proteins identified. However, canonical type I substrate was identified in *Ubr2*$^{-/-}$ MEFs which exhibit vulnerability to UV irradiation as a result of a lack of type I N-end rule degradation of genomic stress regulator SDE2

(Rageul *et al.*, 2019) indicating that there are TI N-end rule substrates *in vivo* and the seven proteins identified require further investigation.

The proteins that were allocated as type I (TI), type II (TII) and non-N-end rule proteins included histones, developmental proteins and transcription factors (Figure 4.8A). UBR2 has a previous role in the turnover of AcSMC3-marked cohesin in ESCs (Karen Dobie, unpublished) but AcSMC3 or SMC3 were not found to have significant changes in the dataset generated from the MS. This is consistent with previous data in the lab showing the UBR2 primarily regulates AcSMC3 in the G2/M phase of the cell cycle, which would only represent a minor population of cells in the MS experiment. The only cohesin subunit that was identified as a potential substrate was the meiosis specific SMC1β cohesin subunit which has previously been shown to be expressed in ESCs (Choi *et al.*, 2022). SMC1β was found to be significantly upregulated in *Ubr2*$^{T2/T2}$, *Ubr2*$^{RD/RD}$ and *Ubr2*$^{-/-}$ ESCs so could be a potential TII peptide. Interestingly, there is no evidence that SMC1β would have a non-methionine N-terminus so may be a substrate for non-acetylated Met-Φ turnover that depends on TII Arg/N-end Rule pathway (Kim and Hwang, 2014; Nguyen *et al.*, 2018, 2019). All the proteins that were allocated to be TI, TII peptides or non-N-end rule could be further investigated to confirm if they do upregulate in ESCs by investigating protein level by Western blotting.

Figure 4.8: Mass spectrometry of Ubr2 mutants can identify potential pathway proteins. (**A**) Venn diagram of proteins upregulated in *Ubr2*$^{-/-}$, *Ubr2*$^{T1/T1}$, *Ubr2*$^{T2/T2}$ and *Ubr2*$^{RD/RD}$ ESCs (**B**) Table of proteins that are potentially specific to either type I N-end rule (7), type II N-end rule (57) or non-N-end rule (21) pathways. All potential N-end rule substrates were upregulated in *Ubr2*$^{-/-}$ and *Ubr2*$^{RD/RD}$ ESCs. Proteins that were only increased in *Ubr2*$^{-/-}$ and *Ubr2*$^{RD/RD}$ ESCs were classified as non-N-end Rule.

A

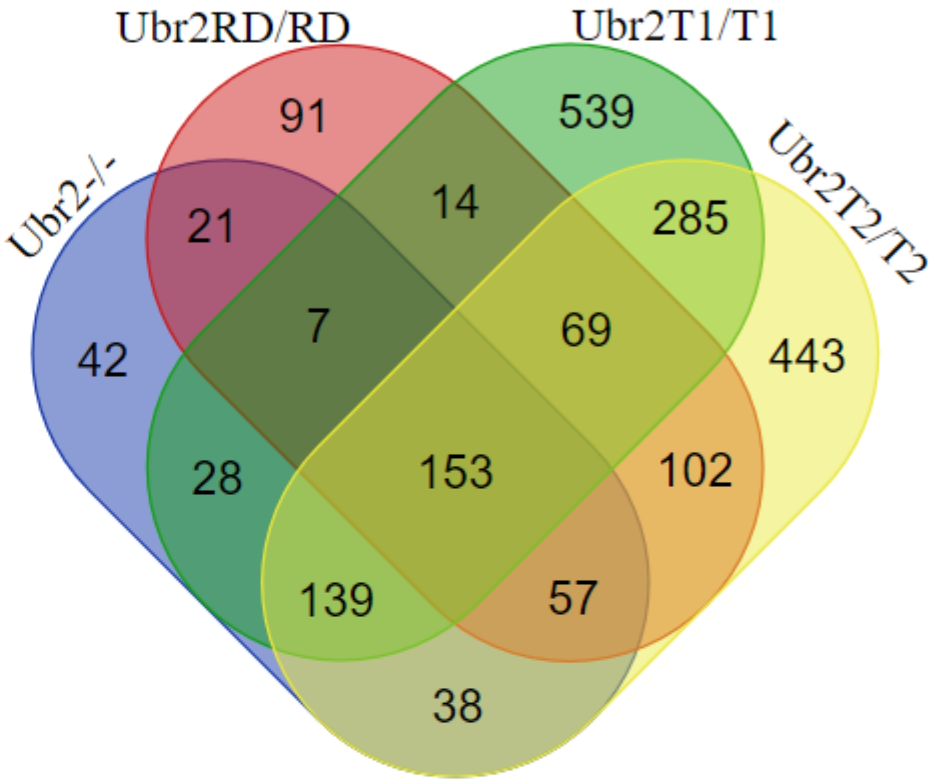

B

Pathway of *Ubr2*	**Genes**	**Upregulated in:**
TI N-end rule	Sra1 Cox7b Mfge8 Fkbp11 Cox16 Dpysl4 Pycard	*Ubr2*$^{-/-}$ *Ubr2*$^{RD/RD}$ *Ubr2*$^{T1/T1}$
TII N-end rule	Abi2 Pou3f1 Dazl Rhox6 Atxn10 Pik3c3 Zscan4f H1-6 Crabp2 Gm21293 Peg10 Krt8 Rab6a Gstk1 Zscan4d Npm1 Rap2c Prdm1 Zscan4-ps3 **Smc1β** Nrk Polr3g Uxs1 Krt15 Zbtb10 Krt19 Ppp1r13l Drap1 Mtmr7 Tmem9 **Dppa3** Pde6d Map2k4 Cnn2 Commd5 Zscan4e Sfn Fbxo15 Dmrt1 Sgpl1 Zscan4c Arhgap1 Dgke Eps8l2 Fermt2 Vtn Usp17le Mreg Prep F5 Myo1c Arf6 Ap3m1 Tuba3a Gm13212 Ube2r2 Helz	*Ubr2*$^{-/-}$ *Ubr2*$^{RD/RD}$ *Ubr2*$^{T2/T2}$
Non-N-end rule	Krt79 Bbx Itgav Pigx Pramef17 Hist2h2bb Sfmbt2 Trmt1l Znf516 **Tfap2c** Phf11 Hba-a1 Ppip5k2 Scoc Plek Fbxl20 Peg3 H2ac1 Ddx17 Crlf1 Ezhip	*Ubr2*$^{-/-}$ *Ubr2*$^{RD/RD}$

One protein identified within the MS data was Transcription Factor AP-2 Gamma (TFAP2C) which is a sequence-specific DNA-binding transcription factor involved in the activation of several developmental genes and chromatin organisation (Yan *et al.*, 2013). TFAP2C is increased 2.6 fold in *Ubr2*$^{-/-}$ and 2.3 fold in *Ubr2*$^{RD/RD}$ ESCs and is a potential non-N-end rule substrate of UBR2. The average raw label-free quantitation (LFQ) of each peptide identified in each ESC line shows the increase in the amount of detected peptides in *Ubr2*$^{-/-}$ and *Ubr2*$^{RD/RD}$ compared to *Ubr2*$^{+/+}$ ESCs (Figure 4.9A). It's apparent that the most N-terminal peptide detected (R120) is upregulated with a LFC of 1.4 (Fold change ~2) and that most peptides detected in *Ubr2*$^{-/-}$ and *Ubr2*$^{RD/RD}$ ESCs are upregulated when compared to *Ubr2*$^{+/+}$ ESCs. There appears to be little N vs C terminal bias in the upgregulated peptides suggesting there is little internal cleavage of proteins which would be consistent with a non-N-end rule substrate (Figure 4.9B).

To check if the ~2-fold increase in the ratio of TFAP2C in *Ubr2*$^{-/-}$ and *Ubr2*$^{RD/RD}$ ESCs compared to *Ubr2*$^{+/+}$ detected in the mass spec corresponds to a detectable increase in protein levels in the ESCs, I took whole cell lysate from the ESCs and ran them on a western blot and probed for TFAP2C. TFAP2C is composed of 449 amino acids with a molecular weight of 49kDa and could be detected by western blot (Figure 4.9C). There was no detectable increase in TFAP2C (Figure 4.9D) suggesting that the increase in protein abundance detected by MS did not correspond to a detectable increase in protein levels by Western blotting. Therefore, it is difficult to conclude whether TFAP2C is regulated by UBR2 in ESCs.

Figure 4.9 TFAP2C is not perturbed in *Ubr2* ESCs. (**A**) Mass spectrometry identification of Tfap2c peptides isolated. Site is the location of R or K within the peptide amino acid, Peptide sequence and *Ubr2*$^{x/x}$ LFQ is the average intensity value of peptide sequence. *Ubr2*$^{x/x}$ LFC is the mean Log_2(Fold change) of *Ubr2*$^{RD/RD}$ and *Ubr2*$^{-/-}$ LFQ compared to *Ubr2*$^{+/+}$. p-value is shown in brackets following Student's T-test. (**B**) Peptide sequence of mouse TFAP2C (Uniprot Q61312). Detected peptide sequences are highlighted in yellow. (**C**) Representative western blots of TFAP2C (~49kDa, Q61312) from whole cell lysate of wild type *Ubr2*$^{+/+}$, *Ubr2*$^{RD/RD}$ and *Ubr2*$^{-/-}$ ESCs and Lamin B1 as a loading control. (**D**) Quantified mean protein levels of TFAP2C from western blotting in C, corrected against Lamin B1 protein level, and relative to the wild type mean. Standard deviation over three pairs of *Ubr2* mutant ESCs. Differences between *Ubr2*$^{+/+}$ and *Ubr2*$^{RD/RD}$ or *Ubr2*$^{-/-}$ are not significant; *Ubr2*$^{RD/RD}$ p=0.46, or *Ubr2*$^{-/-}$ p=0.69 (Student's T-test).

A

Tfap2c		ESC genotype				
Site	**Peptide sequence**	***Ubr2*$^{+/+}$ LFQ**	***Ubr2*$^{RD/RD}$ LFQ**	***Ubr2*$^{RD/RD}$ LFC (p-value)**	***Ubr2*$^{-/-}$ LFQ**	***Ubr2*$^{-/-}$ LFC (p-value)**
R120	QSQEGSSLASHHSR	50542.6	131304.3	1.4 (0.01)	124661.1	1.3 (0.04)
R139	SASLIPHISGLEGGSVSAR	711018.3	2130493	1.6 ($1.5x10^{-5}$)	2378877	1.8 ($4.8x10^{-5}$)
R140	SASLIPHISGLEGGSVSARR	1382667	3313503	1.4 ($2x10^{-4}$)	3711507	1.6 ($7.7x10^{-5}$)
K201	KGPISMTK		256020.5	-		-
R229	DLVGVVMNPSEVFCSVPGR	350039	832572	1.3 (0.004)	646212.3	0.9 (0.05)
K238	DLVGVVMNPSEVFCSVPGRLSLLSSTSK		352856	-	335618	-
K238	LSLLSSTSK	3345407	7551403	1.3 ($3x10^{-4}$)	7353990	1.3 (0.001)
R248	VTVAEVQR	424190	1256900	1.6 (0.07)	999011.3	1.2 (0.03)
R248	YKVTVAEVQR	243458	785569.7	1.7 ($9.2x10^{-6}$)	912054	1.9 (0.001)
R266	RLSPPECLNASLLGGVLR	822007.7	2567117	1.6 ($2.4x10^{-6}$)	2877803	1.8 ($4.8x10^{-5}$)
R266	LSPPECLNASLLGGVLR	634541.3	1600453	1.3 (0.002)	1698793	1.4 (5x10-4)
R267	LSPPECLNASLLGGVLRR	2543620	6505320	1.4 ($6.2x10^{-5}$)	6940423	1.5 ($4.9x10^{-6}$)
R292	IGLNLPAGR	4898660	10107573	1 (0.002)	11877200	1.2 ($6x10^{-4}$)
R292	LDKIGLNLPAGR	227677.3	704808	1.9 (0.002)	807332.7	2.1 ($6x10^{-4}$)
R314	KAAHVTLLTSLVEGEAVHLAR		705749.7	-	722739.7	-
R314	AAHVTLLTSLVEGEAVHLAR	149839.7	426592.7	1.5 ($6x10^{-4}$)	418369	1.5 (0.02)
K327	DFAYVCEAEFPSK	2461513	4737983	0.9 (0.01)	5665490	1.2 ($3x10^{-4}$)
R341	AVADYLTRPHLGGR	1201437	2.23E+06	0.9 (0.15)	3.15E+06	1.4 (0.003)
K359	SMLLAAQQVCK	1140428	2109460	0.9 (0.04)	1857723	0.8 (0.06)
L424	EALIAIDK	2260610	3963213	0.8 (0.02)	4825563	1.1 (0.003)
K439	SYMNPGDQSPADSSK	206055.3	605294.7	1.7 ($8x10^{-4}$)	429474	1.2 (0.002)

B

>sp|Q61312|AP2C_MOUSE OS=Mus musculus OX=10090 GN=Tfap2c PE=1 SV=2

MLWKITDNVK YEEDCEDRHD SSSNGNPRIP HLSSPGQHLY SPAPPLSHTG VAEYQPPPYF

PPPYQQLAYS QSADHYSHLG EAYAAAMNPL HQPAATGSQQ QAWPGR QSQE GSSLASHHSR

SASLIPHISG LEGGSVSARR EVYRRSDLLL PHAHALEAGL AENLGLHEMA HPIEEVQNVD

DAHLLLHDQT VIRKGPISMT KNPLGLPCQK DLVGVVMNPS EVFCSVPGRL SLLSSTSKYK

VTVAEVQRRL SPPECLNASL LGGVLRRAKS KNGGRSLREK LDKIGLNLPA GRRKAAHVTL

LTSLVEGEAV HLARDFAYVC EAEFPSKAVA DYLTRPHLGG RNEMATRKSM LLAAQQVCKE

FTDLLHQDRT PNGNNRPAQV LEPNIQNCLS HFSLITHGFG SQAICAAVSA VQNYIKEALI

AIDKSYMNPG DQSPADSSKT MEKMEKHRK

C

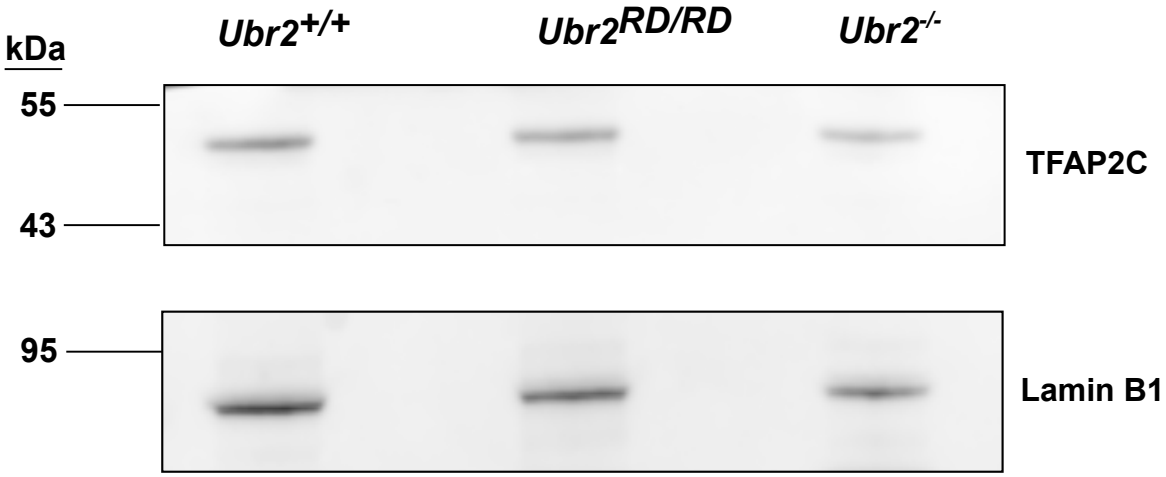
kDa
Ubr2+/+
Ubr2RD/RD
Ubr2-/-
55
43
TFAP2C
95
Lamin B1

D

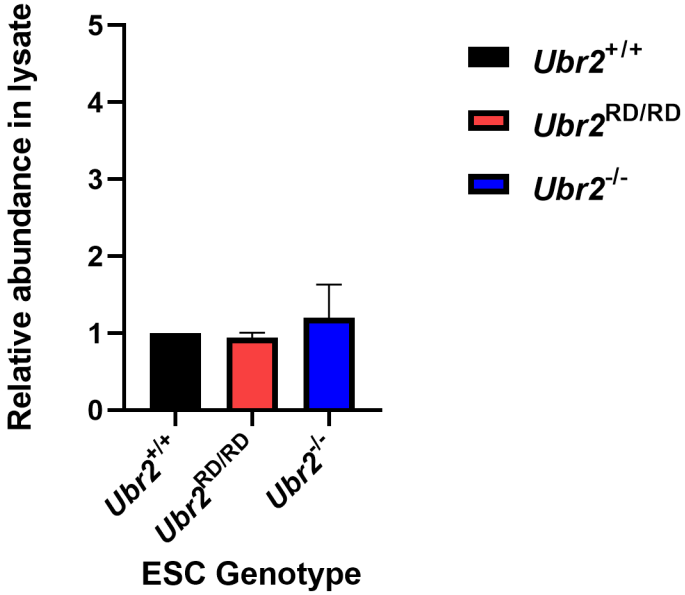
Relative abundance in lysate
5
4
3
2
1
0
Ubr2+/+
Ubr2RD/RD
Ubr2-/-
ESC Genotype
Ubr2+/+
Ubr2RD/RD
Ubr2-/-

A potential type II N-end rule substrate identified in the MS data was DPPA3 (also referred to as Stella or PGC7) which is mainly expressed in primordial germ cells but is also expressed in preimplantation embryos and pluripotent cells (Saitou and Yamaji, 2012). DPPA3 is increased 2.6 fold in *Ubr2*$^{-/-}$, 2.2 fold in *Ubr2*$^{RD/RD}$ and 2.5 fold in *Ubr2*$^{T2/T2}$ ESCs in the MS dataset. The mean raw LFQ of each peptide identified in each ESC line shows the increase in the amount of detected peptides in *Ubr2*$^{-/-}$, *Ubr2*$^{RD/RD}$ and *Ubr2*$^{T2/T2}$ compared to *Ubr2*$^{+/+}$ ESCs (Figure 4.10A). When the peptide sequences identified were mapped onto the protein sequence of DPPA3, most of the peptides were located at the C-terminus (Figure 4.10B). The DPPA3 protein has a cleavage point in at ^{59}LR↓NR^{62} where the C-terminal fragment, which has a N-residue at its amino terminus, is ubiquitinated and degraded (Shin *et al.*, 2017). This c-terminus peptide might be a potential N-end rule substrate but does appear to behave like a type I substrate of the N-end rule pathway in oocytes and early embryos (Shin *et al.*, 2017). DPPA3 was indicated as a type II N-end rule substrate in the MS but the cleavage and processing of DPPA3 may be different in ESCs.

To investigate if an increase in LFC of the peptides detected in the MS data corresponds to an increase in protein levels in the ESCs, whole cell lysate from the ESCs was taken and ran on a Western blot to probe for DPPA3. DPPA3 is a small protein, composed of 150 amino acids with a molecular weight of 20kDa. Two bands were detected by western blot one at 20kDA and a cleavage product of DPPA3 at 17kDa (Figure 4.10C) similar to what was identified in oocytes and early embryos (Shin *et al.*, 2017). Quantification

of the protein levels of three sample lysates showed there was no significant increase in DPPA3 (Figure 4.10D) suggesting that an increase detected protein by MS does not correspond to a detectable increase by Western blotting.

Figure 4.10 DPPA3 is not perturbed in *Ubr2* ESCs. (**A**) Mass spectrometry identification of DPPA3 (Stella) peptides isolated. Site is the location of R or K within the peptide amino acid, Peptide sequence and $Ubr2^{x/x}$ LFQ is the average intensity value of peptide sequence. $Ubr2^{x/x}$ LFC is the mean Log_2(Fold change) of $Ubr2^{T2/T2}$, $Ubr2^{RD/RD}$ and $Ubr2^{-/-}$ LFQ compared to $Ubr2^{+/+}$. p-value is shown in brackets. Student's T-test (**B**) Peptide sequence of mouse DPPA3 (Uniprot Q8QZY3). Detected peptide sequences are highlighted in yellow. (**C**) Representative western blots of DPPA3 (~20kDA, Q8QZY3) from three different whole cell lysate samples of wild type $Ubr2^{+/+}$, $Ubr2^{T2/T2}$, $Ubr2^{RD/RD}$ and $Ubr2^{-/-}$ ESCs. Arrows label 20kDA and 17 kDa bands of DPPA3. Lamin B1 as a loading control. (**D**) Quantified mean protein levels of all DPPA3 protein from western blotting in C, corrected against Lamin B1 protein level, and relative to the $Ubr2^{+/+}$ mean. Standard deviation over three pairs of *Ubr2* mutant ESCs. Differences between $Ubr2^{+/+}$ and $Ubr2^{T2/T2}$, $Ubr2^{RD/RD}$ or $Ubr2^{-/-}$ are not significant; $Ubr2^{T2/T2}$ p=0.80, $Ubr2^{RD/RD}$ p=0.28, or $Ubr2^{-/-}$ p=0.88 (Student's T-test).

A

DPPA3		*ESC Genotype*						
Site	**Peptide sequence**	***Ubr2*$^{+/+}$ LFQ**	***Ubr2*$^{T2/T2}$ LFQ**	***Ubr2*$^{T2/T2}$ LFC (p-value)**	***Ubr2*$^{RD/RD}$ LFQ**	***Ubr2*$^{RD/RD}$ LFC (p-value)**	***Ubr2*$^{-/-}$ LFQ**	***Ubr2*$^{-/-}$ LFC (p-value)**
K71	IAAVPVENK	283000	745666	1.4 (0.03)	775975	1.5 (0.02)	763045.5	1.4 (0.02)
K74	IAAVPVENKSEK	27475.3	90103.1	1.8 (0.001)	70029.7	1.3 (0.01)	73220.9	1.4 (0.005)
K101	TLLSVLKDPIAK	414521.5	639747.3	0.63 (0.05)	56112.3	0.44 (0.15)	784622.3	0.92 (0.006)
R122	LEGNEFER	126216	127368.5	0.2 (0.63)	56099.3	-1.2 (0.21)	170290.3	0.4 (0.26)
R128	LEGNEFERDSEPFR	255740	356185	0.5 (0.52)	296851.3	0.2 (0.33)	619295.3	1.3 (0.001)

B

>sp|Q8QZY3|DPPA3_MOUSE OS=Mus musculus OX=10090 GN=Dppa3 PE=1 SV=1

MEEPSEKVDP MKDPETPQKK DEEDALDDTD VLQPETLVKV MKKLTLNPGV KRSARRRSLR

NRIAAVPVEN KSEKIRREVQ SAFPKRRVRT LLSVLKDPIA KMRRLVRIEQ RQKRLEGNEF

ERDSEPFRCL CTFCHYQRWD PSENAKIGKN

C

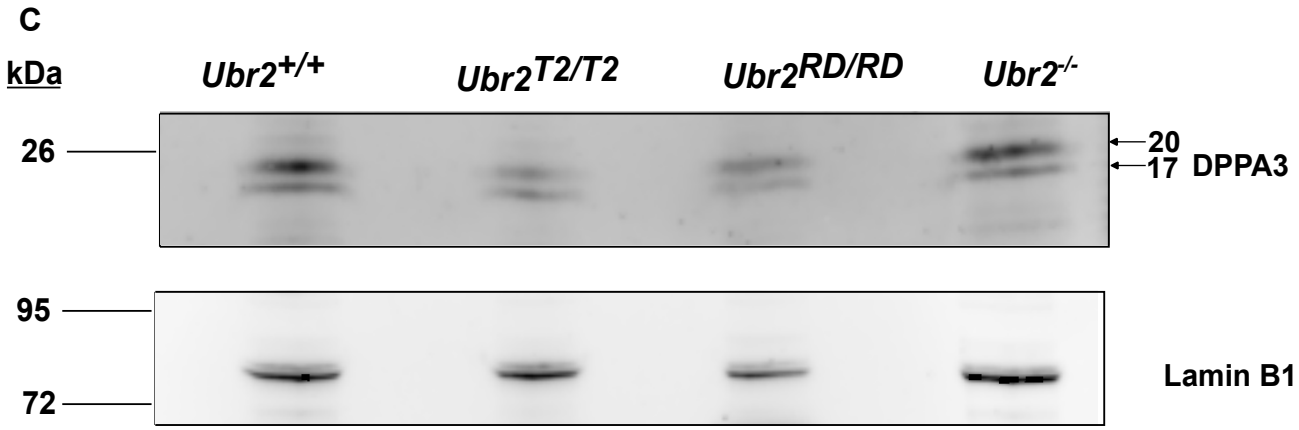

D

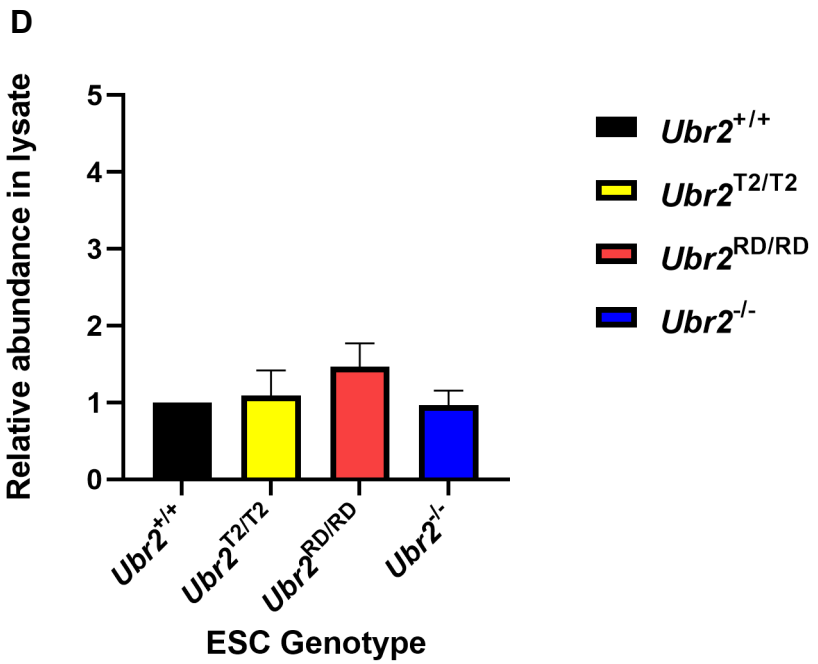

In Chapter 3, FLAG-ELL-UBR2 was shown to have a change in localisation in overexpression in HEK293Ts to be chromatin bound (Figure 3.7). However, it remains unknown whether this mutation leads to any functional changes. To further understand the effects of the K834A mutation in endogenous UBR2, the *Ubr2*$^{ELL/ELL}$ ESCs proteome was determined by MS. Protein abundances of each protein from *Ubr2*$^{ELL/ELL}$ ESCs was compared to wildtype *Ubr2*$^{+/+}$ controls and proteins with log FC> 1.5 were designated as upregulated and those with log FC< -1.5 were downregulated (Figure 4.11A). There were 1033 upregulated proteins and 382 downregulated proteins identified in *Ubr2*$^{ELL/ELL}$ when compared to *Ubr2*$^{+/+}$ control.

There did appear to be a larger number of upregulated proteins that you may expect from an E3 ubiquitin ligase and the upregulated proteins were used to undertake GO enrichment analysis to determine which biological processes these proteins were enriched in (Figure 4.11B). The highest fold enrichment was in the process of ribonucleoside triphosphate metabolic processing which is important in processes such as the pro-inflammatory response (Yu *et al.*, 2019). The *Ubr2*$^{ELL/ELL}$ upregulated proteins were compared to the type I, type II and non-N-end rule substrates identified in the earlier analysis and the majority of these substrates were also identified in the *Ubr2*$^{ELL/ELL}$ MS (Figure 4.11C and 4.11D). This indicates that the ELL mutation is perturbing UBR2 function and the K834 residue is important for UBR2's role in the ubiquitination of proteins.

4.11 Whole proteome of *Ubr2*$^{ELL/ELL}$ ESCs shows that introduction of K834A mutation into *Ubr2* leads to proteomic shift (**A**) Volcano plot of MS results shows the proteins in *Ubr2*$^{ELL/ELL}$ compared to *Ubr2*$^{+/+}$ ESCs. Y-axis represents -$\log_{10}$(p-value) and proteins with a positive Log_2 fold change (Mean Log2 Ratio) are upregulated and negative values represent downregulated proteins in the *Ubr2*$^{ELL/ELL}$ ESCs, respectively. All protein changes have a p=value <0.05 and those that have Fold change >1.5 are highlighted in red, Fold change <-1.5 are highlighted in blue. Upregulated proteins=1033 and downregulated proteins=382. Gene names of proteins with the highest Log(Fold change) are labelled alongside *Smc1b*, *Tfap2c* and *Dppa3*. (**B**) GO term analysis of the biological processes upregulated proteins from *Ubr2*$^{ELL/ELL}$ ESCs. 1033 significant upregulated proteins were compared to the background of 5424 proteins identified by MS. nGenes is number of genes in upregulated group, Pathway genes is the number of genes in the biological processes pathway and Fold enrichment is the calculated increase enrichment compared to the background. (**C**) Venn diagram of TI N-end rule (7), TII N-end rule (57) or non-N-end rule (21) proteins and upregulated proteins in *Ubr2*$^{ELL/ELL}$ ESCs (**D**) Table of proteins that are potentially specific to either TI N-end rule (5), TII N-end rule (53) or non-N-end rule (13) pathways and upregulated in *Ubr2*$^{ELL/ELL}$ ESCs.

A

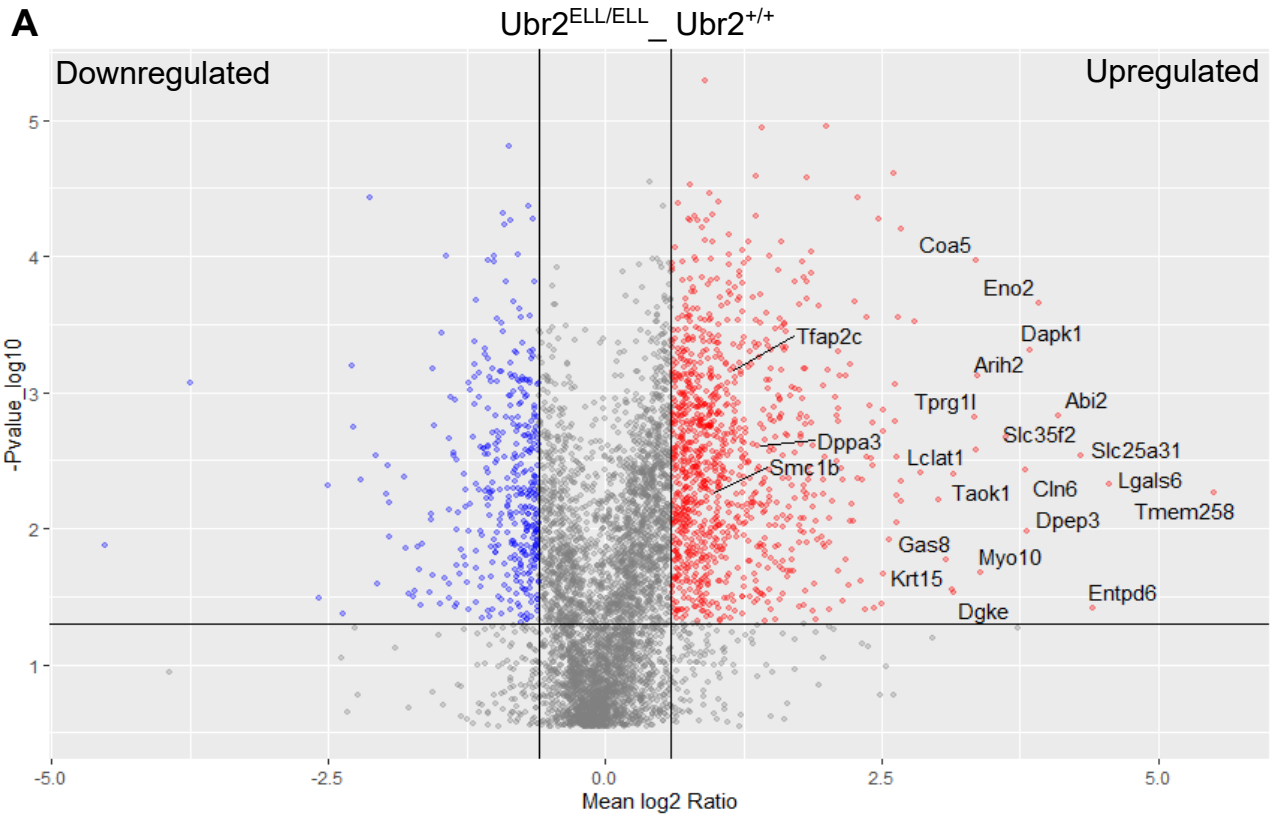

B Upregulated

Enrichment FDR	nGenes	Pathway Genes	Fold Enrichment	GO Biological Processes
1.20E-10	47	91	2.3	Ribonucleoside triphosphate metabolic proc.
3.10E-10	44	83	2.3	Purine ribonucleoside triphosphate metabolic proc.
2.80E-08	35	68	2.3	Purine ribonucleoside triphosphate biosynthetic proc.
9.20E-07	29	52	2.3	Aerobic electron transport chain
1.60E-11	56	116	2.2	Nucleoside triphosphate metabolic proc.
3.30E-09	44	93	2.2	Mitochondrial transmembrane transport
1.10E-08	41	85	2.2	Nucleoside triphosphate biosynthetic proc.
1.4E-07	39	58	2.2	NADH dehydrogenase complex assembly
1.00E-10	63	177	2.1	Purine nucleotide biosynthetic proc.
3.10E-13	95	215	1.9	Cellular respiration

C

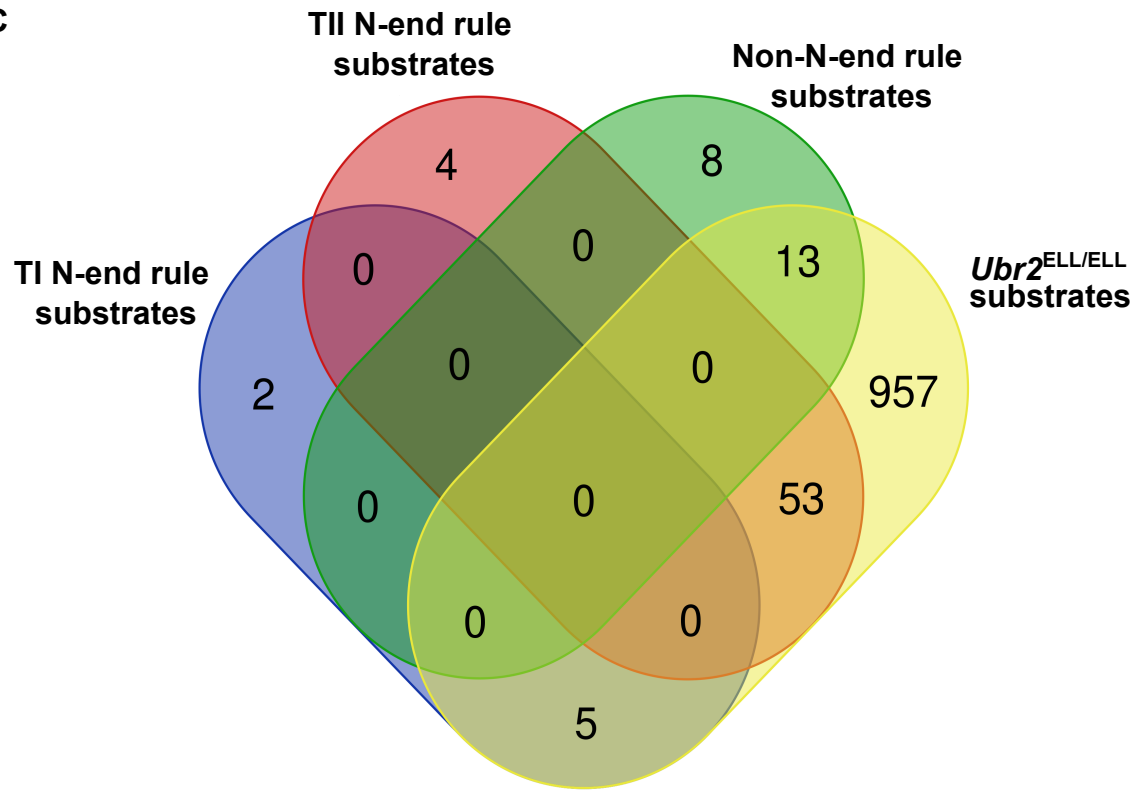

D

Genes	Upregulated in:
TI N-end rule Cox7b Mfge8 Fkbp11 Cox16 Pycard	*Ubr2*$^{-/-}$ *Ubr2*$^{RD/RD}$ *Ubr2*$^{T1/T1}$ *Ubr2*$^{ELL/ELL}$
TII N-end rule Abi2 Pou3f1 Rhox6 Pik3c3 Zscan4f H1-6 Crabp2 Peg10 Krt8 Rab6a Gstk1 Zscan4d Npm1 Rap2c Prdm1 Zscan4-ps3 **Smc1β** Nrk Polr3g Uxs1 Krt15 Zbtb10 Krt19 Ppp1r13l Drap1 Mtmr7 Tmem9 **Dppa3** Pde6d Cnn2 Commd5 Zscan4e Sfn Gm13212 Fbxo15 Dmrt1 Sgpl1 Zscan4c Arhgap1 Dgke Eps8l2 Fermt2 Vtn Mreg Gm21293 PrepF5 Myo1c Arf6 Ap3m1 Helz Ube2r2	*Ubr2*$^{-/-}$ *Ubr2*$^{RD/RD}$ *Ubr2*$^{T2/T2}$ *Ubr2*$^{ELL/ELL}$
Non-N-end rule Krt79 Bbx Itgav Hist2h2bb Sfmbt2 Trmt1l **Tfap2c** Ppip5k2 Scoc Plek Fbxl20 H2ac1 Crlf1	*Ubr2*$^{-/-}$ *Ubr2*$^{RD/RD}$ *Ubr2*$^{ELL/ELL}$

4.3 Discussion

In this chapter, I introduced point mutations into protein-binding interfaces of UBR2 in ESCs to separate out N-end rule and non-N-end rule ubiquitination to identify substrates of these pathways. I identified, by mass spectrometry that *Ubr2*$^{-/-}$ and the other mutant ESCs have a large proteomic shift when compared to *Ubr2*$^{+/+}$ controls and these proteins are from a wide background. However, it was difficult to confirm the proteins that were identified to be potential substrates by Western blotting suggesting that there may be some quantification differences between methods. *Ubr2*$^{ELL/ELL}$ ESCs had a large overlap with proteins identified as potential N-end rule and non-N-end rule substrates suggesting that the K834 residue is important for ubiquitination.

4.3.1 *Ubr2*$^{-/-}$ ESCs proteome indicates a role in turnover of mitochondrial proteins and histones

The *Ubr2*$^{-/-}$ ESCs previously generated in our group contain a premature stop codon in exon 3 leading to an early truncated protein and were used to identify any biological pathways and substrates by investigating their proteome by mass spectrometry. As UBR2 is an E3 ubiquitin ligase of the Arg/N-end rule pathway, I was largely interested in the proteins that were upregulated once UBR2 had been removed.

The largest group of proteins that were upregulated in *Ubr2*$^{-/-}$ ESCs were proteins involved in multiple mitochondria processes indicating a role for UBR2 in the organelle. Mitochondrial processing protease cleaves the N-

terminal of nuclear-encoded mitochondrial proteins when imported into the matrix from the cytosol which results in destabilizing N-terminal residues (Vögtle *et al.*, 2009; Schmidt, Pfanner and Meisinger, 2010). In *S. cerevisiae*, mitochondrial processing peptidases Icp55 and Oct1 remove destabilising residue from the N-terminal to prevent degradation by an N-end rule pathway (Vögtle *et al.*, 2009, 2011). Yet it remains unclear what is the function of the N-end rule pathway and the identity of the *N*-recognin and protease responsible for the recognition and degradation of N-end rule substrates in mitochondria. UBR2 may be an important player in this but further research into the N-end rule pathway of mammalian mitochondria is required.

Also, UBR2 has been implicated in the cytosolic mitochondrial quality control pathway in neurodegenerative diseases such as Parkinson's disease. Tensin homolog (PTEN)-induced kinase 1 (PINK1) plays an essential role in mitochondrial quality control as the N-terminus of PINK1 is inserted into the inner mitochondrial membrane (IMM), where an IMM protease, PARL, cuts PINK1 between residues Ala103 and Phe104, releasing a C-terminal fragment of PINK1 (Phe104-PINK1) into the cytosol (Jin *et al.*, 2010; Greene *et al.*, 2012; Yamano and Youle, 2013). This fragment is recognised by UBR proteins UBR1, UBR2 and UBR4 and removed by the UPS (Yamano and Youle, 2013). PINK1 is expressed in ESCs (Wang *et al.*, 2021) but it was not detected in the MS data. UBR2 may be important for ubiquitination of other mitochondrial proteins in a similar way to PINK1.

The proteins designated as downregulated in *Ubr2*$^{-/-}$ ESCs were enriched in metabolic processes of the cell, RNA activity and Histone H2B ubiquitination. Previously, mammalian UBR2 was associated with the ubiquitination of histone protein H2A (An *et al.*, 2012) and as several histones were detected in the MS, UBR2 is important for multiple histone ubiquitination. This function may be evolutionarily conserved because the yeast ortholog of *Ubr*1 is implicated in the turnover of an H3-like histone (Cheng *et al.*, 2017). *Campos et al* found that the histone, H2B, is a target for UBR7-dependent ubiquitination (Campos *et al.*, 2015) suggesting redundancy in histone ubiquitination between UBR proteins. It was surprising that depletion of an E3 ubiquitin ligase would lead to a large amount of downregulated protein in ESCs suggesting that UBR2 has a role in regulation of inhibitors of proteins that remain to be identified.

4.3.2 Point mutations in protein-binding interfaces of UBR2 identified potential ubiquitin substrates

Point mutations were introduced to *Ubr2* in protein-binding interfaces to test whether these interfaces are required for UBR2 functions in ESCs. The W1177A mutation in *Ubr2*'s RING domain was previously shown to perturb the binding of E2 ubiquitin conjugating enzymes, USE1 and UBE2A, to UBR2 (Lee *et al.*, 2011). Placing this mutation into ESCs allowed for identification of potential N-end rule and Non-N-end rule ubiquitin targets of endogenous UBR2. ~50% of upregulated proteins in *Ubr2*$^{RD/RD}$ ESCs were upregulated in *Ubr2*$^{-/-}$ ESCs and ~40% of downregulated proteins in *Ubr2*$^{RD/RD}$ were

downregulated in *Ubr2*$^{-/-}$ ESCs indicating that the W1177A mutation is impairing UBR2 function in a somewhat similar way to *Ubr2*$^{-/-}$. There are upregulated proteins in *Ubr2*$^{-/-}$ ESCs that are not also upregulated in *Ubr2*$^{RD/RD}$ ESCs. These could be proteins that are UBR2 interactors for other non-canonical functions outside of ubiquitination. The only protein that has been identified as having this type of role with UBR2 is TEX19.1 (Yang *et al.*, 2010; Reichmann *et al.*, 2020).

As UBR2 has a previously characterised role in turnover of chromatin-associated AcSMC3 cohesin in ESCs (Karen Dobie, unpublished), I was particularly interested in cohesin subunits in the MS. As described in Chapter 1, cohesin has multiple subunits that bind to form a tripartite ring where the SMC3 subunit of cohesin is acetylated during S phase to establish cohesion between replicated chromosomes (Beckouët *et al.*, 2010). Multiple cohesin subunits were detected in the MS but the only cohesin subunit that had a significant fold change was the meiosis specific SMC1β subunit. There has been no previous work to determine whether UBR2 has any role in the turnover of SMC1β-containing cohesin. SMC1β is present in ESCs and important for binding of REC8-cohesin complexes that are essential for sister chromatid cohesion (Choi *et al.*, 2022). SMC1β was identified as a potential type II N-end rule peptide from the MS data but the N-terminus of the protein is MGHLELLLVE which would not make it a typical N-end rule substrate as methionine cleavage would lead to N-terminal glycine and no UBR2 binding was observed with peptides bearing N-terminal Glycine residue (Tasaki *et al.*, 2009). Potentially, there may be cleavage of SMC1β protein in ESCs leading

to a C-terminal fragment that has a type II N-end rule degron or it may be a met-Φ substrate of UBR2. Bioinformatic techniques should be used to determine any potential SMC1β cleavage sites and then confirm if cleavage products arise *in vitro*.

In Chapter 3, the introduction of the K834A mutation in the ELL domain of FLAG-UBR2 changed localisation to chromosomes in HEK293T cells. Structural analysis in yeast Ubr1 showed that the proteins base is a helical scaffold consisting of four regions interspaced by three domains: the UBR box, N-domain and the WHD which participates in the interaction with the donor Ub that is transferred during ubiquitination of a substrate (Pan *et al.*, 2021). The WHD is similar to the ELL domain in mouse UBR2 indicating that this domain has a role in ubiquitination. *Ubr2*$^{ELL/ELL}$ ESCs had a large overlap of its upregulated proteins with proteins that were identified as potential N-end rule or non-N-end rule substrates of UBR2 in the MS. This suggests that the ELL domain and the K834 residue is important for ubiquitination of proteins. As the change in localisation in Chapter 3 only occurred with FLAG-ELL-UBR2 and not the other UBR2 mutants, this localisation alteration is not due to the ubiquitination function of UBR2.

Previously, *Ubr2*$^{-/-}$ ESCs have an increase in AcSMC3-marked cohesin levels during G2/M detected by Western blotting (Karen Dobie, unpublished). *Ubr2*$^{T1/T1}$ ESCs did not have an increase in chromatin-associated AcSMC3 during G2/M (Eleanor Raymond, unpublished) suggesting that UBR2's type I N-end rule binding is not important for this role. Synchronising these *Ubr2*

mutants to G2/M and quantifying cohesin subunit protein levels in lysates will help determine whether this change in AcSMC3 is due to type II N-end rule or Non-N-end rule ubiquitination in ESCs. Also the *Ubr2* mutant ESCs could be synchronised to G2/M and then ran on the MS to determine if any of the detected protein changes are found throughout the cell cycle or if there are any specific to mitosis.

4.3.3 Limitations of this study

Comparisons of proteomes of *Ubr2*$^{T1/T1}$ and *Ubr2*$^{T2/T2}$ ESCs could help identify potential substrates of UBR2's function in the N-end rule pathway. Only a small number of proteins were found to be upregulated in the three allocated groups: type I N-end rule (*Ubr2*$^{T1/T1}$, *Ubr2*$^{-/-}$ and *Ubr2*$^{RD/RD}$), type II N-end rule (*Ubr2*$^{T2/T2}$, *Ubr2*$^{-/-}$ and *Ubr2*$^{RD/RD}$) and non-N-end rule (*Ubr2*$^{-/-}$ and *Ubr2*$^{RD/RD}$) substrates. As each *Ubr2* mutant proteome was compared to wildtype *Ubr2*$^{+/+}$ ESCs before being grouped into these categories, proteins that may be upregulated in *Ubr2*$^{T2/T2}$ ESCs when compared to other mutants like *Ubr2*$^{T1/T1}$ are excluded. Further analysis with different combinations of *Ubr2* mutant comparisons, without the initial comparison to *Ubr2*$^{+/+}$, may lead to identification of more upregulated proteins.

There was a large amount of proteins that were upregulated in all ESC mutants suggesting that there is lack of specificity in the proteins detected by MS. A BioID (biotinylated protein identification) or TurboID fusion-UBR2 protein could be generated and expressed in ESCs to allow selective isolation and identification of interacting proteins, like E2 ligases and short-

lived substrates, with affinity capture and MS (Roux, Kim and Burke, 2013; Doerr, 2018). BioID has successfully identified over 50 substrates, in combination with proteasomal inhibition with MG-132, of the RING-type E3 complex Skp Cullin F-box β-TrCP1/2 E3 ligases (Coyaud *et al.*, 2015). All mutant UBR2 proteins could be used as a BioID fusion protein to assess type I, type II and non-N-end rule interactions.

Additionally, alanine-scanning mutagenesis of the UBR box and N-domain of UBR1 identified the two point mutations: D118A and D233A, which specifically interfere with the ability of UBR1 to bind either Type I or Type II substrates, respectively (Tasaki *et al.*, 2009). Peptide pulldowns for D118A and D233A showed a reduction in type I and type II binding ability of UBR2 in ectopically overexpressed FLAG construct in HEK293T cells and a reduction in type II binding ability in endogenous UBR2 in testis (Eleanor Raymond, unpublished). However, this does not necessarily demonstrate a full ablation of type I and type II binding ability. For example, T2-UBR2 may still be able to bind type II substrates that do not contain an N-terminal phenylalanine, which is the most common type II sequence and was used as the TII peptide in these experiments, or with type II-like substrates such as non-acetylated Met-Φ proteins. Examination of the mutant UBR2 proteins by peptide pulldown in ESCs is required and pulldown with different peptide sequences could be used to predict the extent of their binding ability.

Also, even though the W1177A mutation in RING domain led to depletion of E2 ubiquitin conjugating enzymes USE1 and UBE2A binding (Lee *et al.*,

2011), UBR2 has been confirmed to act through a variety of other E2 enzymes including UBE2O and UBE2B (An *et al.*, 2010; Xu *et al.*, 2019). So this point mutation may not necessarily prevent binding of all potential E2 ubiquitin ligases and not generate a fully penetrant catalytic dead mutation. Co-immunoprecipitation assays could be carried out in order to test the extent of the mutation in ESCs, as well as the conservation of the UBR2 RING domain structure between different potential E2 interactors.

The biggest limitation of this study is even though there was over a ~2-fold increase in the MS data for both DPPA3 and TFAP2C this was not observed by Western blotting. MS quantification uses multiple signals (multiple transitions per peptide, multiple peptides per protein, and multiple measurements of each signal) to indicate the protein quantity. Western blotting assay essentially depends on the specificity of the antibodies used which may not be as well characterised. The anti-TFAP2C antibody (PA5-49862) was raised against the 400-450aa end of the protein. As TFAP2C is a non-N-end rule substrate there would be no bias expected in peptides detected in the N-terminus and the C-terminus so quantification of protein levels with an antibody raised against this end of protein should be able to detect changes in protein level by Western blotting. The anti-DPPA3 antibody (Sc-67249) was raised against full length mouse DPPA3 which was able to identify the full length and cleaved protein in the ESC lysate (Figure 4.10C) which was previously identified in mouse oocytes and embryos (Shin *et al.*, 2017). However, quantification by Western blotting has not confirmed what was observed in the MS making it difficult to confirm that DPPA3 is a type II

N-end rule substrate or TFAP2C is a non-N-end rule substrate of UBR2. Further work is needed to confirm that these potential substrates are upregulated in these cells.

4.3.4 Summary

In summary, placing point mutations in protein-binding interfaces of endogenous UBR2 in ESCs does not impair cell growth or the stabilisation of TEX19.1. Mass spectrometry analysis identified potential substrates of N-end-rule or non-N-end rule pathways but these were not confirmed by Western blotting. This leads to difficulty in concluding that these are real substrates of UBR2.

Chapter 5:
Mutations in the RING domain of UBR2 in mice

5.1 Introduction

UBR2 has previously been implicated in genomic stability and homologous recombination in a mitotic context (Ouyang *et al.*, 2006) and is one of four UBR proteins that have been shown to have activity in the N-end rule protein recognition system of the UPS (Tasaki *et al.*, 2009). Although *Ubr2* is relatively ubiquitously expressed, the *Ubr2*$^{-/-}$ mouse has phenotypes in a specific subset of tissues suggesting that UBR2 has essential molecular functions in specific tissues either through N-end rule protein ubiquitination or other non-canonical functions.

One of the best characterised phenotypes of *Ubr2*$^{-/-}$ is in male meiosis, characterised by gross morphological changes in seminiferous tubules of the testis, low testis weight and lack of mature sperm leading to male infertility (Kwon et al., 2003). Chromosome spreads of *Ubr2*$^{-/-}$ testes confirm defects in progression through meiotic prophase, and very few spermatocytes progress through pachytene into diplotene with a significant increase in asynapsis during pachytene (Crichton *et al.*, 2017). These asynapsed chromosomes are present in multiple configurations consistent with defects in meiotic recombination and homolog pairing, similar to those found in *Tex19.1*$^{-/-}$ spermatocytes.

UBR2 has a 1:1 stoichiometric interaction with TEX19.1, which is a germline genome defence protein primarily expressed in hypomethylated tissues, including the ovaries, testes and in ESCs in culture (Öllinger *et al.*, 2008; Maclennan *et al.*, 2017; Reichmann *et al.*, 2020). When ectopically

expressed, TEX19.1 is able to regulate the Type II N-end rule substrate binding activity of UBR2 so can regulate UBR2's ability to target Type II substrates for N-end rule ubiquitination (Tasaki *et al.*, 2005; Reichmann *et al.*, 2020). Further investigation of *Ubr2*$^{-/-}$ testes showed that loss of UBR2 results in loss of TEX19.1 protein but not *Tex19.1* mRNA (Yang *et al.*, 2010), suggesting that UBR2 prevents degradation of TEX19.1, possibly through UBR2 being an obligate binding partner of TEX19.1.

Interestingly, somatic tissues appear unperturbed in adult *Ubr2*$^{-/-}$ males (Kwon *et al.*, 2003) but investigation of the rapidly proliferating adult mouse spleen, where TEX19.1 is not expressed, of *Ubr2*$^{-/-}$ mice found a 2-fold increase in the AcSMC3 chromatin-associated cohesin subunit (Reichmann *et al.*, 2020). UBR2 appear to have a role in regulating AcSMC3 in splenocytes. The introduction of the point mutation D233A into UBR2's N-domain in mice, previously shown to decrease Type II peptide binding, did not cause any of the overt phenotypes seen in *Ubr2*$^{-/-}$ mice (Eleanor Raymond, unpublished). Thus, Type II substrate binding does not appear to be important for the overt *in vivo* functions of UBR2. This, in combination with the UBR box D118A point mutation not causing an increase in the amount of chromatin-associated AcSMC3 at G2/M in mouse embryonic stem cells suggests that neither Type I nor Type II substrate binding are important for the recently uncovered novel role of UBR2 in cohesin regulation (Eleanor Raymond, unpublished). Separation of the TEX19.1-stabilising and non-N-end rule ubiquitination functions of UBR2 at the biochemical level could dissect out which leads to the phenotypes observed in *Ubr2*$^{-/-}$ mice.

In this chapter, I aimed to look at the importance of *Ubr2*'s RING domains in UBR2's major functions and investigate the molecular basis of the null phenotypes. I introduced a mutation in the protein-binding interface of the E2 binding RING domain to understand UBR2's molecular functions more closely. A conserved Tryptophan (W1177) was found in a region of UBR1 and UBR2 proteins and mutating W1177 to an alanine (W1177A) in the RING domain reduced the affinity of the E2 ubiquitin conjugating enzymes USE1 and UBE2A/B (Lee *et al.*, 2011). I generated $Ubr2^{W1177A/W1177A}$ using CRISPR to assess the hypothesis that UBR2 primarily acts through non-canonical functions. The W1177A mutation in the RING domain does lead to a cohesin phenotype and suggests that UBR2 carries out its essential *in vivo* functions through promoting protein degradation through a non-canonical, non N-end rule pathway.

5.2 Results

5.2.1 Generation of RING domain mutants of UBR2

5.2.1.1 Generation of the *Ubr2^{W1177A}* point mutation in mice using genome editing

I utilised CRISPR-Cas9 technology to generate an *Ubr2*^{W1177A} mouse line carrying the W1177A point mutation (Lee *et al.*, 2011) in the RING domain (hereafter referred to as *Ubr2RD*). The introduction of the point mutation into the locus was undertaken by use of a wild type Cas9 for the generation of double-strand breaks (Cong *et al.*, 2013) and a homology directed repair template, which can be introduced into the break site by recombination (Figure 5.1A).

Ubr2$^{-/-}$ males are infertile so I used both a wild type and mutant repair template to reduce the editing efficiency with the mutant repair to ensure that heterozygote mice are generated for further breeding and colony establishment. The repair templates were designed such that either the wild type sequence or the W1177A point mutation could be integrated, with a mutant PAM site in both to prevent re-editing after repair template integration (Figure 5.1B). These were injected alongside the guide complex with tracrRNA into the cytoplasm of single-celled mouse zygotes (Figure 5.1C). The guide sequence was designed specific to a region within 10bp of the target residue, with a PAM sequence on the 3' end which is a NGG motif that is required for Cas9 binding. Following injection, zygotes were cultured overnight then transferred into a surrogate mother in the CD1 background

(Figure 5.1C) and the pups born were screened at weaning (3 weeks post-partum) for successful integration of the repair templates. 40 individuals were successfully born following one round of zygote injections and genotyped as in Figure 5.2. Of these individuals, 24 had undergone active genomic editing with 22 of these mice were identified as being heterozygote for the RD (*Ubr2*^{W1177A}) mutant allele (55% successful editing). However, most of these mice also had at least one *Ubr2* allele containing unintended mutations that presumably arose from error-prone repair of the Cas9-induced DSB. Thus, one round of breeding with wild type C57BL/6J mice was carried out in order to generate *Ubr2*$^{+/RD}$ heterozygous offspring, which were then interbred as a stable mouse colony (Fig. 5.1C), expected to produce 25% *Ubr2*$^{RD/RD}$ animals based on normal Mendelian genetics.

Figure 5.1: Generation of an *Ubr2*^{W1177A} mouse line using CRISPR-Cas9. (**A**) Schematic of CRISPR-wtCas9 homology directed repair. Taken from www.addgene.org/crispr/guide/. (**B**) CRISPR-HDR guide and repair sequences for the UBR2-RD CRISPR experiment. PAM sequence is shown in bold and cut site of wtCas9 enzyme marked by ^. Introduced point mutations are marked in repair templates in green. Homology arms are underlined. (**C**) Schematic representation of zygotic injection of CRISPR components and breeding strategy for *Ubr2*^{W1177A} mouse colony establishment. Components were introduced by injection into the cytoplasm of the single-celled zygote, then cultured and transferred into a CD1 host mother. Pups born were on the C57BL/6J background and those carrying a RD (*Ubr2*^{W1177A}) allele identified then bred with C57BL/6J wild type mice. Heterozygous *Ubr2*$^{RD/+}$ offspring were then crossed together to produce *Ubr2*$^{RD/RD}$ experimental mice and *Ubr2*$^{+/+}$ littermate control animals.

A

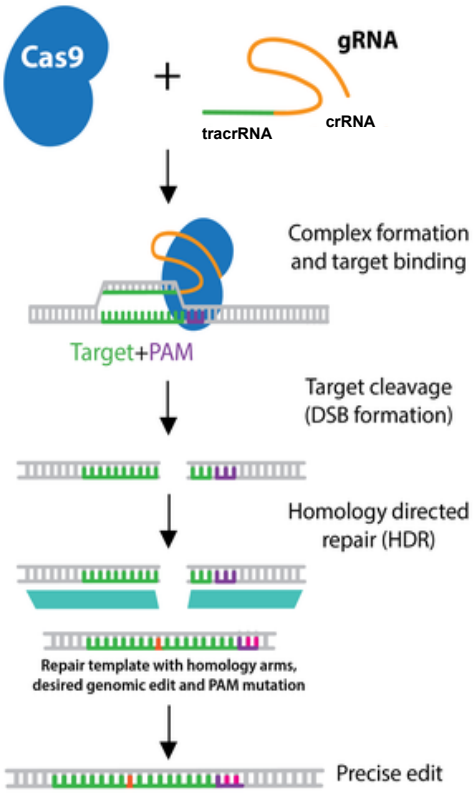

B

Experiment	Guide Sequence	Repair Template	Restriction Site
RD (W1177A) TGG>GCG	Sense: CAAATTACCTT TGCCAA^CAA**T GG**	Mutant: TTGTTTTATAATGCAGAAAAATATGATCCATTA TTCATGCACCCCGATCTGTCTTGTGGGACAC ACACTGGCAGCTGTGGGCACGTTATGCATGC GCATTGT GCGCAAAGGTAATTTGTATTCTTAT ATTACTCAGGGAACACCATCTGAAGGCTCAG GATTGACTTTTAAAGCAAAGGAAAATTTGTGC TGGGGGTGG Wildtype: TTGTTTTATAATGCAGAAAAATATGATCCATTA TTCATGCACCCCGATCTGTCTTGTGGGACAC ACACTGGCAGCTGTGGGCACGTTATGCATGC GCATTGTTGGCAAAGGTAATTTGTATTCTTAT ATTACTCAGGGAACACCATCTGAAGGCTCAG GATTGACTTTTAAAGCAAAGGAAAATTTGTGC TGGGGGTGG	TGC^GCA

C

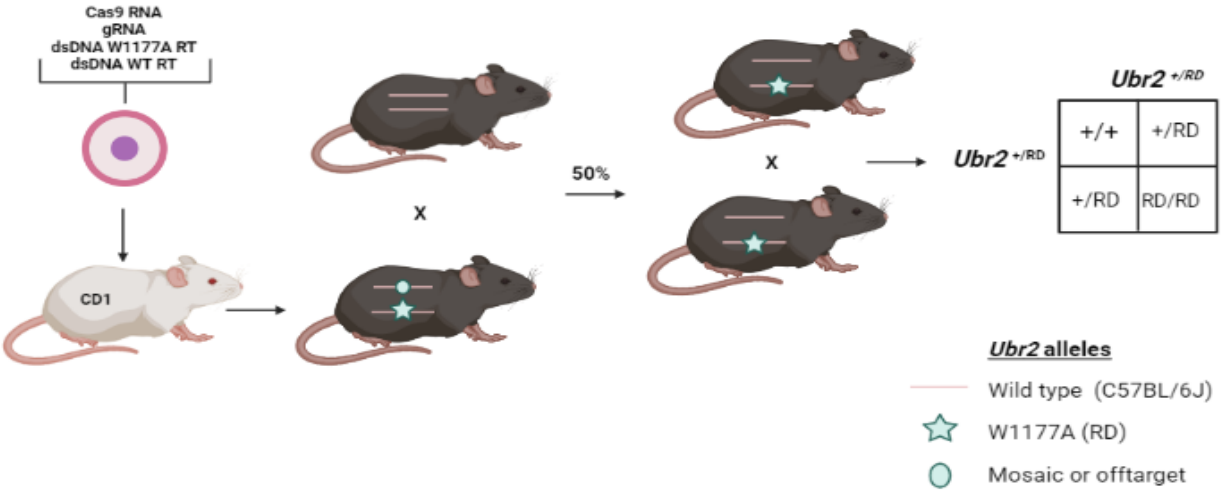

All subsequent colony genotyping was carried out using PCR with primers RD_F and RD_R that flank the edited region of *Ubr2* (Figure 5.2A) to generate a 499bp PCR product, this was followed by restriction digest with the *FspI* restriction enzyme. The *Ubr2*^{W1177A} mutated allele has an *FspI* site (TGC^GCA). Mice generated from heterozygoous (*Ubr2*$^{+/RD}$ x *Ubr2*$^{+/RD}$) intercrosses were genotyped in this way and then assayed by gel electrophoresis (Figure 5.2B). Following digestion, the uncut PCR product gives a band of 499bp, present in wild type (*Ubr2*$^{+/+}$) and heterozygote mice (*Ubr2*$^{+/RD}$). W1177A mutants are cut at TGC^GCA which leads to the production of 2 bands, 431bp and 68bp (Figure 5.2B). However, it can remain difficult to detect the 68bp fragment on the gel but these genotypes can be confirmed using Sanger sequencing of the 499bp PCR fragment (Figure 5.2C). Wild type *Ubr2*$^{+/+}$ mouse 9756 has the Tryptophan (W) TGG codon and a wild type PAM site (CCA, sense TGG). *Ubr2*$^{RD/RD}$ mouse 9760 has the Ala-encoding (A) GCG codon and a silently mutated PAM site (GCA, sense TGC).

Using these genotyping tools, it was possible to generate and maintain a stable mouse line with the *Ubr2*RD (W1177A) mutation. For all further experiments in this chapter, *Ubr2*$^{RD/RD}$ experimental mice were generated from heterozygous (*Ubr2*$^{+/RD}$ × *Ubr2*$^{+/RD}$) crosses, and all control animals used were *Ubr2*$^{+/+}$ or *Ubr2*$^{+/RD}$ from the same colony.

Figure 5.2: Genotyping of *Ubr2* W1177A mouse colony using *Fsp1* restriction digest and Sanger sequencing. **(A)** Location of W1177 in Ubr2 exon 31 and placement of RD_F and RD_R primers used in genotyping. Arrow indicates exon 31 and W1177. (**B**) Representative gel electrophoresis of one litter of mice from a *Ubr2*$^{+/RD}$ × *Ubr2*$^{+/RD}$ heterozygous cross, showing *FspI* digest for RD genotyping. 100bp ladder shown on left. Wild type band is 499bp. Homozygote allele bands following digestion is 400bp and 99bp. * Indicates low levels of undigested PCR product present in homozygous samples. (**C**) Representative Sanger sequencing data generated from earclips of mice: *Ubr2*$^{+/+}$ 9756 and *Ubr2*$^{RD/RD}$ 9760.

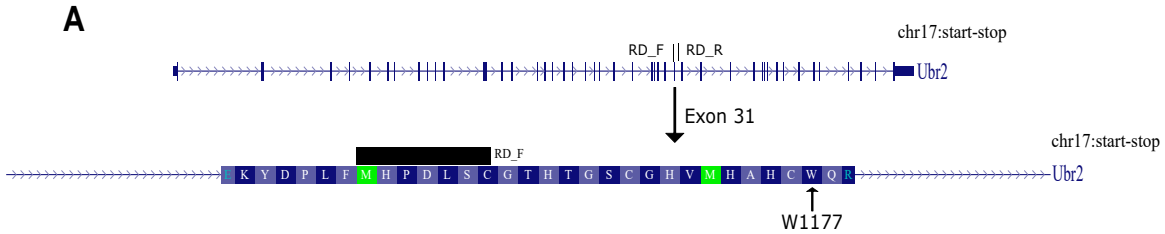
A
chr17:start-stop
RD_F
RD_R
Ubr2
Exon 31
chr17:start-stop
RD_F
Ubr2
W1177

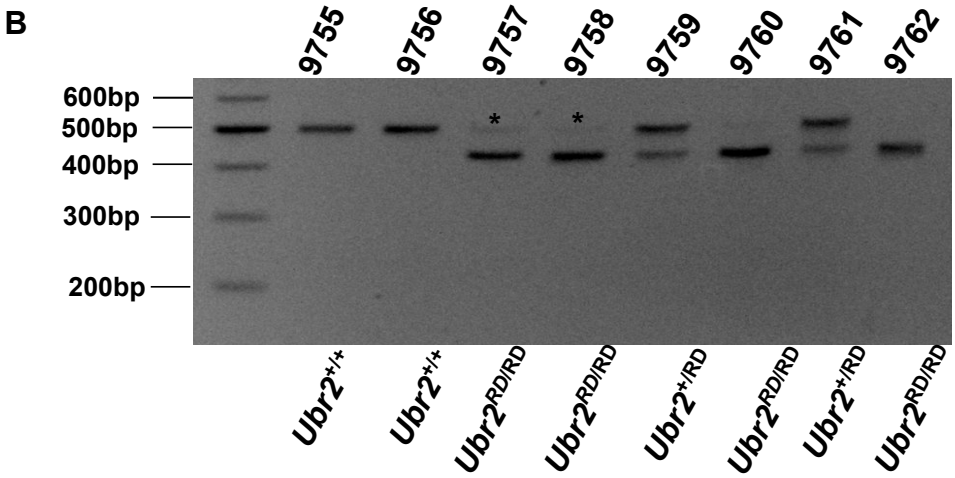
B
9755
9756
9757
9758
9759
9760
9761
9762
600bp
500bp
400bp
300bp
200bp
Ubr2+/+
Ubr2+/+
Ubr2RD/RD
Ubr2RD/RD
Ubr2+/RD
Ubr2RD/RD
Ubr2+/RD
Ubr2RD/RD

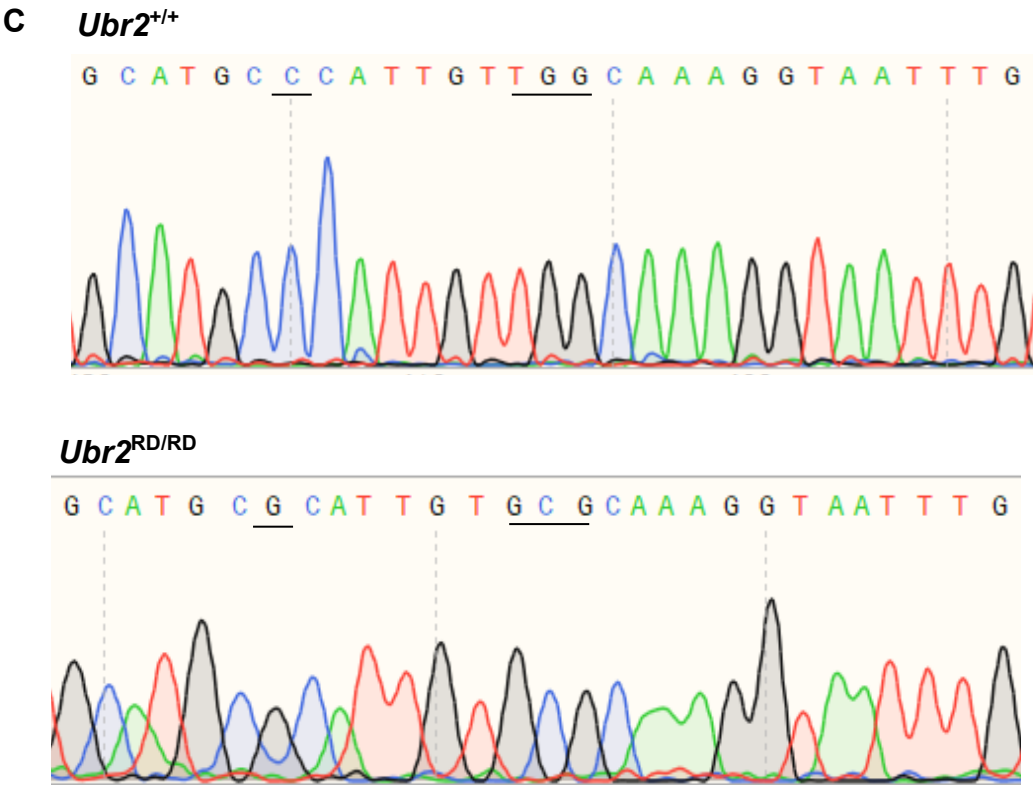
C
Ubr2+/+
G C A T G C C C A T T G T T G G C A A A G G T A A T T T G
Ubr2RD/RD
G C A T G C G C A T T G T G C G C A A A G G T A A T T T G

One of the most initially obvious phenotypes of the *Ubr2*$^{-/-}$ mouse is an underrepresentation of female *Ubr2*$^{-/-}$ animals born from heterozygote (*Ubr2*$^{+/-}$ x *Ubr2*$^{+/-}$) crosses (Kwon et al., 2003, Eleanor Raymond, unpublished). In order to assess whether *Ubr2*'s role in female survival acts through the E2 binding ability of UBR2 protein, the proportions of mice born in the *Ubr2*RD mouse colony from heterozygote (*Ubr2*$^{+/RD}$ × *Ubr2*$^{+/RD}$) crosses were assessed. At weaning (3 weeks post-partum), *Ubr2*$^{RD/RD}$ mice represent 31% of pups born (19 of 61 total mice genotyped) over 9 litters, and heterozygous and wild type littermates make up 50% and 19% of pups, respectively (Figure 5.3). This does not significantly deviate from the expected Mendelian ratio of pups from these crosses. There was no detection of significant deviation from the expected Mendelian frequency in either male or female pups from heterozygous intercrosses. Pups are present at expected Mendelian frequency in the *Ubr2*$^{RD/RD}$ mice, as was observed in *Ubr2*$^{-/-}$ mice at 3 weeks post-partum on the same genetic background (C57BL6/J), (Eleanor Raymond, unpublished). Therefore, the UBR2 W1177A RING domain point mutation, which results in decreased E2 binding *in vitro* (Lee et al., 2011), is not detrimental to embryonic or perinatal survival *in vivo*.

Figure 5.3: *Ubr2*$^{+/RD}$ crosses produce offspring in Mendelian ratios Pie charts to represent the total numbers of *Ubr2*$^{+/+}$, *Ubr2*$^{+/RD}$ and *Ubr2*$^{RD/RD}$ mice at weaning from heterozygous (*Ubr2*$^{+/RD}$ x *Ubr2*$^{+/RD}$) crosses in the RD colony and split into male and females pups born; percentages of all mice, and males and females were calculated. There was no deviation from Mendelian frequency in the RD colony (p=0. 48, χ^2 test) or in the distribution of male and female pups (p=0.33, 0.66 respectively, χ^2 test).

All Animals at Weaning

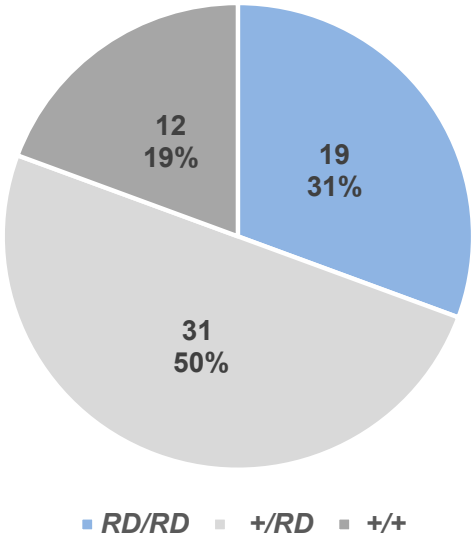

Female

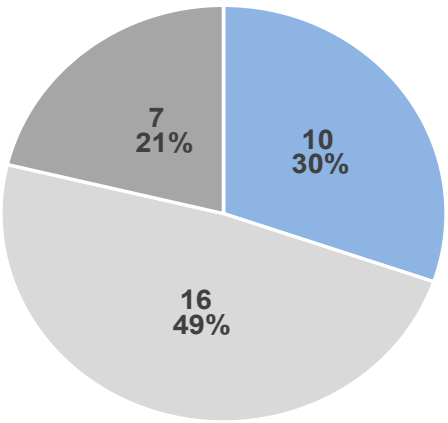

Male

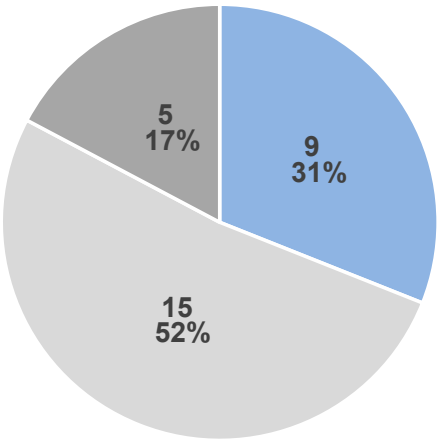

5.2.1.2 There are no gross infertility phenotypes observed in a *Ubr2*$^{RD/RD}$ male mouse

One of the most well characterised phenotypes of *Ubr2*$^{-/-}$ mice is the role of UBR2 during spermatogenesis (Kwon *et al.*, 2003; An *et al.*, 2010; Yang *et al.*, 2010; Crichton *et al.*, 2017). *Ubr2*$^{-/-}$ spermatocytes are reported to arrest and apoptose in prophase I due to defects in the repair of DSBs, homologous chromosome pairing, and SC formation (Kwon *et al.*, 2003; An *et al.*, 2012). *Ubr2*$^{-/-}$ mice from our group, which is on a C57BL/6J inbred background, results from a premature stop codon in the N-terminal region of UBR2 within the UBR domain that binds N-end rule substrates. These *Ubr2*$^{-/-}$ mice have no detectable UBR2 protein in their testes, 68% reduction in testis weight and no detectable sperm in their epididymis due to a partial meiotic arrest (Crichton *et al.*, 2017).

To investigate the abundance of the RD-UBR2 protein in the *Ubr2*$^{RD/RD}$ testis, whole testis protein extract was isolated and Western blotting was used to assess the protein level of UBR2 in *Ubr2*$^{RD/RD}$ and age matched *Ubr2*$^{+/+}$ testis (Figure 5.4). The UBR2 protein is expected to be around 200kDa (Uniprot Q6WKZ8) and is observed in both *Ubr2*$^{RD/RD}$ and *Ubr2*$^{+/+}$ testis protein extracts. Therefore, endogenous UBR2 protein is stable in Ubr2$^{RD/RD}$ mice, and this will be a useful mouse model to test the W1177A mutation in UBR2's RING domain is affecting UBR2's ability in prophase I progression and does not lead to undetectable UBR2 protein levels.

Figure 5.4: UBR2 protein is stable in the *Ubr2*$^{RD/RD}$ testis Representative Western blot for UBR2 (~200Kda) and loading control Lamin B1 (~80kDa) in testis protein extract from one of three *Ubr2*$^{RD/RD}$ mouse and one of three *Ubr2*$^{+/+}$ control animal.

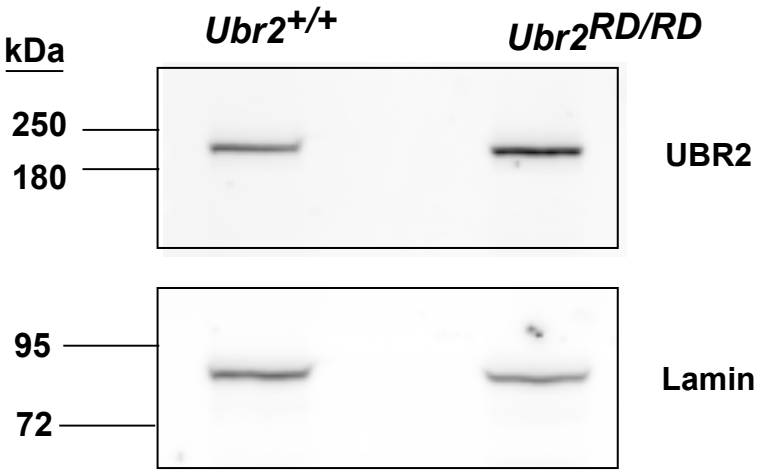
kDa
Ubr2+/+
Ubr2RD/RD
250
180
UBR2
95
72
Lamin

In order to investigate if the W1177A point mutation in UBR2's RING domain had an impact on male fertility, mouse testes from *Ubr2*$^{+/+}$ and *Ubr2*$^{RD/RD}$ males between 8-12 weeks old were dissected and weighed. We have previously reported a 67.6% reduction in testis weight between *Ubr2*$^{+/+}$ and *Ubr2*$^{-/-}$ males, and an undetectable level of sperm isolated from the epididymis of *Ubr2*$^{-/-}$ testes (Crichton *et al.*, 2017). In this study, the average weight of each testis in an *Ubr2*$^{+/+}$ male is 96.4 ±10.8mg (± standard deviation), and *Ubr2*$^{RD/RD}$ testes are 105.2 ±11.2mg; these are not significantly different in size (Figure 5.5A). This indicates a lack of gross fertility phenotypes in the *Ubr2*$^{RD/RD}$ male.

To investigate the *Ubr2*$^{RD/RD}$ testis in more detail, the epididymis of each testis was dissected from these mice and sperm was counted using a haemocytometer. I calculated an estimated mean of $9.7x10^6$±$2.5x10^6$ cells mature sperm produced by an *Ubr2*$^{+/+}$ testis, and an estimated mean of $10.6x10^6$±$1.5x10^6$ cells produced by an *Ubr2*$^{RD/RD}$ testis. The difference between these counts are not statistically significant (Figure 5.5B). The sperm counted in this assay had a normal morphology (data not shown).Thus *Ubr2*$^{RD/RD}$ mice do not have the overt spermatogenesis defects that are present in *Ubr2*$^{-/-}$ mice.

To assess the *Ubr2*$^{RD/RD}$ testis morphology in more detail, Jen Lawson in our group performed tissue sections and stained with H&E to look at the seminiferous tubules (Figure 5.5C). Spermatogenesis occurs within each seminiferous tubule and as spermatocytes develop and go through meiosis,

they advance towards the lumen, which is the centre of the tubules in these sections. *Ubr2*$^{-/-}$ seminiferous tubules have an accumulation of zygotene-like arrested cells and absence of round and elongated mature spermatids that indicates meiotic arrest and cell death which is observed as large spaces in the seminiferous tubule lumen (Crichton *et al.*, 2017). There are no clear morphological defects in the *Ubr2*$^{RD/RD}$ sections as compared to *Ubr2*$^{+/+}$ testes, and both round and elongated spermatids are in seminiferous tubules examined here. Therefore, consistent with the normal epididymal sperm counts and testis weights in these mice, there is no grossly overt male meiotic phenotype in *Ubr2*$^{RD/RD}$ testis.

Figure 5.5: *Ubr2*$^{RD/RD}$ males have no overt defects in spermatogenesis

(**A**) Testis weights, as an average of both testes per mouse in wild type (*Ubr2*$^{+/+}$) and homozygote W1177A mutant (*Ubr2*$^{RD/RD}$) males (N=4 mice per genotype) at 8-12 weeks post-partum. Black bars are means. p=0.24, Student's T-test (**B**) Counts of mature sperm from the same males as in (**A**), isolated from the epididymis. Black bars are means. p= 0.32, Student's T-test (**C**) Representative H&E stained 5µm-thick testis sections from wild type *Ubr2*$^{+/+}$ and homozygous mutant *Ubr2*$^{RD/RD}$ males. Scale bar is 100µm. ST: seminiferous tubule, L: lumen, arrow indicates direction of meiotic progression, black arrowhead: elongated spermatids, white arrowheads: round spermatids.

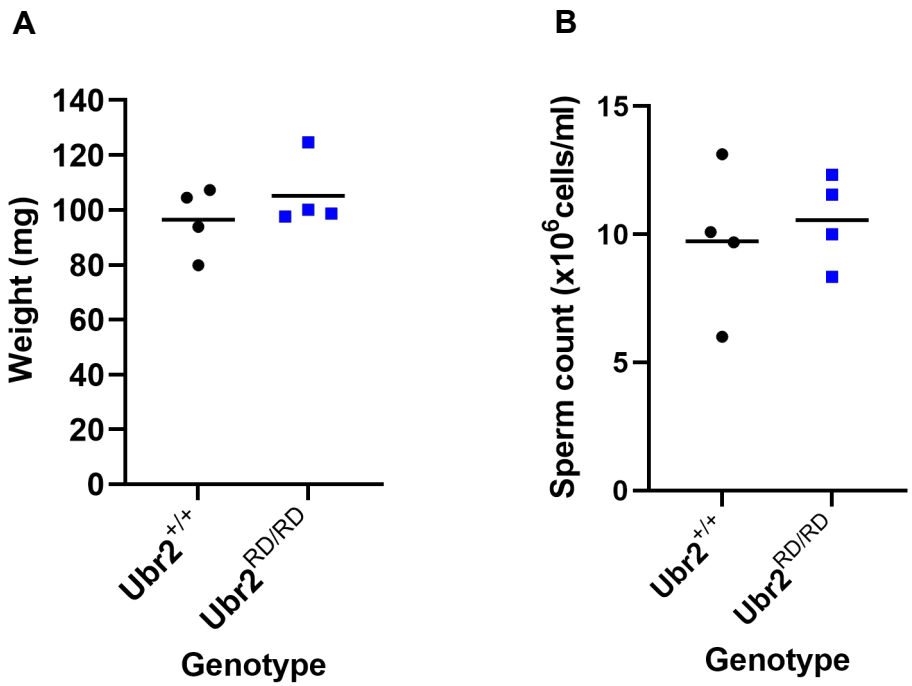

C

Ubr2$^{+/+}$

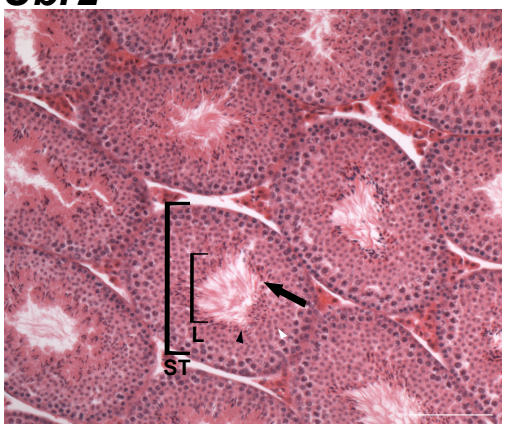

Ubr2$^{RD/RD}$

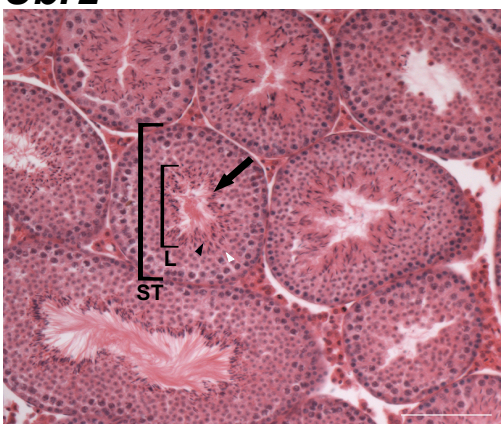

Chromosome spreads from *Ubr2*$^{-/-}$ testes show that removal of UBR2 leads to defects in progression through meiotic prophase, and very few spermatocytes progress through pachytene into diplotene (Crichton *et al.*, 2017). Chromosome spreads were made from *Ubr2*$^{+/+}$ and *Ubr2*$^{RD/RD}$ mice. These were stained for synaptonemal complex proteins SYCP3 and SYCP1 to monitor chromosome synapsis and stage progression through prophase I as defined in Chapter 2 (Figure 5.6A). Around 8.79% ± 2.6 (±standard deviation) of pachytene nuclei of *Ubr2*$^{RD/RD}$ spermatocytes from three animals exhibited some asynapsis which is not significantly different from the 12.4% ±0.5 pachytene nuclei in *Ubr2*$^{+/+}$ animals. This is markedly different from the 65.9% ± 2.5 of *Ubr2*$^{-/-}$ pachytene nuclei exhibiting asynapsis in *Ubr2*$^{-/-}$ animals ($p<0.001$, Student's T test) (Crichton *et al.*, 2017). This suggests that the W1177A mutation in the RING domain does not lead to synapsis problems in prophase I.

Figure 5.6: *Ubr2*$^{RD/RD}$ males can continue through meiosis (**A**) Representative images of chromosome spreads from testes from three *Ubr2*$^{+/+}$ and three *Ubr2*$^{RD/RD}$ animals were immunostained with antibodies to SYCP3 (red) and SYCP1 (green). Asynapsed chromosomes were identified due to the presence of at least one completely synapsed pair of autosomes and at least one incompletely synapsed pair of autosomes exhibiting asynapsis along at least half its length. Scale bar 10 μm. (**B**) Boxplot of the percentage of SYCP3-positive nuclei scored for meiotic substage from three *Ubr2*$^{+/+}$ shown as black unfilled dot (n=51, 41, 50,) and three *Ubr2*$^{RD/RD}$ animals shown as blue unfilled dot (n= 53, 55, 44). *Ubr2*$^{RD/RD}$ spreads contained no significant change in percentage of asynapsed pachytene compared to *Ubr2*$^{+/+}$ controls (n=3, p=0.44, Student's T-test). Solid point in black is mean percentage of *Ubr2*$^{+/+}$ and solid point in blue is mean percentage of *Ubr2*$^{RD/RD}$.

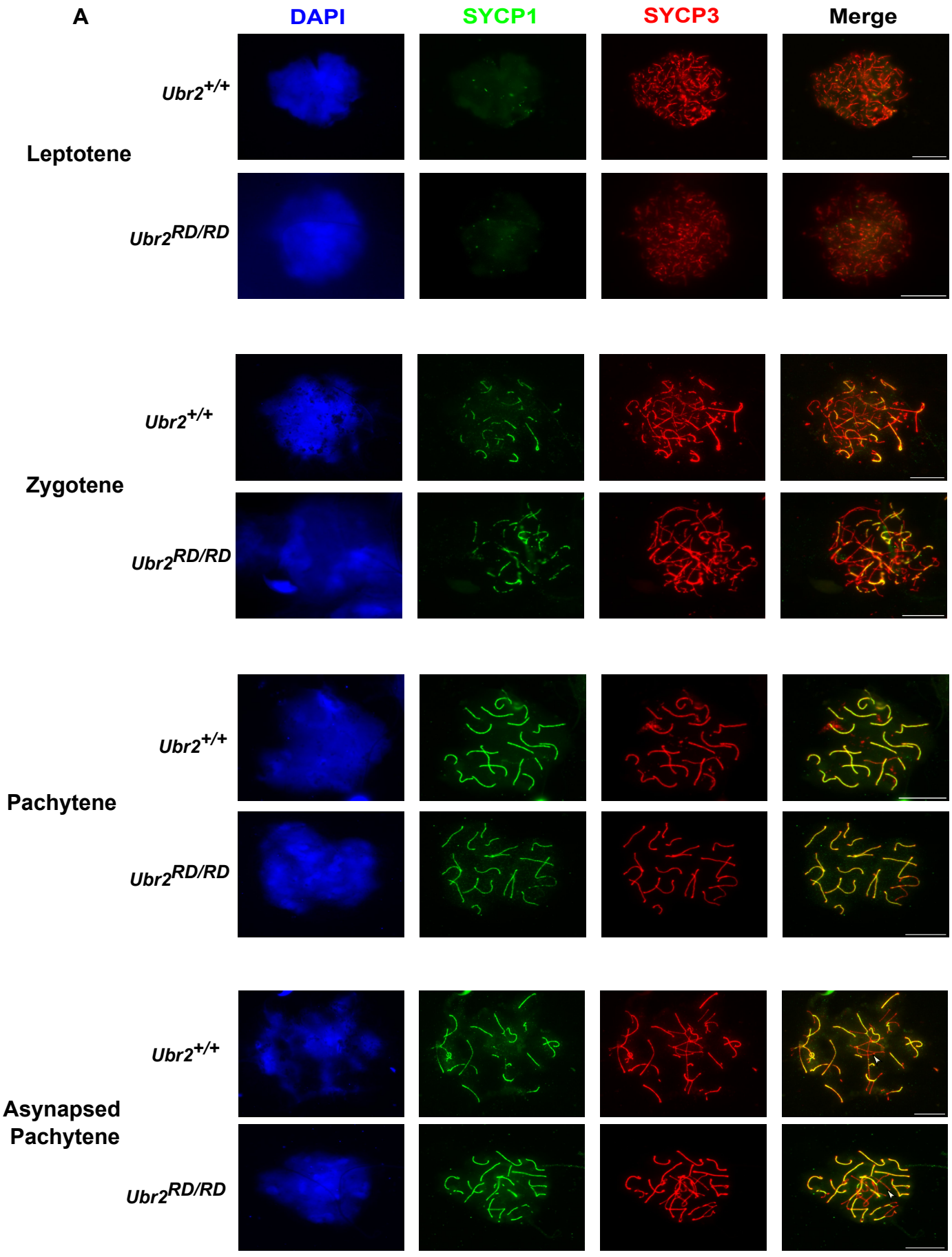
A
DAPI
SYCP1
SYCP3
Merge
Leptotene
Ubr2+/+
Ubr2RD/RD
Zygotene
Ubr2+/+
Ubr2RD/RD
Pachytene
Ubr2+/+
Ubr2RD/RD
Asynapsed Pachytene
Ubr2+/+
Ubr2RD/RD

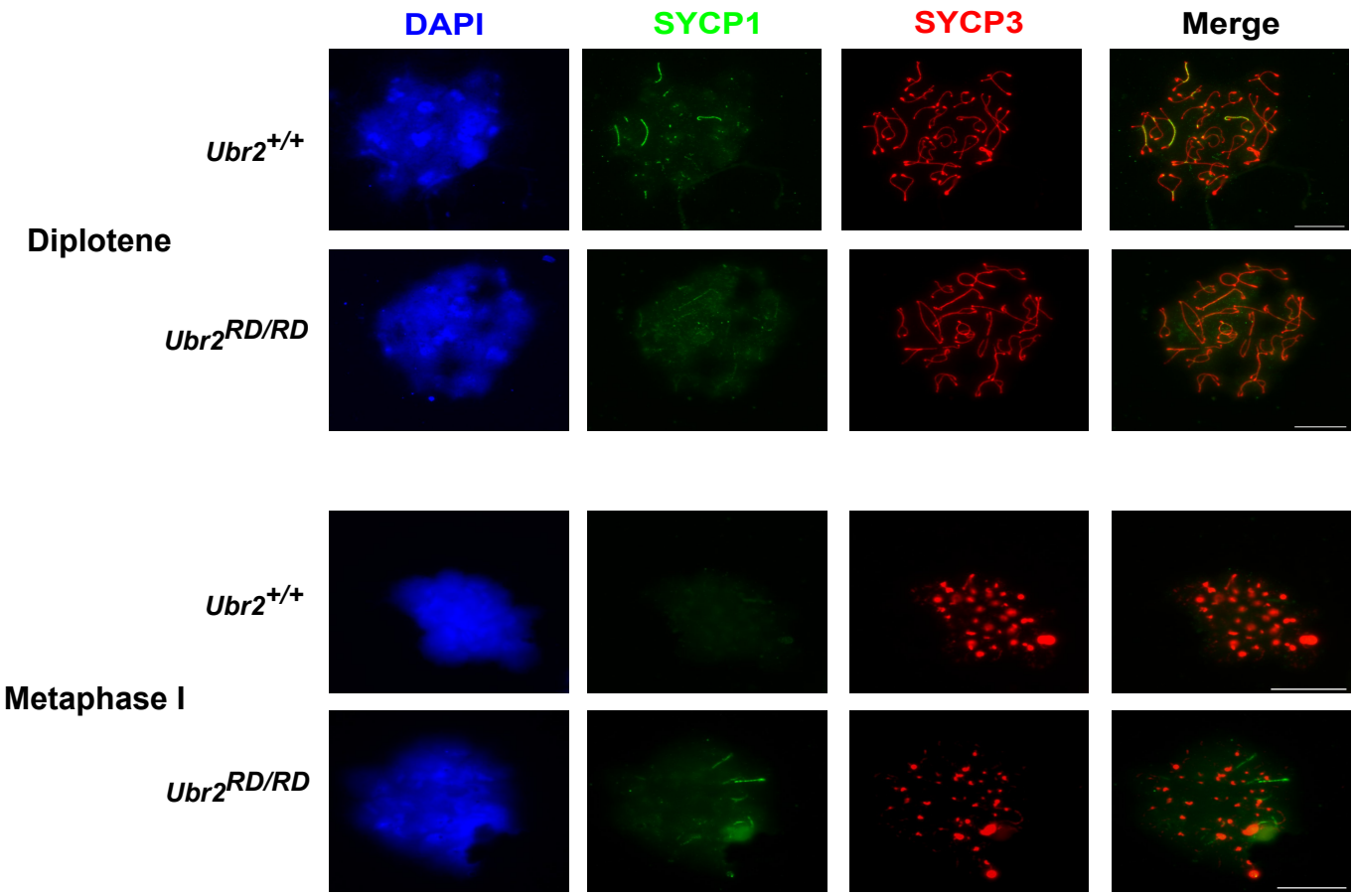
DAPI
SYCP1
SYCP3
Merge
Diplotene
Ubr2+/+
Ubr2RD/RD
Metaphase I
Ubr2+/+
Ubr2RD/RD

B

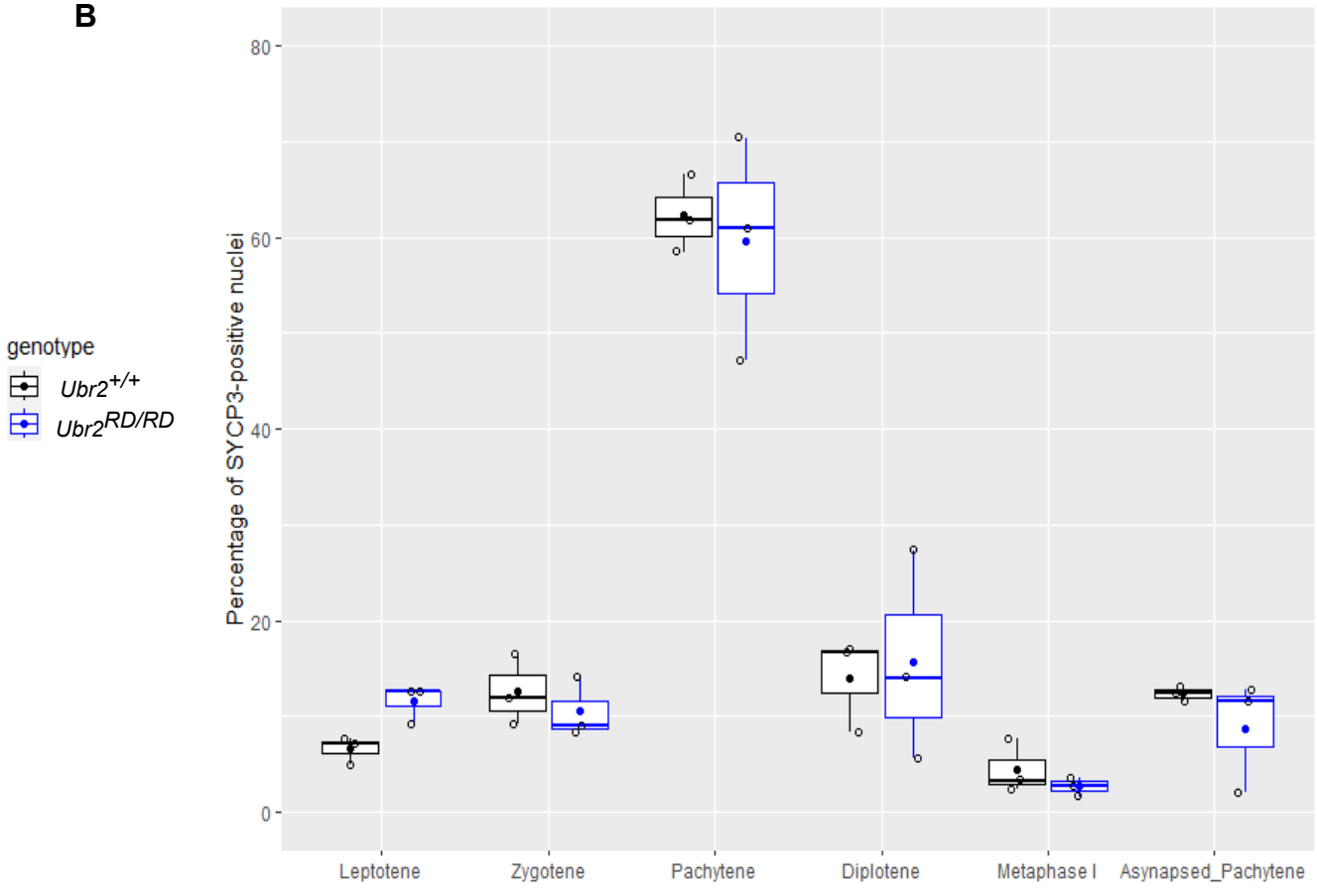
genotype
Ubr2+/+
Ubr2RD/RD
Percentage of SYCP3-positive nuclei
0
20
40
60
80
Leptotene
Zygotene
Pachytene
Diplotene
Metaphase I
Asynapsed_Pachytene

Baarends et al reported that loss of mammalian ubiquitin-conjugating enzyme UBE2B in mice leads to male infertility due to spermatogenesis being affected during postmeiotic steps. UBE2B mutant mice that progress through to pachytene have 20% longer SC length as well as more MLH1 foci and chiasma than wild type mice (Baarends *et al.*, 2003). It was suggested that the increased length of the SC represents a decrease in chromatin compaction.

As UBE2B is one of the E2 ubiquitin ligase partners for UBR2, it may have a role in regulating chromosome axis length. Axis length was measured from autosomes in pachytene stage nuclei of chromosome spreads identified by SYCP3 immunostaining from *Ubr2*$^{RD/RD}$ and Ubr2$^{+/+}$ control mouse using the SNT software in FIJI (Figure 5.7A). The mean total SC length in *Ubr2*$^{+/+}$ mice is 123.6 ±16.7 µm and 129.1 ±16.7 µm in *Ubr2*$^{RD/RD}$ mice. There was no significant change in SC length between *Ubr2*$^{+/+}$ and *Ubr2*$^{RD/RD}$ mice (Figure 5.7B). Taken together, the data presented in this section show that *Ubr2*$^{RD/RD}$ males do not grossly phenocopy the overt spermatogenesis defects seen in *Ubr2*$^{-/-}$ males, and so the major functions of UBR2 in the testis are not impaired by the W1177A mutation in the RING domain.

Figure 5.7: *Ubr2*$^{RD/RD}$ does not have longer synaptonemal complex length (**A**) Autosomes from pachytene stage nuclei were measured using the SNT using the ImageJ software by drawing along the length of the axis and measuring the length in µm. (**B**) Total measured Chromosome length in wild-type *Ubr2*$^{+/+}$ (n = 11) and *Ubr2*$^{RD/RD}$ (n =12) spermatocyte spreads. The mean total length in *Ubr2*$^{+/+}$ mice is 123.6 ±16.7 µm (± standard deviation) and *Ubr2*$^{RD/RD}$ was 129.1 ±16.7 µm (p= 0.3474, Student's T test).

A

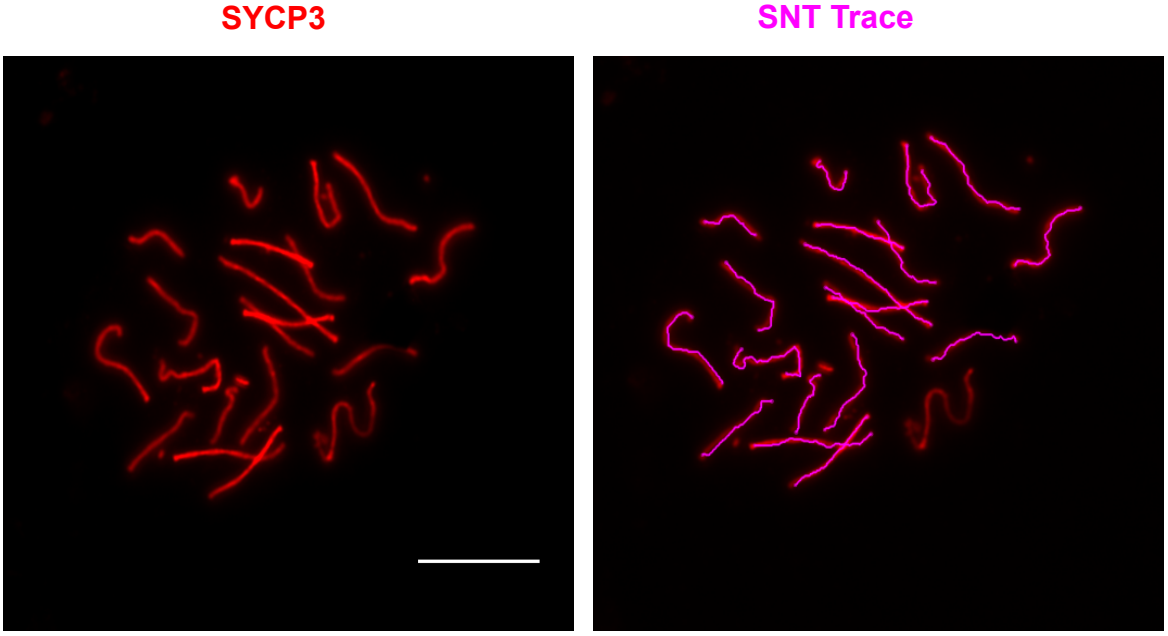

Pachytene

B

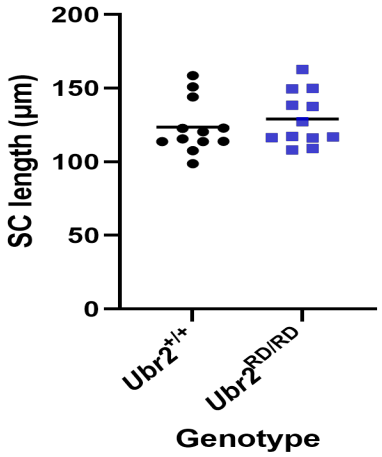

5.2.2 Generation of TT insertion in UBR2's RING domain leads to a premature stop codon

As a result of CRISPR editing of the original embryos a founder mouse with a two base pair (TT) insertion at the position 55655 in exon 31 of the *Ubr2* gene was identified. This mutation is predicted to cause a frame shift and eventually a premature termination codon in the UBR2 protein (Figure 5.8A). The W1177 amino acid follows this insertion and becomes W1177F (Tryptophan to Phenylalanine) and this frameshift leads to a premature stop codon at the amino acid location of 1204 in exon 32 (Figure 5.8B). This is predicted to truncate the UBR2 protein in the RING domain and may impact the function of the domain and completely removes the auto inhibitory domain that is located after the RING domain (Figure 5.8C).

Following identification of the TT insertion, one round of breeding with wild type C57BL/6J mice was carried out in order to generate heterozygous offspring, which were then inter-crossed to give a stable mouse colony. All subsequent colony genotyping was carried out using PCR with the same primers, RD_F and RD_R, used to genotype $Ubr2^{RD/RD}$ mice, that flank the edited region of *Ubr2* (Figure 5.2A) to generate a 499bp PCR product and was sequenced with Sanger sequence (Figure 5.8C). For all further experiments in this chapter, $Ubr2^{TT/TT}$ experimental and $Ubr2^{+/+}$ control mice were generated from heterozygote ($Ubr2^{+/TT}$ × $Ubr2^{+/TT}$) crosses.

Figure 5.8 TT insertion in UBR2 RING domain leads to frame shift mutation. (**A**) An image of UBR2 exon 31 and an arrow indicates site of TT bases insertion into UBR2 exon 31 (**B**) The amino acid sequence of wild type UBR2 and the amino acid sequence of UBR2 with the TT insertion. ^ in red indicates the amino acid site where TT bases were inserted at position 55655. The location of the amino acids where the UBR2 antibody (Aviva, OAEB 00482) binds in the UBR2 protein is in yellow. (**C**) Schematic of UBR2's domain structure in *Ubr2*$^{+/+}$ mice and after the introduction of the TT insertion in *Ubr2*$^{TT/TT}$ mice to indicate the predicted structure of truncated UBR2 following the premature stop codon. (**D**) Representative Sanger sequencing data generated from earclips of mice at weaning *Ubr2*$^{+/+}$ 9335 and *Ubr2*$^{TT/TT}$ *9337*. TT insertion underlined.

A

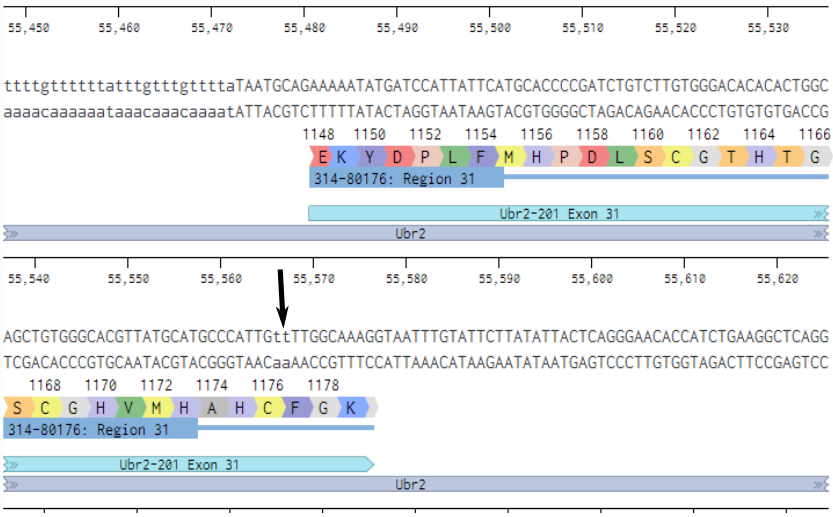

B **WT UBR2**

>NP_666190.2 E3 ubiquitin-protein ligase UBR2 isoform 1 [Mus musculus]
MASEMEPEVQAIDRSLLECSAEEIAGRWLQATDLNREVYQHLAHCVPKIYCRGPNPFPQKEDTLAQHILL
GPMEWYICAEDPALGFPKLEQANKPSHLCGRVFKVGEPTYSCRDCAVDPTCVLCMECFLGSIHRDHRYRM
TTSGGGGFCDCGDTEAWKEGPYCQKHKLSSSEVVEEEDPLVHLSEDVIARTYNIFAIMFRYAVDILTWEK
ESELPEDLEVAEKSDTYYCMLFNDEVHTYEQVIYTLQKAVNCTQKEAIGFATTVDRDGRRSVRYGDFQYC
DQAKTVIVRNTSRQTKPLKVQVMHSSVAAHQNFGLKALSWLGSVIGYSDGLRRILCQVGLQEGPDGENSS
LVDRLMLNDSKLWKGARSVYHQLFMSSLLMDLKYKKLFALRFAKNYRQLQRDFMEDDHERAVSVTALSVQ
FFTAPTLARMLLTEENLMTVIIKAFMDHLKHRDAQGRFQFERYTALQAFKFRRVQSLILDLKYVLISKPT
EWSDELRQKFLQGFDAFLELLKCMQGMDPITRQVGQHIEMEPEWEAAFTLQMKLTHVISMVQDWCALDEK
VLIEAYKKCLAVLTQCHGGFTDGEQPITLSICGHSVETIRYCVSQEKVSIHLPISRLLAGLHVLLSKSEV
AYKFPELLPLSELSPPMLIEHPLRCLVLCAQVHAGMWRRNGFSLVNQIYYYHNVKCRREMFDKDIVMLQT
GVSMMDPNHFLMIMLSRFELYQLFSTPDYGKRFSSEVTHKDVVQQNNTLIEEMLYLIIMLVGERFNPGVG
QVAATDEIKREIIHQLSIKPMAHSELVKSLPEDENKETGMESVIESVAHFKKPGLTGRGMYELKPECAKE
FNLYFYHFSRAEQSKAEEAQRKLKRENKEDTALPPPALPPFCPLFASLVNILQCDVML^YIMGTILQWAVE
HHGSAWSESMLQRVLHLIGMALQEEKHHLENAVEGHVQTFTFTQKISKPGDAPHNSPSILAMLETLQNAP
SLEAHKDMIRWLLKMFNAIKKIRECSSSSPVAEAEGTIMEESSRDKDKAERKRKAEIARLRREKIMAQMS
EMQRHFIDENKELFQQTLELDTSASATLDSSPPVSDAALTALGPAQTQVPEPRQFVTCILCQEEQEVTVG
SRAMVLAAFVQRSTVLSKDRTKTIADPEKYDPLFMHPDLSCGTHTGSCGHVMHAHC^WQRYFDSVQAKEQR
RQQRLRLHTSYDVENGEFLCPLCECLSNTVIPLLLPPRSILSRRLNFSDQPDLAQWTRAVTQQIKVVQML
RRKHNAADTSSSEDTEAMNIIPIPEGFRPDFYPRNPYSDSIKEMLTTFGTAAYKVGLKVHPNEGDPRVPI
LCWGTCAYTIQSIERILSDEEKPVFGPLPCRLDDCLRSLTRFAAAHWTVALLPVVQGHFCKLFASLVPSD
SYEDLPCILDIDMFHLLVGLVLAFPALQCQDFSGSSLATGDLHIFHLVTMAHIVQILLTSCTEENGMDQE
NPTGEEELAILSLHKTLHQYTGSALKEAPSGWHLWRSVRAAIMPFLKCSALFFHYLNGVPAPPDLQVSGT
SHFEHLCNYLSLPTNLIHLFQENSDIMNSLIESWCQNSEVKRYLNGERGAISYPRGANKLIDLPEDYSSL
INQASNFSCPKSGGDKSRAPTLCLVCGSLLCSQSYCCQAELEGEDVGACTAHTYSCGSGAGIFLRVRECQ
VLFLAGKTKGCFYSPPYLDDYGETDQGLRRGNPLHLCQERFRKIQKLWQQHSITEEIGHAQEANQTLVGI
DWQHL

TT insertion

>NP_666190.2 E3 ubiquitin-protein ligase UBR2 isoform 1 [Mus musculus]
MASEMEPEVQAIDRSLLECSAEEIAGRWLQATDLNREVYQHLAHCVPKIYCRGPNPFPQKEDTLAQHILL
GPMEWYICAEDPALGFPKLEQANKPSHLCGRVFKVGEPTYSCRDCAVDPTCVLCMECFLGSIHRDHRYRM
TTSGGGGFCDCGDTEAWKEGPYCQKHKLSSSEVVEEEDPLVHLSEDVIARTYNIFAIMFRYAVDILTWEK
ESELPEDLEVAEKSDTYYCMLFNDEVHTYEQVIYTLQKAVNCTQKEAIGFATTVDRDGRRSVRYGDFQYC
DQAKTVIVRNTSRQTKPLKVQVMHSSVAAHQNFGLKALSWLGSVIGYSDGLRRILCQVGLQEGPDGENSS
LVDRLMLNDSKLWKGARSVYHQLFMSSLLMDLKYKKLFALRFAKNYRQLQRDFMEDDHERAVSVTALSVQ
FFTAPTLARMLLTEENLMTVIIKAFMDHLKHRDAQGRFQFERYTALQAFKFRRVQSLILDLKYVLISKPT
EWSDELRQKFLQGFDAFLELLKCMQGMDPITRQVGQHIEMEPEWEAAFTLQMKLTHVISMVQDWCALDEK
VLIEAYKKCLAVLTQCHGGFTDGEQPITLSICGHSVETIRYCVSQEKVSIHLPISRLLAGLHVLLSKSEV
AYKFPELLPLSELSPPMLIEHPLRCLVLCAQVHAGMWRRNGFSLVNQIYYYHNVKCRREMFDKDIVMLQT
GVSMMDPNHFLMIMLSRFELYQLFSTPDYGKRFSSEVTHKDVVQQNNTLIEEMLYLIIMLVGERFNPGVG
QVAATDEIKREIIHQLSIKPMAHSELVKSLPEDENKETGMESVIESVAHFKKPGLTGRGMYELKPECAKE
FNLYFYHFSRAEQSKAEEAQRKLKRENKEDTALPPPALPPFCPLFASLVNILQCDVML^YIMGTILQWAVE
HHGSAWSESMLQRVLHLIGMALQEEKHHLENAVEGHVQTFTFTQKISKPGDAPHNSPSILAMLETLQNAP
SLEAHKDMIRWLLKMFNAIKKIRECSSSSPVAEAEGTIMEESSRDKDKAERKRKAEIARLRREKIMAQMS
EMQRHFIDENKELFQQTLELDTSASATLDSSPPVSDAALTALGPAQTQVPEPRQFVTCILCQEEQEVTVG
SRAMVLAAFVQRSTVLSKDRTKTIADPEKYDPLFMHPDLSCGTHTGSCGHVMHAHC^FGKGILIPFKPRS
SEGSSGCACTLATM*

C

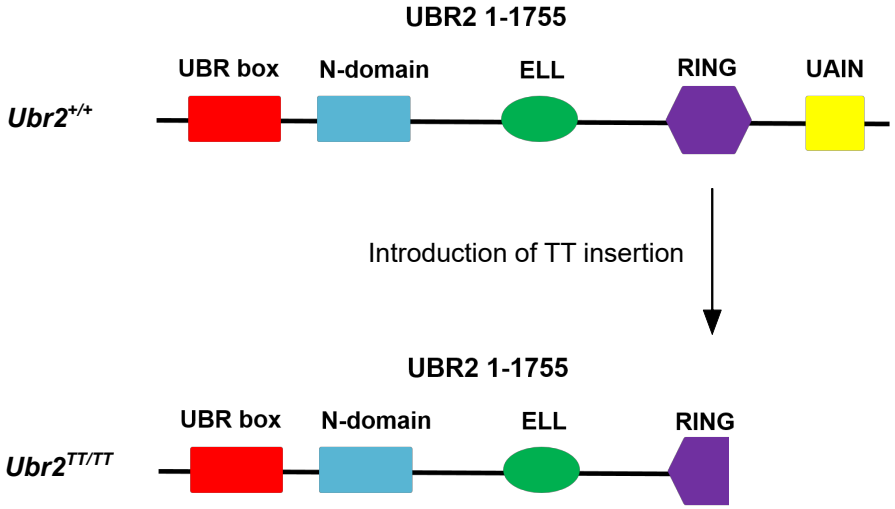
UBR2 1-1755
UBR box
N-domain
ELL
RING
UAIN
Ubr2+/+
Introduction of TT insertion
UBR2 1-1755
UBR box
N-domain
ELL
RING
Ubr2TT/TT

D

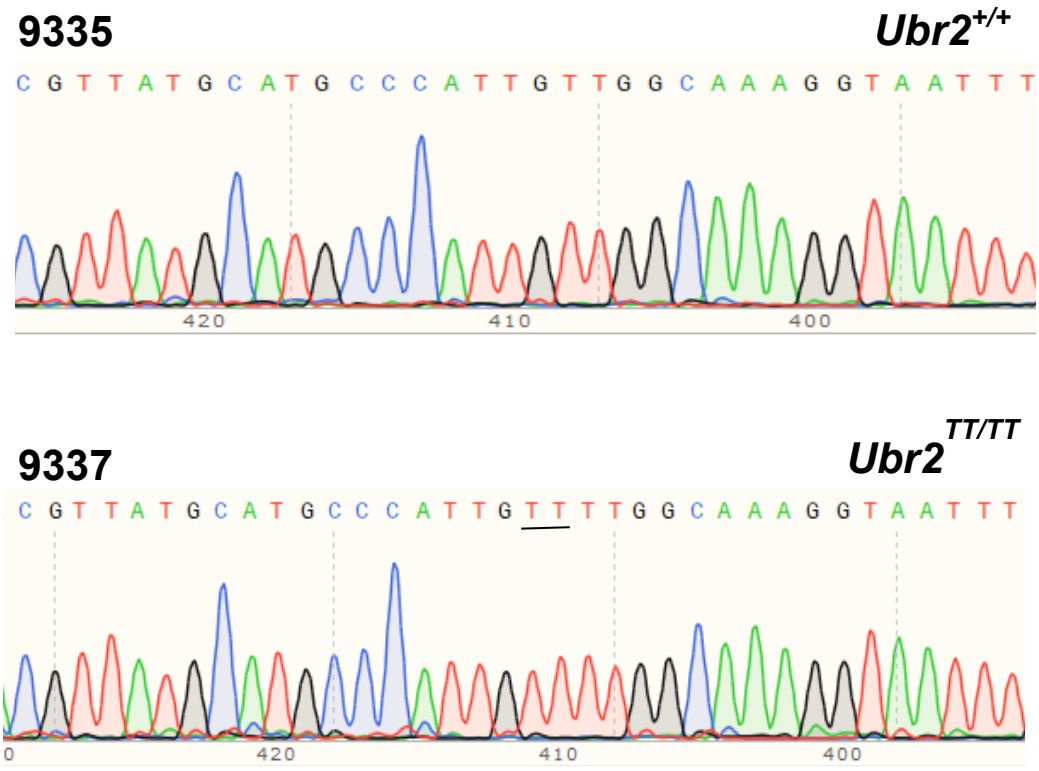
9335
Ubr2+/+
C G T T A T G C A T G C C C A T T G T T G G C A A A G G T A A T T T
420
410
400
9337
Ubr2TT/TT
C G T T A T G C A T G C C C A T T G T T T T G G C A A A G G T A A T T T
0
420
410
400

As previously stated one of the obvious phenotypes of the *Ubr2*$^{-/-}$ mouse is an underrepresentation of female *Ubr2*$^{-/-}$ animals born from heterozygote (*Ubr2*$^{+/-}$ x *Ubr2*$^{+/-}$) crosses (Kwon *et al.*, 2003). At weaning, *Ubr2*$^{TT/TT}$ mice represent 18% of pups born (12 of 66 total mice genotyped) over 9 litters, and heterozygous and wild type littermates make up 46% and 36% of pups, respectively (Fig. 5.9). This does not significantly deviate from the expected Mendelian ratio of pups from these crosses.

However, after partitioning these pups by sex, *Ubr2*$^{TT/TT}$ mice represent 0% of all female mice genotyped over these 9 litters (0 of 30 females) (Figure 5.9) whereas *Ubr2*$^{TT/TT}$ mice represent 34% of all 36 male mice in these 9 litters. Therefore, there is lethality in *Ubr2*$^{TT/TT}$ females only, as has been observed in the *Ubr2*$^{-/-}$ genotype indicating that the TT insertion at 55655 in exon 31 is detrimental to embryonic survival.

Figure 5.9: *Ubr2*$^{+/TT}$ crosses produce no homozygote female pups. Pie charts to represent the total numbers of *Ubr2*$^{+/+}$, *Ubr2*$^{+/TT}$ and *Ubr2*$^{TT/TT}$ mice at weaning from heterozygous (*Ubr2*$^{+/TT}$ x *Ubr2*$^{+/TT}$) crosses in the TT colony and split into male and females pups born; percentages of all mice, and males and females were calculated. There was no significant deviation from Mendelian frequency in the total TT colony ($p=0.19$, χ^2 test) or in the distribution of male pups ($p=0.06$, χ^2 test). Significant deviation from Mendelian frequency was detected in female pups as 0 *Ubr2*$^{TT/TT}$ pups were born ($p<0.0001$, χ^2 test).

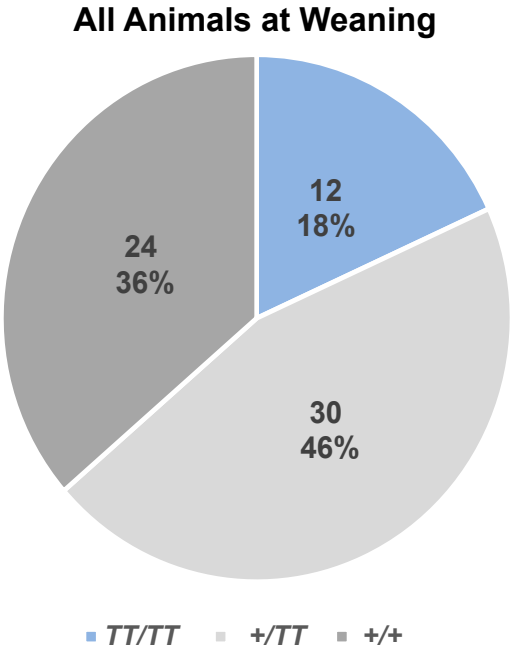
All Animals at Weaning
12
18%
24
36%
30
46%
TT/TT
+/TT
+/+

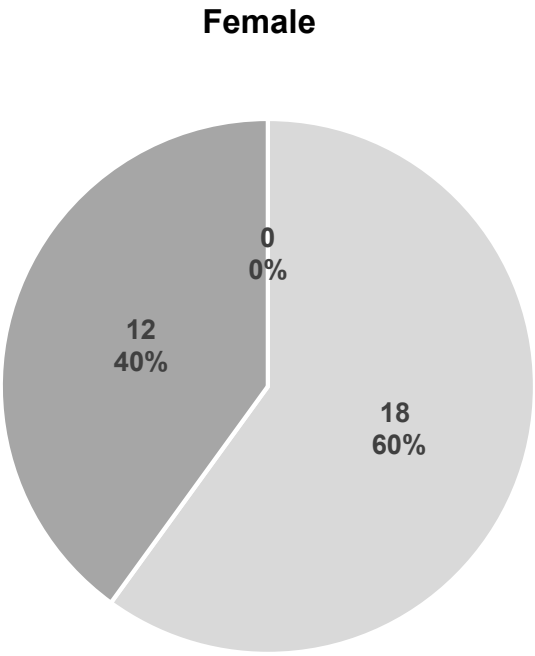
Female
0
0%
12
40%
18
60%

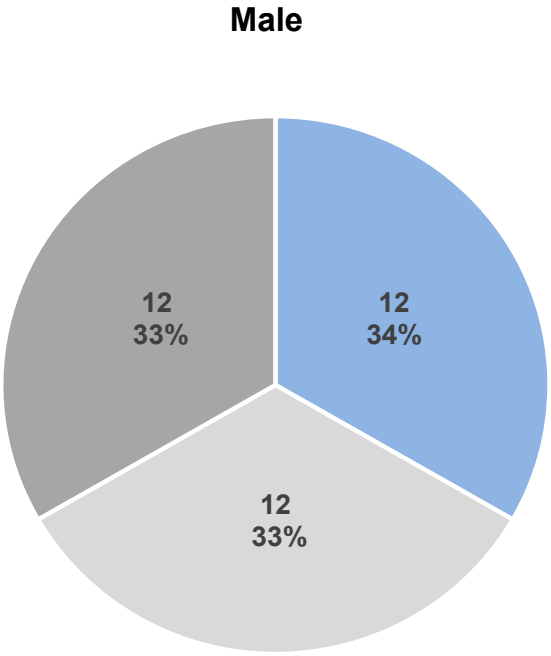
Male
12
34%
12
33%
12
33%

5.2.2.1 *Ubr2*$^{TT/TT}$ male mice have a gross testis phenotype

As previously stated, the most well characterised phenotypes of *Ubr2*$^{-/-}$ mice are those resulting from the role of UBR2 during spermatogenesis (Kwon *et al.*, 2003; An *et al.*, 2010; Yang *et al.*, 2010; Crichton *et al.*, 2017). *Ubr2*$^{-/-}$ mice have no detectable UBR2 in their testes, 68% reduction in testis weight and no detected sperm in their epididymis due to meiotic arrest (Crichton *et al.*, 2017).

To investigate the stability of the UBR2 protein in the *Ubr2*$^{TT/TT}$ testis, whole testis protein extract was isolated and carried out Western blotting to assess the protein level of UBR2 in *Ubr2*$^{TT/TT}$ and age matched *Ubr2*$^{+/+}$ testis (Figure 5.10). The UBR2 protein is only observed in *Ubr2*$^{+/+}$ testis protein extracts not the *Ubr2*$^{TT/TT}$ testis. Therefore, endogenous UBR2 protein is not detectable in *Ubr2*$^{TT/TT}$ mice with this antibody (Aviva, OAEB 00482) due to the binding site of the antibody used in this chapter and Chapter 4 binds to the C terminus of UBR2 which is removed in *Ubr2*$^{TT/TT}$ mutant (shown in Figure 5.8). Use of an UBR2 antibody that binds to an early part of the protein is required to identify if a UBR2 protein is detected in the testes.

Figure 5.10: UBR2 protein is not detectable in the *Ubr2*$^{TT/TT}$ testis.
Western blotting assay for UBR2 (~200Kda) and loading control Lamin B1 (~80kDa) in testis protein extract from an *Ubr2*$^{TT/TT}$ mouse and *Ubr2*$^{+/+}$ control animal.

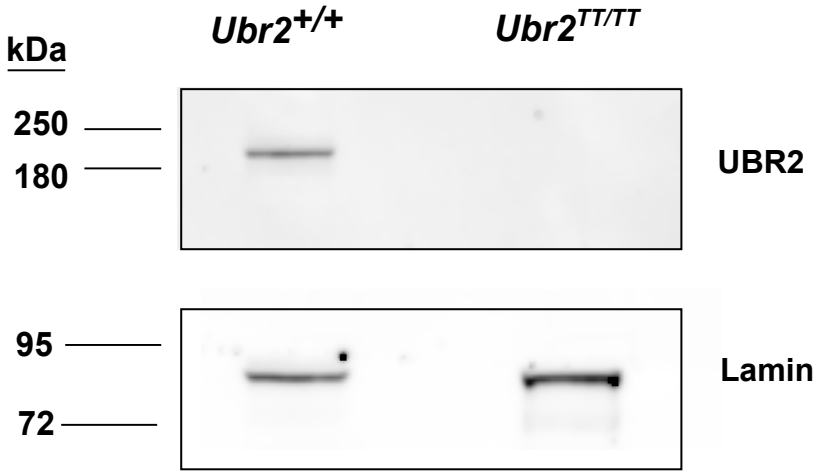
kDa
Ubr2+/+
Ubr2TT/TT
250
180
UBR2
95
72
Lamin

In order to investigate if the TT insertion into UBR2's RING domain which leads to a frame shift had an impact on male fertility, mouse testes from *Ubr2*$^{+/+}$ and *Ubr2*$^{TT/TT}$ males were dissected between 8-12 weeks old and assessed the weight. In this study, the average weight of each testis in an *Ubr2*$^{+/+}$ male is 100.5 ±2.7mg (± standard deviation), and *Ubr2*$^{TT/TT}$ testes are 33.1±4.9mg; *Ubr2*$^{TT/TT}$ mice have a significant 67% reduction in testis size compared to *Ubr2*$^{+/+}$ (Figure 5.11A). This reduction is testis weight is comparable to that previously reported in *Ubr2*$^{-/-}$ testes (Crichton *et al.*, 2017).

To investigate any defects in spermatogenesis in *Ubr2*$^{TT/TT}$ mice in more detail, I dissected the epididymis of each testis from these mice and performed sperm counts using a haemocytometer. There was a mean of $17.9x10^6$±$5.7x10^6$ cells mature sperm produced by an *Ubr2*$^{+/+}$ testis, and a mean of $10.6x10^5$±$0.5x10^5$ cells produced by an *Ubr2*$^{TT/TT}$ testis. There is a significantly 95% reduction in sperm counted in *Ubr2*$^{TT/TT}$ compared to *Ubr2*$^{+/+}$ mice (Figure 5.11B). This is different to the *Ubr2*$^{-/-}$ mice where there is no detected sperm in the epididymis whereas there is some sperm detected in *Ubr2*$^{TT/TT}$ mice. The sperm counted in this assay had a normal morphology (data not shown) so they do not have any overt spermatogenesis defects.

To assess the *Ubr2*$^{TT/TT}$ testis morphology in more detail, Jen Lawson in our group prepared tissue sections and stained with H&E to look at the seminiferous tubules (Figure 5.11C). There are no clear morphological

defects in the *Ubr2*$^{TT/TT}$ sections as compared to *Ubr2*$^{+/+}$ testes, and both round and elongated spermatids are in seminiferous tubules examined here. Therefore, it could be a post meiotic consequence leading to the reduction in sperm detected in the epididymis of *Ubr2*$^{TT/TT}$ testis.

Figure 5.11: *Ubr2*$^{TT/TT}$ males have overt defects in spermatogenesis (**A**) Testis weights, as an average of both testes per mouse in wild type (*Ubr2*$^{+/+}$) and homozygote mutant (*Ubr2*$^{TT/TT}$) males (N=3 mice per genotype) at 8-12 weeks pp. Black bars are means. p=0.006, Student's T-test (**B**) Counts of mature sperm from the same males as in (**A**), isolated from the epididymis. Black bars are means. p= 0.0002, Student's T-test (**C**) Representative H&E stained 5µm-thick testis sections from wild type *Ubr2*$^{+/+}$ and homozygous mutant *Ubr2*$^{TT/TT}$ males. Scale bar is 100µm. ST: seminiferous tubule, L: lumen, arrow indicates direction of meiotic progression, black arrowhead: elongated spermatids, white arrowheads: round spermatids.

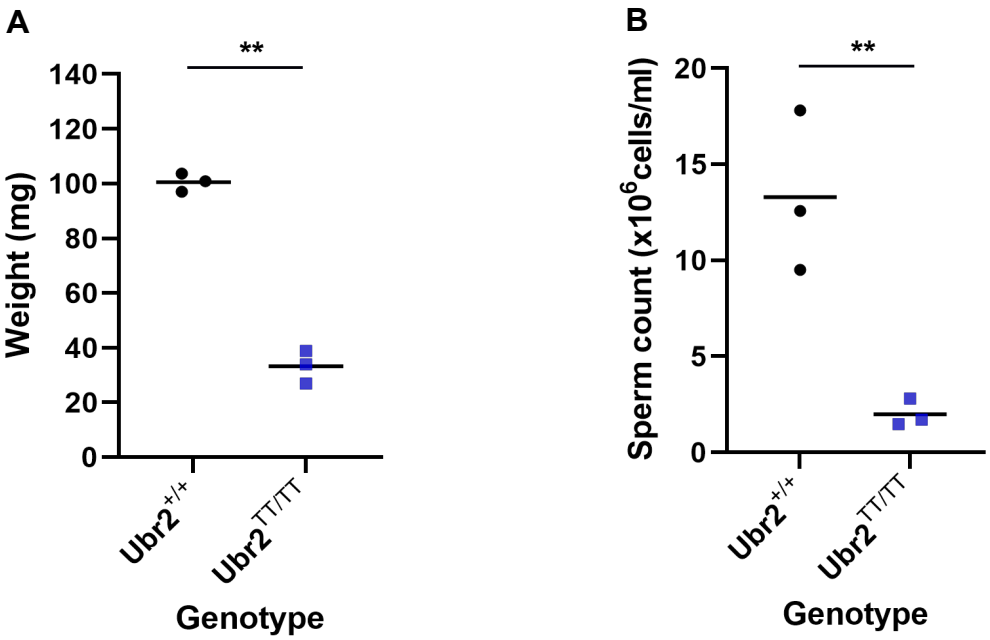
A
**
140
120
100
80
60
40
20
0
Weight (mg)
Ubr2+/+
Ubr2TT/TT
Genotype
B
**
20
15
10
5
0
Sperm count (x10^6cells/ml)
Ubr2+/+
Ubr2TT/TT
Genotype

C

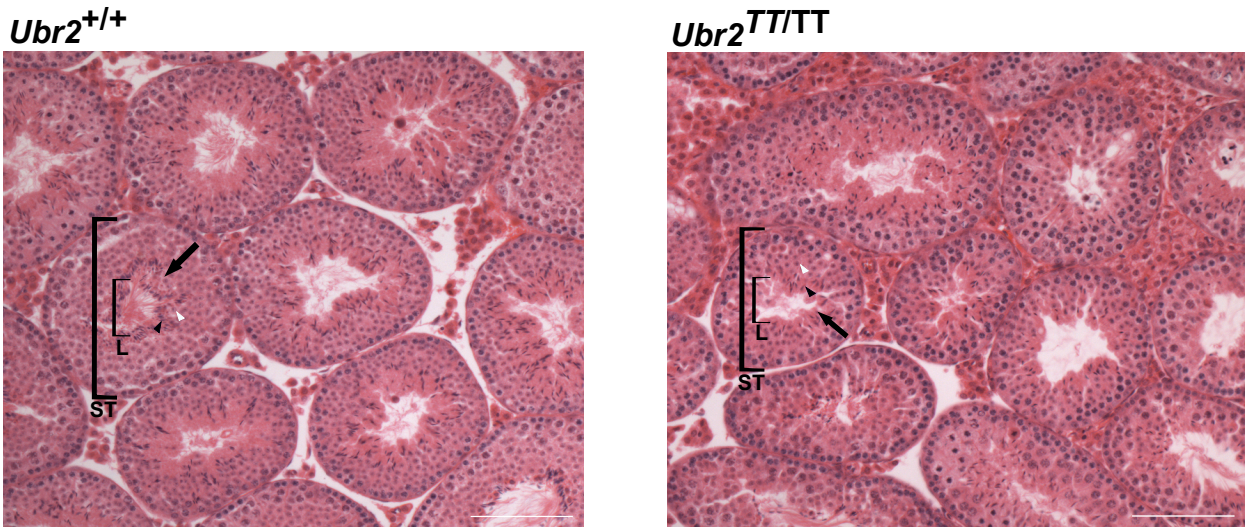
Ubr2+/+
L
ST
Ubr2TT/TT
L
ST

Chromosome spreads from *Ubr2*$^{-/-}$ testes show that loss of UBR2 leads to defects in progression through meiotic prophase, and very few spermatocytes progress through pachytene into diplotene (Crichton *et al.*, 2017). Chromosome spreads were made from *Ubr2*$^{+/+}$ and *Ubr2*$^{TT/TT}$ mice. These were stained for synaptonemal complex proteins SYCP3 and SYCP1 and staged throughout prophase I as defined in Chapter 2.5.3.2 (Figure 5.12A).

Around 29.7% ± 7.2 (±standard deviation) of pachytene nuclei of *Ubr2*$^{TT/TT}$ spermatocytes from three animals had chromosome asynapsis which is significantly greater than the 10% ±5.3 pachytene nuclei from three *Ubr2*$^{+/+}$ animals (Figure 5.12B). Also, there is a significant reduction in the percentage of diplotene nuclei identified in *Ubr2*$^{TT/TT}$ testis, 7.9% ±2.5 compared to 22.2% ±4.7 in *Ubr2*$^{+/+}$ testis. The percentage of metaphase I identified in the *Ubr2*$^{TT/TT}$ mice is not different to the percentage observed in *Ubr2*$^{+/+}$ (1.6% ±0.2 compared to 2% ±1.7, p= 0.77, Student's T-test). So even though there is a significant increase in incomplete synapsis leading to pachytene arrest in *Ubr2*$^{TT/TT}$ mice than observed in *Ubr2*$^{+/+}$ control mice, some spermatocytes are still undergoing normal synapsis and can complete meiosis I. This increase in asynapsis could contribute to the reduction in sperm counts in the epididymis.

The percentage of nuclei with pachytene asynapsis in *Ubr2*$^{TT/TT}$ mice (29.7% ± 7.2) is around half that reported in *Ubr2*$^{-/-}$ mice (65.9% ± 2.5) (Crichton *et al.*, 2017). This suggests that the TT insertion in the RING domain does lead

to synapsis problems in prophase I but not to the same extent observed in *Ubr2*$^{-/-}$ mice. Furthermore, *Ubr2*$^{TT/TT}$ mice can still produce sperm, albeit a much lower amount, compared to *Ubr2*$^{-/-}$ mice (Crichton *et al.*, 2017) indicating that this frameshift is a partial phenocopy to *Ubr2*$^{-/-}$ mice with the main deviation being the lack of total ablation of mature sperm.

Figure 5.12: *Ubr2*$^{TT/TT}$ males can continue through meiosis. (**A**) Chromosome spreads from testes from three *Ubr2*$^{+/+}$ and three *Ubr2*$^{TT/TT}$ animals were immunostained with antibodies to SYCP3 (red) and SYCP1 (green). Asynapsed chromosomes were identified due to the presence of at least one completely synapsed pair of autosomes and at least one incompletely synapsed pair of autosomes exhibiting asynapsis along at least half its length. Scale bar 10 μm. (**B**) Boxplot to present percentage of SYCP3-positive nuclei scored for meiotic substage from three *Ubr2*$^{+/+}$ shown as dot with black rim (n=43, 51, 62) and three *Ubr2*$^{TT/TT}$ animals shown as dot with blue rim (n=46, 50, 54). *Ubr2*$^{TT/TT}$ spreads had higher significant percentage of asynapsed pachytene (p=0.035, Student's T-test) and lower percentage of diplotene nuclei (p= 0.02, Student's T-test) compared to *Ubr2*$^{+/+}$ controls. Solid point in black is mean percentage of *Ubr2*$^{+/+}$ and solid point in blue is mean percentage of *Ubr2*$^{TT/TT}$ mice.

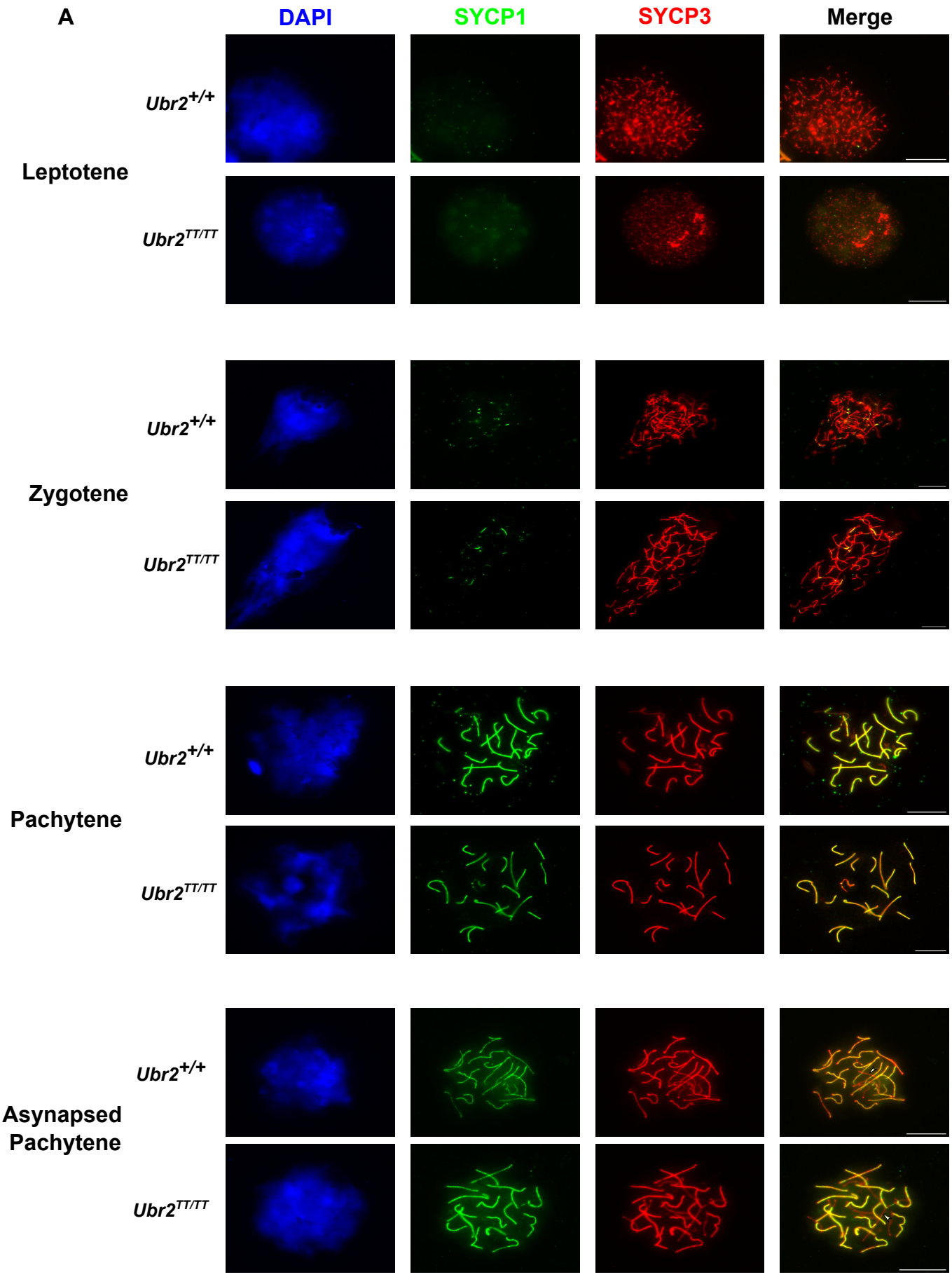
A
DAPI
SYCP1
SYCP3
Merge
Leptotene
Ubr2+/+
Ubr2TT/TT
Zygotene
Ubr2+/+
Ubr2TT/TT
Pachytene
Ubr2+/+
Ubr2TT/TT
Asynapsed Pachytene
Ubr2+/+
Ubr2TT/TT

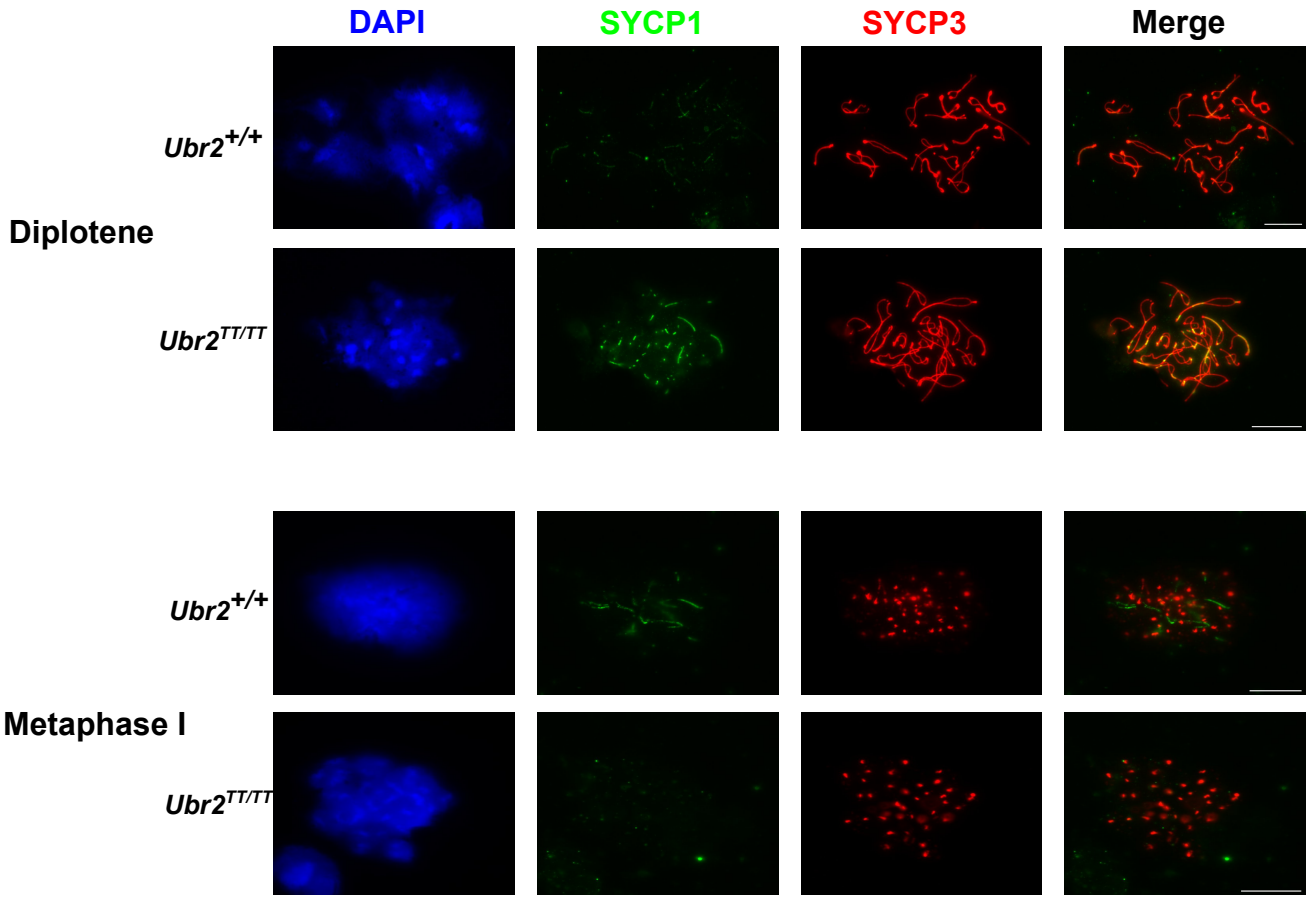
DAPI
SYCP1
SYCP3
Merge
Diplotene
Ubr2+/+
Ubr2TT/TT
Metaphase I
Ubr2+/+
Ubr2TT/TT

B

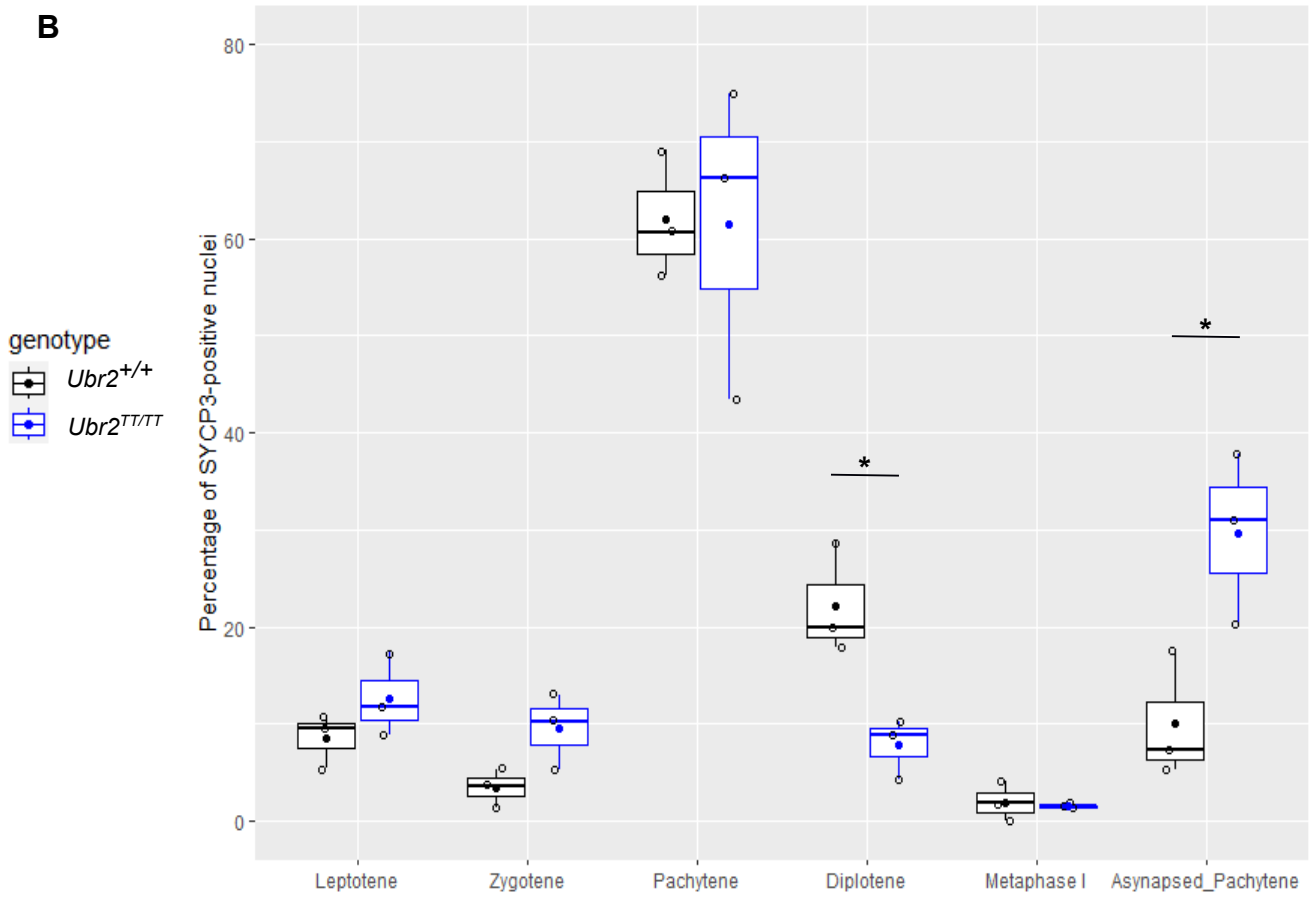
genotype
Ubr2+/+
Ubr2TT/TT
Percentage of SYCP3-positive nuclei
0
20
40
60
80
Leptotene
Zygotene
Pachytene
Diplotene
Metaphase I
Asynapsed_Pachytene
*
*

5.2.3 The W1177A mutation disrupts the novel role of *Ubr2* in cohesin regulation

We have previously shown that *Ubr2* has a role in splenocytes in the regulation of the AcSMC3-containing subpopulation of cohesin complexes, which is thought to mediate sister chromatid cohesin (Reichmann *et al.*, 2020). *Ubr2* specifically regulates the relatively minor population of cohesin, the AcSMC3-containing cohesin complexes, and usually effects on this population typically do not cause detectable changes in the abundance of other cohesin subunits, such as total SMC3.

In order to investigate if this role of *Ubr2* is perturbed in the *Ubr2*$^{RD/RD}$ mutant mouse, the chromatin-associated cohesin levels from splenocytes isolated from the *Ubr2*$^{RD/RD}$ spleen were determined. *Ubr2*$^{-/-}$ chromatin preparation from spleens have a ~2-fold increase in AcSMC3 and no detectable change in other subunits (SMC3, SMC1, RAD21 and SA2) (Reichmann *et al.*, 2020). The level of total chromatin-associated cohesin was investigated in the *Ubr2*$^{RD/RD}$ spleen using SMC3, SMC1, Rad21 and SA2 subunits as well as the AcSMC3 subunit, by Western blotting of chromatin prepared from the spleens of 4 independent mice (Figure 5.13A). Upon quantification of these proteins, which are normalised to the intensity of chromatin-associated histone H3 protein detected in these samples, there was a significant 2.3 fold change in AcSMC3 levels in *Ubr2*$^{RD/RD}$ ($p = 0.037$, Student's T-Test) (Figure 5.13B). There is a significant 2-fold increase in total SMC3 levels and 1.5-fold increase in SMC1 levels that was not seen *Ubr2*$^{-/-}$ spleen. There was no

detectable change in the levels of RAD21. SA2 protein levels had a significant 2-fold increase that is not seen in *Ubr2*$^{-/-}$ spleen.

This implies that the W1177A mutation in the RING domain is having an effect on UBR2's function in the spleen and that regulation of AcSMC3 cohesin depends on the normal level of E2 ligases binding to UBR2's RING domain. However, there also seems to be a change in the SMC3, SMC1 and SA2 subunits in the chromatin-associated cohesin in spleen, which is suggesting that this mutation is having an effect on cohesin subunits not seen in *Ubr2*$^{-/-}$ mice.

Figure 5.13: Mitotic cohesin regulation is perturbed in the *Ubr2*$^{RD/RD}$ mouse (**A**) Representative western blots of chromatin-associated proteins AcSMC3, SMC3, SMC1, RAD21 and SA2 isolated from spleens of 4 pairs of *Ubr2*$^{+/+}$ and homozygous W1177A mutant *Ubr2*$^{RD/RD}$ mice, and chromatin-associated histone H3 protein as a loading control. (**B**) Quantified mean protein levels of cohesin subunits from western blotting in A and corrected against histone H3 protein level. Standard deviation over four pairs of wild type and homozygous mutant mice shown. Differences between wild type and RD are significant; AcSMC3: p=0.037, SMC3: p=0.047 and SA2 p=0.045, SMC1: p=0.031; but are not significant for RAD21: p=0.830 (Student's T-test). Each pair of histone H3 and cohesin bands are from the same gel lane; the high concentration of histones in chromatin causes the sample to spread laterally at low molecular weights.

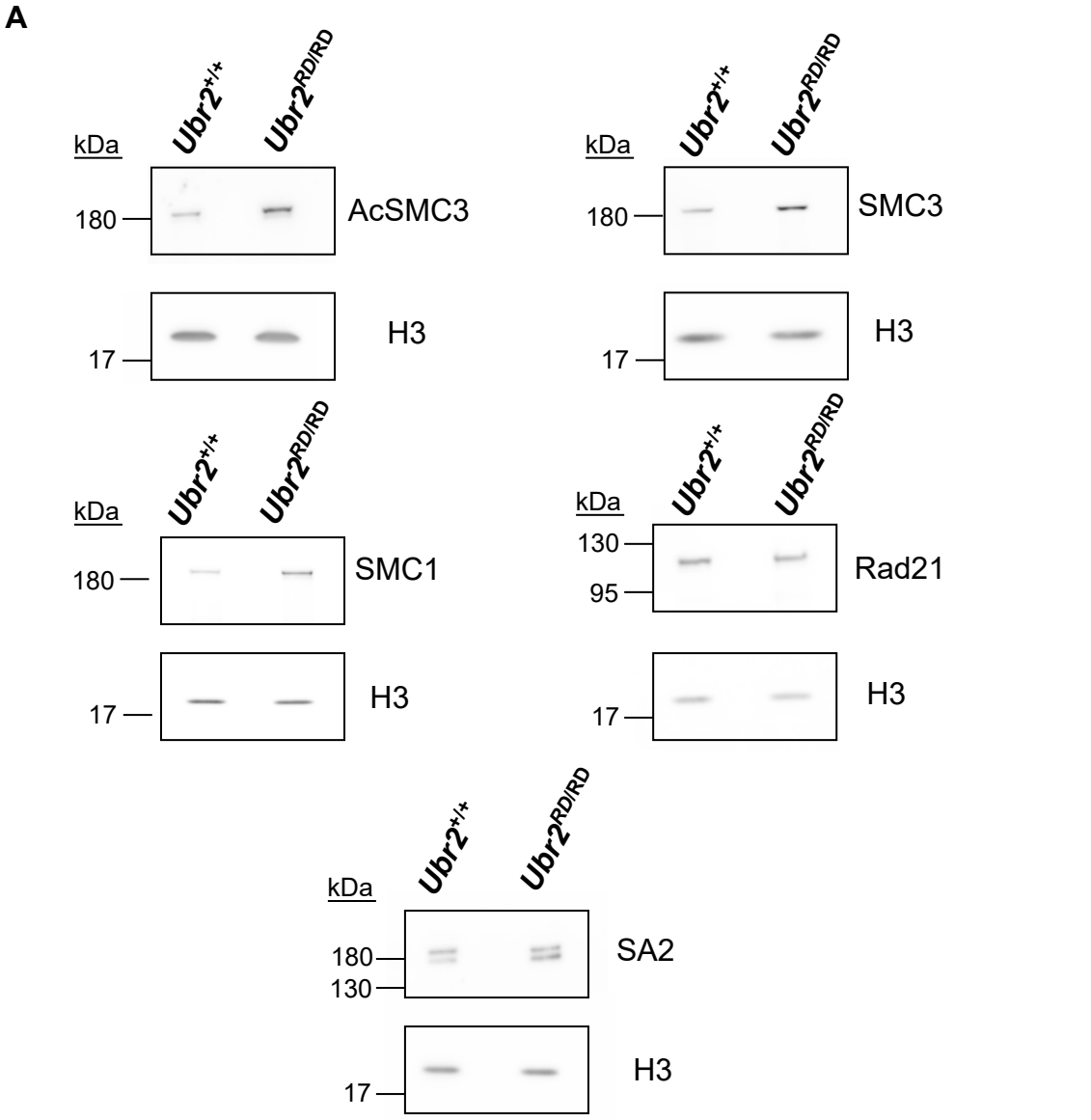
A
Ubr2+/+
Ubr2RD/RD
kDa
180
AcSMC3
17
H3
SMC3
SMC1
130
95
Rad21
SA2
B
Relative abundance in Chromatin
0
1
2
3
4
5
*
AcSMC3
SMC3
SMC1
RAD21
SA2
Cohesin Subunit
Ubr2+/+
Ubr2RD/RD

As the W1177A point mutation in UBR2's RING domain had an impact on chromatin-associated cohesin, I wanted to check that this did not perturb the spleen gross morphology. To assess the *Ubr2*$^{RD/RD}$ spleen morphology in detail, Jen Lawson in our group performed tissue sections and stained with H&E to look at the spleen (Figure 5.14A) The W1177A mutation in *Ubr2* does not dramatically alter the histological appearance or cell type composition of the spleen. Furthermore, the average weight of each spleen in an *Ubr2*$^{+/+}$ male is 95.7±18.9mg (± standard deviation), and *Ubr2*$^{RD/RD}$ spleen is 91.4 ±11mg; these are not significantly different in size (Figure 5.14B). The cell cycle distribution of *Ubr2*$^{RD/RD}$ splenocytes, analysed by flow cytometry, is not different to *Ubr2*$^{+/+}$ mice (Figure 5.14C). The W1177A mutation in *Ubr2* does not grossly perturb the cell cycle distribution and gross morphology of the spleen tissue.

Figure 5.14: *Ubr2*$^{RD/RD}$ mice have no overt defects in spleen. (A) Hematoxylin and eosin–stained paraffin sections of *Ubr2*$^{+/+}$ and *Ubr2*$^{RD/RD}$ spleen. W1177A mutation in UBR2 does not dramatically alter the histological appearance or cell type composition of the spleen. Scale bar, 100 μm. (**B**) Spleen weights in wild type (*Ubr2*$^{+/+}$) and homozygote W1177A mutant (*Ubr2*$^{RD/RD}$) males (N=4 mice per genotype) at 8-12 weeks pp. Black bars are means. p=0.73, Student's T-test (**C**) Flow cytometry of *Ubr2*$^{+/+}$ and *Ubr2*$^{RD/RD}$ splenocytes.

A

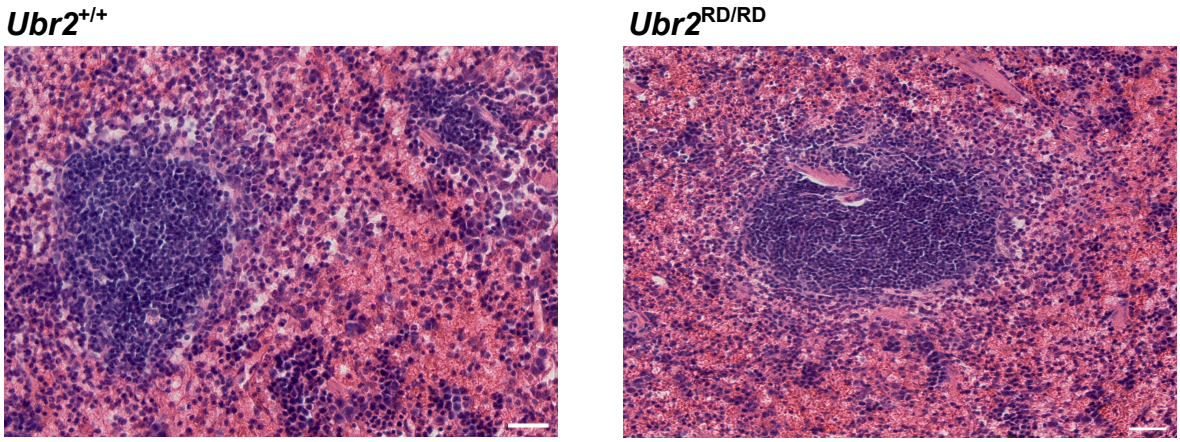
Ubr2+/+
Ubr2RD/RD

B

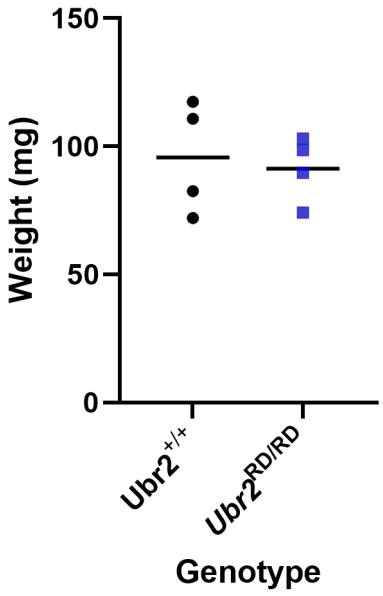
150
100
50
0
Weight (mg)
Ubr2+/+
Ubr2RD/RD
Genotype

C

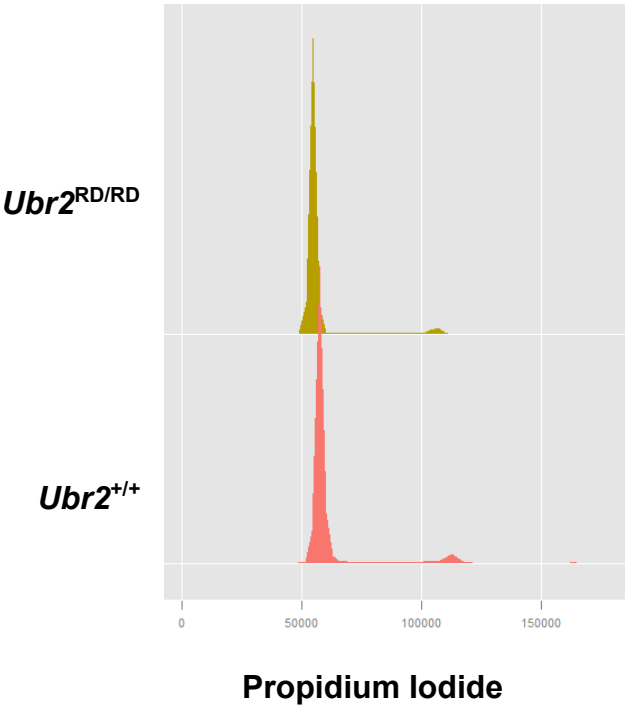
Ubr2RD/RD
Ubr2+/+
0
50000
100000
150000
Propidium Iodide

5.2.4 The TT insertion does not disrupt the novel role of *Ubr2* in cohesin regulation

As previously stated, UBR2 has a role in the regulation of the AcSMC3-containing subpopulation of cohesin complexes, which is thought to mediate sister chromatid cohesin, in splenocytes (Reichmann *et al.*, 2020). In order to investigate if this role of *Ubr2* is perturbed in the *Ubr2*$^{TT/TT}$ mutant mouse, I looked at the chromatin-associated cohesin levels from splenocytes isolated from the *Ubr2*$^{TT/TT}$ spleen. The level of total chromatin-associated cohesin was quantified in the *Ubr2*$^{TT/TT}$ spleen using anti- SMC3, SMC1, RAD21, SA2 and AcSMC3 antibodies in Western blotting of chromatin prepared from the spleens of 3 independent mice (Figure 5.15A).

Upon quantification of these proteins, normalised to the intensity of chromatin-associated histone H3 protein detected in these samples, I was unable to detect a significant change in any of the cohesin protein levels (Figure 5.15B). The TT insertion in *Ubr2* does not dramatically alter the histological appearance cell type composition or average weight of the spleen (Figure 5.15C and D). This implies that the TT insertion that leads to a frameshift in UBR2 does not have an impact on cohesin levels suggesting that UBR2 is still functional in the spleen unlike in *Ubr2*$^{-/-}$ mice. However, the TT insertion in the RING domain gives a different phenotype than that observed in *Ubr2*$^{RD/RD}$ mice which suggests the TT insertion that leads to an amino acid change (W1177F) and the premature stop codon does not inhibit E2 binding and ubiquitination of substrates. Additional biochemical assays

would have to be performed to confirm the Ub activity of *Ubr2*$^{TT/TT}$ and *Ubr2*$^{RD/RD}$ mice.

Figure 5.15: Mitotic cohesin regulation is not perturbed in the *Ubr2*$^{TT/TT}$ mouse (**A**) Representative western blots of chromatin-associated proteins AcSMC3, SMC3, SMC1, Rad21 and SA2 isolated from spleens of 3 pairs of *Ubr2*$^{+/+}$ and homozygous *Ubr2*$^{TT/TT}$ mice, and chromatin-associated histone H3 protein as a loading control. (**B**) Quantified mean protein levels of cohesin subunits from western blotting in A and normalised to histone H3 protein level. Standard deviation over three pairs of wild type and homozygous mutant mice shown. Differences between *Ubr2*$^{+/+}$ and *Ubr2*$^{TT/TT}$ are not significant; AcSMC3: p=0.11, SMC3: p=0.75, SMC1: p=0.85 and RAD21: p= 0.70 and SA2 p=0.76 (Student's T-test). Each pair of histone H3 and cohesin bands are from the same gel lane; the high concentration of histones in chromatin causes the sample to spread laterally at low molecular weights. (**C**) Hematoxylin and eosin–stained paraffin sections of *Ubr2*$^{+/+}$ and *Ubr2*$^{TT/TT}$ spleen. TT insertion in UBR2 does not dramatically alter the histological appearance or cell type composition of the spleen. Scale bar, 100 μm. (**D**) Spleen weights in wild type (*Ubr2*$^{+/+}$) and homozygote TT insertion mutant (*Ubr2*$^{TT/TT}$) males (N=3 mice per genotype). Black bars are means. p= 0.89, Student's T-test.

A

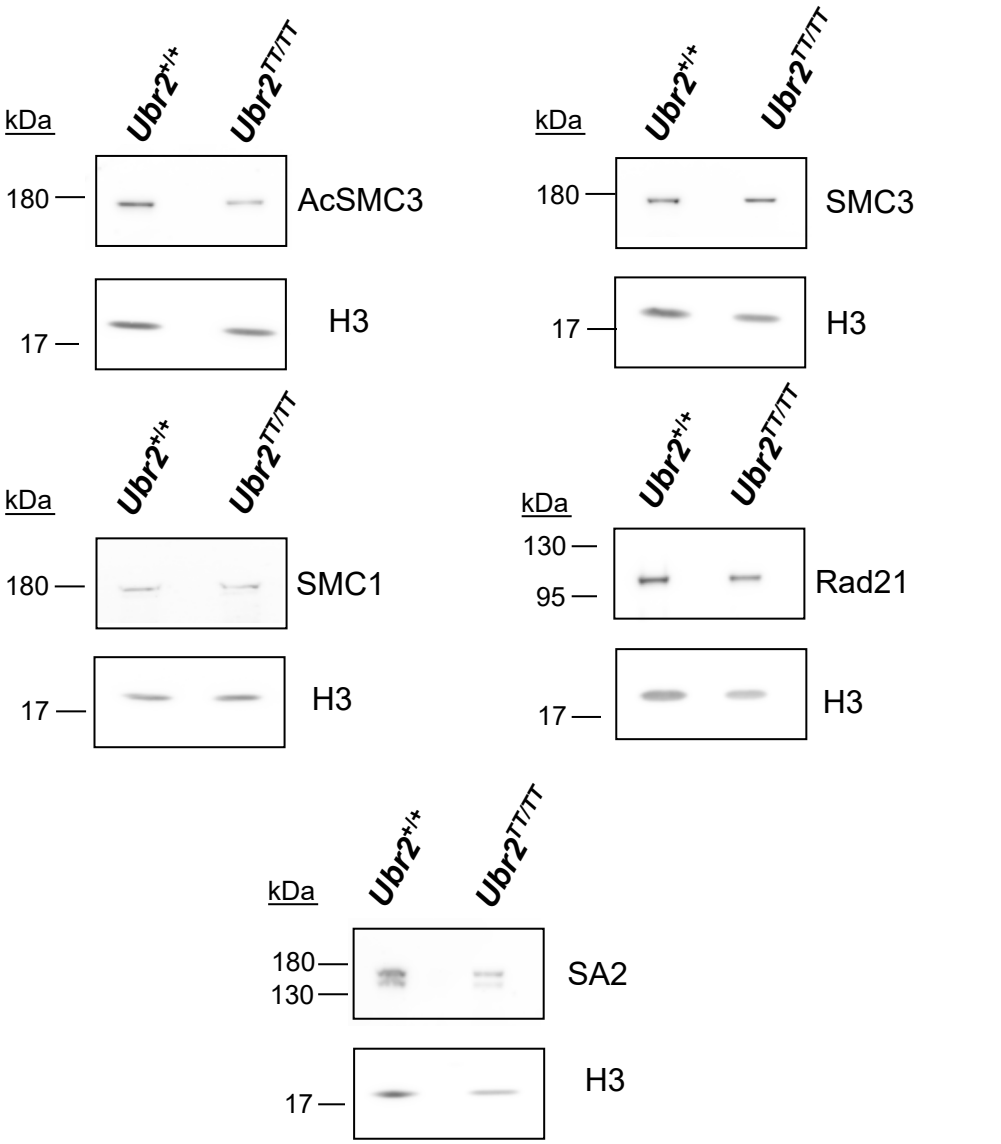
kDa
Ubr2+/+
Ubr2TT/TT
180
AcSMC3
17
H3
kDa
Ubr2+/+
Ubr2TT/TT
180
SMC3
17
H3
kDa
Ubr2+/+
Ubr2TT/TT
180
SMC1
17
H3
kDa
Ubr2+/+
Ubr2TT/TT
130
95
Rad21
17
H3
kDa
Ubr2+/+
Ubr2TT/TT
180
130
SA2
17
H3

B

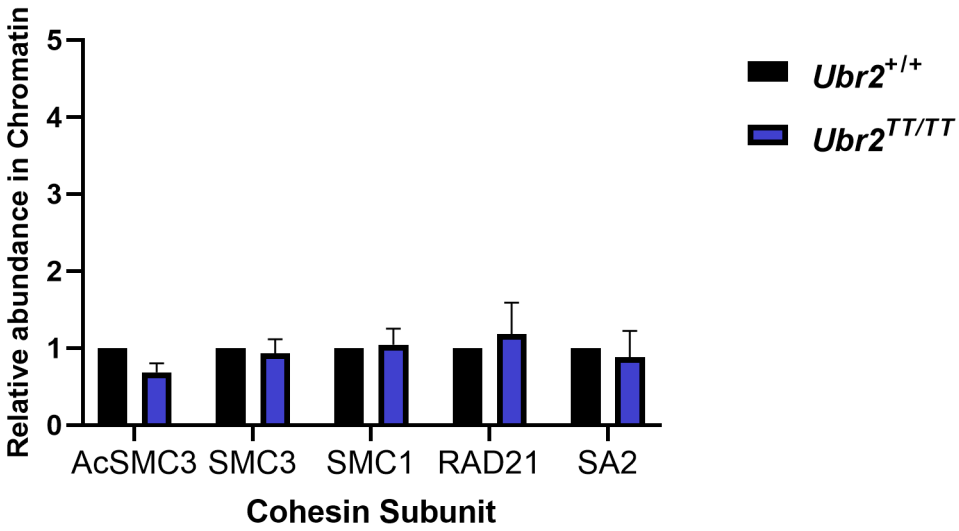
Relative abundance in Chromatin
5
4
3
2
1
0
AcSMC3
SMC3
SMC1
RAD21
SA2
Cohesin Subunit
Ubr2+/+
Ubr2TT/TT

C

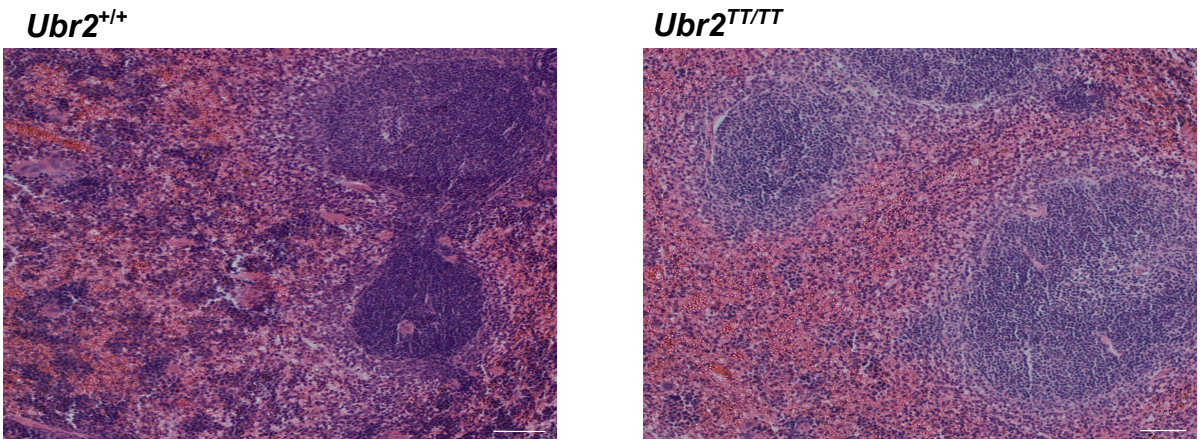
Ubr2+/+
Ubr2TT/TT

D

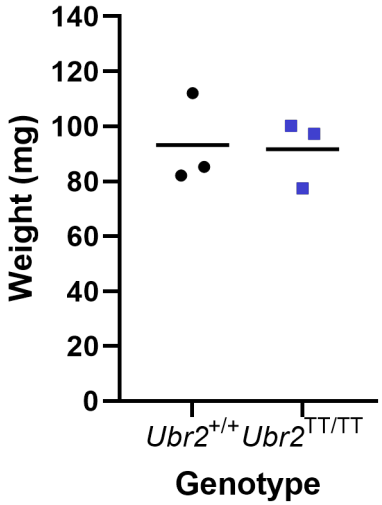
140
120
100
80
60
40
20
0
Weight (mg)
Ubr2+/+
Ubr2TT/TT
Genotype

5.3 Discussion

In this chapter, I carried out the implementation of a genetic point mutation in the *Ubr2* gene in order to investigate the molecular basis of the RING domain of the E3 ubiquitin ligase. The point mutation W1177A has been shown *in vitro* to perturb UBR2's ability to binding of E2 ligases such as USE1 and UBE2A (Lee *et al.*, 2011). The TT insertion at position 55655 in exon 31 of the *Ubr2* gene leads to a frame shift in the UBR2 protein which would lead to a premature stop codon in the RING domain, ablating all functions that require the domains following this insertion. As has been previously described, in our group and by others (Crichton et al., 2017; Kwon et al., 2003; Reichmann et al., 2020; Yang et al., 2010; Eleanor Raymond, unpublished), *Ubr2* is required *in vivo* for normal meiosis and spermatogenesis in males, female embryonic development and for regulation of the chromatin-associated AcSMC3 component of the cohesin complex in the rapidly replicating mitotic spleen.

Stable introduction of W1177A into the *Ubr2* gene in a mouse line by CRISPR-Cas9 homology directed repair allowed investigation into the three major phenotypes of the $Ubr2^{-/-}$ mouse, and showed the that male infertility and female embryonic lethality phenotypes are not present in $Ubr2^{RD/RD}$ mice, indicating that they do not act through UBR2's role in N-end rule or non-N-end rule ubiquitination for protein turnover. $Ubr2^{RD/RD}$ mice have a cohesin phenotype in mitotic spleen indicating that cohesin turnover is due to non-N-end rule ubiquitination. However, $Ubr2^{RD/RD}$ leads to an increase in all

cohesin subunits, except RAD21, which is not observed in *Ubr2*$^{-/-}$ mice indicating that ubiquitination is important but there is some previously uncharacterised role of UBR2 with cohesin.

5.3.1 UBR2 and TEX19.1 in spermatogenesis

The *Ubr2*$^{-/-}$ spermatogenesis phenotypes were previously thought to be due to UBR2's well characterised role in the N-end rule pathway for protein degradation (Tasaki *et al.*, 2005). Previous work by Eleanor Raymond on *Ubr2*$^{T2/T2}$ mice and *Ubr2*$^{RD/RD}$ mice in this chapter indicate that UBR2's essential role in spermatogenesis does not act through ubiquitination of type II or non-N-end rule substrates.

UBR2's role in spermatogenesis may be through its role in TEX19.1 stabilisation. *Ubr2*$^{-/-}$ testes showed that loss of UBR2 results in loss of TEX19.1 protein but not *Tex19.1* mRNA (Yang *et al.*, 2010), suggesting that UBR2 prevents degradation of TEX19.1, possibly through UBR2 being an obligate binding partner of TEX19.1. Also, *Ubr2*$^{-/-}$ spermatocytes have a phenocopy of the recombination deficits and asynapsis observed in the *Tex19.1*$^{-/-}$ spermatocyte (Crichton *et al.*, 2017) which could be due to a lack of functional TEX19.1-UBR2 complex as UBR2 is required for TEX19.1 stabilisation in the testes.

Binding and stabilisation of proteins like TEX19.1 is unique to UBR2 as it has not been observed in other E3 ubiquitin ligases. The location of the TEX19.1 binding site on UBR2 is unknown. As it appears that the stabilisation of the TEX19.1:UBR2 complex is the important role of UBR2 in spermatogenesis,

the region that is lost in *Ubr2*$^{TT/TT}$ protein could be an important location for the identification of the TEX19.1 binding site. As *Ubr2*$^{TT/TT}$ mice had a testis phenotype similar to what is observed in *Ubr2*$^{-/-}$ mice, albeit could still produce a small quantity of sperm. Further work to identify TEX19.1 protein levels in the *Ubr2*$^{TT/TT}$ testes should be determined to confirm whether TEX19.1 is stable in this tissue. If TEX19.1 is not detectable, this could give an idea of the location of this binding site.

5.3.2 UBR2's role in cohesin regulation

Ubr2 has been implicated in cohesin regulation, both alongside and in absence of *Tex19.1* (Reichmann et al., 2020; Eleanor Raymond, unpublished). Sister chromatid cohesion is one of the best-studied roles for cohesin during the mitotic cell cycle, to allow even chromosome division and prevent aneuploidy, which can cause cell death. *Ubr2* has been implicated in the regulation of acetylated cohesin subpopulation (AcSMC3) which is required for recruitment of cohesin-maintenance factors such as sororin (Nishiyama *et al.*, 2010; Ladurner *et al.*, 2016). During the cell cycle, efficient and timely loading and removal of the cohesin complex is vital for correct chromosome segregation during cell division, and maintenance of the acetylated cohesin complex in mitosis is important.

Ubr2$^{RD/RD}$ splenocytes had an increase in all cohesin subunits, except for RAD21, protein levels in the spleen which is not identical to *Ubr2*$^{-/-}$ mice where only the AcSMC3-supopulation of cohesin was increased (Reichmann *et al.*, 2020). Implying that the W1177A mutation in the RING domain is

leading to changes in all chromatin-bound cohesin not just the AcSMC3-marked subpopulation of cohesin. This suggests that UBR2 has the ability to turn over cohesin or increase cohesin loading in splenocytes through non-N-end rule ubiquitination of cohesin or via intermediates. Substrates of UBR2 can still bind to the mutant UBR2 protein in the *Ubr2*$^{RD/RD}$ mice but their ubiquitination by E2 ligases leading to their degradation by the 26s proteasome will be impaired. Examples of substrates of this ubiquitination function of UBR2 has been identified including LINE-1, histone H2A and ATF3 (An et al., 2012; Maclennan et al., 2017; Vu and Varshavsky, 2020). However, the functional domain through which UBR2 is able to bind these substrates is unknown so further structural analysis of UBR2 may identify regions of interest outside of the UBR box and N-domain.

One that may be of interest could be the UBR auto-inhibitory domain (UAIN) domain which follows the RING domain in UBR2's structure. *S. cerevisiae* Ubr1 can bind to the transcriptional repressor CUP9 through an internal degron site, that has been limited to a c-terminal 33-residue region (Turner, Du and Varshavsky, 2000; Du *et al.*, 2002). Ubr1 recognition of CUP9 depends on the C-terminus proximal UAIN (Zenker *et al.*, 2005) and carries out auto-inhibition in Ubr1 by binding the N-terminal, blocking binding of Ubr1 to CUP9 (Du *et al.*, 2002). The recognition domain for CUP9 within Ubr1 has not been identified so it is not fully understood how the UAIN blocks CUP9 interactions (Du *et al.*, 2002; Xia *et al.*, 2008). Furthermore the UAIN domain can interact with the Ubr-Box and Winged helix domain through a putative zinc-binding site in Ubr1 (Pan *et al.*, 2021) but it remains unclear how this

links to function and study of the UAIN domain has not been published in mammalian UBR proteins.

Previous work has identified that the internal degron ubiquitination target, ATF3, can bind to an 81 kDa Ct-fragment of human UBR2 (1072-1755) in Split-Ub assays but not the Nt-fragment or full length UBR2 (Vu and Varshavsky, 2020). This fragmented UBR2 includes part of the RING domain and UAIN so the UAIN may be important for ubiquitin substrate binding outside of the N-end rule.

Ubr2$^{TT/TT}$ mice lack any cohesin phenotype in the spleen indicating that the changing of tryptophan at W1177 to phenylalanine (W1177F) following the TT insertion may not perturb E2 binding so ubiquitination occurs normally in these mice. Co-immunoprecipitation assays with USE1 and UBE2A antibody's and spleen lysate may identify whether this mutation does not perturb binding between this UBR2 protein and E2 ligases. These mice would not have a UAIN domain in UBR2 due to the location of the premature stop codon so it is unlikely that this domain is important for non-N-end rule substrate binding.

The kleisin subunit, RAD21, was the only cohesin subunit that was not affected by the W1177A mutation in the spleen. RAD21 binds to the V-shaped SMC1 and SMC3 heterodimer, forming a tripartite ring-like structure (Gligoris *et al.*, 2014) and then recruits SA1/SA2 which binds to STAG domain on RAD21 to reinforce the cohesin ring (Gruber, Haering and Nasmyth, 2003). RAD21 is proteolytically cleaved by separase which is

required for the dissociation of the cohesin complex for the orderly segregation of the sister chromatids during mitosis (Nasmyth, Peters and Uhlmann, 2000). Human and mouse RAD21 are 96% identical and contain two separase cleavage sites with the ExxR motif (Hauf, Waizenegger and Peters, 2001). In yeast, the separase-generated C-terminal fragment of Scc1 retained some affinity to the rest of the cohesin complex (Rao *et al.*, 2001). The model for the Scc1 Ct fragments affinity for the cohesin complex would require incorporation into new cohesin complexes loaded onto the chromosomes during S phase in the next cell cycle. Previously, the C-terminal separase cleavage products of RAD21 were shown to be stable and long lived in mice unlike the short-lived fragments of meiotic REC8 cleaved in the same region (Liu *et al.*, 2016) indicating that RAD21 cleaved products are more stable and could incorporate into the cohesin complex in spleenocytes. The cohesin that is increased in *Ubr2*$^{RD/RD}$ mice may be complexes with C-terminal RAD21 incorporated rather than full length and this may not be detected with the anti-RAD21 antibody. However, the epitope recognized by Anti-RAD21 antibody (ab992) maps to a region between residue 575 and the C-terminus (residue 631) of RAD21 so would have shown an increase in both fragments.

In addition to proteolytic cleavage of RAD21 during mitosis, RAD21 is cleaved during apoptosis (Chen *et al.*, 2002; Pati, Zhang and Plon, 2002). It remains unclear what protease is important for this cleavage but it appears that there is a novel caspase or caspase-like molecule in the nucleus that cleaves RAD21 early in apoptosis (Panigrahi and Pati, 2009). RAD21 also

has critical roles in multiple developmental processes, transcriptional programmes, chromatin structure regulation and acts as an oncogene (Nitzsche *et al.*, 2011; Xu *et al.*, 2011; Monahan *et al.*, 2012; Galeev *et al.*, 2016). Such findings indicate multiple roles of RAD21 outside of sister chromatid cohesion and there are multiple pathways that are involved in maintaining RAD21 protein levels. Although it is unclear as to why it is the only cohesin subunit not affected in *Ubr2*$^{RD/RD}$ spleen, the potential impairment of ubiquitination in the spleen may lead to accumulation of a substrate responsible for depleting RAD21 from chromatin. The differences in *Ubr2*$^{-/-}$, *Ubr2*$^{RD/RD}$ and *Ubr2*$^{TT/TT}$ all leading to different cohesin phenotypes shows that understanding UBR2's interactions with cohesin is not complete.

As there was an increase in cohesin levels in *Ubr2*$^{RD/RD}$ mice spleen, it would be worth determining cohesin levels in female oocytes. Misregulation of the cohesin complex in oocytes, has been associated with chromosome missegregation, aneuploidy and subfertility (Jessberger, 2012; Herbert *et al.*, 2015). Due to the female embryonic lethality observed in *Ubr2*$^{-/-}$ mice (Kwon *et al.*, 2003) it has been difficult to determine if UBR2 has a role in cohesin turnover in oocytes. As *Ubr2*$^{RD/RD}$ mice do not have the female embryonic lethality it is a potential model that could be used to investigate cohesin subunit levels by IF on metaphase I spreads and determine any effect on chromosome cohesion.

5.3.3 Limitations of this study

It should be noted that the study conducted in this chapter does not have the scope to fully prevent ubiquitination by UBR2. The W1177A mutation in the RING domain of UBR2 was shown to lower, but not fully prevent, pulldown of E2 ligases UBE2A and USE1 in a co-immunoprecipitation assay (Lee *et al.*, 2011). Although this is a highly conserved domain, UBR2 has been confirmed to act through a variety of other E2 ubiquitin conjugating enzymes, including UBE2O and UBE2B (An *et al.*, 2010; Xu *et al.*, 2019) , and so this point mutation may not necessarily prevent binding of all potential E2 ubiquitin ligases and not generate a fully penetrant catalytic dead mutation. In future work, co-immunoprecipitation assays should be carried out in order to test the extent of the mutation on UBE2A and USE1 binding in the mouse, as well as the conservation of the UBR2 RING domain structure between different potential E2 interactors.

Ubr2$^{TT/TT}$ mice may have no detectable UBR2 protein as a result of misfolding which would explain why the female homozygote lethality and reduction in testis size matched what is observed in *Ubr2*$^{-/-}$ mice (Kwon *et al.*, 2003; Crichton *et al.*, 2017). However, asynpasis is not as profound and spermatocytes can still complete meiosis leading to detectable sperm in the epididymis suggesting that there is some UBR2 function remaining in these tissues. Identification of the level of expression of this UBR2 protein has not been completed in this study so it is not clear if UBR2 is still expressed in these tissues. Identifying and using an antibody that binds to the protein

before the mutation site is required, as the binding site of the antibody used in this chapter binds to the C-terminus of UBR2 which is removed in the TT insertion mutant (Figure 5.10). Bioinformatic analyses could be applied to identify conserved structural domains within this lost region of the UBR2 protein, as compared to known mouse proteins, and structural folding could be predicted.

5.3.4 Further study of UBR2 protein-binding domains.

Further investigation into the role of UBR2's affinity to type I N-end rule binding is required to confirm that ubiquitination of non-N-end rule substrates is important for cohesin in *Ubr2*$^{RD/RD}$ mice. Initially, the D118A point mutation was identified in the Ubr1 gene using an alanine screen of the N-end rule substrate-binding domains (Tasaki *et al.*, 2009). D118 is within the UBR box's active site, conserved between species and UBR1/UBR2 which conjugates water to the sidechain of the N-terminal arginine, so gives the UBR box specific type I substrate binding (Tasaki *et al.*, 2009; Matta-Camacho *et al.*, 2010; Muñoz-Escobar, Kozlov and Gehring, 2017). Placing the D118A mutation into *Ubr2* in ESCs did not lead to any effect on AcSMC3 protein levels at G2/M (Eleanor Raymond, unpublished) which did not match the increase in AcSMC3 levels in *Ubr2*$^{-/-}$ ESCs and mouse spleen suggesting that type I substrate binding to UBR2 is not important for the cohesin phenotype. However, *Ubr2*$^{RD/RD}$ mice had a different cohesin phenotype, not observed in an *Ubr2*$^{-/-}$ spleen, indicating that this UBR2 protein leads to specific phenotypes which may involve type I substrate binding.

Even though UBR2 was first thought to have a limited role in the type I N-end Rule pathway instead acting more in the turnover of type II substrates (Tasaki *et al.*, 2005). Studies have identified canonical type I substrates, i.e. encoding an N-terminal arginine that depends on one or both of UBR1 and UBR2, the most highly conserved members of the UBR family (Rageul *et al.*, 2019). *Ubr2*$^{-/-}$ MEFs (mouse embryonic fibroblasts) exhibit a vulnerability to UV irradiation as a result of a lack of type I N-end rule degradation of genomic stress regulator SDE2 (Rageul *et al.*, 2019) indicating that UBR2 does have a role in type I-N-end rule pathway *in vivo*. Introduction of the D118A mutation into mice, could determine if the cohesin phenotype in *Ubr2*$^{RD/RD}$ requires type I abilities.

5.4 Summary

In this chapter, I have demonstrated that the RING domain of UBR2, impaired by the W1177A mutation, is required for one of the major essential roles of the protein in the mouse. It appears that the increase in AcSMC3 levels in the spleen identified in the *Ubr2*$^{-/-}$ mouse line depends on the non-canonical ubiquitination of UBR2. However, this mutation also appears to be affecting all of the cohesin subunits, except RAD21, so impairing E2 binding is leading to phenotypes not observed in *Ubr2*$^{-/-}$ mice and could lead to increase in total cohesin loading. The male meiotic phenotype is through a non-canonical function, not ubiquitination, rather another function of the UBR2 protein altogether such as its interaction with TEX19.1.

Further work to generate more genetic models that can be used to separate out other functions of UBR2 and possibly other UBR proteins will give an insight into the full scope of UBR2's roles in the mouse, and potentially lead to a greater understanding of the UBR protein family.

Chapter 6

Discussions and Conclusion

The main aim of the work presented in this thesis was to study the E3 ubiquitin ligase UBR2's mechanism of action in the essential roles that have previously been identified in the mouse, particularly in spermatogenesis, cohesin maintenance and in embryonic survival. A summary of the phenotypes identified in *Ubr2*$^{-/-}$ mice and the *Ubr2* mutants is shown in Table 6.1.

In order to study this using a genetic approach, I introduced a mutation into the RING domain of UBR2 which perturbs its role in E2 binding, and showed that this essential function of the protein does not perturb spermatogenesis and embryonic survival indicating the importance of non-canonical roles of UBR2 outside of ubiquitination. The mutant allele does impact chromatin-associated cohesin in mitotic spleen. This poses the question of non-N-end Rule activities of UBR2 as previous work shows that cohesin maintenance is not through the N-end rule pathway. Even though UBR2 has a role in the maintenance of chromatin-associated cohesin in mitotic tissue, UBR2 does not localise to chromatin during G2/M. UBR2's ELL-like structural domain may be important for ubiquitination and introduction of a mutation, which may disturb its structure, alters the localisation of UBR2 towards chromosomes. This poses the question of UBR2's structure in relation to its function.

	Phenotype		
***Ubr2* mutants**	**Embryonic lethality**	**Chromatin-associated cohesin**	**Spermatogenesis and testis development**
***Ubr2*$^{-/-}$**	- Female embryonic lethality	- Increase in the AcSMC3 subunit of chromatin-associated cohesin in spleen	- No detectable sperm - Reduced testis size - Increase in asynapsed pachytene and stalled Meiosis I
***Ubr2*$^{T2/T2}$**	- No embryonic lethality	- No increase in cohesin subunits in spleen	- Normal sperm count - No change in testis size - No change in prophase staging of Meiosis I
***Ubr2*$^{RD/RD}$**	- No embryonic lethality	- Increase in all chromatin-associated cohesin subunits in spleen except for RAD21	- Normal sperm count - No change in testis size - No change in prophase staging of Meiosis I
***Ubr2*$^{TT/TT}$**	- Female embryonic lethality	- No increase in cohesin subunits in spleen	- Reduction in sperm count - Reduced testis size - Increase in asynapsed pachytene but Meiosis I can be completed

Table 6.1: Summary of phenotypes identified in all *Ubr2* mouse mutants

6.1 UBR2 in spermatogenesis and development

UBR2 is ubiquitously expressed in a wide variety of tissues in the mouse yet the majority of the phenotypes identified in *Ubr2*$^{-/-}$ mouse arise in tissues that also express TEX19.1, which is able to form a 1:1 stoichiometric complex with the UBR2 protein (Yang *et al.*, 2010; Reichmann *et al.*, 2020). In the testis, UBR2 is required for TEX19.1 protein stability (Yang *et al.*, 2010), presumably due to the requirement for a stable TEX19.1-UBR2 complex. Unsurprisingly, the mammalian *Ubr2*$^{-/-}$ spermatocyte has a partial phenocopy of the recombination deficits and asynapsis leading to infertility observed in the *Tex19.1*$^{-/-}$ mouse. The *Ubr2*$^{RD/RD}$ mice had none of the developmental or male testis phenotypes identified in *Ubr2*$^{-/-}$ mice indicating that UBR2's role in protein ubiquitination of either N-end rule or non-N-end rule substrates is not important in these processes. This suggests that these phenotypes in *Ubr2*$^{-/-}$ mice are due to the loss of a stable TEX19.1-UBR2 complex. TEX19.1 is not a substrate of UBR2 as the protein is not degraded in the presence of UBR2 (Maclennan *et al.*, 2017) rather a regulatory protein or cofactor.

Further work will be required to separate TEX19.1 and UBR2 functions to confirm the importance of this interaction between them. This could be done by perturbing the TEX19.1-UBR2 interaction itself and by identifying the interaction site between TEX19.1 and UBR2 which remains unknown. UBR2 is a large 200kDA protein (Tasaki *et al.*, 2009) with only a small proportion being fully mapped and studied i.e. the UBR box, N-domain and the RING domain. Identification of structural domains within the UBR2 protein by

comparing to known mouse proteins led to the identification of the ELL-like domain in UBR2. Yeast Ubr1 has a WHD that is important for ubiquitination of substrates bound to the protein (Pan *et al.*, 2021) which may be conserved in UBR2. Further characterisation of this area could determine whether it has a role in substrate binding for ubiquitination or binding to cofactor proteins like TEX19.1.

The TT insertion into the RING domain led to female lethality and gross testis phenotypes that are observed in *Ubr2*$^{-/-}$ mice but the *Ubr2*$^{TT/TT}$ mouse is only a partial phenocopy of *Ubr2*$^{-/-}$ as some sperm is still detectable. The part of the protein that is lost in the *Ubr2*$^{TT/TT}$ mouse may be important for TEX19.1 binding and may highlight an important role for the UAIN domain which follows the RING domain in UBR2's structure. Further characterisation of the protein created in this mouse should be completed to confirm if this area of the protein is important for TEX19.1 binding.

6.2 UBR2 and cohesin

Even though UBR2 has a role in protein turnover in a wide variety of tissues from the innate immune response to neuron degeneration (Xu *et al.*, 2019; Eldeeb *et al.*, 2022), only one phenotype thus far identified outside of the TEX19.1 expression pattern is the misregulation of the acetylated SMC3 cohesin subunit in the splenocyte (Reichmann *et al.*, 2020). An *Ubr2*$^{-/-}$ mouse embryonic fibroblast (MEF) cell line, which also does not express *Tex19.1*, exhibits nuclear localisation and chromatin-associated ubiquitination as a result of DNA damage by UV radiation. This indicates a regulatory role for

UBR2 in DNA damage response, possibly through regulatory monoubiquitination of histone H2A (An *et al.*, 2012) but this association is not fully confirmed. One other explanation for the increased DNA damage could be the misregulation of the cohesin complex. Cohesionopathies, such as WABs, have a DNA breakage phenotype resulting from the misregulation of cohesin during S phase and replication fork instability (Cortone *et al.*, 2018; Pisani *et al.*, 2018). To determine the cause of genomic instability in the *Ubr2*$^{-/-}$ MEFs, cohesin localisation or chromatin capture assays could be assessed in these cells.

The role of *Ubr2* in cohesin regulation is complex. The upregulation of the chromatin-associated AcSMC3 subunit of cohesin in the spleen is *Tex19.1*-independent, ESCs in culture express both *Tex19.1* and *Ubr2*, and *Ubr2*$^{-/-}$ ESCs exhibit a similar increase in chromatin-associated cohesin. *Tex19.1*$^{-/-}$ ESCs have a significant reduction in chromatin-associated AcSMC3 (Karen Dobie, unpublished) so TEX19.1 may act to regulate UBR2's control of AcSMC3 levels in ESCs. The *Ubr* mutant ESCs in this thesis had detectable levels of TEX19.1 protein so it would be worth identifying cohesin protein levels to try identify which of UBR2's protein-binding interfaces are important for this role in the presence of TEX19.1. Also, it would be interesting to investigate if the response to DNA damage in *Ubr2*$^{-/-}$ MEFs is the same in *Ubr2*$^{-/-}$ ESCs compared to MEFs or if having *Tex19.1* expression alters UBR2's role in the DNA damage response.

Ubr2$^{-/-}$ mice have increased levels of the AcSMC3-subunit of cohesin in splenocytes (Reichmann *et al.*, 2020) which is also observed in *Ubr2*$^{-/-}$ ESCs (Karen Dobie, unpublished). Acetylation of the SMC3 subunit of cohesin during mitotic S phase recruits cohesin maintenance factors like sororin, which antagonises WAPL to maintain chromosome cohesion throughout G2 (Nishiyama *et al.*, 2010; Losada, 2014). Therefore, AcSMC3 is seen as a marker of cohesive cohesin on chromatin which is important for chromosome cohesion during the cell cycle.

Ubr2$^{RD/RD}$ mice had an increase in AcSMC3-subunit to a similar to what is observed in *Ubr2*$^{-/-}$ spleen but also had an increase in all other cohesin subunits except RAD21. This suggests that UBR2 has a role in either maintaining all cohesin levels not just the AcSMC3-subpopulation in splenocytes or an increase in cohesin loading. RAD21 being unaffected in this mutant was unexpected. Previously, the C-terminal separase cleavage products of RAD21 were shown to be stable and long lived in mice unlike the fragments meiotic REC8 (Liu *et al.*, 2016) indicating that RAD21 may have a different pathway for its turnover from other cohesin subunits.

Previous work showed that the cohesin phenotype was not due to UBR2's role in N-end rule pathway (Eleanor Raymond, unpublished), UBR2's role in cohesin turnover may be a non-canonical function likely a non-N-end Rule ubiquitination function. Yeast paralog of the mouse UBR family, Ubr1, has been shown to bind ubiquitination targets such as the CUP9 transcriptional repressor through an internal degron (Xia et al., 2008). Also, human UBR2

was shown to have a role in ubiquitination of transcription factor ATF3 through an internal degron (Vu and Varshavsky, 2020) suggesting this function is conserved between species. UBR2 may be binding to cohesin directly or through intermediates via an internal degron site. Further work is required to determine the location of the internal degron binding site within UBR2 which could be done genetically or by breaking the UBR2 protein into smaller regions and observing which region or combination of regions are important for its role in cohesin turnover.

6.3 Localisation of UBR2 and identification of substrates

UBR2 has functions with many chromatin-associated proteins including cohesin and histones. However, it remains unknown whether UBR2 directly interacts with these proteins or through intermediates which could be determined by identifying the localisation of UBR2 throughout the cell cycle. An *Ubr2*$^{-/-}$ MEF cell line exhibited UBR2 nuclear localisation in interphase by IF and a rapid increase in nuclear-associated UBR2 protein levels during G2/M by cell fractionation and Western blotting (An *et al.*, 2012). In Chapter 3, FLAG-UBR2 was localised to the nucleus during interphase but did not colocalise with chromosomes during G2/M suggesting that UBR2 does not directly bind to chromatin-associated proteins at this point in the cell cycle. Future work should investigate the localisation of endogenous UBR2 in cells that have phenotypes in *Ubr2*$^{-/-}$ context. Stable tagging of endogenous UBR2 with a fluorescent label in ESCs or MEFs would allow for live cell imaging throughout the cell cycle to confirm localisation patterns which have been contradictory.

Mass spectrometry is a high-powered way of identifying significant changes in the proteome and did lead to identification of potential substrates of UBR2 by comparing *Ubr2*$^{-/-}$ and *Ubr* mutants to wildtype *Ubr2*$^{+/+}$ ESCs. However, these substrates still need to be verified. Mass spectrometry associated with co-immunoprecipitation (coIP) with the UBR2 protein may be better in identifying UBR2 interactions, similar to what was done in Chapter 3. Following transfection of FLAG-UBR2 or FLAG-ELL-UBR2 in HEK293Ts at G2/M, there were ~700 proteins that were pulled down with either of the UBR2 proteins indicating a large number of UBR2 interactors. To compile a list of proteins that could be divided into N-end-rule, non-N-end rule and interacting cofactors like TEX19.1, the FLAG-UBR2 mutants (T1, T2 and RD) could be used in a FLAG-IP and MS experiment. To compile a more specific list of potential UBR2 interactors for the essential roles in ESCs, a BioID or TurboID fusion-UBR2 protein could be generated and expressed to allow selective isolation and identification of more transiently interacting proteins, like E2 ligases and short-lived substrates, with affinity capture and MS (Roux, Kim and Burke, 2013; Doerr, 2018). This could be undertaken with the UBR2 protein in *Ubr2*$^{RD/RD}$, *Ubr2*$^{T1/T1}$ *and Ubr2*$^{T2/T2}$ ESCs to assess more specific Type I, Type II or non-N-end rule interactions.

6.4 Conclusion

Although the N-end Rule has long been recognised as a primary substrate recognition pathway of the UPS and protein degradation, our current understanding of E3 ubiquitin ligases is shifting towards non-canonical roles, whether within regulatory functions of ubiquitination, or outside of the ubiquitin-proteasome system altogether. The major finding of this thesis is that UBR2 does appear to act through non-canonical roles, for a variety of essential functions in testis and cohesin maintenance in splenocytes. Future work must consider the possibilities of different molecular abilities within this protein by combining both genetic and proteomic approaches.

References

Adelfalk, C. *et al.* (2009) 'Cohesin SMC1β protects telomeres in meiocytes', *Journal of Cell Biology*, 187(2), pp. 185–199. Available at: https://doi.org/10.1083/jcb.200808016.

Aichem, A. *et al.* (2010) 'USE1 is a bispecific conjugating enzyme for ubiquitin and FAT10, which FAT10ylates itself in cis', *Nature Communications*, 1(1), p. 13. Available at: https://doi.org/10.1038/ncomms1012.

Alibhoy, A.A. and Chiang, H.-L. (2011) 'Vacuole import and degradation pathway: Insights into a specialized autophagy pathway', *World Journal of Biological Chemistry*, 2(11), pp. 239–245. Available at: https://doi.org/10.4331/wjbc.v2.i11.239.

Allers, T. and Lichten, M. (2001) 'Differential Timing and Control of Noncrossover and Crossover Recombination during Meiosis', *Cell*, 106(1), pp. 47–57. Available at: https://doi.org/10.1016/S0092-8674(01)00416-0.

Alomer, R.M. *et al.* (2017) 'Esco1 and Esco2 regulate distinct cohesin functions during cell cycle progression', *Proceedings of the National Academy of Sciences*, 114(37), pp. 9906–9911. Available at: https://doi.org/10.1073/pnas.1708291114.

An, J.Y. *et al.* (2006) 'Impaired neurogenesis and cardiovascular development in mice lacking the E3 ubiquitin ligases UBR1 and UBR2 of the N-end rule pathway', *Proceedings of the National Academy of Sciences of the United States of America*, 103(16), pp. 6212–6217. Available at: https://doi.org/10.1073/pnas.0601700103.

An, J.Y. *et al.* (2010) 'UBR2 mediates transcriptional silencing during spermatogenesis via histone ubiquitination', *Proceedings of the National Academy of Sciences of the United States of America*, 107(5), pp. 1912–1917. Available at: https://doi.org/10.1073/pnas.0910267107.

An, J.Y., Kim, E., Zakrzewska, A., Yoo, Y.D., Jang, J.M., Han, D.H., Lee, M.J., Seo, J.W., Lee, Y.J., Kim, T.Y., *et al.* (2012a) 'UBR2 of the N-end rule pathway is required for chromosome stability via histone ubiquitylation in spermatocytes and somatic cells', *PLoS ONE*, 7(5). Available at: https://doi.org/10.1371/journal.pone.0037414.

An, J.Y., Kim, E., Zakrzewska, A., Yoo, Y.D., Jang, J.M., Han, D.H., Lee, M.J., Seo, J.W., Lee, Y.J., Kim, T.-Y., *et al.* (2012) 'UBR2 of the N-End Rule Pathway Is Required for Chromosome Stability via Histone Ubiquitylation in Spermatocytes and Somatic Cells', *PLoS ONE*, 7(5), p. e37414. Available at: https://doi.org/10.1371/journal.pone.0037414.

An, J.Y., Kim, E., Zakrzewska, A., Yoo, Y.D., Jang, J.M., Han, D.H., Lee, M.J., Seo, J.W., Lee, Y.J., Kim, T.Y., *et al.* (2012b) 'UBR2 of the N-end rule pathway is required for chromosome stability via histone ubiquitylation in spermatocytes and somatic cells', *PLoS ONE*, 7(5). Available at: https://doi.org/10.1371/journal.pone.0037414.

Anderson, L.K. *et al.* (1999) 'Distribution of crossing over on mouse synaptonemal complexes using immunofluorescent localization of MLH1 protein.', *Genetics*, 151(4), pp. 1569–1579.

Baarends, W. *et al.* (2003) 'Loss of HR6B ubiquitin-conjugating activity results in damaged synaptonemal complex structure and increased crossing-over frequency during the male meiotic prophase.' Available at: https://repub.eur.nl/pub/3207 (Accessed: 27 October 2022).

Baek, K. *et al.* (2020) 'NEDD8 nucleates a multivalent cullin–RING–UBE2D ubiquitin ligation assembly', *Nature*, 578(7795), pp. 461–466. Available at: https://doi.org/10.1038/s41586-020-2000-y.

Baier, A., Alsheimer, M. and Benavente, R. (2007) 'Synaptonemal complex protein SYCP3: Conserved polymerization properties among vertebrates', *Biochimica et Biophysica Acta (BBA) - Proteins and Proteomics*, 1774(5), pp. 595–602. Available at: https://doi.org/10.1016/j.bbapap.2007.03.008.

Banerji, R., Skibbens, R.V. and Iovine, M.K. (2017) 'How many roads lead to cohesinopathies?', *Developmental Dynamics*, 246(11), pp. 881–888. Available at: https://doi.org/10.1002/dvdy.24510.

Bannister, L.A. *et al.* (2004) 'Positional cloning and characterization of mouse mei8, a disrupted allele of the meiotic cohesin Rec8', *genesis*, 40(3), pp. 184–194. Available at: https://doi.org/10.1002/gene.20085.

Bansal, R. *et al.* (2020) 'SMARCAL1, the annealing helicase and the transcriptional co-regulator', *IUBMB Life*, 72(10), pp. 2080–2096. Available at: https://doi.org/10.1002/iub.2354.

Bansbach, C.E. *et al.* (2009) 'The annealing helicase SMARCAL1 maintains genome integrity at stalled replication forks', *Genes & Development*, 23(20), pp. 2405–2414. Available at: https://doi.org/10.1101/gad.1839909.

Bastié, N. *et al.* (2022) 'Smc3 acetylation, Pds5 and Scc2 control the translocase activity that establishes cohesin-dependent chromatin loops', *Nature Structural & Molecular Biology*, 29(6), pp. 575–585. Available at: https://doi.org/10.1038/s41594-022-00780-0.

Baudat, F., Imai, Y. and De Massy, B. (2013) 'Meiotic recombination in mammals: Localization and regulation', *Nature Reviews Genetics*, 14(11), pp. 794–806. Available at: https://doi.org/10.1038/nrg3573.

Baudat, F. and de Massy, B. (2007) ‘Regulating double-stranded DNA break repair towards crossover or non-crossover during mammalian meiosis’, *Chromosome Research*, 15(5), pp. 565–577. Available at: https://doi.org/10.1007/s10577-007-1140-3.

Baumann, C. *et al.* (2017) ‘Error-prone meiotic division and subfertility in mice with oocyte-conditional knockdown of pericentrin’, *Journal of Cell Science*, 130(7), pp. 1251–1262. Available at: https://doi.org/10.1242/jcs.196188.

Beckouët, F. *et al.* (2010) ‘An Smc3 Acetylation Cycle Is Essential for Establishment of Sister Chromatid Cohesion’, *Molecular Cell*, 39(5), pp. 689–699. Available at: https://doi.org/10.1016/j.molcel.2010.08.008.

Bedford, L. *et al.* (2010) ‘Assembly, structure, and function of the 26S proteasome’, *Trends in Cell Biology*, 20(7), pp. 391–401. Available at: https://doi.org/10.1016/j.tcb.2010.03.007.

Ben-Saadon, R. *et al.* (2006) ‘The Polycomb Protein Ring1B Generates Self Atypical Mixed Ubiquitin Chains Required for Its In Vitro Histone H2A Ligase Activity’, *Molecular Cell*, 24(5), pp. 701–711. Available at: https://doi.org/10.1016/j.molcel.2006.10.022.

Ben-Shahar, T.R. *et al.* (2008) ‘Eco1-Dependent Cohesin Acetylation During Establishment of Sister Chromatid Cohesion’, *Science*, 321, pp. 563–567. Available at: https://doi.org/10.1101/cshperspect.a011130.

Bergink, S. and Jentsch, S. (2009) ‘Principles of ubiquitin and SUMO modifications in DNA repair’, *Nature*, 458(7237), pp. 461–467. Available at: https://doi.org/10.1038/nature07963.

Bermudez, V.P. *et al.* (2012) ‘In vitro loading of human cohesin on DNA by the human Scc2-Scc4 loader complex’, *Proceedings of the National Academy of Sciences*, 109(24), pp. 9366–9371. Available at: https://doi.org/10.1073/pnas.1206840109.

Berndsen, C.E. and Wolberger, C. (2014) ‘New insights into ubiquitin E3 ligase mechanism’, *Nature Structural and Molecular Biology*, 21(4), pp. 301–307. Available at: https://doi.org/10.1038/nsmb.2780.

Biswas, U. *et al.* (2013) ‘Meiotic Cohesin SMC1β Provides Prophase I Centromeric Cohesion and Is Required for Multiple Synapsis-Associated Functions’, *PLoS Genetics*. Edited by R.S. Hawley, 9(12), p. e1003985. Available at: https://doi.org/10.1371/journal.pgen.1003985.

Biswas, U. *et al.* (2016) ‘Distinct Roles of Meiosis-Specific Cohesin Complexes in Mammalian Spermatogenesis’, *PLOS Genetics*, 12(10), p. e1006389. Available at: https://doi.org/10.1371/journal.pgen.1006389.

Biswas, U., Stevense, M. and Jessberger, R. (2018) 'SMC1α Substitutes for Many Meiotic Functions of SMC1β but Cannot Protect Telomeres from Damage', *Current Biology*, 28(2), pp. 249-261.e4. Available at: https://doi.org/10.1016/j.cub.2017.12.020.

Bolcun-Filas, E. *et al.* (2007) 'SYCE2 is required for synaptonemal complex assembly, double strand break repair, and homologous recombination', *Journal of Cell Biology*, 176(6), pp. 741–747. Available at: https://doi.org/10.1083/jcb.200610027.

Bolcun-Filas, E. *et al.* (2009) 'Mutation of the Mouse Syce1 Gene Disrupts Synapsis and Suggests a Link between Synaptonemal Complex Structural Components and DNA Repair', *PLOS Genetics*, 5(2), p. e1000393. Available at: https://doi.org/10.1371/journal.pgen.1000393.

Bolcun-Filas, E. and Handel, M.A. (2018) 'Meiosis: the chromosomal foundation of reproduction', *Biology of Reproduction*, 99(1), pp. 112–126. Available at: https://doi.org/10.1093/biolre/ioy021.

Bolor, H. *et al.* (2009) 'Mutations of the SYCP3 Gene in Women with Recurrent Pregnancy Loss', *The American Journal of Human Genetics*, 84(1), pp. 14–20. Available at: https://doi.org/10.1016/j.ajhg.2008.12.002.

Borde, V. and de Massy, B. (2013) 'Programmed induction of DNA double strand breaks during meiosis: setting up communication between DNA and the chromosome structure', *Current Opinion in Genetics & Development*, 23(2), pp. 147–155. Available at: https://doi.org/10.1016/j.gde.2012.12.002.

Borton, M.T. *et al.* (2016) 'Multiple Levels of Regulation of Sororin by Cdk1 and Aurora B: R EGULATION O F S ORORIN B Y C DK1 A ND A URORA B', *Journal of Cellular Biochemistry*, 117(2), pp. 351–360. Available at: https://doi.org/10.1002/jcb.25277.

Brieño-Enríquez, M.A. *et al.* (2016) 'Cohesin Removal along the Chromosome Arms during the First Meiotic Division Depends on a NEK1-PP1γ-WAPL Axis in the Mouse', *Cell Reports*, 17(4), pp. 977–986. Available at: https://doi.org/10.1016/j.celrep.2016.09.059.

Brower, C.S., Piatkov, K.I. and Varshavsky, A. (2013) 'Neurodegeneration-Associated Protein Fragments As Short-Lived Substrates of the N-End Rule Pathway', *Molecular cell*, 50(2), pp. 161–171. Available at: https://doi.org/10.1016/j.molcel.2013.02.009.

Brower, C.S. and Varshavsky, A. (2009) 'Ablation of Arginylation in the Mouse N-End Rule Pathway: Loss of Fat, Higher Metabolic Rate, Damaged Spermatogenesis, and Neurological Perturbations', *PLOS ONE*, 4(11), p. e7757. Available at: https://doi.org/10.1371/journal.pone.0007757.

Buonomo, S.B.C. *et al.* (2000) ‘Disjunction of Homologous Chromosomes in Meiosis I Depends on Proteolytic Cleavage of the Meiotic Cohesin Rec8 by Separin’, *Cell*, 103(3), pp. 387–398. Available at: https://doi.org/10.1016/S0092-8674(00)00131-8.

Burgoyne, P.S., Mahadevaiah, S.K. and Turner, J.M.A. (2009) ‘The consequences of asynapsis for mammalian meiosis’, *Nature Reviews Genetics*, 10(3), pp. 207–216. Available at: https://doi.org/10.1038/nrg2505.

Burkhardt, S. *et al.* (2016) ‘Chromosome Cohesion Established by Rec8-Cohesin in Fetal Oocytes is Maintained without Detectable Turnover in Oocytes Arrested for Months in Mice’, *Current Biology*, 26(5), pp. 678–685. Available at: https://doi.org/10.1016/j.cub.2015.12.073.

Byrd, C., Turner, G.C. and Varshavsky, A. (1998) ‘The N-end rule pathway controls the import of peptides through degradation of a transcriptional repressor’, *The EMBO Journal*, 17(1), pp. 269–277. Available at: https://doi.org/10.1093/emboj/17.1.269.

Çamdere, G.Ö., Carlborg, K.K. and Koshland, D. (2018) ‘Intermediate step of cohesin’s ATPase cycle allows cohesin to entrap DNA’, *Proceedings of the National Academy of Sciences of the United States of America*, 115(39), pp. 9732–9737. Available at: https://doi.org/10.1073/pnas.1807213115.

Campos, E.I. *et al.* (2015) ‘Analysis of the Histone H3.1 Interactome: A Suitable Chaperone for the Right Event’, *Molecular Cell*, 60(4), pp. 697–709. Available at: https://doi.org/10.1016/j.molcel.2015.08.005.

Canudas, S. *et al.* (2007) ‘Protein requirements for sister telomere association in human cells’, *The EMBO Journal*, 26(23), pp. 4867–4878. Available at: https://doi.org/10.1038/sj.emboj.7601903.

Canudas, S. and Smith, S. (2009) ‘Differential regulation of telomere and centromere cohesion by the Scc3 homologues SA1 and SA2, respectively, in human cells’, *Journal of Cell Biology*, 187(2), pp. 165–173. Available at: https://doi.org/10.1083/jcb.200903096.

Carretero, M. *et al.* (2013) ‘Pds5B is required for cohesion establishment and Aurora B accumulation at centromeres’, *The EMBO Journal*, 32(22), pp. 2938–2949. Available at: https://doi.org/10.1038/emboj.2013.230.

Chapard, C. *et al.* (2019) ‘Sister DNA Entrapment between Juxtaposed Smc Heads and Kleisin of the Cohesin Complex’, *Molecular Cell*, 75(2), pp. 224-237.e5. Available at: https://doi.org/10.1016/j.molcel.2019.05.023.

Charalambous, C., Webster, A. and Schuh, M. (2023) ‘Aneuploidy in mammalian oocytes and the impact of maternal ageing’, *Nature Reviews Molecular Cell Biology*, 24(1), pp. 27–44. Available at: https://doi.org/10.1038/s41580-022-00517-3.

Chen, F. *et al.* (2002) ‘Caspase Proteolysis of the Cohesin Component RAD21 Promotes Apoptosis *’, *Journal of Biological Chemistry*, 277(19), pp. 16775–16781. Available at: https://doi.org/10.1074/jbc.M201322200.

Chen, S.-J. *et al.* (2017) ‘An N-end rule pathway that recognizes proline and destroys gluconeogenic enzymes’, *Science*, 355(6323), p. eaal3655. Available at: https://doi.org/10.1126/science.aal3655.

Cheng, H. *et al.* (2017) ‘Multiple E3s promote the degradation of histone H3 variant Cse4’, *Scientific Reports*, 7(1), p. 8565. Available at: https://doi.org/10.1038/s41598-017-08923-w.

Cheng, L. *et al.* (2019) ‘PES1 is a critical component of telomerase assembly and regulates cellular senescence’, *Science Advances*, 5(5), p. eaav1090. Available at: https://doi.org/10.1126/sciadv.aav1090.

Chiang, T. *et al.* (2010) ‘Evidence that weakened centromere cohesion is a leading cause of age-related aneuploidy in oocytes’, *Current Biology* [Preprint]. Available at: https://doi.org/10.1016/j.cub.2010.06.069.

Choi, E.-H. *et al.* (2022) ‘Meiosis-specific cohesin complexes display essential and distinct roles in mitotic embryonic stem cell chromosomes’, *Genome Biology*, 23(1), p. 70. Available at: https://doi.org/10.1186/s13059-022-02632-y.

Ciosk, R. *et al.* (2000) ‘Cohesin’s Binding to Chromosomes Depends on a Separate Complex Consisting of Scc2 and Scc4 Proteins’, *Molecular Cell*, 5(2), pp. 243–254. Available at: https://doi.org/10.1016/S1097-2765(00)80420-7.

Clift, D., Bizzari, F. and Marston, A.L. (2009) ‘Shugoshin prevents cohesin cleavage by PP2ACdc55-dependent inhibition of separase’, *Genes & Development*, 23(6), pp. 766–780. Available at: https://doi.org/10.1101/gad.507509.

Cohen, D.E. and Lee, J.T. (2002) ‘X-chromosome inactivation and the search for chromosome-wide silencers’, *Current Opinion in Genetics & Development*, 12(2), pp. 219–224. Available at: https://doi.org/10.1016/S0959-437X(02)00289-7.

Coleman, M.A. *et al.* (2003) ‘Identification of chromatin-related protein interactions using protein microarrays’, *PROTEOMICS*, 3(11), pp. 2101–2107. Available at: https://doi.org/10.1002/pmic.200300593.

Collier, J.E. and Nasmyth, K.A. (2022) ‘DNA passes through cohesin’s hinge as well as its Smc3–kleisin interface’, *eLife*, 11, p. e80310. Available at: https://doi.org/10.7554/eLife.80310.

Cong, L. *et al.* (2013) ‘Cong, L., Ran, F. A., Cox, D., Lin, S., Barretto, R., Habib, N., … Zhang, F. (2013). Multiplex Genome Engineering Using

CRISPR/Cas Systems. Science (New York, N.Y.)', *Science (New York, N.Y.)*, 339(6121), pp. 819–823. Available at: https://doi.org/10.1126/science.1231143.Multiplex.

Cortone, G. *et al.* (2018) 'Interaction of the Warsaw breakage syndrome DNA helicase DDX11 with the replication fork-protection factor Timeless promotes sister chromatid cohesion', *PLOS Genetics*, 14(10), p. e1007622. Available at: https://doi.org/10.1371/journal.pgen.1007622.

Costa, Y. *et al.* (2005) 'Two novel proteins recruited by synaptonemal complex protein 1 (SYCP1) are at the centre of meiosis', *Journal of Cell Science*, 118(12), pp. 2755–2762. Available at: https://doi.org/10.1242/jcs.02402.

Couch, F.B. *et al.* (2013) 'ATR phosphorylates SMARCAL1 to prevent replication fork collapse', *Genes & Development*, 27(14), pp. 1610–1623. Available at: https://doi.org/10.1101/gad.214080.113.

Coyaud, E. *et al.* (2015) 'BioID-based Identification of Skp Cullin F-box (SCF)β-TrCP1/2 E3 Ligase Substrates', *Molecular & cellular proteomics: MCP*, 14(7), pp. 1781–1795. Available at: https://doi.org/10.1074/mcp.M114.045658.

Crichton, J.H. *et al.* (2017) 'Tex19.1 promotes Spo11-dependent meiotic recombination in mouse spermatocytes', *PLoS Genetics*, pp. 1–25.

Crichton, J.H. *et al.* (2023) 'Structural maturation of SYCP1-mediated meiotic chromosome synapsis by SYCE3', *Nature Structural & Molecular Biology*, 30(2), pp. 188–199. Available at: https://doi.org/10.1038/s41594-022-00909-1.

Daniel, K. *et al.* (2011) 'Meiotic homologue alignment and its quality surveillance are controlled by mouse HORMAD1', *Nature Cell Biology*, 13(5), pp. 599–610. Available at: https://doi.org/10.1038/ncb2213.

Darweesh, M. *et al.* (2022) 'ZC3H11A loss of function enhances NF-κB signaling through defective IκBα protein expression', *Frontiers in Immunology*, 13. Available at: https://www.frontiersin.org/articles/10.3389/fimmu.2022.1002823 (Accessed: 10 February 2023).

Dasgupta, T. *et al.* (2016) 'HDAC8 Inhibition Blocks SMC3 Deacetylation and Delays Cell Cycle Progression without Affecting Cohesin-dependent Transcription in MCF7 Cancer Cells', *Journal of Biological Chemistry*, 291(24), pp. 12761–12770. Available at: https://doi.org/10.1074/jbc.M115.704627.

Deardorff, M.A. *et al.* (2007) 'Mutations in Cohesin Complex Members SMC3 and SMC1A Cause a Mild Variant of Cornelia de Lange Syndrome with

Predominant Mental Retardation', *The American Journal of Human Genetics*, 80(3), pp. 485–494. Available at: https://doi.org/10.1086/511888.

Deardorff, M.A., Bando, M., *et al.* (2012) 'HDAC8 mutations in Cornelia de Lange syndrome affect the cohesin acetylation cycle', *Nature*, 489(7415), pp. 313–317. Available at: https://doi.org/10.1038/nature11316.

Deardorff, M.A., Wilde, J.J., *et al.* (2012) 'RAD21 Mutations Cause a Human Cohesinopathy', *The American Journal of Human Genetics*, 90(6), pp. 1014–1027. Available at: https://doi.org/10.1016/j.ajhg.2012.04.019.

Deshaies, R.J. and Joazeiro, C.A.P. (2009) 'RING Domain E3 Ubiquitin Ligases', *Annual Review of Biochemistry*, 78(1), pp. 399–434. Available at: https://doi.org/10.1146/annurev.biochem.78.101807.093809.

Doerr, A. (2018) 'Proximity labeling with TurboID', *Nature Methods*, 15(10), p. 764. Available at: https://doi.org/10.1038/s41592-018-0158-0.

Du, F. *et al.* (2002) 'Pairs of dipeptides synergistically activate the binding of substrate by ubiquitin ligase through dissociation of its autoinhibitory domain', *Proceedings of the National Academy of Sciences*, 99(22), pp. 14110–14115. Available at: https://doi.org/10.1073/pnas.172527399.

Dunne, O.M. and Davies, O.R. (2019) 'Molecular structure of human synaptonemal complex protein SYCE1', *Chromosoma*, 128(3), pp. 223–236. Available at: https://doi.org/10.1007/s00412-018-00688-z.

Dupont, C. *et al.* (2014) '3D-FISH analysis reveals chromatid cohesion defect during interphase in Roberts syndrome', *Molecular Cytogenetics*, 7(1), p. 59. Available at: https://doi.org/10.1186/s13039-014-0059-6.

Eisele, F. and Wolf, D.H. (2008) 'Degradation of misfolded protein in the cytoplasm is mediated by the ubiquitin ligase Ubr1', *FEBS Letters*, 582(30), pp. 4143–4146. Available at: https://doi.org/10.1016/j.febslet.2008.11.015.

Eldeeb, M.A. *et al.* (2022a) 'Regulation of Neurodegeneration-associated Protein Fragments by the N-degron Pathways', *Neurotoxicity Research*, 40(1), pp. 298–318. Available at: https://doi.org/10.1007/s12640-021-00396-0.

Eldeeb, M.A. *et al.* (2022b) 'Regulation of Neurodegeneration-associated Protein Fragments by the N-degron Pathways', *Neurotoxicity Research*, 40(1), pp. 298–318. Available at: https://doi.org/10.1007/s12640-021-00396-0.

Ellnati, E. *et al.* (2017) 'DNA damage response protein TOPBP1 regulates X chromosome silencing in the mammalian germ line', *Proceedings of the National Academy of Sciences*, 114(47), pp. 12536–12541. Available at: https://doi.org/10.1073/pnas.1712530114.

Elizondo, L.I. *et al.* (2009) 'Schimke immuno-osseous dysplasia: SMARCAL1 loss-of-function and phenotypic correlation', *Journal of Medical Genetics*, 46(1), pp. 49–59. Available at: https://doi.org/10.1136/jmg.2008.060095.

Ellis, N. and Goodfellow, P.N. (1989) 'The mammalian pseudoautosomal region', *Trends in Genetics*, 5, pp. 406–410. Available at: https://doi.org/10.1016/0168-9525(89)90199-6.

Falque, M. *et al.* (2007) 'Patterns of Recombination and MLH1 Foci Density Along Mouse Chromosomes: Modeling Effects of Interference and Obligate Chiasma', *Genetics*, 176(3), pp. 1453–1467. Available at: https://doi.org/10.1534/genetics.106.070235.

Fan, Y. *et al.* (2010) 'Lysine 63-linked Polyubiquitination of TAK1 at Lysine 158 Is Required for Tumor Necrosis Factor α- and Interleukin-1β-induced IKK/NF-κB and JNK/AP-1 Activation *', *Journal of Biological Chemistry*, 285(8), pp. 5347–5360. Available at: https://doi.org/10.1074/jbc.M109.076976.

Faustman, D.L. and Davis, M. (2010) 'Stem cells in the spleen: Therapeutic potential for Sjogren's syndrome, type I diabetes, and other disorders', *The international journal of biochemistry & cell biology*, 42(10), pp. 1576–1579. Available at: https://doi.org/10.1016/j.biocel.2010.06.012.

Fenger-Grøn, M. *et al.* (2005) 'Multiple Processing Body Factors and the ARE Binding Protein TTP Activate mRNA Decapping', *Molecular Cell*, 20(6), pp. 905–915. Available at: https://doi.org/10.1016/j.molcel.2005.10.031.

Fernandez-Capetillo, O. *et al.* (2003) 'H2AX Is Required for Chromatin Remodeling and Inactivation of Sex Chromosomes in Male Mouse Meiosis', *Developmental Cell*, 4(4), pp. 497–508. Available at: https://doi.org/10.1016/S1534-5807(03)00093-5.

Ferrara, F. *et al.* (2022) 'Ubiquitination as a key regulatory mechanism for O3-induced cutaneous redox inflammasome activation', *Redox Biology*, 56, p. 102440. Available at: https://doi.org/10.1016/j.redox.2022.102440.

Freemont, P.S. (1993) 'The RING Finger', *Annals of the New York Academy of Sciences*, 684(1), pp. 174–192. Available at: https://doi.org/10.1111/j.1749-6632.1993.tb32280.x.

Freemont, P.S., Hanson, I.M. and Trowsdale, J. (1991) 'A novel gysteine-rich sequence motif', *Cell*, 64(3), pp. 483–484. Available at: https://doi.org/10.1016/0092-8674(91)90229-R.

Fukuda, T. *et al.* (2014) 'STAG3-mediated stabilization of REC8 cohesin complexes promotes chromosome synapsis during meiosis', *EMBO Journal*, 33(11), pp. 1243–1255. Available at: https://doi.org/10.1002/embj.201387329.

Galeev, R. *et al.* (2016) ‘Genome-wide RNAi Screen Identifies Cohesin Genes as Modifiers of Renewal and Differentiation in Human HSCs’, *Cell Reports*, 14(12), pp. 2988–3000. Available at: https://doi.org/10.1016/j.celrep.2016.02.082.

Gandhi, R., Gillespie, P.J. and Hirano, T. (2006) ‘Human Wapl Is a Cohesin-Binding Protein that Promotes Sister-Chromatid Resolution in Mitotic Prophase’, *Current Biology*, 16(24), pp. 2406–2417. Available at: https://doi.org/10.1016/j.cub.2006.10.061.

Gao, S. *et al.* (2022) ‘UBR2 targets myosin heavy chain IIb and IIx for degradation: Molecular mechanism essential for cancer-induced muscle wasting’, *Proceedings of the National Academy of Sciences*, 119(43), p. e2200215119. Available at: https://doi.org/10.1073/pnas.2200215119.

Gligoris, T.G. *et al.* (2014) ‘Closing the cohesin ring: Structure and function of its Smc3-kleisin interface’, *Science*, 346(6212), pp. 963–967. Available at: https://doi.org/10.1126/science.1256917.

Gómez-H, L. *et al.* (2016) ‘C14ORF39/SIX6OS1 is a constituent of the synaptonemal complex and is essential for mouse fertility’, *Nature Communications*, 7(1), p. 13298. Available at: https://doi.org/10.1038/ncomms13298.

Gonsalves, J. *et al.* (2004) ‘Defective recombination in infertile men’, *Human Molecular Genetics*, 13(22), pp. 2875–2883. Available at: https://doi.org/10.1093/hmg/ddh302.

Gordillo, M. *et al.* (2008) ‘The molecular mechanism underlying Roberts syndrome involves loss of ESCO2 acetyltransferase activity’, *Human Molecular Genetics*, 17(14), pp. 2172–2180. Available at: https://doi.org/10.1093/hmg/ddn116.

Green, C.D. *et al.* (2018) ‘A Comprehensive Roadmap of Murine Spermatogenesis Defined by Single-Cell RNA-Seq’, *Developmental Cell*, 46(5), pp. 651-667.e10. Available at: https://doi.org/10.1016/j.devcel.2018.07.025.

Greene, A.W. *et al.* (2012) ‘Mitochondrial processing peptidase regulates PINK1 processing, import and Parkin recruitment’, *EMBO reports*, 13(4), pp. 378–385. Available at: https://doi.org/10.1038/embor.2012.14.

Grive, K.J. *et al.* (2019) ‘Dynamic transcriptome profiles within spermatogonial and spermatocyte populations during postnatal testis maturation revealed by single-cell sequencing’, *PLOS Genetics*, 15(3), p. e1007810. Available at: https://doi.org/10.1371/journal.pgen.1007810.

Gruber, S., Haering, C.H. and Nasmyth, K. (2003) ‘Chromosomal Cohesin Forms a Ring’, *Cell*, 112(6), pp. 765–777. Available at: https://doi.org/10.1016/S0092-8674(03)00162-4.

Gutiérrez-Caballero, C. *et al.* (2011) ‘Identification and molecular characterization of the mammalian α-kleisin RAD21L’, *Cell Cycle*, 10(9), pp. 1477–1487. Available at: https://doi.org/10.4161/cc.10.9.15515.

Haering, C.H. *et al.* (2002) ‘Molecular Architecture of SMC Proteins and the Yeast Cohesin Complex’, *Molecular Cell*, 9(4), pp. 773–788. Available at: https://doi.org/10.1016/S1097-2765(02)00515-4.

Haglund, K., Fiore, P.P.D. and Dikic, I. (2003) ‘Distinct monoubiquitin signals in receptor endocytosis’, *Trends in Biochemical Sciences*, 28(11), pp. 598–604. Available at: https://doi.org/10.1016/j.tibs.2003.09.005.

Hamazaki, J., Hirayama, S. and Murata, S. (2015) ‘Redundant Roles of Rpn10 and Rpn13 in Recognition of Ubiquitinated Proteins and Cellular Homeostasis’, *PLoS Genetics*, 11(7), pp. 1–20. Available at: https://doi.org/10.1371/journal.pgen.1005401.

Hamer, G. *et al.* (2008) ‘Progression of meiotic recombination requires structural maturation of the central element of the synaptonemal complex’, *Journal of Cell Science*, 121(15), pp. 2445–2451. Available at: https://doi.org/10.1242/jcs.033233.

Handel, M.A. (2004) ‘The XY body: a specialized meiotic chromatin domain’, *Experimental Cell Research*, 296(1), pp. 57–63. Available at: https://doi.org/10.1016/j.yexcr.2004.03.008.

Handel, M.A. and Eppig, J.J. (1997) ‘10 Sexual Dimorphism in the Regulation of Mammalian Meiosis’, in M.A. Handel (ed.) *Current Topics in Developmental Biology*. Academic Press (Meiosis and Gamteogenesis), pp. 333–358. Available at: https://doi.org/10.1016/S0070-2153(08)60179-9.

Hansen, A.S. *et al.* (2017) ‘CTCF and cohesin regulate chromatin loop stability with distinct dynamics’, *eLife*, 6, pp. 1–33. Available at: https://doi.org/10.7554/eLife.25776.

Hara, K. *et al.* (2014) ‘Structure of cohesin subcomplex pinpoints direct shugoshin-Wapl antagonism in centromeric cohesion’, *Nature Structural & Molecular Biology*, 21(10), pp. 864–870. Available at: https://doi.org/10.1038/nsmb.2880.

Harami, G.M., Gyimesi, M. and Kovács, M. (2013) ‘From keys to bulldozers: Expanding roles for winged helix domains in nucleic-acid-binding proteins’, *Trends in Biochemical Sciences*, 38(7), pp. 364–371. Available at: https://doi.org/10.1016/j.tibs.2013.04.006.

Hasegawa, K. *et al.* (2015) 'SCML2 Establishes the Male Germline Epigenome through Regulation of Histone H2A Ubiquitination', *Developmental Cell*, 32(5), pp. 574–588. Available at: https://doi.org/10.1016/j.devcel.2015.01.014.

Hassold T and Hunt P (2001) 'To err (meiotically) is human: the genesis of human aneuploidy.', *Nature reviews. Genetics*, 2(4), pp. 280–91.

Hauf, S., Waizenegger, I.C. and Peters, J.-M. (2001) 'Cohesin Cleavage by Separase Required for Anaphase and Cytokinesis in Human Cells', *Science*, 293(5533), pp. 1320–1323. Available at: https://doi.org/10.1126/science.1061376.

Heck, J.W., Cheung, S.K. and Hampton, R.Y. (2010) 'Cytoplasmic protein quality control degradation mediated by parallel actions of the E3 ubiquitin ligases Ubr1 and San1', *Proceedings of the National Academy of Sciences*, 107(3), pp. 1106–1111. Available at: https://doi.org/10.1073/pnas.0910591107.

Herbert, M. *et al.* (2015) 'Meiosis and maternal aging: Insights from aneuploid oocytes and trisomy births', *Cold Spring Harbor Perspectives in Biology*, 7(4). Available at: https://doi.org/10.1101/cshperspect.a017970.

Hernández-Hernández, A. *et al.* (2016) 'The central element of the synaptonemal complex in mice is organized as a bilayered junction structure', *Journal of Cell Science*, 129(11), pp. 2239–2249. Available at: https://doi.org/10.1242/jcs.182477.

Herrán, Y. *et al.* (2011) 'The cohesin subunit RAD21L functions in meiotic synapsis and exhibits sexual dimorphism in fertility', *EMBO Journal*, 30(15), pp. 3091–3105. Available at: https://doi.org/10.1038/emboj.2011.222.

Hicke, L. (2001) 'Protein regulation by monoubiquitin', *Nature Reviews Molecular Cell Biology*, 2(3), pp. 195–201. Available at: https://doi.org/10.1038/35056583.

Higgins, J.M.G. (2010) 'Haspin: a newly discovered regulator of mitotic chromosome behavior', *Chromosoma*, 119(2), pp. 137–147. Available at: https://doi.org/10.1007/s00412-009-0250-4.

Hirano, T. (2002) 'The ABCs of SMC proteins: two-armed ATPases for chromosome condensation, cohesion, and repair', *Genes & Development*, 16(4), pp. 399–414. Available at: https://doi.org/10.1101/gad.955102.

Hochstrasser, M. (2010) 'Origin and Function of Ubiquitin-like Protein Conjugation Mark', *Nature*, 458(7237), pp. 1–19. Available at: https://doi.org/10.1038/nature07958.Origin.

Hodges, C.A. *et al.* (2005) 'SMC1B-deficient female mice provide evidence that cohesins are a missing link in age-related nondisjunction', *Nature*

Genetics, 37(12), pp. 1351–1355. Available at: https://doi.org/10.1038/ng1672.

Holland, A.J. *et al.* (2007) 'Protein Phosphatase 2A and Separase Form a Complex Regulated by Separase Autocleavage *', *Journal of Biological Chemistry*, 282(34), pp. 24623–24632. Available at: https://doi.org/10.1074/jbc.M702545200.

Hons, M.T. *et al.* (2016) 'Topology and structure of an engineered human cohesin complex bound to Pds5B', *Nature Communications*, 7(1), p. 12523. Available at: https://doi.org/10.1038/ncomms12523.

Hopkins, J. *et al.* (2014) 'Meiosis-Specific Cohesin Component, Stag3 Is Essential for Maintaining Centromere Chromatid Cohesion, and Required for DNA Repair and Synapsis between Homologous Chromosomes', *PLoS Genetics*, 10(7). Available at: https://doi.org/10.1371/journal.pgen.1004413.

Hormaechea-Agulla, D. *et al.* (2018) 'New Insights into the Role of E2s in the Pathogenesis of Diseases: Lessons Learned from UBE2O', *Molecules and Cells*, 41(3), pp. 168–178. Available at: https://doi.org/10.14348/molcells.2018.0008.

Horn-Ghetko, D. *et al.* (2021) 'Ubiquitin ligation to F-box protein targets by SCF–RBR E3–E3 super-assembly', *Nature*, 590(7847), pp. 671–676. Available at: https://doi.org/10.1038/s41586-021-03197-9.

Hou, F. and Zou, H. (2005) 'Two Human Orthologues of Eco1/Ctf7 Acetyltransferases Are Both Required for Proper Sister-Chromatid Cohesion', *Molecular Biology of the Cell*, 16(8), pp. 3908–3918. Available at: https://doi.org/10.1091/mbc.e04-12-1063.

Hu, J., Sun, F. and Handel, M.A. (2018) 'Nuclear localization of EIF4G3 suggests a role for the XY body in translational regulation during spermatogenesis in mice†', *Biology of Reproduction*, 98(1), pp. 102–114. Available at: https://doi.org/10.1093/biolre/iox150.

Hunt, P.A. and Hassold, T.J. (2008) 'Human female meiosis: what makes a good egg go bad?', *Trends in Genetics*, 24(2), pp. 86–93. Available at: https://doi.org/10.1016/j.tig.2007.11.010.

Hwang, C.-S., Shemorry, A. and Varshavsky, A. (2010) 'N-Terminal Acetylation of Cellular Proteins Creates Specific Degradation Signals', *Science*, 327(5968), pp. 973–977. Available at: https://doi.org/10.1126/science.1183147.

Ichijima, Y. *et al.* (2011) 'MDC1 directs chromosome-wide silencing of the sex chromosomes in male germ cells', *Genes & Development*, 25(9), pp. 959–971. Available at: https://doi.org/10.1101/gad.2030811.

Ichijima, Y., Sin, H.-S. and Namekawa, S.H. (2012) ‘Sex chromosome inactivation in germ cells: emerging roles of DNA damage response pathways’, *Cellular and Molecular Life Sciences*, 69(15), pp. 2559–2572. Available at: https://doi.org/10.1007/s00018-012-0941-5.

Imai, Y. *et al.* (2017) ‘The PRDM9 KRAB domain is required for meiosis and involved in protein interactions’, *Chromosoma*, 126(6), pp. 681–695. Available at: https://doi.org/10.1007/s00412-017-0631-z.

Ishiguro, K. *et al.* (2014) ‘Meiosis-specific cohesin mediates homolog recognition in mouse spermatocytes’, *Genes & Development*, 28(6), pp. 594–607. Available at: https://doi.org/10.1101/gad.237313.113.

Ishiguro, K. (2019) ‘The cohesin complex in mammalian meiosis’, *Genes to Cells*, 24(1), pp. 6–30. Available at: https://doi.org/10.1111/gtc.12652.

Ishiguro, K.I. *et al.* (2011) ‘A new meiosis-specific cohesin complex implicated in the cohesin code for homologous pairing’, *EMBO Reports*, 12(3), pp. 267–275. Available at: https://doi.org/10.1038/embor.2011.2.

Jessberger, R. (2010) ‘Deterioration without replenishment—the misery of oocyte cohesin’, *Genes & Development*, 24(23), pp. 2587–2591. Available at: https://doi.org/10.1101/gad.2000610.

Jessberger, R. (2012) ‘Age-related aneuploidy through cohesion exhaustion’, *EMBO Reports*, 13(6), pp. 539–546. Available at: https://doi.org/10.1038/embor.2012.54.

Jin, S.M. *et al.* (2010) ‘Mitochondrial membrane potential regulates PINK1 import and proteolytic destabilization by PARL’, *Journal of Cell Biology*, 191(5), pp. 933–942. Available at: https://doi.org/10.1083/jcb.201008084.

Jo, U. *et al.* (2016) ‘PCNA-Dependent Cleavage and Degradation of SDE2 Regulates Response to Replication Stress’, *PLOS Genetics*, 12(12), p. e1006465. Available at: https://doi.org/10.1371/journal.pgen.1006465.

Joazeiro, C.A.P. and Weissman, A.M. (2000) ‘RING Finger Proteins: Mediators of Ubiquitin Ligase Activity’, *Cell*, 102(5), pp. 549–552. Available at: https://doi.org/10.1016/S0092-8674(00)00077-5.

Joglekar, A.P. and Kukreja, A.A. (2017) ‘How Kinetochore Architecture Shapes the Mechanisms of Its Function’, *Current Biology*, 27(16), pp. R816–R824. Available at: https://doi.org/10.1016/j.cub.2017.06.012.

Jordan, P.W., Karppinen, J. and Handel, M.A. (2012) ‘Polo-like kinase is required for synaptonemal complex disassembly and phosphorylation in mouse spermatocytes’, *Journal of Cell Science*, 125(21), pp. 5061–5072. Available at: https://doi.org/10.1242/jcs.105015.

Kaiser, F.J. *et al.* (2014) 'Loss-of-function HDAC8 mutations cause a phenotypic spectrum of Cornelia de Lange syndrome-like features, ocular hypertelorism, large fontanelle and X-linked inheritance', *Human Molecular Genetics*, 23(11), pp. 2888–2900. Available at: https://doi.org/10.1093/hmg/ddu002.

Kawai, K. *et al.* (2014) 'Functional Implications and Ubiquitin-Dependent Degradation of the Peptide Transporter Ptr2 in Saccharomyces cerevisiae', *Eukaryotic Cell*, 13(11), pp. 1380–1392. Available at: https://doi.org/10.1128/EC.00094-14.

Kawasumi, R. *et al.* (2017) 'ESCO1/2's roles in chromosome structure and interphase chromatin organization', *Genes & Development*, 31(21), pp. 2136–2150. Available at: https://doi.org/10.1101/gad.306084.117.

Kim, J.G. *et al.* (2021) 'Signaling Pathways Regulated by UBR Box-Containing E3 Ligases', *International Journal of Molecular Sciences*, 22(15), p. 8323. Available at: https://doi.org/10.3390/ijms22158323.

Kim, J.-M. *et al.* (2018) 'Formyl-methionine as an N-degron of a eukaryotic N-end rule pathway', *Science*, 362(6418), p. eaat0174. Available at: https://doi.org/10.1126/science.aat0174.

Kim, J.-M. and Hwang, C.-S. (2014) 'Crosstalk between the Arg/N-end and Ac/N-end rule', *Cell Cycle*, 13(9), pp. 1366–1367. Available at: https://doi.org/10.4161/cc.28751.

Kitajima, T.S. *et al.* (2003) 'Rec8 cleavage by separase is required for meiotic nuclear divisions in fission yeast', *The EMBO Journal*, 22(20), pp. 5643–5653. Available at: https://doi.org/10.1093/emboj/cdg527.

Kitajima, T.S. *et al.* (2006) 'Shugoshin collaborates with protein phosphatase 2A to protect cohesin', *Nature*, 441(7089), pp. 46–52. Available at: https://doi.org/10.1038/nature04663.

Klaasen, S.J. and Kops, G.J.P.L. (2022) 'Chromosome Inequality: Causes and Consequences of Non-Random Segregation Errors in Mitosis and Meiosis', *Cells*, 11(22), p. 3564. Available at: https://doi.org/10.3390/cells11223564.

Kline, A.D. *et al.* (2018) 'Diagnosis and management of Cornelia de Lange syndrome: first international consensus statement', *Nature Reviews Genetics*, 19(10), pp. 649–666. Available at: https://doi.org/10.1038/s41576-018-0031-0.

Kobayashi, W. *et al.* (2017) 'SYCP3 regulates strand invasion activities of RAD51 and DMC1', *Genes to Cells*, 22(9), pp. 799–809. Available at: https://doi.org/10.1111/gtc.12513.

Kong, X. *et al.* (2014) 'Distinct Functions of Human Cohesin-SA1 and Cohesin-SA2 in Double-Strand Break Repair', *Molecular and Cellular Biology*, 34(4), pp. 685–698. Available at: https://doi.org/10.1128/MCB.01503-13.

Kouznetsova, A., Benavente, R. and Pastink, A. (2011) 'Meiosis in Mice without a Synaptonemal Complex', *PLoS ONE*, 6(12), p. 13.

Kragelund, B.B. *et al.* (2016) 'DSS1/Sem1, a Multifunctional and Intrinsically Disordered Protein', *Trends in Biochemical Sciences*, 41(5), pp. 446–459. Available at: https://doi.org/10.1016/j.tibs.2016.02.004.

Krantz, I.D. *et al.* (2004) 'Cornelia de Lange syndrome is caused by mutations in NIPBL, the human homolog of Drosophila melanogaster Nipped-B', *Nature Genetics*, 36(6), pp. 631–635. Available at: https://doi.org/10.1038/ng1364.

Kriegenburg, F. *et al.* (2014) 'A Chaperone-Assisted Degradation Pathway Targets Kinetochore Proteins to Ensure Genome Stability', *PLOS Genetics*, 10(1), p. e1004140. Available at: https://doi.org/10.1371/journal.pgen.1004140.

Kudo, N.R. *et al.* (2006) 'Resolution of Chiasmata in Oocytes Requires Separase-Mediated Proteolysis', *Cell*, 126(1), pp. 135–146. Available at: https://doi.org/10.1016/j.cell.2006.05.033.

Kudo, N.R. *et al.* (2009) 'Role of cleavage by separase of the Rec8 kleisin subunit of cohesin during mammalian meiosis I', *Journal of Cell Science*, 122(15), pp. 2686–2698. Available at: https://doi.org/10.1242/jcs.035287.

Kueng, S. *et al.* (2006) 'Wapl Controls the Dynamic Association of Cohesin with Chromatin', *Cell*, 127(5), pp. 955–967. Available at: https://doi.org/10.1016/j.cell.2006.09.040.

Kulak, N.A. *et al.* (2014) 'Minimal, encapsulated proteomic-sample processing applied to copy-number estimation in eukaryotic cells', *Nature Methods*, 11(3), pp. 319–324. Available at: https://doi.org/10.1038/nmeth.2834.

Kwon, Y.T. *et al.* (2001) 'Construction and analysis of mouse strains lacking the ubiquitin ligase UBR1 (E3alpha) of the N-end rule pathway', *Molecular and cellular biology*, 21(23), pp. 8007–8021. Available at: https://doi.org/10.1128/mcb.21.23.8007-8021.2001.

Kwon, Y.T. *et al.* (2002) 'An Essential Role of N-Terminal Arginylation in Cardiovascular Development', *Science*, 297(5578), pp. 96–99. Available at: https://doi.org/10.1126/science.1069531.

Kwon, Y.T. *et al.* (2003a) 'Female lethality and apoptosis of spermatocytes in mice lacking the UBR2 ubiquitin ligase of the N-end rule pathway.', *Molecular*

and cellular biology, 23(22), pp. 8255–71. Available at: https://doi.org/10.1128/MCB.23.22.8255.

Kwon, Y.T. *et al.* (2003b) 'Female lethality and apoptosis of spermatocytes in mice lacking the UBR2 ubiquitin ligase of the N-end rule pathway.', *Molecular and cellular biology*, 23(22), pp. 8255–71. Available at: https://doi.org/10.1128/MCB.23.22.8255.

Kwon, Y.T., Kashina, A.S. and Varshavsky, A. (1999) 'Alternative splicing results in differential expression, activity, and localization of the two forms of arginyl-tRNA-protein transferase, a component of the N-end rule pathway', *Molecular and Cellular Biology*, 19(1), pp. 182–193. Available at: https://doi.org/10.1128/MCB.19.1.182.

Ladurner, R. *et al.* (2016) 'Sororin actively maintains sister chromatid cohesion', *The EMBO journal*, 35(6), pp. 635–653. Available at: https://doi.org/10.15252/embj.201592532.

Lafont, A.L., Song, J. and Rankin, S. (2010) 'Sororin cooperates with the acetyltransferase Eco2 to ensure DNA replication-dependent sister chromatid cohesion', *Proceedings of the National Academy of Sciences*, 107(47), pp. 20364–20369. Available at: https://doi.org/10.1073/pnas.1011069107.

Lammers, J.H. *et al.* (1994) 'The gene encoding a major component of the lateral elements of synaptonemal complexes of the rat is related to X-linked lymphocyte-regulated genes.', *Molecular and Cellular Biology*, 14(2), pp. 1137–1146.

Lao, J.P. and Hunter, N. (2010) 'Trying to Avoid Your Sister', *PLOS Biology*, 8(10), p. e1000519. Available at: https://doi.org/10.1371/journal.pbio.1000519.

LaPlante, G. and Zhang, W. (2021) 'Targeting the Ubiquitin-Proteasome System for Cancer Therapeutics by Small-Molecule Inhibitors', *Cancers*, 13(12), p. 3079. Available at: https://doi.org/10.3390/cancers13123079.

Lara-Gonzalez, P., Westhorpe, F.G. and Taylor, S.S. (2012) 'Review- The Spindle Assembly Checkpoint (Higher Eukaryotes)', *Current Biology*, 22(22), pp. R966–R980. Available at: https://doi.org/10.1016/j.cub.2012.10.006.

Lee, J. *et al.* (2008) 'Unified mode of centromeric protection by shugoshin in mammalian oocytes and somatic cells', *Nature Cell Biology*, 10(1), pp. 42–52. Available at: https://doi.org/10.1038/ncb1667.

Lee, J. and Hirano, T. (2011) 'RAD21L, a novel cohesin subunit implicated in linking homologous chromosomes in mammalian meiosis', *Journal of Cell Biology*, 192(2), pp. 263–276. Available at: https://doi.org/10.1083/jcb.201008005.

Lee, P.C.W. *et al.* (2011a) 'Alternative Ubiquitin Activation/Conjugation Cascades Interact with N-End Rule Ubiquitin Ligases to Control Degradation of RGS Proteins', *Molecular Cell*, 43(3), pp. 392–405. Available at: https://doi.org/10.1016/j.molcel.2011.05.034.

Lee, P.C.W. *et al.* (2011b) 'Alternative Ubiquitin Activation/Conjugation Cascades Interact with N-End Rule Ubiquitin Ligases to Control Degradation of RGS Proteins', *Molecular Cell*, 43(3), pp. 392–405. Available at: https://doi.org/10.1016/j.molcel.2011.05.034.

Li, W. *et al.* (2008) 'Genome-Wide and Functional Annotation of Human E3 Ubiquitin Ligases Identifies MULAN, a Mitochondrial E3 that Regulates the Organelle's Dynamics and Signaling', *PLOS ONE*, 3(1), p. e1487. Available at: https://doi.org/10.1371/journal.pone.0001487.

Li, W. and Ye, Y. (2008) 'Polyubiquitin chains: Functions, structures, and mechanisms', *Cellular and Molecular Life Sciences*, 65(15), pp. 2397–2406. Available at: https://doi.org/10.1007/s00018-008-8090-6.

Li, X.C., Bolcun-Filas, E. and Schimenti, J.C. (2011) 'Genetic Evidence That Synaptonemal Complex Axial Elements Govern Recombination Pathway Choice in Mice', *Genetics*, 189(1), pp. 71–82. Available at: https://doi.org/10.1534/genetics.111.130674.

Lianga, N. *et al.* (2018) 'Cdk1 phosphorylation of Esp1/Separase functions with PP2A and Slk19 to regulate pericentric Cohesin and anaphase onset', *PLOS Genetics*, 14(3), p. e1007029. Available at: https://doi.org/10.1371/journal.pgen.1007029.

Lister, L.M. *et al.* (2010) 'Age-related meiotic segregation errors in mammalian oocytes are preceded by depletion of cohesin and Sgo2', *Current Biology*, 20(17), pp. 1511–1521. Available at: https://doi.org/10.1016/j.cub.2010.08.023.

Liu, J. and Nussinov, R. (2010) 'Molecular Dynamics Reveal the Essential Role of Linker Motions in the Function of Cullin–RING E3 Ligases', *Journal of Molecular Biology*, 396(5), pp. 1508–1523. Available at: https://doi.org/10.1016/j.jmb.2010.01.022.

Liu, L. and Keefe, D.L. (2008) 'Defective cohesin is associated with age-dependent misaligned chromosomes in oocytes', *Reproductive BioMedicine Online*, 16(1), pp. 103–112. Available at: https://doi.org/10.1016/S1472-6483(10)60562-7.

Liu, Y.-J. *et al.* (2016a) 'Degradation of the Separase-cleaved Rec8, a Meiotic Cohesin Subunit, by the N-end Rule Pathway*', *Journal of Biological Chemistry*, 291(14), pp. 7426–7438. Available at: https://doi.org/10.1074/jbc.M116.714964.

Liu, Y.-J. *et al.* (2016b) ‘Degradation of the Separase-cleaved Rec8, a Meiotic Cohesin Subunit, by the N-end Rule Pathway *’, *Journal of Biological Chemistry*, 291(14), pp. 7426–7438. Available at: https://doi.org/10.1074/jbc.M116.714964.

Llano, E. *et al.* (2008) ‘Shugoshin-2 is essential for the completion of meiosis but not for mitotic cell division in mice’, *Genes & Development*, 22(17), pp. 2400–2413. Available at: https://doi.org/10.1101/gad.475308.

Llano, E. *et al.* (2012) ‘Meiotic cohesin complexes are essential for the formation of the axial element in mice’, *Journal of Cell Biology*, 197(7), pp. 877–885. Available at: https://doi.org/10.1083/jcb.201201100.

Losada, A. (2014) ‘Cohesin in cancer: chromosome segregation and beyond’, *Nature Reviews Cancer*, 14(6), pp. 389–393. Available at: https://doi.org/10.1038/nrc3743.

Losada, A., Yokochi, T. and Hirano, T. (2005) ‘Functional contribution of Pds5 to cohesin-mediated cohesion in human cells and Xenopus egg extracts’, *Journal of Cell Science*, 118(10), pp. 2133–2141. Available at: https://doi.org/10.1242/jcs.02355.

Luo, M. *et al.* (2015) ‘Polycomb Protein SCML2 Associates with USP7 and Counteracts Histone H2A Ubiquitination in the XY Chromatin during Male Meiosis’, *PLOS Genetics*, 11(1), p. e1004954. Available at: https://doi.org/10.1371/journal.pgen.1004954.

Luo, S. and Tong, L. (2018) ‘Structural biology of the separase–securin complex with crucial roles in chromosome segregation’, *Current Opinion in Structural Biology*, 49, pp. 114–122. Available at: https://doi.org/10.1016/j.sbi.2018.01.012.

MacLennan, M. *et al.* (2015) ‘Oocyte development, meiosis and aneuploidy’, *Seminars in Cell and Developmental Biology*, 45, pp. 68–76. Available at: https://doi.org/10.1016/j.semcdb.2015.10.005.

Maclennan, M. *et al.* (2017) ‘Mobilization of LINE-1 retrotransposons is restricted by Tex19 . 1 in mouse embryonic stem cells’, *eLIFE*, 1, pp. 1–32. Available at: https://doi.org/10.7554/eLife.26152.

Maezawa, S. *et al.* (2020) ‘Super-enhancer switching drives a burst in gene expression at the mitosis-to-meiosis transition’, *Nature Structural & Molecular Biology*, 27(10), pp. 978–988. Available at: https://doi.org/10.1038/s41594-020-0488-3.

Masson, N. *et al.* (2019) ‘Conserved N-terminal cysteine dioxygenases transduce responses to hypoxia in animals and plants’, *Science*, 365(6448), pp. 65–69. Available at: https://doi.org/10.1126/science.aaw0112.

Matta-Camacho, E. *et al.* (2010) 'Structural basis of substrate recognition and specificity in the N-end rule pathway', *Nature Structural and Molecular Biology*, 17(10), pp. 1182–1187. Available at: https://doi.org/10.1038/nsmb.1894.

Matzuk, M.M. and Lamb, D.J. (2002) 'Genetic dissection of mammalian fertility pathways', *Nature Medicine*, 8(10), pp. S40–S40. Available at: https://doi.org/10.1038/nm-fertilityS41.

McKay, M.J. *et al.* (1996) 'Sequence Conservation of therad21 Schizosaccharomyces pombeDNA Double-Strand Break Repair Gene in Human and Mouse', *Genomics*, 36(2), pp. 305–315. Available at: https://doi.org/10.1006/geno.1996.0466.

Melnykov, A., Chen, S.-J. and Varshavsky, A. (2019) 'Gid10 as an alternative N-recognin of the Pro/N-degron pathway', *Proceedings of the National Academy of Sciences*, 116(32), pp. 15914–15923. Available at: https://doi.org/10.1073/pnas.1908304116.

Menssen, R. *et al.* (2012) 'Exploring the Topology of the Gid Complex, the E3 Ubiquitin Ligase Involved in Catabolite-induced Degradation of Gluconeogenic Enzymes *', *Journal of Biological Chemistry*, 287(30), pp. 25602–25614. Available at: https://doi.org/10.1074/jbc.M112.363762.

Metzger, M.B. *et al.* (2014a) 'RING-type E3 ligases: Master manipulators of E2 ubiquitin-conjugating enzymes and ubiquitination', *Biochimica et Biophysica Acta - Molecular Cell Research*, 1843(1), pp. 47–60. Available at: https://doi.org/10.1016/j.bbamcr.2013.05.026.

Metzger, M.B. *et al.* (2014b) 'RING-type E3 ligases: Master manipulators of E2 ubiquitin-conjugating enzymes and ubiquitination', *Biochimica et Biophysica Acta - Molecular Cell Research*, 1843(1), pp. 47–60. Available at: https://doi.org/10.1016/j.bbamcr.2013.05.026.

Meuwissen, R. l. *et al.* (1992) 'A coiled-coil related protein specific for synapsed regions of meiotic prophase chromosomes.', *The EMBO Journal*, 11(13), pp. 5091–5100. Available at: https://doi.org/10.1002/j.1460-2075.1992.tb05616.x.

Mfarej, M.G. and Skibbens, R.V. (2020) 'An ever-changing landscape in Roberts syndrome biology: Implications for macromolecular damage', *PLOS Genetics*, 16(12), p. e1009219. Available at: https://doi.org/10.1371/journal.pgen.1009219.

Minamino, M. *et al.* (2015) 'Esco1 Acetylates Cohesin via a Mechanism Different from That of Esco2', *Current Biology*, 25(13), pp. 1694–1706. Available at: https://doi.org/10.1016/j.cub.2015.05.017.

Mogessie, B., Scheffler, K. and Schuh, M. (2018) ‘Assembly and Positioning of the Oocyte Meiotic Spindle’, *Annual Review of Cell and Developmental Biology*, 34(1), pp. 381–403. Available at: https://doi.org/10.1146/annurev-cellbio-100616-060553.

Monahan, K. *et al.* (2012) ‘Role of CCCTC binding factor (CTCF) and cohesin in the generation of single-cell diversity of Protocadherin-α gene expression’, *Proceedings of the National Academy of Sciences of the United States of America*, 109(23), pp. 9125–9130. Available at: https://doi.org/10.1073/pnas.1205074109.

Mondal, G. *et al.* (2019) ‘A requirement for STAG2 in replication fork progression creates a targetable synthetic lethality in cohesin-mutant cancers’, *Nature Communications*, 10. Available at: https://www.nature.com/articles/s41467-019-09659-z (Accessed: 10 October 2022).

Morelli, M.A. and Cohen, P.E. (2005) ‘Not all germ cells are created equal: Aspects of sexual dimorphism in mammalian meiosis’, *Reproduction*, 130(6), pp. 761–781. Available at: https://doi.org/10.1530/rep.1.00865.

Moriya, H. (2015) ‘Quantitative nature of overexpression experiments’, *Molecular Biology of the Cell*, 26(22), pp. 3932–3939. Available at: https://doi.org/10.1091/mbc.E15-07-0512.

Mukhopadhyay, H. and Lee, N.Y. (2020) ‘Multifaceted roles of TAK1 signaling in cancer’, *Oncogene*, 39(7), pp. 1402–1413. Available at: https://doi.org/10.1038/s41388-019-1088-8.

Mulugeta Achame, E. *et al.* (2010) ‘The ubiquitin-conjugating enzyme HR6B is required for maintenance of X chromosome silencing in mouse spermatocytes and spermatids’, *BMC Genomics*, 11, p. 367. Available at: https://doi.org/10.1186/1471-2164-11-367.

Muñoz-Escobar, J., Kozlov, G. and Gehring, K. (2017) ‘Crystal structure of the UBR-box from UBR6/FBXO11 reveals domain swapping mediated by zinc binding’, *Protein Science*, 26(10), pp. 2092–2097. Available at: https://doi.org/10.1002/pro.3227.

Nagaoka, S.I., Hassold, T.J. and Hunt, P.A. (2012) ‘Human aneuploidy: Mechanisms and new insights into an age-old problem’, *Nature Reviews Genetics*, 13(7), pp. 493–504. Available at: https://doi.org/10.1038/nrg3245.

Nasmyth, K. (2001) ‘Disseminating the Genome: Joining, Resolving, and Separating Sister Chromatids During Mitosis and Meiosis’, *Annual Review of Genetics*, 35(1), pp. 673–745. Available at: https://doi.org/10.1146/annurev.genet.35.102401.091334.

Nasmyth, K. and Haering, C.H. (2009) ‘Cohesin: Its Roles and Mechanisms’, *Annual Review of Genetics*, 43(1), pp. 525–558. Available at: https://doi.org/10.1146/annurev-genet-102108-134233.

Nasmyth, K., Peters, J.-M. and Uhlmann, F. (2000) ‘Splitting the Chromosome: Cutting the Ties That Bind Sister Chromatids’, *Science*, 288(5470), pp. 1379–1384. Available at: https://doi.org/10.1126/science.288.5470.1379.

Neale, M.J. and Keeney, S. (2006) ‘Clarifying the mechanics of DNA strand exchange in meiotic recombination’, *Nature*, 442(7099), pp. 153–158. Available at: https://doi.org/10.1038/nature04885.

Neale, M.J., Pan, J. and Keeney, S. (2005) ‘Endonucleolytic processing of covalent protein-linked double-strand breaks’, *Nature*, 436(7053), pp. 1053–1057. Available at: https://doi.org/10.1038/nature03872.

Nerusheva, O.O. *et al.* (2014) ‘Tension-dependent removal of pericentromeric shugoshin is an indicator of sister chromosome biorientation’, *Genes & Development*, 28(12), pp. 1291–1309. Available at: https://doi.org/10.1101/gad.240291.114.

Nezi, L. and Musacchio, A. (2009) ‘Sister chromatid tension and the spindle assembly checkpoint’, *Current Opinion in Cell Biology*, 21(6), pp. 785–795. Available at: https://doi.org/10.1016/j.ceb.2009.09.007.

Nguyen, K.T. *et al.* (2018) ‘Control of protein degradation by N-terminal acetylation and the N-end rule pathway’, *Experimental & Molecular Medicine*, 50(7), pp. 1–8. Available at: https://doi.org/10.1038/s12276-018-0097-y.

Nguyen, K.T. *et al.* (2019) ‘N-terminal acetylation and the N-end rule pathway control degradation of the lipid droplet protein PLIN2’, *Journal of Biological Chemistry*, 294(1), pp. 379–388. Available at: https://doi.org/10.1074/jbc.RA118.005556.

Nillegoda, N.B. *et al.* (2010) ‘Ubr1 and Ubr2 Function in a Quality Control Pathway for Degradation of Unfolded Cytosolic Proteins’, *Molecular Biology of the Cell*, 21(13), pp. 2102–2116. Available at: https://doi.org/10.1091/mbc.e10-02-0098.

Nishiyama, T. *et al.* (2010) ‘Sororin Mediates Sister Chromatid Cohesion by Antagonizing Wapl’, *Cell*, 143(5), pp. 737–749. Available at: https://doi.org/10.1016/j.cell.2010.10.031.

Nishiyama, T. *et al.* (2013) ‘Aurora B and Cdk1 mediate Wapl activation and release of acetylated cohesin from chromosomes by phosphorylating Sororin’, *Proceedings of the National Academy of Sciences*, 110(33), pp. 13404–13409. Available at: https://doi.org/10.1073/pnas.1305020110.

Nitzsche, A. *et al.* (2011) ‘RAD21 Cooperates with Pluripotency Transcription Factors in the Maintenance of Embryonic Stem Cell Identity’, *PLOS ONE*, 6(5), p. e19470. Available at: https://doi.org/10.1371/journal.pone.0019470.

Nuebler, J. *et al.* (2018) ‘Chromatin organization by an interplay of loop extrusion and compartmental segregation’, *Proceedings of the National Academy of Sciences*, 115(29). Available at: https://doi.org/10.1073/pnas.1717730115.

Ohtake, F. *et al.* (2018) ‘K63 ubiquitylation triggers proteasomal degradation by seeding branched ubiquitin chains’, *Proceedings of the National Academy of Sciences of the United States of America*, 115(7), pp. E1401–E1408. Available at: https://doi.org/10.1073/pnas.1716673115.

Öllinger, R. *et al.* (2008a) ‘Deletion of the pluripotency-associated Tex19.1 gene causes activation of endogenous retroviruses and defective spermatogenesis in mice’, *PLoS Genetics*, 4(9). Available at: https://doi.org/10.1371/journal.pgen.1000199.

Öllinger, R. *et al.* (2008b) ‘Deletion of the pluripotency-associated Tex19.1 gene causes activation of endogenous retroviruses and defective spermatogenesis in mice’, *PLoS Genetics*, 4(9). Available at: https://doi.org/10.1371/journal.pgen.1000199.

Olsen, S.K. and Lima, C.D. (2013) ‘Structure of a Ubiquitin E1-E2 Complex: Insights to E1-E2 Thioester Transfer’, *Molecular Cell*, 49(5), pp. 884–896. Available at: https://doi.org/10.1016/j.molcel.2013.01.013.

Ouyang, Y. *et al.* (2006a) ‘Loss of Ubr2, an E3 ubiquitin ligase, leads to chromosome fragility and impaired homologous recombinational repair’, *Mutation Research - Fundamental and Molecular Mechanisms of Mutagenesis*, 596(1-2 SPEC. ISS.), pp. 64–75. Available at: https://doi.org/10.1016/j.mrfmmm.2005.12.016.

Ouyang, Y. *et al.* (2006b) ‘Loss of Ubr2, an E3 ubiquitin ligase, leads to chromosome fragility and impaired homologous recombinational repair’, *Mutation Research - Fundamental and Molecular Mechanisms of Mutagenesis*, 596(1-2 SPEC. ISS.), pp. 64–75. Available at: https://doi.org/10.1016/j.mrfmmm.2005.12.016.

Page, S.L. and Hawley, R.S. (2004) ‘The Genetics and Molecular Biology of the Synaptonemal Complex’, *Annual Review of Cell and Developmental Biology*, 20(1), pp. 525–558. Available at: https://doi.org/10.1146/annurev.cellbio.19.111301.155141.

Pan, M. *et al.* (2021) ‘Structural insights into Ubr1-mediated N-degron polyubiquitination’, *Nature*, 600(7888), pp. 334–338. Available at: https://doi.org/10.1038/s41586-021-04097-8.

Panigrahi, A.K. and Pati, D. (2009) ‘Road to the crossroads of life and death: Linking sister chromatid cohesion and separation to aneuploidy, apoptosis and cancer’, *Critical Reviews in Oncology/Hematology*, 72(3), pp. 181–193. Available at: https://doi.org/10.1016/j.critrevonc.2008.12.002.

Paraskevopoulos, K. *et al.* (2014) ‘Dss1 is a 26S proteasome ubiquitin receptor’, *Molecular Cell*, 56(3), pp. 453–461. Available at: https://doi.org/10.1016/j.molcel.2014.09.008.

Parisi, S. *et al.* (1999) ‘Rec8p, a Meiotic Recombination and Sister Chromatid Cohesion Phosphoprotein of the Rad21p Family Conserved from Fission Yeast to Humans’, *Molecular and Cellular Biology*, 19(5), pp. 3515–3528. Available at: https://doi.org/10.1128/MCB.19.5.3515.

Park, S.-E. *et al.* (2015) ‘Control of mammalian G protein signaling by N-terminal acetylation and the N-end rule pathway’, *Science*, 347(6227), pp. 1249–1252. Available at: https://doi.org/10.1126/science.aaa3844.

Parra, M.T. *et al.* (2004) ‘Involvement of the cohesin Rad21 and SCP3 in monopolar attachment of sister kinetochores during mouse meiosis I’, *Journal of Cell Science*, 117(7), pp. 1221–1234. Available at: https://doi.org/10.1242/jcs.00947.

Parvanov, E.D., Petkov, P.M. and Paigen, K. (2010) ‘Prdm9 Controls Activation of Mammalian Recombination Hotspots’, *Science (New York, N.Y.)*, 327(5967), p. 835. Available at: https://doi.org/10.1126/science.1181495.

Patel, A., Sibbet, G.J. and Huang, D.T. (2019) ‘Structural insights into non-covalent ubiquitin activation of the cIAP1-UbcH5B~ubiquitin complex’, *Journal of Biological Chemistry*, 294(4), pp. 1240–1249. Available at: https://doi.org/10.1074/jbc.RA118.006045.

Pati, D., Zhang, N. and Plon, S.E. (2002) ‘Linking Sister Chromatid Cohesion and Apoptosis: Role of Rad21’, *Molecular and Cellular Biology*, 22(23), pp. 8267–8277. Available at: https://doi.org/10.1128/MCB.22.23.8267-8277.2002.

Perera, D. *et al.* (2004) ‘TopBP1 and ATR Colocalization at Meiotic Chromosomes: Role of TopBP1/Cut5 in the Meiotic Recombination Checkpoint’, *Molecular Biology of the Cell*, 15(4), pp. 1568–1579. Available at: https://doi.org/10.1091/mbc.e03-06-0444.

Peters, J.M. and Nishiyama, T. (2012) ‘Sister chromatid cohesion’, *Cold Spring Harbor Perspectives in Biology*, 4(11). Available at: https://doi.org/10.1101/cshperspect.a011130.

Pickart, C.M. and Eddins, M.J. (2004) ‘Ubiquitin: Structures, functions, mechanisms’, *Biochimica et Biophysica Acta - Molecular Cell Research*,

1695(1–3), pp. 55–72. Available at: https://doi.org/10.1016/j.bbamcr.2004.09.019.

Pisani, F.M. *et al.* (2018) 'Molecular and Cellular Functions of the Warsaw Breakage Syndrome DNA Helicase DDX11', *Genes*, 9(11), p. E564. Available at: https://doi.org/10.3390/genes9110564.

Polevoda, B., Arnesen, T. and Sherman, F. (2009) 'A synopsis of eukaryotic Nα-terminal acetyltransferases: nomenclature, subunits and substrates', *BMC Proceedings*, 3(Suppl 6), p. S2. Available at: https://doi.org/10.1186/1753-6561-3-S6-S2.

Powers, N.R. *et al.* (2016) 'The Meiotic Recombination Activator PRDM9 Trimethylates Both H3K36 and H3K4 at Recombination Hotspots In Vivo', *PLOS Genetics*, 12(6), p. e1006146. Available at: https://doi.org/10.1371/journal.pgen.1006146.

Prieto, I. *et al.* (2001) 'Mammalian STAG3 is a cohesin specific to sister chromatid arms in meiosis I', *Nature Cell Biology*, 3(8), pp. 761–766. Available at: https://doi.org/10.1038/35087082.

Prieto, I. *et al.* (2002) 'STAG2 and Rad21 mammalian mitotic cohesins are implicated in meiosis', *EMBO reports*, 3(6), pp. 543–550. Available at: https://doi.org/10.1093/embo-reports/kvf108.

Primorac, I. and Musacchio, A. (2013) 'Panta rhei: The APC/C at steady state', *Journal of Cell Biology*, 201(2), pp. 177–189. Available at: https://doi.org/10.1083/jcb.201301130.

Qian, H. *et al.* (2020) 'Structure and function of HECT E3 ubiquitin ligases and their role in oxidative stress', *Journal of Translational Internal Medicine*, 8(2), pp. 71–79. Available at: https://doi.org/10.2478/jtim-2020-0012.

Rageul, J. *et al.* (2019) 'Conditional degradation of SDE2 by the Arg/N-End rule pathway regulates stress response at replication forks', *Nucleic acids research*, 47(8), pp. 3996–4010. Available at: https://doi.org/10.1093/nar/gkz054.

Ramasamy, R. *et al.* (2015) 'Fluorescence in situ hybridization detects increased sperm aneuploidy in men with recurrent pregnancy loss', *Fertility and Sterility*, 103(4), pp. 906-909.e1. Available at: https://doi.org/10.1016/j.fertnstert.2015.01.029.

Ran, F.A. *et al.* (2013) 'Genome engineering using the CRISPR-Cas9 system', *Nature Protocols*, 8(11), pp. 2281–2308. Available at: https://doi.org/10.1038/nprot.2013.143.

Rao, H. *et al.* (2001) 'Degradation of a cohesin subunit by the N-end rule pathway is essential for chromosome stability', *Nature*, 410(6831), pp. 955–959. Available at: https://doi.org/10.1038/35073627.

Reichmann, J. *et al.* (2013) ‘The genome-defence gene Tex19.1 suppresses LINE-1 retrotransposons in the placenta and prevents intra-uterine growth retardation in mice’, *Human Molecular Genetics*, 22(9), pp. 1791–1806. Available at: https://doi.org/10.1093/hmg/ddt029.

Reichmann, J. *et al.* (2020) ‘Tex19.1 inhibits the N-end rule pathway and maintains acetylated SMC3 cohesin and sister chromatid cohesion in oocytes’, *Journal of Cell Biology*, 219(5). Available at: https://doi.org/10.1083/jcb.201702123.

Revenkova, E. *et al.* (2001) ‘Novel Meiosis-Specific Isoform of Mammalian SMC1’, *Molecular and Cellular Biology*, 21(20), pp. 6984–6998. Available at: https://doi.org/10.1128/MCB.21.20.6984-6998.2001.

Revenkova, E. *et al.* (2004) ‘Cohesin SMC1 β is required for meiotic chromosome dynamics , sister chromatid cohesion and DNA recombination’, 6(6), pp. 555–562. Available at: https://doi.org/10.1038/ncb1135.

Rinaldi, V.D. *et al.* (2017) ‘The DNA Damage Checkpoint Eliminates Mouse Oocytes with Chromosome Synapsis Failure’, *Molecular Cell*, 67(6), pp. 1026-1036.e2. Available at: https://doi.org/10.1016/j.molcel.2017.07.027.

Robert, T. *et al.* (2016) ‘The TopoVIB-Like protein family is required for meiotic DNA double-strand break formation’, *Science*, 351(6276), pp. 943–949. Available at: https://doi.org/10.1126/science.aad5309.

Rogacheva, M.V. *et al.* (2014) ‘Mlh1-Mlh3, a Meiotic Crossover and DNA Mismatch Repair Factor, Is a Msh2-Msh3-stimulated Endonuclease*’, *Journal of Biological Chemistry*, 289(9), pp. 5664–5673. Available at: https://doi.org/10.1074/jbc.M113.534644.

RONG, M. *et al.* (2016) ‘Meiotic cohesin subunits RAD21L and REC8 are positioned at distinct regions between lateral elements and transverse filaments in the synaptonemal complex of mouse spermatocytes’, *The Journal of Reproduction and Development*, 62(6), pp. 623–630. Available at: https://doi.org/10.1262/jrd.2016-127.

Roux, K.J., Kim, D.I. and Burke, B. (2013) ‘BioID: A Screen for Protein-Protein Interactions’, *Current Protocols in Protein Science*, 74(1), p. 19.23.1-19.23.14. Available at: https://doi.org/10.1002/0471140864.ps1923s74.

Royo, H. *et al.* (2010) ‘Evidence that Meiotic Sex Chromosome Inactivation Is Essential for Male Fertility’, *Current Biology*, 20(23), pp. 2117–2123. Available at: https://doi.org/10.1016/j.cub.2010.11.010.

Royo, H. *et al.* (2013) ‘ATR acts stage specifically to regulate multiple aspects of mammalian meiotic silencing’, *Genes & Development*, 27(13), pp. 1484–1494. Available at: https://doi.org/10.1101/gad.219477.113.

van Ruiten, M.S. *et al.* (2022) ‘The cohesin acetylation cycle controls chromatin loop length through a PDS5A brake mechanism’, *Nature Structural & Molecular Biology*, 29(6), pp. 586–591. Available at: https://doi.org/10.1038/s41594-022-00773-z.

Rusnac, D.-V. and Zheng, N. (2020) ‘Structural Biology of CRL Ubiquitin Ligases’, in Y. Sun, W. Wei, and J. Jin (eds) *Cullin-RING Ligases and Protein Neddylation: Biology and Therapeutics*. Singapore: Springer (Advances in Experimental Medicine and Biology), pp. 9–31. Available at: https://doi.org/10.1007/978-981-15-1025-0_2.

Sacristan, C. and Kops, G.J.P.L. (2015) ‘Joined at the hip: kinetochores, microtubules, and spindle assembly checkpoint signaling’, *Trends in Cell Biology*, 25(1), pp. 21–28. Available at: https://doi.org/10.1016/j.tcb.2014.08.006.

Sadowski, M. *et al.* (2012) ‘Protein monoubiquitination and polyubiquitination generate structural diversity to control distinct biological processes’, *IUBMB Life*, 64(2), pp. 136–142. Available at: https://doi.org/10.1002/iub.589.

Sadowski, M. and Sarcevic, B. (2010) ‘Mechanisms of mono- and poly-ubiquitination: Ubiquitination specificity depends on compatibility between the E2 catalytic core and amino acid residues proximal to the lysine’, *Cell Division*, 5, pp. 1–5. Available at: https://doi.org/10.1186/1747-1028-5-19.

Saitou, M. and Yamaji, M. (2012) ‘Primordial Germ Cells in Mice’, *Cold Spring Harbor Perspectives in Biology*, 4(11), p. a008375. Available at: https://doi.org/10.1101/cshperspect.a008375.

Sakakibara, Y. *et al.* (2015) ‘Bivalent separation into univalents precedes age-related meiosis i errors in oocytes’, *Nature Communications*, 6(May), pp. 1–8. Available at: https://doi.org/10.1038/ncomms8550.

Sakuno, T. *et al.* (2011) ‘Repositioning of Aurora B Promoted by Chiasmata Ensures Sister Chromatid Mono-Orientation in Meiosis I’, *Developmental Cell*, 21(3), pp. 534–545. Available at: https://doi.org/10.1016/j.devcel.2011.08.012.

Sakuno, T., Tada, K. and Watanabe, Y. (2009) ‘Kinetochore geometry defined by cohesion within the centromere’, *Nature*, 458(7240), pp. 852–858. Available at: https://doi.org/10.1038/nature07876.

Sarcevic, B. *et al.* (2002) ‘Regulation of the ubiquitin-conjugating enzyme hHR6A by CDK-mediated phosphorylation’, *The EMBO Journal*, 21(8), pp. 2009–2018. Available at: https://doi.org/10.1093/emboj/21.8.2009.

Schimenti, J. (2005) ‘Synapsis or silence’, *Nature Genetics*, 37(1), pp. 11–13. Available at: https://doi.org/10.1038/ng0105-11.

Schmidt, O., Pfanner, N. and Meisinger, C. (2010) 'Mitochondrial protein import: from proteomics to functional mechanisms', *Nature Reviews Molecular Cell Biology*, 11(9), pp. 655–667. Available at: https://doi.org/10.1038/nrm2959.

Schmitz, J. *et al.* (2007) 'Sororin Is Required for Stable Binding of Cohesin to Chromatin and for Sister Chromatid Cohesion in Interphase', *Current Biology*, 17(7), pp. 630–636. Available at: https://doi.org/10.1016/j.cub.2007.02.029.

Schramm, S. *et al.* (2011) 'A Novel Mouse Synaptonemal Complex Protein Is Essential for Loading of Central Element Proteins, Recombination, and Fertility', *PLOS Genetics*, 7(5), p. e1002088. Available at: https://doi.org/10.1371/journal.pgen.1002088.

Schulman, B.A. and Wade Harper, J. (2009) 'Ubiquitin-like protein activation by E1 enzymes: The apex for downstream signalling pathways', *Nature Reviews Molecular Cell Biology*, 10(5), pp. 319–331. Available at: https://doi.org/10.1038/nrm2673.

Schultz, N., Hamra, F.K. and Garbers, D.L. (2003) 'A multitude of genes expressed solely in meiotic or postmeiotic spermatogenic cells offers a myriad of contraceptive targets', *Proceedings of the National Academy of Sciences*, 100(21), pp. 12201–12206. Available at: https://doi.org/10.1073/pnas.1635054100.

Schwarzer, W. *et al.* (2017) 'Two independent modes of chromatin organization revealed by cohesin removal', *Nature*, 551(7678), pp. 51–56. Available at: https://doi.org/10.1038/nature24281.

Scott, D.C. *et al.* (2017) 'Blocking an N-terminal acetylation–dependent protein interaction inhibits an E3 ligase', *Nature Chemical Biology*, 13(8), pp. 850–857. Available at: https://doi.org/10.1038/nchembio.2386.

Seitan, V.C. *et al.* (2006) 'Metazoan Scc4 Homologs Link Sister Chromatid Cohesion to Cell and Axon Migration Guidance', *PLOS Biology*, 4(8), p. e242. Available at: https://doi.org/10.1371/journal.pbio.0040242.

Sgarbi, G. *et al.* (2006) 'Inefficient coupling between proton transport and ATP synthesis may be the pathogenic mechanism for NARP and Leigh syndrome resulting from the T8993G mutation in mtDNA', *Biochemical Journal*, 395(Pt 3), pp. 493–500. Available at: https://doi.org/10.1042/BJ20051748.

Shah, S.S. and Kumar, S. (2021) 'Adaptors as the regulators of HECT ubiquitin ligases', *Cell Death & Differentiation*, 28(2), pp. 455–472. Available at: https://doi.org/10.1038/s41418-020-00707-6.

Shemorry, A., Hwang, C.-S. and Varshavsky, A. (2013) 'Control of Protein Quality and Stoichiometries by N-Terminal Acetylation and the N-End Rule

Pathway', *Molecular Cell*, 50(4), pp. 540–551. Available at: https://doi.org/10.1016/j.molcel.2013.03.018.

Shibuya, H. and Watanabe, Y. (2014) 'The meiosis-specific modification of mammalian telomeres', *Cell Cycle*, 13(13), pp. 2024–2028. Available at: https://doi.org/10.4161/cc.29350.

Shima, J.E. *et al.* (2004) 'The Murine Testicular Transcriptome: Characterizing Gene Expression in the Testis During the Progression of Spermatogenesis1', *Biology of Reproduction*, 71(1), pp. 319–330. Available at: https://doi.org/10.1095/biolreprod.103.026880.

Shin, S.-W. *et al.* (2017) 'Cytoplasmic cleavage of DPPA3 is required for intracellular trafficking and cleavage-stage development in mice', *Nature Communications*, 8, p. 1643. Available at: https://doi.org/10.1038/s41467-017-01387-6.

Shin, Y.-H., McGuire, M.M. and Rajkovic, A. (2013) 'Mouse HORMAD1 Is a Meiosis I Checkpoint Protein That Modulates DNA Double-Strand Break Repair During Female Meiosis1', *Biology of Reproduction*, 89(2), pp. 29, 1–12. Available at: https://doi.org/10.1095/biolreprod.112.106773.

Shintomi, K. and Hirano, T. (2009) 'Releasing cohesin from chromosome arms in early mitosis: opposing actions of Wapl–Pds5 and Sgo1', *Genes & Development*, 23(18), pp. 2224–2236. Available at: https://doi.org/10.1101/gad.1844309.

Skibbens, R.V. (2019) 'Condensins and cohesins – one of these things is not like the other!', *Journal of Cell Science*, 132(3), p. jcs220491. Available at: https://doi.org/10.1242/jcs.220491.

Sluimer, J. and Distel, B. (2018) 'Regulating the human HECT E3 ligases', *Cellular and Molecular Life Sciences*, 75(17), pp. 3121–3141. Available at: https://doi.org/10.1007/s00018-018-2848-2.

Smith, J.S. *et al.* (2016) 'Loss of Function Cohesin Complex Gene Mutations Create Neomorphic Cell States Advantageous to Oncogenesis', *Blood*, 128(22), p. 1564. Available at: https://doi.org/10.1182/blood.V128.22.1564.1564.

Solari, A.J. (1974) 'The Behavior of the XY Pair in Mammals', in G.H. Bourne, J.F. Danielli, and K.W. Jeon (eds) *International Review of Cytology*. Academic Press, pp. 273–317. Available at: https://doi.org/10.1016/S0074-7696(08)60928-6.

Song, J. *et al.* (2012) 'Cohesin Acetylation Promotes Sister Chromatid Cohesion Only in Association with the Replication Machinery *', *Journal of Biological Chemistry*, 287(41), pp. 34325–34336. Available at: https://doi.org/10.1074/jbc.M112.400192.

Sultana, R., Theodoraki, M.A. and Caplan, A.J. (2012) 'UBR1 promotes protein kinase quality control and sensitizes cells to Hsp90 inhibition', *Experimental Cell Research*, 318(1), pp. 53–60. Available at: https://doi.org/10.1016/j.yexcr.2011.09.010.

Summers, D.W. *et al.* (2013) 'The Type II Hsp40 Sis1 Cooperates with Hsp70 and the E3 Ligase Ubr1 to Promote Degradation of Terminally Misfolded Cytosolic Protein', *PLOS ONE*, 8(1), p. e52099. Available at: https://doi.org/10.1371/journal.pone.0052099.

Sun, F. *et al.* (2015) 'Nuclear localization of PRDM9 and its role in meiotic chromatin modifications and homologous synapsis', *Chromosoma*, 124(3), pp. 397–415. Available at: https://doi.org/10.1007/s00412-015-0511-3.

Sun, F. and Handel, M.A. (2008) 'Regulation of the meiotic prophase I to metaphase I transition in mouse spermatocytes', *Chromosoma*, 117(5), pp. 471–485. Available at: https://doi.org/10.1007/s00412-008-0167-3.

Sun, F., Palmer, K. and Handel, M.A. (2010) 'Mutation of Eif4g3, encoding a eukaryotic translation initiation factor, causes male infertility and meiotic arrest of mouse spermatocytes', *Development*, 137(10), pp. 1699–1707. Available at: https://doi.org/10.1242/dev.043125.

Sun, Y. *et al.* (2009) 'Separase Is Recruited to Mitotic Chromosomes to Dissolve Sister Chromatid Cohesion in a DNA-Dependent Manner', *Cell*, 137(1), pp. 123–132. Available at: https://doi.org/10.1016/j.cell.2009.01.040.

SZOLLOSI, D., CALARCO, P. and DONAHUE, R.P. (1972) 'Absence of Centrioles in the First and Second Meiotic Spindles of Mouse Oocytes', *Journal of Cell Science*, 11(2), pp. 521–541. Available at: https://doi.org/10.1242/jcs.11.2.521.

Takahashi, T.S. *et al.* (2019) 'Structural basis of ubiquitin recognition by the winged-helix domain of Cockayne syndrome group B protein', *Nucleic acids research*, 47(7), pp. 3784–3794. Available at: https://doi.org/10.1093/nar/gkz081.

Takayanagi-Kiya, S. *et al.* (2014) 'Splicing Variants of NOL4 Differentially Regulate the Transcription Activity of Mlr1 and Mlr2 in Cultured Cells', *Zoological Science*, 31(11), pp. 735–740. Available at: https://doi.org/10.2108/zs140049.

Tarabay, Y. *et al.* (2013) 'The mammalian-specific Tex19.1 gene plays an essential role in spermatogenesis and placenta-supported development', *Human Reproduction*, 28(8), pp. 2201–2214. Available at: https://doi.org/10.1093/humrep/det129.

Tasaki, T. *et al.* (2005) 'A Family of Mammalian E3 Ubiquitin Ligases That Contain the UBR Box Motif A Family of Mammalian E3 Ubiquitin Ligases

That Contain the UBR Box Motif and Recognize N-Degrons', *Molecular and cellular biology*, 25(16), pp. 7120–7136. Available at: https://doi.org/10.1128/MCB.25.16.7120.

Tasaki, T. *et al.* (2009a) 'The substrate recognition domains of the N-end rule pathway', *Journal of Biological Chemistry*, 284(3), pp. 1884–1895. Available at: https://doi.org/10.1074/jbc.M803641200.

Tasaki, T. *et al.* (2009b) 'The substrate recognition domains of the N-end rule pathway', *Journal of Biological Chemistry*, 284(3), pp. 1884–1895. Available at: https://doi.org/10.1074/jbc.M803641200.

Tasaki, T. *et al.* (2012) 'The N-End Rule Pathway', *Annual Review of Biochemistry*, 81(1), pp. 261–289. Available at: https://doi.org/10.1146/annurev-biochem-051710-093308.

Tedeschi, A. *et al.* (2013) 'Wapl is an essential regulator of chromatin structure and chromosome segregation', *Nature*, 501(7468), pp. 564–568. Available at: https://doi.org/10.1038/nature12471.Wapl.

Thomas, G.E., Renjith, M.R. and Manna, T.K. (2017) 'Kinetochore–microtubule interactions in chromosome segregation: lessons from yeast and mammalian cells', *Biochemical Journal*, 474(21), pp. 3559–3577. Available at: https://doi.org/10.1042/BCJ20170518.

Toda, K. *et al.* (2012) 'APC/C-Cdh1-dependent anaphase and telophase progression during mitotic slippage', *Cell Division*, 7(1), p. 4. Available at: https://doi.org/10.1186/1747-1028-7-4.

Tonkin, E.T. *et al.* (2004) 'NIPBL, encoding a homolog of fungal Scc2-type sister chromatid cohesion proteins and fly Nipped-B, is mutated in Cornelia de Lange syndrome', *Nature Genetics*, 36(6), pp. 636–641. Available at: https://doi.org/10.1038/ng1363.

Tsuchiya, H. *et al.* (2017) 'In Vivo Ubiquitin Linkage-type Analysis Reveals that the Cdc48-Rad23/Dsk2 Axis Contributes to K48-Linked Chain Specificity of the Proteasome', *Molecular Cell*, 66(4), pp. 488-502.e7. Available at: https://doi.org/10.1016/j.molcel.2017.04.024.

Tsutsumi, M. *et al.* (2014) 'Age-related decrease of meiotic cohesins in human oocytes', *PLoS ONE*, 9(5). Available at: https://doi.org/10.1371/journal.pone.0096710.

Turner, G.C., Du, F. and Varshavsky, A. (2000) 'Peptides accelerate their uptake by activating a ubiquitin-dependent proteolytic pathway', *Nature*, 405(6786), pp. 579–583. Available at: https://doi.org/10.1038/35014629.

Turner, J.M.A. (2015) 'Meiotic Silencing in Mammals', *Annual Review of Genetics*, 49(1), pp. 395–412. Available at: https://doi.org/10.1146/annurev-genet-112414-055145.

Uhlmann, F., Lottspeich, F. and Nasmyth, K. (1999) 'Sister-chromatid separation at anaphase onset is promoted by cleavage of the cohesin subunit Scc1', *Nature*, 400(6739), pp. 37–42. Available at: https://doi.org/10.1038/21831.

Varshavsky, A. (2008) 'Discovery of Cellular Regulation by Protein Degradation', *Journal of Biological Chemistry*, 283(50), pp. 34469–34489. Available at: https://doi.org/10.1074/jbc.X800009200.

Varshavsky, A. (2019) 'N-degron and C-degron pathways of protein degradation', *Proceedings of the National Academy of Sciences*, 116(2), pp. 358–366. Available at: https://doi.org/10.1073/PNAS.1816596116.

Verma, R., Mohl, D. and Deshaies, R.J. (2020) 'Harnessing the Power of Proteolysis for Targeted Protein Inactivation', *Molecular Cell*, 77(3), pp. 446–460. Available at: https://doi.org/10.1016/j.molcel.2020.01.010.

Vögtle, F.-N. *et al.* (2009) 'Global Analysis of the Mitochondrial N-Proteome Identifies a Processing Peptidase Critical for Protein Stability', *Cell*, 139(2), pp. 428–439. Available at: https://doi.org/10.1016/j.cell.2009.07.045.

Vögtle, F.-N. *et al.* (2011) 'Mitochondrial protein turnover: role of the precursor intermediate peptidase Oct1 in protein stabilization', *Molecular Biology of the Cell*, 22(13), pp. 2135–2143. Available at: https://doi.org/10.1091/mbc.E11-02-0169.

de Vries, F.A.T. *et al.* (2005) 'Mouse Sycp1 functions in synaptonemal complex assembly, meiotic recombination, and XY body formation', *Genes & Development*, 19(11), pp. 1376–1389. Available at: https://doi.org/10.1101/gad.329705.

Vu, T.T.M. and Varshavsky, A. (2020a) 'The ATF3 Transcription Factor Is a Short-Lived Substrate of the Arg/N-Degron Pathway', *Biochemistry*, 59(30), pp. 2796–2812. Available at: https://doi.org/10.1021/acs.biochem.0c00514.

Vu, T.T.M. and Varshavsky, A. (2020b) 'The ATF3 Transcription Factor Is a Short-Lived Substrate of the Arg/N-Degron Pathway', *Biochemistry*, 59(30), pp. 2796–2812. Available at: https://doi.org/10.1021/acs.biochem.0c00514.

Waizenegger, I.C. *et al.* (2000) 'Two Distinct Pathways Remove Mammalian Cohesin from Chromosome Arms in Prophase and from Centromeres in Anaphase', *Cell*, 103(3), pp. 399–410. Available at: https://doi.org/10.1016/S0092-8674(00)00132-X.

Wang, C. *et al.* (2007) 'Regulation of E2F1 function by the nuclear corepressor KAP1', *Journal of Biological Chemistry*, 282(41), pp. 29902–29909. Available at: https://doi.org/10.1074/jbc.M704757200.

Wang, C. *et al.* (2021) ‘PINK1-mediated mitophagy maintains pluripotency through optineurin’, *Cell Proliferation*, 54(5), p. e13034. Available at: https://doi.org/10.1111/cpr.13034.

Wang, M. and Kaufman, R.J. (2016) ‘Protein misfolding in the endoplasmic reticulum as a conduit to human disease’, *Nature*, 529(7586), pp. 326–335. Available at: https://doi.org/10.1038/nature17041.

Wang, M. and Pickart, C.M. (2005) ‘Different HECT domain ubiquitin ligases employ distinct mechanisms of polyubiquitin chain synthesis’, *The EMBO Journal*, 24(24), pp. 4324–4333. Available at: https://doi.org/10.1038/sj.emboj.7600895.

Ward, A. *et al.* (2016) ‘Genetic interactions between the meiosis-specific cohesin components, STAG3, REC8, and RAD21L’, *G3: Genes, Genomes, Genetics*, 6(6), pp. 1713–1724. Available at: https://doi.org/10.1534/g3.116.029462.

Wassmann, K. (2013) ‘Sister chromatid segregation in meiosis II : Deprotection through phosphorylation’, *Cell Cycle*, 12(9), pp. 1352–1359. Available at: https://doi.org/10.4161/cc.24600.

Wassmann, K. (2022) ‘Separase Control and Cohesin Cleavage in Oocytes: Should I Stay or Should I Go?’, *Cells*, 11(21), p. 3399. Available at: https://doi.org/10.3390/cells11213399.

Watanabe, Y. (2012) ‘Geometry and force behind kinetochore orientation: lessons from meiosis’, *Nature Reviews Molecular Cell Biology*, 13(6), pp. 370–382. Available at: https://doi.org/10.1038/nrm3349.

Watrin, E. *et al.* (2006) ‘Human Scc4 Is Required for Cohesin Binding to Chromatin, Sister-Chromatid Cohesion, and Mitotic Progression’, *Current Biology*, 16(9), pp. 863–874. Available at: https://doi.org/10.1016/j.cub.2006.03.049.

Wendt, K.S. *et al.* (2008) ‘Cohesin mediates transcriptional insulation by CCCTC-binding factor’, *Nature*, 451(7180), pp. 796–801. Available at: https://doi.org/10.1038/nature06634.

Whelan, G. *et al.* (2012) ‘Cohesin acetyltransferase Esco2 is a cell viability factor and is required for cohesion in pericentric heterochromatin’, *EMBO Journal*, 31(1), pp. 71–82. Available at: https://doi.org/10.1038/emboj.2011.381.

Winters, T., McNicoll, F. and Jessberger, R. (2014) ‘Meiotic cohesin STAG3 is required for chromosome axis formation and sister chromatid cohesion’, *The EMBO Journal*, 33(11), pp. 1256–1270. Available at: https://doi.org/10.1002/embj.201387330.

Wojtasz, L. *et al.* (2012) 'Meiotic DNA double-strand breaks and chromosome asynapsis in mice are monitored by distinct HORMAD2-independent and -dependent mechanisms', *Genes & Development*, 26(9), pp. 958–973. Available at: https://doi.org/10.1101/gad.187559.112.

Wolf, P.G. *et al.* (2018) 'Studying meiotic cohesin in somatic cells reveals that Rec8-containing cohesin requires Stag3 to function and is regulated by Wapl and sororin', *Journal of Cell Science*, 131(11), p. jcs212100. Available at: https://doi.org/10.1242/jcs.212100.

Wutz, G. *et al.* (2017) 'Topologically associating domains and chromatin loops depend on cohesin and are regulated by CTCF, WAPL, and PDS5 proteins', *The EMBO Journal*, 36(24), pp. 3573–3599. Available at: https://doi.org/10.15252/embj.201798004.

Xia, Z. *et al.* (2008) 'Substrate-binding Sites of UBR1, the Ubiquitin Ligase of the N-end Rule Pathway *', *Journal of Biological Chemistry*, 283(35), pp. 24011–24028. Available at: https://doi.org/10.1074/jbc.M802583200.

Xu, H. *et al.* (2004) 'A new role for the mitotic RAD21/SCC1 cohesin in meiotic chromosome cohesion and segregation in the mouse', *EMBO reports*, 5(4), pp. 378–384. Available at: https://doi.org/10.1038/sj.embor.7400121.

Xu, H. *et al.* (2011) 'Enhanced RAD21 cohesin expression confers poor prognosis and resistance to chemotherapy in high grade luminal, basal and HER2 breast cancers', *Breast Cancer Research*, 13(1), p. R9. Available at: https://doi.org/10.1186/bcr2814.

Xu, H. *et al.* (2019) 'The N-end rule ubiquitin ligase UBR2 mediates NLRP1B inflammasome activation by anthrax lethal toxin', *The EMBO Journal*, p. e101996. Available at: https://doi.org/10.15252/embj.2019101996.

Yamano, K. and Youle, R.J. (2013) 'PINK1 is degraded through the N-end rule pathway', *Autophagy*, 9(11), pp. 1758–1769. Available at: https://doi.org/10.4161/auto.24633.

Yan, L. *et al.* (2013) 'Single-cell RNA-Seq profiling of human preimplantation embryos and embryonic stem cells', *Nature Structural & Molecular Biology*, 20(9), pp. 1131–1139. Available at: https://doi.org/10.1038/nsmb.2660.

Yanagitani, K., Juszkiewicz, S. and Hegde, R.S. (2017) 'UBE2O is a quality control factor for orphans of multiprotein complexes', *Science*, 357(6350), pp. 472–475. Available at: https://doi.org/10.1126/science.aan0178.

Yang, F. *et al.* (2010a) 'The ubiquitin ligase Ubr2, a recognition E3 component of the N-end rule pathway, stabilizes Tex19.1 during spermatogenesis', *PLoS ONE*, 5(11), pp. 1–7. Available at: https://doi.org/10.1371/journal.pone.0014017.

Yang, F. *et al.* (2010b) ‘The ubiquitin ligase Ubr2, a recognition E3 component of the N-end rule pathway, stabilizes Tex19.1 during spermatogenesis’, *PLoS ONE*, 5(11), pp. 1–7. Available at: https://doi.org/10.1371/journal.pone.0014017.

Yoo, Y.D. *et al.* (2018) ‘N-terminal arginylation generates a bimodal degron that modulates autophagic proteolysis’, *Proceedings of the National Academy of Sciences*, 115(12), pp. E2716–E2724. Available at: https://doi.org/10.1073/pnas.1719110115.

Young, D.J. *et al.* (2014) ‘Knockdown of Hnrnpa0, a del(5q) gene, alters myeloid cell fate in murine cells through regulation of AU-rich transcripts’, *Haematologica*, 99(6), pp. 1032–1040. Available at: https://doi.org/10.3324/haematol.2013.098657.

Yu, W. *et al.* (2019) ‘One-Carbon Metabolism Supports S-Adenosylmethionine and Histone Methylation to Drive Inflammatory Macrophages’, *Molecular Cell*, 75(6), pp. 1147-1160.e5. Available at: https://doi.org/10.1016/j.molcel.2019.06.039.

Yuan, L. *et al.* (no date) ‘The Murine SCP3 Gene Is Required for Synaptonemal Complex Assembly, Chromosome Synapsis, and Male Fertility’, *Molecular Cell*, p. 11.

Yusufzai, T. and Kadonaga, J.T. (2008) ‘HARP Is an ATP-Driven Annealing Helicase’, *Science*, 322(5902), pp. 748–750. Available at: https://doi.org/10.1126/science.1161233.

Zelazowski, M.J. and Cole, F. (2016) ‘X marks the spot: PRDM9 rescues hybrid sterility by finding hidden treasure in the genome’, *Nature Structural & Molecular Biology*, 23(4), pp. 267–269. Available at: https://doi.org/10.1038/nsmb.3201.

Zenker, M. *et al.* (2005) ‘Deficiency of UBR1, a ubiquitin ligase of the N-end rule pathway, causes pancreatic dysfunction, malformations and mental retardation (Johanson-Blizzard syndrome)’, *Nature Genetics*, 37(12), pp. 1345–1350. Available at: https://doi.org/10.1038/ng1681.

Zhang, J. *et al.* (2008) ‘Acetylation of Smc3 by Eco1 Is Required for S Phase Sister Chromatid Cohesion in Both Human and Yeast’, *Molecular Cell*, 31(1), pp. 143–151. Available at: https://doi.org/10.1016/j.molcel.2008.06.006.

Zhang, N. *et al.* (2013) ‘Characterization of the interaction between the cohesin subunits Rad21 and SA1/2’, *PloS One*, 8(7), p. e69458. Available at: https://doi.org/10.1371/journal.pone.0069458.

Zhang, X. *et al.* (2017) ‘An Atomic Structure of the Human Spliceosome’, *Cell*, 169(5), pp. 918-929.e14. Available at: https://doi.org/10.1016/j.cell.2017.04.033.

Zhou, C. *et al.* (2021) ‘The cohesin stabilizer Sororin drives G2-M transition and spindle assembly in mammalian oocytes’, *Science Advances*, 7(39), p. eabg9335. Available at: https://doi.org/10.1126/sciadv.abg9335.

Zhou, H. *et al.* (2017) ‘A potent small-molecule inhibitor of the DCN1-UBC12 interaction that selectively blocks cullin 3 neddylation’, *Nature Communications*, 8(1), p. 1150. Available at: https://doi.org/10.1038/s41467-017-01243-7.

Zickler, D. and Kleckner, N. (1999) ‘Meiotic chromosomes: Integrating structure and function’, *Annual Review of Genetics*, 33, pp. 603–754. Available at: https://doi.org/10.1146/annurev.genet.33.1.603.

Zielinska, A.P. *et al.* (2015) ‘Sister kinetochore splitting and precocious disintegration of bivalents could explain the maternal age effect’, *eLife*, 4(DECEMBER2015), pp. 1–19. Available at: https://doi.org/10.7554/eLife.11389.